S.V. Starodubtsev, A.M.Romanov

The Passage of Charged Particles through Matter

Translation of "Prokhozhdenie zaryazhennykh chastits cherez veshchestvo"
Izdatel'stvo Akademii Nauk Uzbekskoi SSR Tashkent 1962

Israel Program for Scientific Translations
Jerusalem 1965

AKADEMIYA NAUK UZBEKSKOI SSR. FIZIKO-TEKHNICHESKII INSTITUT
Academy of Sciences of the Uzbek SSR. Physico-Technical Institute

S. V. STARODUBTSEV and A. M. ROMANOV

The Passage of Charged Particles through Matter

(Prokhozhdenie zaryazhennykh chastits cherez veshchestvo)

Izdatel'stvo Akademii Nauk Uzbekskoi SSR
Tashkent 1962

Translated from Russian

Israel Program for Scientific Translations
Jerusalem 1965

AEC-tr-6468

Published Pursuant to an Agreement with
THE U. S. ATOMIC ENERGY COMMISSION
and
THE NATIONAL SCIENCE FOUNDATION, WASHINGTON, D. C.

Copyright © 1965
Israel Program for Scientific Translations
IPST Cat. No. 1246
Translated and Edited by IPST Staff

Printed in Jerusalem by S. Monson
Binding: K. Wiener
Price: $ 6.00

Available from the
U. S. DEPARTMENT OF COMMERCE
Clearinghouse for Federal Scientific and Technical Information
Springfield, Va. 22151

IX/5/3.5

TABLE OF CONTENTS

Chapter I. PASSAGE OF HEAVY CHARGED PARTICLES THROUGH MATTER . 1
§ 1. Introduction 1
§ 2. Elastic collisions and energy transfer in elastic scattering of particles by nuclei (atoms) 3
§ 3. Excitation of nuclei and nuclear reactions induced by fast charged particles 34
§ 4. Theory of energy loss of particles in inelastic collisions with atomic electrons 40
§ 5. Experimental verification of the stopping theory and data on the ionization energy losses of fast protons and α-particles 66
§ 6. Experimental data on the relation between range and energy for fast protons and for α-particles 85
§ 7. Inelastic collisions of heavy charged particles with atoms. The stopping process and the ranges of heavy ions in matter 112
§ 8. Relation between energy losses and ionization 140
§ 9. Vavilov-Cerenkov radiation 149
§ 10. Some methods of identifying fast charged particles and their energy measurements 151

CHAPTER II. PASSAGE OF ELECTRONS THROUGH MATTER 158
§ 11. Introduction 158
§ 12. Elastic scattering of electrons (positrons) 159
§ 13. Ionization energy losses 175
§ 14. Radiation energy losses. Total energy lost by an electron 184
§ 15. Relationship between range and energy of electrons 192
§ 16. Connection between energy losses and ionization 199

BIBLIOGRAPHY 207

EXPLANATORY LIST OF ABBREVIATIONS . . . . . .

This book gives a basic account of the theory of interaction and the results of numerous experimental investigations on the passage of heavy charged particles and electrons through matter.

The book deals mainly with problems of the energy loss of charged particles and the resulting ionization, with relations between the range and the energy of particles, and related topics. Extensive data are presented which should prove useful for physicists and engineers.

The book is intended for research scientists, university lecturers, and for postgraduate students specializing in fields of physics and engineering physics.

Chapter I

PASSAGE OF HEAVY CHARGED PARTICLES THROUGH MATTER

§ 1. Introduction

Short review of the interactions of heavy charged particles with matter. When charged particles pass through matter the following processes may take place:

1) inelastic collisions with the bound electrons of the retarding medium, in which the energy lost by the particle is spent on the excitation or ionization of atoms and molecules. The energy losses in this kind of collisions are called ionization losses, to distinguish them from radiation losses which are connected with the generation of bremsstrahlung in inelastic collisions of charged particles with electrons;

2) inelastic collisions with nuclei, leading to the production of bremsstrahlung quanta, to the excitation of nuclear levels, or to nuclear reactions;

3) elastic collisions with nuclei (or with whole atoms), in which part of the kinetic energy of the incident particle is transferred to the recoil atoms; in this case the total kinetic energy of the colliding particles remains unchanged;

4) elastic collisions with bound electrons;

5) the Vavilov-Cerenkov effect, i.e., emission of light by particles passing through matter with a velocity exceeding the phase velocity of light waves in the given medium.

The nature of these processes and their relative importance in reducing the intensity of particle beams and in stopping them depend on the mass of the charged particles and on their velocities. In this connection, when problems connected with the passage of particles through matter are considered, heavy charged particles and electrons (positrons) are dealt with separately.

In this context heavy particles are particles whose mass exceeds the electron mass by a large factor (mesons, protons, deuterons, alpha-particles, etc.).

Inelastic collisions with nuclei and elastic collisions with electrons are relatively unimportant in reducing the intensity of a beam of heavy charged particles as compared to inelastic ionization collisions with electrons and elastic collisions with nuclei (atoms) of the retarding medium*. In turn, the importance of electronic and atomic collisions in reducing the intensity

* For a proton energy $\gtrsim 10^9$ ev and a μ-meson energy $\approx 10^{11}$ ev inelastic nuclear interactions begin to be of major importance (see § 3).

of a beam of heavy charged particles and in their retarding depends both on their charge and on their velocity.

Two extreme cases should be distinguished: when the incident particles have a small charge ($z \approx 1$) and a high velocity ($v > \frac{cZ}{137}$) and, conversely, a large charge ($z \gg 1$) and a "low" velocity ($v < \frac{cZ}{137}$). Here z is the effective charge (taking into account the electron screening) of the incident particles, and Z is the effective charge of the nuclei of the retarding medium; c is the velocity of light.

In the first case, the theoretical description of particle retardation was successful and anticipated the results of experimental investigations (§ 4 — 6). For fast particles of small charge, the energy is lost mainly in small amounts during inelastic collisions with electrons. The effective charge of the particle remains unchanged along a large section of its path, at least as long as the velocity of the particle considerably exceeds the velocity of the electrons in its K-shell. Owing to the large difference in masses, the heavy particle K— hardly deviates from its initial direction during collisions with electrons. Particles of the same energy proceed until they are stopped practically along their initial path. This is clearly illustrated by photographs of tracks of alpha-particles and protons in a cloud chamber or in a photoemulsion.

When the velocity of the charged particles becomes comparable to that of the orbiting electrons ($v \sim \frac{cZ}{137}$), these become less effective in retarding the particles. This is taken into account in the theory by introducing corrections for the electron binding effect (§ 4). Finally, as the velocity decreases further, charge exchange, i.e., the process of capture and loss of electrons by particles, begins to be of importance (§ 7). At this stage of retardation, the effective charge of the particle continuously decreases, the rate of energy loss due to inelastic collisions with electrons also becomes smaller, and at the same time elastic collisions with atoms become more important (§ 2). Charge exchange is one of the possible ways of energy loss by incident particles, since it is connected with the formation of ion pairs. When protons with an energy of ~25 kev pass through hydrogen, charge-exchange losses amount to 15 — 17% of the total energy losses /132/. Unfortunately, there is no satisfactory theory at present of charge exchange and energy loss of retarded charged particles. However, a large body experimental data are available (§ 5 — 7) which facilitate the formulation of some general characteristic features of this phenomenon.

For charged particles of relativistic velocities the energy losses dependent on the spin of the particle have to be considered, as well as the influence of the density of the retarding medium and its dielectric properties (§ 4).

Only a small amount of energy is lost by fast charged particles in the Vavilov-Cerenkov radiation compared with ionization and other losses; this radiation, however, is very important in the high-energy range. The Vavilov-Cerenkov radiation is discussed in § 9.

For highly charged slow particles, charge exchange processes are important. As the velocity of the particle decreases, the effective charge and the ionization energy losses rapidly decrease, which is also observed in the final range of particles of small charge (protons, alpha-particles). At the same time, the neutralization of the particles and the decrease in their

velocity lead to the increasing importance of elastic collisions. At some stage of the retardation, the ionization produced by the recoil atoms may constitute a considerable fraction of the total ionization produced by a slow heavy particle. Most of the data on the passage of slow highly charged particles through matter is of an empirical nature (§ 7).

This chapter deals mainly with the theoretical and experimental aspects of the energy losses associated with the passage of particles through matter, with the relations between the range and the energy of heavy charged particles in various media, and with relations between the energy loss and the ionization. Information of this kind is important in the design and set-up of a wide range of experimental investigations, as well as in the interpretation of their results. For example, the characteristics of recording and analyzing devices used in nuclear and atomic physics are determined in the last analysis by the nature of the interaction of the charged particles with the substance constituting the sensitive volume of the detector. Many methods of physical investigation (see, for example, § 10) are connected with phenomena observed when particles pass through matter.

The study of the interaction of particles with matter is also significant in understanding the physical and chemical changes occurring in the retarding layer due to radiation.

Interaction cross section. The probability of an interaction is characterized by the concept of the cross section. It is defined as follows:

Suppose a particle with an energy E passes through a substance of thickness dx, containing n interaction centers (atoms, nuclei or electrons) per 1 cm^3. Then $\sigma(E)ndx$ is the probability that an interaction occurs between the incident particle and a particle of the substance. The quantity $\sigma(E)$ is called the effective interaction cross section, and, according to the definition, it is numerically equal to the probability that an interaction occurs when one particle passes through a target containing one interaction center per 1 cm^2. The cross section has the dimension of area.

If N particles with an energy E pass through a target containing ndx centers, then a fraction dN of the particles undergo interaction (dN interactions occur). We have then

$$dN = \sigma(E)Nndx. \tag{1.1}$$

The differential cross section $\sigma(E,Q\vartheta,\varphi)$ determines the number of interactions of a particle with a target containing one center per 1 cm^2. These events are accompanied by an energy change from Q to $Q + dQ$ and a deflection of the incident particle in the solid angle from Ω to $\Omega + d\Omega$, so that

$$dN = \sigma(E, Q, \vartheta, \varphi)Nndxd Qd\Omega, \tag{1.2}$$

where

$$d\Omega = \sin\vartheta d\vartheta d\varphi$$

is the solid-angle element in spherical coordinates (r,ϑ,φ).

§ 2. Elastic collisions and energy transfer in elastic scattering of particles by nuclei (atoms)

The kinematics of elastic collisions (non-relativistic case). Let us consider the most frequently encountered case of an elastic collision of

two free particles, one, with the mass m_2, was stationary before the collision, and the other, with the mass m_1, had the velocity $\vec{v}$ in the laboratory system of coordinates (LS) before the collision. As a result of the collision the particles acquire the velocities $\vec{v}_1$ and $\vec{v}_2$, flying away at the angles ϑ_1 and ϑ_2 to the direction of the vector $\vec{v}$ (Figure 1). The velocities of the particles after the collision can be easily determined using the laws of conservation of energy and momentum. In the non-relativistic approximation ($\beta = \frac{v}{c} \ll 1$, where c is the velocity of light), the corresponding calculations

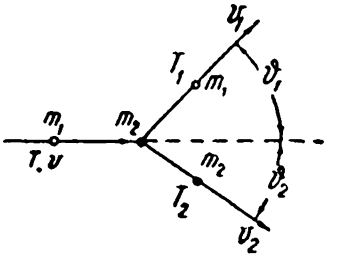

FIGURE 1. Collision of two particles

lead to the following expressions:

$$\left.\begin{aligned} v_1 &= \frac{m_1}{m_1+m_2}\left[\cos\vartheta_1 \pm \sqrt{\left(\frac{m_2}{m_1}\right)^2 - \sin^2\vartheta_1}\right] v = v\,\frac{\sin\vartheta_2}{\sin(\vartheta_1+\vartheta_2)} \\ v_2 &= v\left(\frac{2m_1}{m_1+m_2}\right)\cos\vartheta_2. \end{aligned}\right\} \quad (2.1)$$

For $m_1 < m_2$ both the positive and the negative sign before the square root in the first of expressions (2.1), are permitted; for $m_2 < m_1$ the positive sign is taken. It can also be shown that for $m_1 > m_2$ the deflection angles of the colliding particles cannot exceed

$$\vartheta_{1\max} = \arcsin\left(\frac{m_2}{m_1}\right),$$

$$\vartheta_{2\max} = \arcsin\left(\frac{m_1-m_2}{2m_1}\right)^{1/2}.$$

For example, in the elastic scattering of alpha-particles by hydrogen, the particles cannot be deflected from their initial direction by an angle larger than 14°30'. The relation between the kinetic energies of the particles before and after the collision is given by

$$\left.\begin{aligned} T_1 &= T\left(\frac{m_1}{m_1+m_2}\right)^2\left[\cos\vartheta_1 \pm \sqrt{\left(\frac{m_2}{m_1}\right)^2 - \sin^2\vartheta_1}\right]^2 = T\left[\frac{\sin\vartheta_1}{\sin(\vartheta_1+\vartheta_2)}\right]^2 \\ T_2 &\equiv Q = T\frac{4m_1m_2}{(m_1+m_2)^2}\cos^2\vartheta_2 = T\frac{m_1}{m_2}\left[\frac{\sin\vartheta_1}{\sin(\vartheta_1+\vartheta_2)}\right]^2 \end{aligned}\right\} \quad (2.2)$$

In a head-on collision ($\vartheta_2 = 0$) the stationary particle receives the maximum energy, which is equal to

$$T_{2\max} \equiv Q_{\max} = \frac{4m_1 m_2}{(m_1 + m_2)^2} T. \tag{2.3}$$

Thus, for example, in the elastic head-on collision of a neutron with a proton, the neutron is completely stopped, and the energy of the recoil proton is equal to the initial energy of the neutron. In the elastic scattering of neutrons by deuterium and carbon, the maximum energy of the recoil nuclei is respectively 89% and 28% of the energy of the scattered neutrons. Thus, light elements are effective neutron moderators, a fact which is widely applied in nuclear physics and engineering.

Let us consider an elastic collision in a system of coordinates in which the center of mass of the colliding particles is stationary (center of mass system, CMS).

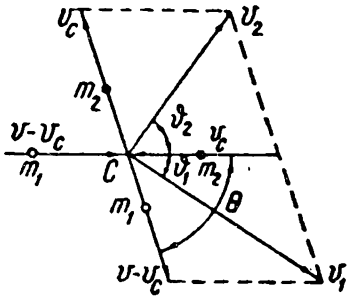

FIGURE 2. Velocity diagram of the particles in an elastic collision

In CMS the interacting particles have zero, total momentum, so that the velocities of the particles are inversely proportional to their mass.

Prior to collision, the particle with the mass m_1 moves towards the center of mass C of the system (Figure 2) with a velocity

$$v_{1C} = v - v_C = v \frac{m_2}{m_1 + m_2} = v \frac{\mu}{m_1},$$

and the particle with the mass m_2 moves towards the center of mass in the opposite direction with the velocity

$$v_{2C} = v_C = v \frac{m_1}{m_1 + m_2} = v \frac{\mu}{m_2}.$$

Here and in the following μ represents the reduced mass of a system of particles,

$$\mu = \frac{m_1 m_2}{m_1 + m_2}. \tag{2.4}$$

According to the conservation laws, the velocities (momenta) of the particles in CMS after collision are unchanged in magnitude and oppositely directed. The result of an elastic collision of particles in CMS is rotation of the direction of all the velocities by the same angle θ (Figure 2), which is called the scattering angle in CMS.

The result of any interaction of particles is determined by the energy of their relative motion in CMS, which is equal to

$$T_c = \frac{m_2}{m_1 + m_2} T = \frac{1}{2} \mu v^2. \tag{2.5}$$

According to (2.5), for example, in the scattering of alpha-particles by gold the collision energy in CMS amounts to 98% of the collision energy in LS, and in the scattering by Li^6 atoms to 60% only.

The relation between the scattering angles in LS and CMS can be derived from Figure 2. It is seen that $\vec{v}_1$ and $\vec{v}_2$ are the vector sums of the velocities of the corresponding particles in CMS (after the collision) and of the velocity of the center of mass in LS.

The scattering angles in CMS and LS are related in the following manner:

$$\operatorname{tg}\vartheta_1 = \frac{(v-v_C)\sin\Theta}{v_C+(v-v_C)\cos\Theta} = \frac{\sin\Theta}{k+\cos\Theta}, \tag{2.6}$$

$$\vartheta_2 = \frac{1}{2}(\pi-\Theta), \tag{2.7}$$

$$\sin(\Theta-\vartheta_1) = k\sin\vartheta_1; \tag{2.8}$$

where

$$k = \frac{m_1}{m_2}.$$

The following general conclusions can be drawn from the above expressions.

When $k<1$, or $m_1<m_2$, the angle ϑ_1 increases continuously from 0 to π as Θ increases from 0 to π. Here $\vartheta_1 > \frac{\Theta}{2}$, and $(\vartheta_1+\vartheta_2) > \frac{\pi}{2}$. In the limiting case of $m_1 \ll m_2$, $\vartheta_1 \approx \Theta$ and $\vartheta_1+\vartheta_2 \approx \frac{\pi+\Theta}{2}$.

For collisions between identical particles $(k=1)$

$$\vartheta_1 = \frac{\Theta}{2} \text{ and } \vartheta_1+\vartheta_2 = \frac{\pi}{2},$$

i.e., the angle of divergence of the particles after the collision in LS is equal to $\frac{\pi}{2}$ and no back scattering occurs. If Θ varies from 0 to π, then ϑ_1 also varies from 0 to $\frac{\pi}{2}$.

For $m_1 > m_2 (k>1)$

$$\vartheta_1 < \frac{\Theta}{2} < \frac{\pi}{2} \text{ and } \vartheta_1+\vartheta_2 < \frac{\pi}{2}.$$

In this case, the angle ϑ_1 increases from 0 to the maximum value of $\arcsin\left(\frac{1}{k}\right) < \frac{\pi}{2}$ as Θ increases from 0 to $\arccos\left(-\frac{1}{k}\right)$; with a further increase in Θ, ϑ_1 decreases reaching zero for $\Theta=\pi$.

The magnitudes of v_1 and v_2 in LS are related to the scattering angle Θ in the following way:

$$\left.\begin{aligned} v_1 &= \frac{\sqrt{m_1^2+m_2^2+2m_1m_2\cos\Theta}}{m_1+m_2}v \\ v_2 &= \frac{2m_1}{m_1+m_2}v\sin\frac{\Theta}{2} \end{aligned}\right\}. \tag{2.9}$$

The second of expressions (2.2), giving the energy transferred in the collision, can be written, according to (2.3) and (2.7), in the form

$$Q = Q_{max}\sin^2\frac{\Theta}{2}. \tag{2.10}$$

Expression (2.10) can also be applied in the relativistic case, if the appropriate value of Q_{max} is used (see below).

The kinematic relations given here and in the following part of this section are based on the application of the conservation laws. No assumptions are made concerning the nature of the deflection forces acting on the particles in the collision. However, to determine the scattering angle in a single event or the distribution of particles over the scattering angles, it is necessary to solve the equations of motion of the particles using the actual law of interaction.

Kinematics of elastic collisions of relativistic particles. The scattering of a relativistic particle with a rest mass m_1 and an energy $E=T+m_1c^2$ on a stationary particle with a rest mass m_2 is given by the following kinematic relations /13, 65/:

$$\left.\begin{aligned} E_1 &= E - \frac{m_2\left(E^2 - m_1^2 c^4\right)}{m_1c^2+m_2c^2+2m_2E}(1-\cos\Theta) \\ E_2 &= m_2c^2 + \frac{m_2\left(E^2 - m_1^2 c^4\right)}{m_1^2 c^2 + m_2^2 c^2 + 2m_2 E}(1-\cos\Theta) \end{aligned}\right\}, \tag{2.11}$$

whence

$$\left.\begin{aligned} T_{2max} &= Q_{max} = \frac{2m_2\left(E^2 - m_1^2 c^4\right)}{\left(m_1^2 + m_2^2\right)c^2 + 2m_2E} \\ \frac{T_{1min}}{T} &= \frac{(m_1 - m_2)^2}{m_1^2 + m_2^2 + \frac{2}{c^2}m_2E} \end{aligned}\right\}. \tag{2.12}$$

E_1 and E_2 are the total energies (including the rest mass) of the particles after the collision in LS; Θ is the scattering angle in CMS.

According to (2.12), a fast relativistic particle may transfer a considerable fraction of its initial energy to the particle it collides with both when $m_1 \gg m_2$, and when $m_1 \ll m_2$ (it follows from the preceding formulas of non-relativistic mechanics that for these mass ratios in the non-relativistic case the incident particle transfers a negligible fraction of the initial energy). For $m_1 \gg m_2$ it is necessary that

$$E \gtrsim \frac{m_1^2}{m_2}c^2,$$

and for $m_1 \ll m_2$

$$E \gg m_2c^2.$$

The deflection angles of the particles after the collision in LS are given by the expressions

$$\left.\begin{aligned} \cos\vartheta_1 &= \frac{E_1\left(E+m_2c^2\right) - Em_2c^2 - m_1^2c^4}{pp_1c^2} \\ \cos\vartheta_2 &= \frac{\left(E+m_2c^2\right)\left(E_2 - m_2c^2\right)}{pp_2c^2} \end{aligned}\right\}, \tag{2.13}$$

where p is the momentum of the incident particle, p_1 and p_2 are the momenta of the particles after the collision in LS. Then

$$\vec{p} = \frac{m\vec{v}}{\sqrt{1-\beta^2}}, \tag{2.14}$$

and

$$\beta = \frac{v}{c} \tag{214}$$

$$\frac{E}{c^2} = p^2 + m^2 c^4 = \frac{m}{\sqrt{1-\beta^2}}. \tag{2.15}$$

As in the non-relativistic case, for $m_1 > m_2$ the scattering angle of the incident particle cannot exceed

$$\vartheta_{1\max} = \arcsin \frac{m_2}{m_1}.$$

If the parameter $Q \equiv T_2$ (the energy transferred in the collision) is applied, then the deflection angles in LS satisfy the relations

$$\left.\begin{aligned} \cos\vartheta_1 &= \frac{E^2 - m_1^2 c^4 - Q(E + m_2 c^2)}{\sqrt{(E^2 - m_1^2 c^4)\left[(E-Q)^2 - m_1^2 c^4\right]}} \\ \cos\vartheta_2 &= \frac{Q(E + m_2 c^2)}{\sqrt{(E^2 - m_1^2 c^4)\left[(m_2 c^2 + Q^2) - m_2^2 c^4\right]}} \end{aligned}\right\}. \tag{2.16}$$

When the masses of the colliding particles are equal ($m_1 = m_2 = m$) we have

$$\left.\begin{aligned} \operatorname{tg}\vartheta_1 &= \sqrt{\frac{2mc^2}{E+mc^2}\,\frac{Q}{E-Q-mc^2}} \\ \operatorname{tg}\vartheta_2 &= \sqrt{\frac{2mc^2}{E+mc^2}\,\frac{E-Q-mc^2}{Q}} \end{aligned}\right\} \tag{2.17}$$

and

$$\operatorname{tg}\frac{\theta}{2} = \sqrt{\frac{Q}{E-Q-mc^2}}. \tag{2.18}$$

Motion in a central Coulomb field. The resolution of the motion of a system of two particles into the motion of the center of mass and motion relative to the center of mass simplifies the two-body problem to the problem of motion of a single particle with a mass μ (reduced mass) in a potential field $U(r)$, which is symmetric with respect to a stationary center of force. A field in which the potential energy depends only on the distance to some fixed point is called central. For example, the description of colliding particles with charges $Z_1 e$ and $Z_2 e$, whose interaction obeys Coulomb's law reduces to the solution of the motion of a particle with a mass μ in a central force field with the potential

$$U(r) = \frac{Z_1 Z_2 e^2}{r}. \tag{2.19}$$

The corresponding calculations (e.g., /62/) show that the trajectory of such a particle is a hyperbola whose focus is at the center of mass. It is symmetric with respect to the straight line connecting the center of mass C with the point on the trajectory nearest to it (Figure 3). The angle φ_0 between this line and the asymptotes to the trajectory can be determined from the laws of conservation of energy and angular momentum in polar coordinates (r, φ):

$$\varphi_0 = \int_{r_{\min}}^{\infty} \frac{\rho\,\frac{dr}{r^2}}{\left(1 - \rho^2/r^2 - \frac{U}{T_c}\right)^{1/2}},$$

where ρ is the impact parameter, i.e., the distance from the center which the particle would reach in the absence of the force field;

r_{min} is the minimum distance of the particle from the center of mass;

T_c is the energy of the relative motion of the particles in CMS given by expression (2.5).

From Figure 3 the angles φ_0 and θ are related by

$$\theta = |\pi - 2\varphi_0|. \tag{2.20}$$

Integration of the expression for φ_0 using (2.19) and (2.20) leads to an expression connecting the scattering angle θ with the impact parameter ρ*

$$\operatorname{tg}\frac{\theta}{2} = \frac{Z_1 Z_2 e^2}{\mu \rho v^2} = \frac{b}{2\rho}. \tag{2.21}$$

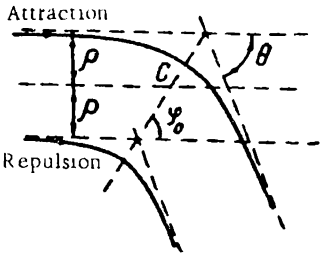

FIGURE 3. Trajectory of a particle in a central force field

Here b is the distance of closest approach of the particles in a head-on collision $(\rho = 0)$,

$$b = \frac{Z_1 Z_2 e^2}{T_c} = \frac{Z_1 Z_2 e^2}{(\frac{1}{2}\mu v^2)}. \tag{2.22}$$

Cross section for particle scattering in a Coulomb field. Suppose a beam of particles with uniform velocity $\vec{v}$ falls on a scattering center. If N is the number of particles passing in one second through 1 cm^2 cross section of the beam, then the number of particles in the beam, having an impact parameter from ρ to $(\rho + d\rho)$, will be

$$dN = N 2\pi \rho d\rho.$$

The ratio

$$\frac{dN}{N} = 2\pi \rho d\rho$$

is (see § 1) the differential cross section for collision with an impact parameter ρ.

Since a single-valued relation exists between the impact parameter and the scattering angle (see formula (2.21), we may introduce the concept of

* This formula is only valid for non-relativistic particles. For relativistic velocities and small scattering angles we have

$$\theta = \frac{\Delta p}{p} = \frac{2 Z_1 Z_2 e^2}{v p \rho}, \tag{2.21a}$$

where p is the momentum of the incident particle, and ρ is confined to distances at which the field is a pure Coulomb field.

differential cross section for scattering at an anlge Θ

$$d\sigma(\Theta) = 2\pi p(\Theta)\left|\frac{dp}{d\Theta}\right| d\Theta$$

or, expressing the cross section in terms of a solid-angle element $d\Omega = 2\pi \sin\Theta d\Theta$, we have

$$d\sigma(\Theta) = \frac{p\Theta}{\sin\Theta}\left|\frac{dp}{d\Theta}\right| d\Omega.$$

Applying (2.21) and simplifying, we obtain an expression for the scattering cross section in a Coulomb field

$$d\sigma = \frac{\pi b^2}{4}\cos\frac{\Theta}{2}\operatorname{cosec}^3\frac{\Theta}{2}d\Theta \qquad (2.23)$$

or

$$\sigma(\Theta) = \frac{d\sigma}{d\Omega} = \frac{b^2}{16}\operatorname{cosec}^4\frac{\Theta}{2} = \frac{Z_1^2 Z_2^2 e^4}{16T_c^2}\operatorname{cosec}^4\frac{\Theta}{2}. \qquad (2.24)$$

For $\Theta > \frac{\pi}{2}$, the impact parameter $p < \frac{b}{2}$ and the cross section for back scattering is equal to $\frac{\pi b^2}{4}$. Therefore b is sometimes referred to as the impact diameter.

Formula (2.24) is known as the Rutherford formula. A form convenient for practical calculations is

$$\sigma_R(\Theta) = \frac{1{,}295 Z_1^2 Z_2^2}{T_c^2\ (\text{Mev})}\operatorname{cosec}^4\frac{\Theta}{2}\ \text{mbarn/sterad}. \qquad (2.24a)$$

The relative magnitudes of the Rutherford scattering cross sections showing the variation of cross section with the angle are given in Table 1 (for $\frac{b}{a} = 0$).

The integral cross section for scattering at an angle exceeding Θ_0 is given by

$$\sigma_{R\Theta} = \int_{\Theta_0}^{\pi} d\sigma_R = \frac{16{,}2 Z_1^2 Z_2^2}{T_c^2\ (\text{Mev})}\operatorname{ctg}^2\frac{\Theta_0}{2}\ \text{mbarn} \qquad (2.25)$$

Thus the integral cross section for the scattering of 5 Mev protons by carbor at angles exceeding 10^0 (CMS) is equal to $\sim$3 barn ($3\cdot10^{-24}$ cm^2), and 527 barn for scattering by gold. The corresponding probabilities for proton scattering at angles greater than 10^0 on passing 10 μ in graphite and in gold* are $4\cdot10^{-4}$ and $4.3\cdot10^{-3}$, respectively.

If the mass m_1 of the incident particle is much smaller than the mass m_2 of the stationary scattering particle, then $\Theta \approx \vartheta_1$ and $T_c \approx T$ (the energy of the incident particle in LS). In this case, when calculating the scattering cross sections from (2.24) the values of ϑ_1 and T can be used instead of Θ and T_c.

In the general case, scattering in LS is represented by the formula**

$$\sigma(\vartheta_1) = \frac{d\sigma}{d\omega_1} = \frac{Z_1^2 Z_2^2 e^4}{4T^2} \times \frac{1}{\sin^4\vartheta_1} \frac{\left[\cos\vartheta_1 \pm \sqrt{1-\left(\frac{m_1}{m_2}\right)^2\sin^2\vartheta_1}\right]^2}{\pm\sqrt{1-\left(\frac{m_1}{m_2}\right)^2\sin^2\vartheta_1}}, \qquad (2.26)$$

* The mean range of 5 Mev protons in graphite is 180 microns, and in gold 61 microns (see § 4).

** This formula is sometimes referred to as Darwin's formula.

where $d\omega_1 = 2\pi \sin\vartheta_1 d\vartheta_1$ is the element of solid angle in LS.

For $m_1 < m_2$, the positive sign of the square root in (2.26) should be taken. If $m_1 > m_2$, the calculation for a given angle ϑ_1 has to be performed for both the plus and the minus sign of the square root, and the results added. When the masses of the scattered and scattering particles are equal ($m_1 = m_2$)

$$\sigma(\vartheta_1) = \frac{Z_1^2 Z_2^2 e^4}{T^2} \frac{\cos\vartheta_1}{\sin^4\vartheta_1}. \tag{2.27}$$

If the scattered and the scattering particles are moreover identical, the quantum-mechanical exchange effect has to be taken into account. Then the scattering cross section in LS is determined by Mott's formula (see, for example, /71/:

$$\sigma(\vartheta) = \frac{d\sigma}{d\omega} = \frac{Z^2 e^4 \cos\vartheta}{T^2}\left\{\frac{1}{\sin^4\vartheta} + \frac{1}{\cos^4\vartheta} + \right.$$
$$\left. + \begin{matrix} +2 \\ -1 \end{matrix}\left[\frac{1}{\sin^2\vartheta\cos^2\vartheta}\cos\frac{2\pi Z^2 e^2}{h v}\ln\operatorname{tg}^2\vartheta\right]\right., \tag{2.28}$$

where h is Planck's constant;

$\vartheta = \frac{\Theta}{2}$ is the scattering angle in LS. +2 is put in front of the square brackets if the particles have zero spin, and −1 if their spin is 1/2.

The cross section for the scattering particles (the "recoil cross section") in LS can be easily obtained from (2.23) and (2.7):

$$\sigma(\vartheta_2) = \frac{d\sigma}{d\omega_2} = \frac{Z_1^2 Z_2^2 e^4}{4T^4} \frac{1}{\cos^3\vartheta_2}, \tag{2.29}$$

$$(d\omega_2 = 2\pi \sin\vartheta_2 d\vartheta_2).$$

In the following the relations between the scattering cross sections in LS and CMS, which are necessary for practical calculations, will be given.

The number of particles scattered in an infinitesimal solid angle $d\Omega$ in the direction Θ is equal to the number of particles scattered in the solid angle $d\omega$ in the direction ϑ:

$$\sigma(\Theta)\, d\Omega = \sigma(\vartheta)\, d\omega \tag{2.30}$$

or

$$\sigma(\Theta) = \sigma(\vartheta)\left(\frac{\sin\vartheta}{\sin\Theta}\right)\frac{d\vartheta}{d\Theta}.$$

Using expression (2.8), we have

$$\sigma(\Theta) = \sigma(\vartheta_1)\left(\frac{\sin\vartheta_1}{\sin\Theta}\right)^2 \cos(\Theta - \vartheta_1).$$

Similarly, from expressions (2.30) and (2.7) we obtain

$$\sigma(\Theta) = \sigma(\vartheta_2)\left(\frac{\sin\vartheta_2}{\sin\Theta}\right)\frac{d\vartheta_2}{d\Theta}. \tag{2.31}$$

When the masses of the scattered and the scattering particles are equal,

$$\sigma(\Theta) = \frac{\sigma(\vartheta_1)}{4\cos\vartheta_1}.$$

TABLE 1

Calculated values of the distances of closest approach r_{min}, of the impact parameters ρ, and of the differential cross sections σ_{scr} for scattering in a potential field (2.34) for different screening lengths a. According to Everhardt /236/

$\frac{\Theta}{\pi}$	$\frac{b}{a}=0$ ($a=\infty$)			$\frac{b}{a}=0.1$			$\frac{b}{a}=0.2$			$\frac{b}{a}=0.5$		
	$\frac{r_{min}}{b}$	$\frac{\rho}{b}$	$\frac{\sigma_R(\Theta)}{b^2}$	$\frac{r_{min}}{b}$	$\frac{\rho}{b}$	$\frac{\sigma_{scr}(\Theta)}{b^2}$	$\frac{r_{min}}{b}$	$\frac{\rho}{b}$	$\frac{\sigma_{scr}(\Theta)}{b^2}$	$\frac{r_{min}}{b}$	$\frac{\rho}{b}$	$\frac{\sigma_{scr}(\Theta)}{b^2}$
0.01	32.3	31,8	$1.03\cdot10^{6}$	14.3	14.2	$1.02\cdot10^{5}$	9,59	9.51	$3.6\cdot10^{4}$	5.26	5.22	$8.1\cdot10^{3}$
0.02	16.4	15,9	$6.42\cdot10^{4}$	9.85	9.65	$1.47\cdot10^{4}$	7.11	6.99	$6.3\cdot10^{3}$	4.16	4.10	$1.70\cdot10^{3}$
0.03	11.1	10.6	$1.27\cdot10^{4}$	7.63	7.36	$4.27\cdot10^{3}$	5.77	5.62	$2.01\cdot10^{3}$	3.56	3.48	$6.1\cdot10^{2}$
0.04	8.46	7.95	$4.02\cdot10^{3}$	6.28	6.00	$1.71\cdot10^{3}$	4.94	4.75	$8.8\cdot10^{2}$	3.14	3.04	$2.91\cdot10^{2}$
0.06	5.81	5.29	$7.97\cdot10^{2}$	4.69	4.37	$4.45\cdot10^{2}$	3.87	3.63	$2.62\cdot10^{2}$	2.60	2.46	$9.8\cdot10^{1}$
0.08	4.49	3.96	$2.53\cdot10^{2}$	3.78	3.42	$1.62\cdot10^{2}$	3.19	2.92	$1.06\cdot10^{2}$	2.22	2.06	$4.32\cdot10^{1}$
0.10	3.70	3.16	$1.04\cdot10^{2}$	3,19	2.81	$7.4\cdot10^{1}$	2.74	2.44	$5.1\cdot10^{1}$	1.99	1.80	$2.26\cdot10^{1}$
0.15	2.64	2.08	$2.11\cdot10^{1}$	2.35	1.91	$1.67\cdot10^{1}$	2.09	1.73	$1.29\cdot10^{1}$	1,59	1.35	$6.5\cdot10^{0}$
0.20	2.12	1.54	$6.85\cdot10^{0}$	1.90	1.43	$5.7\cdot10^{0}$	1.73	1.32	$4.65\cdot10^{0}$	1.35	1.07	$2.57\ 10^{0}$
0.30	1.60	0.981	$1.47\cdot10^{0}$	1.45	0.924	$1.28\cdot10^{0}$	1.34	0.865	$1.09\cdot10^{0}$	1.08	0.729	$6.9\cdot10^{-1}$
0.40	11.35	0.688	$5.23\cdot10^{-1}$	1.24	0.651	$4.64\cdot10^{-1}$	1.13	0.615	$4.06\cdot10^{-1}$	0.931	0.529	$2.78\cdot10^{-1}$
0.50	1.21	0.500	$2.50\cdot10^{-1}$	1.10	0.474	$2.23\cdot10^{-1}$	1.02	0.450	$1.99\cdot10^{-1}$	0.839	0.391	$1.43\cdot10^{-1}$
0.75	1.04	0.207	$8.57\cdot10^{-2}$	0.961	0.197	$7.7\cdot10^{-2}$	0.878	0.187	$7.0\cdot10^{-2}$	0.738	0.166	$5.4\cdot10^{-2}$
1.00	1.00	0	$6.25\cdot10^{-2}$	0.913	0	$5.65\cdot10^{-2}$	0.845	0	$5.14\cdot10^{-2}$	0.703	0	$4.01\cdot10^{-2}$

TABLE 1 (continued)

$\frac{\Theta}{\pi}$	$\frac{b}{a}=1$			$\frac{b}{a}=2$			$\frac{b}{a}=5$			$\frac{b}{a}=10$		
	$\frac{r_{min}}{b}$	$\frac{\rho}{b}$	$\frac{\sigma_{scr}(\Theta)}{b^2}$	$\frac{r_{min}}{b}$	$\frac{\rho}{b}$	$\frac{\sigma_{scr}(\Theta)}{b^2}$	$\frac{r_{min}}{b}$	$\frac{\rho}{b}$	$\frac{\sigma_{scr}(\Theta)}{b^2}$	$\frac{r_{min}}{b}$	$\frac{\rho}{b}$	$\frac{\sigma_{scr}(\Theta)}{b^2}$
0.01	3.22	3.20	$2.80\cdot10^{3}$	1.91	1.90	$8.5\cdot10^{2}$	0.919	0.914	$1.66\cdot10^{2}$	0.523	0.520	$4.75\cdot10^{1}$
0.02	2.63	2.59	$5.7\cdot10^{2}$	1.61	1.59	$1.86\cdot10^{2}$	0.798	0.789	$3.63\cdot10^{1}$	0.460	0.455	$1.06\cdot10^{1}$
0.03	2.30	2.25	$2.15\cdot10^{2}$	1.43	1.40	$7.2\cdot10^{1}$	0.727	0.715	$1.50\cdot10^{1}$	0.425	0.418	$4.36\cdot10^{0}$
0.04	2.08	2.02	$1.06\cdot10^{2}$	1.31	1.28	$3.61\cdot10^{1}$	0.679	0.662	$7.8\cdot10^{0}$	0.398	0.389	$2.31\cdot10^{0}$
0.06	1.78	1.70	$3.82\cdot10^{1}$	1.15	1.10	$1.31\cdot10^{1}$	0.610	0.587	$3.13\cdot10^{0}$	0.363	0.350	$9.5\cdot10^{-1}$
0.08	1.58	1.47	$1.81\cdot10^{1}$	1.04	0.975	$6.6\cdot10^{0}$	0.561	0.531	$1.64\cdot10^{0}$	0.338	0.321	$5.1\cdot10^{-1}$
0.10	1.41	1.29	$9.8\cdot10^{0}$	0.957	0.880	$3.76\cdot10^{0}$	0.525	0.487	$9.7\cdot10^{-1}$	0.319	0.299	$3.15\cdot10^{-1}$
0.15	1.16	1.00	$3.13\cdot10^{0}$	0.817	0.712	$1.34\cdot10^{0}$	0.465	0.411	$3.80\cdot10^{-1}$	0.284	0.254	$1.28\cdot10^{-1}$
0.20	1.03	0.828	$1.37\cdot10^{0}$	0.723	0.595	$6.3\cdot10^{-1}$	0.420	0.352	$1.90\cdot10^{-1}$	0.263	0.222	$6.8\cdot10^{-2}$
0.30	0.844	0.588	$4.25\cdot10^{-1}$	0.610	0.438	$2.14\cdot10^{-1}$	0.360	0.267	$7.1\cdot10^{-2}$	0.230	0.173	$2.74\cdot10^{-2}$
0.40	0.736	0.435	$1.83\cdot10^{-1}$	0.592	0.332	$1.00\cdot10^{-1}$	0.329	0.209	$3.58\cdot10^{-2}$	0.211	0.138	$1.48\cdot10^{-2}$
0.50	0.671	0.326	$9.8\cdot10^{-2}$	0.497	0.252	$5.6\cdot10^{-2}$	0.305	0.162	$2.17\cdot10^{-2}$	0.198	0.109	$9.2\cdot10^{-3}$
0.75	0.593	0.140	$3.84\cdot10^{-2}$	0.440	0.110	$2.36\cdot10^{-2}$	0.273	0.073	$1.02\cdot10^{-2}$	0.180	0.050	$4.74\cdot10^{-3}$
1.00	0.967	0	$2.90\cdot10^{-2}$	0.426	0	$1.83\cdot10^{-2}$	0.265	0	$3.14\cdot10^{-3}$	0.175	0	$3.84\cdot10^{-3}$

The relations between the scattering cross sections of relativistic particles in LS and CMS are:

$$\left.\begin{aligned} \sigma(\vartheta_1) &= \sigma(\Theta)\,\frac{\left[\sin^2\Theta+\gamma^2(k+\cos\Theta)^2\right]^{3/2}}{\gamma(1+k\cos\Theta)} \\ \sigma(\vartheta_2) &= \sigma(\Theta)\,\frac{4(1-\beta^2)\cos\vartheta_2}{(1-\beta^2\cos^2\vartheta_2)^2} \end{aligned}\right\}, \tag{2.32}$$

$$\sigma(\Theta) = \sigma(\vartheta_1)\,\frac{\gamma(1+k\cos\Theta)\sin^3\vartheta_1}{\sin^3\Theta}. \tag{2.33}$$

where $\gamma = (1-\beta^2)^{-1/2}$ and $k = \frac{m_1}{m_2}$.

Scattering cross section in a screened Coulomb field. If we neglect the exchange effect and the relativistic corrections, the results of the quantum-mechanical calculations of the scattering cross sections in a pure Coulomb field are the same as the preceding results calculated by the methods of classical mechanics (see, for example, /64, 71/). However, rigorously we have to take into consideration that the colliding particles are complex systems, consisting of nuclei of finite dimensions screened by electrons. In investigating the scattering of heavy charged particles of between 10^3 and 10^7 ev, particularly for small-angle scattering, the deviation from a pure Coulomb field due to the electron screening of the nuclei has first to be taken into account.

Usually, in screening problems the atom is replaced by a spherically-symmetric force field which coincides with the nuclear Coulomb field at small (atomic) distances and which falls off at large distances faster than the Coulomb field.

The interaction potential in a screened Coulomb field can be represented, for example, by the expression

$$U_{scr}(r) = \frac{Z_1 Z_2 e^2}{r}\exp\left(-\frac{r}{a}\right), \tag{2.34}$$

where a is the screening length, which for nuclear (atomic) collisions has the form /12/

$$a = a_0\left(Z_1^{1/2} + Z_2^{1/2}\right)^{-\frac{1}{2}}; \tag{2.35}$$

Z_1 and Z_2 are the atomic numbers of the colliding particles;

a_0 is the Bohr radius of the hydrogen atom ($0.53\cdot10^{-8}$ cm).

The classical calculations of scattering cross sections are only applicable when the following two conditions are fulfilled /12, 71/:

1) the de Broglie wavelength $\lambda = \frac{\hbar}{mv}$ of the incident particles is smaller than the characteristic dimensions of the region in which the scattering field varies appreciably;

2) the product of the increment of the particle momentum in scattering and of the characteristic dimension of the region of scattering satisfies Heisenberg's uncertainty relation.

In the case of zero screening ($a = \infty$), it is convenient to take $\frac{b}{2}$ as the characteristic dimension; this is half the distance of closest approach in a head-on collision (see (2.22)). Then both requirements lead to the same condition

$$\alpha = \frac{\pi b}{\lambda} = \frac{2\pi Z_1 Z_2 e^2}{\hbar v} = \frac{Z_1 Z_2}{137\beta} \gg 1 \tag{2.36}$$

or

$$v \ll Z_1 Z_2 u_0, \tag{2.36a}$$

where v is the velocity of the incident particle;

$u_0 = \frac{e^2 2\pi}{h} = 2.2\ 10^8$ cm/sec is the orbital velocity of the electron in the hydrogen atom. In this case, the scattering is given by the Rutherford formula for all scattering angles.

If the screening cannot be neglected but is nevertheless weak, i.e., if

$$\xi = \frac{b}{2a} \ll 1, \tag{2.37}$$

then the scattering is given by the Rutherford formula for all angles larger than a certain minimum angle

$$\theta_a^* \cong \frac{b}{2a}. \tag{2.38}$$

The value of this angle is determined by substituting the screening length a for the impact parameter ρ in (2.21).

For $\theta < \theta_a$, the elastic nuclear collision cross section is smaller than that obtaining from the Rutherford formula. In other words, the screening is exhibited by a decrease in the scattering probability at small angles. In certain cases (see below), the scattering probability at angles $\theta < \theta_a^*$ is assumed equal to zero and the energy losses through collisions in which the incident particle is deflected by an angle $\theta < \theta_a^*$ are neglected.

Using (2.22) and (2.35), the screening parameter may be expressed in terms of the constants of the colliding particles

$$\xi = Z_1 Z_2 (Z_1^{1/3} + Z_2^{1/3})^{1/2} \left(\frac{m_1 + m_2}{m_2}\right) \frac{1}{T(\mathrm{Ry})}. \tag{2.37a}$$

The energy loss of the incident particle in elastic scattering at an angle $\theta = \theta_a^*$ is, according to expressions (2.3), (2.7) and (2.37a),

$$Q_a^* = \frac{m_1}{m_2} (Z_1^{2/3} + Z_2^{1/3})\ Z_1 Z_2 \frac{\mathrm{Ry}}{T(\mathrm{Ry})}. \tag{2.38a}$$

Here $T(\mathrm{Ry})$ is the energy of the incident particle in LS, expressed in Rydbergs: $1\mathrm{Ry} = \frac{e^2}{2a_0} = 13.6$ ev.

Classical mechanics can also be applied for strong screening ($\xi > 1$), but here, in addition to (2.36), the following condition must be satisfied

$$\frac{\lambda}{2\pi a} << 1 \tag{2.39}$$

or

$$\alpha >> \xi = \frac{b}{2a}. \tag{2.39a}$$

By virtue of Heisenberg's uncertainty relation, classical mechanics only applies to scattering at angles exceeding

$$\theta_{\min} \approx \frac{\lambda}{2\pi a} = \frac{\xi}{a}$$

Table 1 gives the distances of closest approach $r_{\min}$, the impact parameter ρ, and the differential cross sections σ_{scr} for scattering in a potential

field (2.34), calculated by classical methods /236/. The case $\frac{b}{a} = 0$ corresponds to scattering in a pure Coulomb field (Rutherford scattering).

Following /236/, we now consider the scattering of neon ions with an energy of = 100 kev by argon atoms. In this case $\mu = 13.36$ and $T_c = 67$ kev. The reduced de Broglie wavelength $\frac{\lambda}{2\pi} = 3.32 \cdot 10^{-13}$, the screening length $a = 1.56 \cdot 10^{-9}$ cm, and the impact diameter $b = 3.40 \cdot 10^{-10}$ cm will be used. The condition for the validity of the concept of classical orbits (2.36) is satisfied ($\alpha = 588$); this is a case of moderate screening ($\frac{b}{a} = 0.25$). From Table 1 we see that for $\frac{b}{a} = 0.250$ the absolute values of the scattering cross sections for fairly large angles should be smaller than the scattering cross sections in a pure Coulomb field. This is confirmed by experimental results. The points in Figure 4 give the measured differential cross sections for the scattering of neon ions with energies of 25, 50, and 100 kev

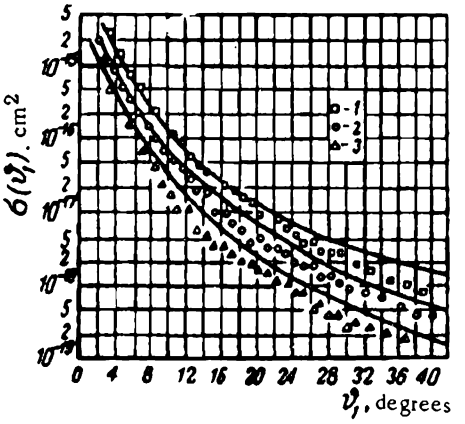

FIGURE 4. Experimental cross sections for the scattering of neon ions by argon atoms /247/:

1 — $T = 25$ kev ($b/a = 1.0$); 2 — $T = 50$ kev ($b/a = 0.5$); 3 — $T = 100$ kcv ($b/a = 0.25$). The curves are calculated according to /236/.

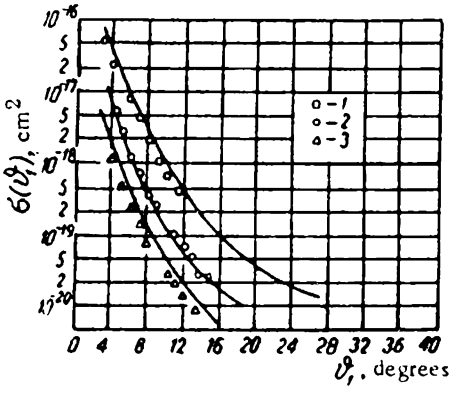

FIGURE 5. Experimental scattering cross sections of helium ions by helium:

1 — $T = 25$ kev ($b/a = 0.016$); 2 — $T = 50$ kev ($b/a = 0.0078$); 3 — $T = 100$ kev ($b/a = 0.0039$). The curves were calculated from the Rutherford formula (2.27).

by argon /247/. The solid lines in this figure were calculated (Table 1) for the corresponding values of $\frac{b}{a}$. A satisfactory agreement between the experimental and calculated data for scattering at relatively small angles ($\vartheta_1 < 20°$) is obtained. For large scattering angles, the experimental cross sections are smaller than the theoretical ones (taking screening into account), which in the authors' opinion is connected with the nonelastic character of the collisions (multiple ionization, charge exchange, see § 7) and with the poor choice of the screening field potential.

For $\frac{b}{a} \approx 1$ (see, for example, Figure 4), a small difference was observed between the theoretical and the experimental cross sections in the entire range of angles investigated (4 — 40°). However, for very small

values of the parameter $\frac{b}{a}$, the scattering, as was also to be expected, was practically identical to the Rutherford scattering. This is illustrated by Figure 5 /247/, which gives the experimental cross sections for the scattering of He^+ ions by helium for energies of 25 kev $\left(\frac{b}{a}=0.016\right)$, 50 kev $\left(\frac{b}{a}=0.0078\right)$, and 100 kev $\left(\frac{b}{a}=0.0039\right)$. The solid curves were calculated from formula (2.27).

O. B. Firsov has shown /114/ that for interatomic distances of $<10^{-8}$ cm, the atomic interaction is better represented by the potential

$$V(r)=\frac{Z_1 Z_2 e^2}{r}\chi\left[\left(Z_1^{1/2}+Z_2^{1/2}\right)^{2/3}\frac{r}{a_{TF}}\right], \tag{2.40}$$

where χ is the Thomas-Fermi screening function (its values are tabulated, e.g., in /35, 62/);

$a_{TF}=0.885\cdot a_0=4.68\cdot 10^{-9}$ cm is the characteristic dimension of the atom in the Thomas-Fermi (TF) model.

Using the potential (2.40), Firsov calculated the impact parameters and differential scattering cross sections in atomic collisions /112, 113/. The results are given as functions of the dimensionless energy and impact parameters, which are defined as follows:

$$\varepsilon=\frac{T_C\, a_{TF}}{Z_1 Z_2\left(Z_1^{1/2}+Z_2^{1/2}\right)^{2/3}e^2}=\frac{T_C\ (\text{ev})}{Z_1 Z_2\left(Z_1^{1/2}+Z_2^{1/2}\right)^{2/3}\cdot 30.4},$$

$$\rho'=\frac{\left(Z_1^{1/2}+Z_2^{1/2}\right)^{2/3}\rho}{a_{TF}}=\frac{\left(Z_1^{1/2}+Z_2^{1/2}\right)^{2/3}\rho\ (\text{cm})}{4.68\cdot 10^{-9}}.$$

where T_C is the collision energy in CMS;

ρ is the impact parameter.

Table 2 gives the dependence of the reduced impact parameter on Θ (the scattering angle in CMS) and on ε (the reduced energy). For the calculation of the scattering cross sections the data of Table 2 should be used and the known relations (see above):

$$\left.\begin{aligned}\sigma(\Theta)&=\frac{\rho d\rho}{\sin\Theta d\Theta}=\frac{a_{TF}^2}{\left(Z_1^{1/2}+Z_2^{1/2}\right)^{4/3}}\frac{\rho' d\rho'}{\sin\Theta d\Theta}\\ \sigma^*&=2\pi\int_0^{\infty}(1-\cos\Theta)\rho d\rho=\pi\frac{a_{TF}^2}{\left(Z_1^{1/2}+Z_2^{1/2}\right)^{4/3}}\int_0^{\pi}\rho'\sin\Theta d\Theta\end{aligned}\right\}. \tag{2.41}$$

For $\varepsilon\geqslant 0.02$, a good approximation is

$$\sigma^*=\frac{\pi Z_1^2 Z_2^2 e^4}{T_C^2}\ln\left[1+\frac{0.62\ T_C\left(\frac{h}{2\pi}\right)^2}{me^4 Z_1 Z_2\left(Z_1^{1/2}+Z_2^{1/2}\right)^{2/3}}\right].$$

The data of Tables 1 and 2 are applicable for experiments on collisions of heavy atoms in the range of 1—100 kev, for investigations on the penetration depth of ions in solid targets, etc. These data can also be used for the description of inelastic collisions, if only the inelastic energy losses are small as compared with the collision energy. In this case, the kinematics of inelastic processes are essentially similar to those of elastic collisions.

An analysis of experimental data on the scattering cross sections of heavy ions with energies of tens of kev /55, 56, 220, 247/ shows /112/ that calculations based on the Thomas-Fermi screening function (Table 2) are in better agreement with the experimental data than those using an exponential screening function (Table 1). Potential (2.34) is quite different

TABLE 2

Calculated values of ρ' for scattering in a potential field (2.40), according to Firsov /112, 113/

ε \ θ	0.3	0.5	0.7	1	1.5	2	2.5	$2.5 < \theta < \pi$
0.02	8.8	6.7	5.6	4.2	2.8	1.8	1.0	—
0.03	7.4	5.8	4.6	3.5	2.3	1.5	0.8	1.3 $(\pi-\theta)$
0.05	6.0	4.6	3.8	2.9	1.9	1.2	0.65	1.0 $(\pi-\theta)$
$0.05<\varepsilon<1$	$\rho' \approx (\pi-\theta)\left[\frac{0.45}{(2\pi-\theta)\,\theta\varepsilon}\right]^{\frac{1}{2}}$							
1	1.45	1.00	0.76	0.55	0.34	0.21	0.11	0.18 $(\pi-\theta)$
1.5	1.10	0.78	0.58	0.41	0.25	0.15	0.08	0.12 $(\pi-\theta)$
2	1.90	0.63	0.47	0.33	0.19	0.12	0.06	0.09 $(\pi-\theta)$
3	0.72	0.47	0.33	0.23	0.15	0.09	0.045	0.07 $(\pi-\theta)$
4	0.60	0.37	0.26	0.18	0.11	0.07	0.035	0.053 $(\pi-\theta)$
5	0.50	0.30	0.23	0.15	0.093	0.060	0.030	0.045 $(\pi-\theta)$
7	0.36	0.23	0.17	0.12	0.07	0.042	0.022	0.033 $(\pi-\theta)$
10	0.28	0.18	0.11	0.087	0.050	0.029	0.016	0.024 $(\pi-\theta)$

from potential (2.40) for $\chi \gg 1$ and yields too low values. This sometimes leads (see below) to low calculated values of the impact parameters and of the scattering cross sections for relatively large angles, when the potential, and not only its derivative, are important. The smaller value of the potential (2.34) is partly compensated by the larger value of its derivative /112/.

The data in Table 3 facilitate the comparison of the experimental values of the impact parameter in collisions of Ne^+ ions and neon atoms /247/ with the theoretical values calculated from the Thomas-Fermi screening function. The agreement in the whole range of angles and energies investigated is quite satisfactory. The theoretical values of ρ' calculated according to Everhardt (Table 1) are smaller than the experimental values ρ'_{exp} and they increase more slowly than ρ_{exp} with decreasing θ.

If condition (2.37) for weak screening is fulfilled, but $\frac{\pi b}{\lambda} < 1$ or $v > Z_1 Z_2 u_0$, then the calculation of the scattering cross sections in the screened field should be performed by quantum-mechanical methods. The general solution is very complicated, but when the condition $\frac{\pi b}{\lambda} \ll 1$ is satisfied, or when

$$\alpha = \frac{2\pi Z_1 Z_2 e^2}{h v} = \frac{Z_1 Z_2}{137\beta} \ll 1 , \qquad (2.42)$$

the problem of scattering in a weakly screened Coulomb field can be solved in the Born approximation, which corresponds to the case of a small perturbation of the plane wave representing the incident particle.

TABLE 3

Experimental /247/ and theoretical /112/ values of the impact parameter in the scattering of Ne^+ ions by neon atoms

Kinetic energy (kev) and energy parameter	θ, radians	0.07	0.14	0.21	0.28	0.42	0.56	0.70	0.84	0.98
	ϑ_1, degrees	2	4	6	8	12	16	20	24	28
$T=25$	$10^9 \rho_{exp}$, cm	3.7	2.8	2.3	1.57	1.27	1.15	0.94	0.77	0.70
$\varepsilon=1.2$	ρ'_{exp}	2.8	2.0	1.68	1.14	0.91	0.76	0.68	0.56	0.51
	ρ_{theor}	3.05	2.15	1.73	1.15	1.05	0.75	0.68	0.58	0.51
$T=50$	$10^9 \rho_{exp}$, cm	2.7	1.79	1.35	1.09	0.81	0.62	0.51	0.43	0.37
$\varepsilon=2.4$	ρ'_{exp}	1.98	1.31	0.99	0.80	0.59	0.45	0.38	0.32	0.27
	ρ_{theor}	2.2	2.2	1.10	0.90	0.66	0.50	0.40	0.33	0.27
$T=100$	$10^9 \rho_{exp}$, cm	1.9	1.19	0.87	0.70	0.47	0.36	0.30	0.25	0.22
$\varepsilon=4.8$	ρ'_{exp}	1.40	0.87	0.63	0.51	0.34	0.26	0.22	0.18	0.16
	ρ_{theor}	1.45	0.95	0.70	0.56	0.39	0.29	0.24	0.20	0.16

For screening in potential field (2.34), the scattering amplitude in the Born approximation is given by the expression

$$f_B(\theta) = \frac{2Z_1 Z_2 e^2 m_1 (2\pi)^2}{h^2\left[q^2 + \left(\frac{1}{a}\right)^2\right]} = \frac{f_R(\theta)}{\left[1 + \left(\frac{\lambda}{4\pi a \sin\frac{\theta}{2}}\right)^2\right]},$$

where

$$q = 2k\sin\left(\frac{\theta}{2}\right) = \left(\frac{4\pi}{\lambda}\right)\sin\frac{\theta}{2};$$

$f_R(\theta)$ is the Rutherford scattering amplitude.

Consequently, in this case the differential scattering cross section in a screened Coulomb field is connected with the scattering cross section in an unscreened field (Rutherford cross section) by

$$\sigma_B(\theta) = \sigma_R(\theta)\left[1 + \left(\frac{\lambda}{4\pi a \sin\frac{\theta}{2}}\right)^2\right]^{-2}. \qquad (2.43)$$

The integral cross section will be small compared with πa^2 for all values of the screening length a. It follows from (2.43) that for $\frac{\lambda}{2\pi} \ll a$ there exists a range of angles where the scattering cross section is practically equal to the Rutherford cross section, $\sigma_B = \sigma_R$. The boundary of this range is determined by the screening angle

$$\theta_a^{**} \cong \frac{\lambda}{2\pi a} = \frac{\xi}{a}. \qquad (2.44)$$

For $\frac{\lambda}{2\pi} \sim a$ this cross section differs from Rutherford's for all the scattering angles.

Moliere /388/ showed that a more general expression for the scattering cross section of fast charged particles in a screened Coulomb field can be obtained by the quasi-classical Wentzel-Kramers-Brillou method in /509/. In order to take screening into account, the author used an electron distribution according to the Thomas-Fermi atomic model, i.e., instead of (2.34) she used the more accurate expression (2.40). The results of Moliere's calculations are summarized in the following.

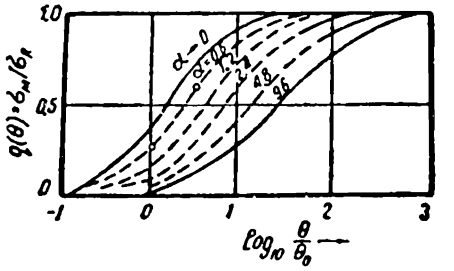

FIGURE 6. Dependence of the screening function according to Moliere /389/ on the scattering angle for various values of the parameter α

For a wide range of variation of the parameter α and for $q(\theta)>0.9$

$$q(\theta)=\frac{\sigma_M(\theta)}{\sigma_R(\theta)}=\left[1-\frac{8.85}{(\theta/\theta_0)^2}\left[1+\alpha^2\cdot 2.303\log_{10}\frac{0.00072\,\theta^4}{\left(0.13+\frac{\alpha^2}{3}+\alpha^4\right)\theta_0^4}\right]\right],$$

where $q(\theta)$ is Moliere's screening function.

The quantity

$$\theta_0=\frac{\lambda}{2\pi r_{TF}}=\frac{\lambda/2\pi}{0.885\,a_0 Z_2^{-1/3}} \tag{2.44a}$$

is the ratio of the reduced wavelength of the incident particle to the characteristic dimension of the atom in the Thomas-Fermi model. In the other cases, the variation of the screening function is established by the interpolation formula

$$\theta_q=\theta_0(A_q+B_q\,\alpha^2)^{1/2},$$

where θ_q is the angle at which the scattering function assumes a given value q.

The values of the coefficients A_q and B_q are tabulated in Moliere's work /388/. The dependence of q on θ/θ_0 calculated by the interpolation formula is represented by the dashed curves in Figure 6. We note that θ_0 is almost exactly equal to the screening angle θ_a^{∞} in (2.44), corresponding to the first Born approximation and to a potential (2.34). The more accurate value of the screening angle θ_a according to Moliere, which includes corrections of the calculations in the first Born approximation, is given by

$$\theta_a^2=\theta_0^2\,[1.13+3.76\,\alpha^2]. \tag{2.45}$$

Moliere assumed the screening angle (2.45) to be valid for large variations of the parameter α. However, in a recent work Nigam et al. /404/ have shown that the applicability of Moliere's calculations is practically limited by condition (2.42). The actual relation between Θ_a^2 and Θ_0^2, taking into account the exact relativistic expression for the cross section of single scattering /229/ and terms of the order of α^2 is given by a more complicated expression

$$\Theta_a^2 = \Theta_0^2\left\{1 + 4\alpha\beta\Theta_0\left[\left(\frac{1-\beta^2}{\beta}\right)\ln\Theta_0 + \frac{0.231}{\beta} + 1.448\beta\right]\right\}, \qquad (2.45a)$$

where Θ_0 is determined by (2.44a) taking the Thomas-Fermi potential (2.40) and is equal to $k\frac{\lambda}{2\pi r_{TF}}$ for the potential (2.34) (k is a factor of the order of unity).

Until now, we only consider collisions in which a considerable overlapping of the electronic shells of the colliding particles is observed and the outer electrons do not affect the interaction potential.

If $\frac{\lambda}{2\pi} \gg a$, or when the kinetic energy of the particle is lower than the interaction potential of the nuclei separated by the screening length, hard-sphere collisions occur. The upper limit of the energy at which this approximation is applicable taking the potential (2.34) can be given roughly by the expression

$$T = (2\,\mathrm{Ry})\, Z_1 Z_2 \left(Z_1^{1/3} + Z_2^{1/3}\right)^{1/2} \frac{m_1 + m_2}{m_1}. \qquad (2.46)$$

According to the laws of hard-sphere collisions scattering in CMS has spherically symmetric angular distribution

$$d\sigma(\Theta) = \frac{\pi a'^2}{2}\sin\Theta d\Theta = \frac{\sigma}{4\pi}d\Omega, \qquad (2.47)$$

where $\sigma \cong \pi a'^2$ is the integral scattering cross section;

a' is the diameter of the effective sphere, being of the same order of magnitude as the screening length a.

The corresponding expression for the scattering cross section in LS can be obtained by (2.6).

For $m_1 < m_2$

$$\sigma(\vartheta_1) = \frac{d\sigma(\vartheta_1)}{d\omega_1} = \frac{a'^2}{4}\left[2\frac{m_1}{m_2}\cos\vartheta_1 + \frac{1 + \frac{m_1^2}{m_2^2}\cos 2\vartheta_1}{\left(1 - \frac{m_1^2}{m_2^2}\sin^2\vartheta_1\right)^{1/2}}\right]; \qquad (2.47a)$$

for $m_1 > m_2$

$$\sigma(\vartheta_1) = \frac{a'^2}{2}\frac{1 + \left(m_1^2/m_2^2\right)\cos 2\vartheta_1}{\left[1 - \left(m_1^2/m_2^2\right)\sin^2\vartheta_2\right]^{1/2}}. \qquad (2.47b)$$

Let us now summarize.

In the case of weak screening ($\xi < 1$), the problems of scattering of heavy charged particles by atoms can be solved by classical methods or by the Born method. For $\alpha \sim 1$, both methods give the same results. In all cases the scattering is identical to Rutherford scattering in a wide range of angles.

If the screening is strong ($\xi > 1$), the scattering differs from Rutherford scattering at all angles. However, as was shown above, in this case

(for example, when condition (2.39) is fulfilled), the collisions may often be described by classical mechanics, and for $\xi \gg 1$ they approach the hard-sphere collisions.

In special cases when both the classical theory and the quantum-mechanical perturbation theory are inapplicable, a more accurate quantum-mechanical scattering formula and a corresponding method of calculation have to be used; see, for example, references /12, 16, 17, 62, 401/.

Elastic scattering of high-energy charged particles. Deviations from Rutherford formula due to nuclear force fields. Let us consider some experimental results on the elastic scattering of high energy α-particles ($T > 10$ Mev) which show deviations from the cross sections determined by the Rutherford formula*. Analysis of these deviations provides information on the radii of the scattering nuclei and α-particles, as well as on the interaction potential of α-particles with nuclei in the non-Coulombian range. For these investigations faster α-particles are required than those from natural radioactive sources ($T = 4 - 9$ Mev). Therefore, although early observations of deviations from the Rutherford formula were made in the scattering on light nuclei, a systematic investigation became possible only with the appearance of high-energy accelerators.

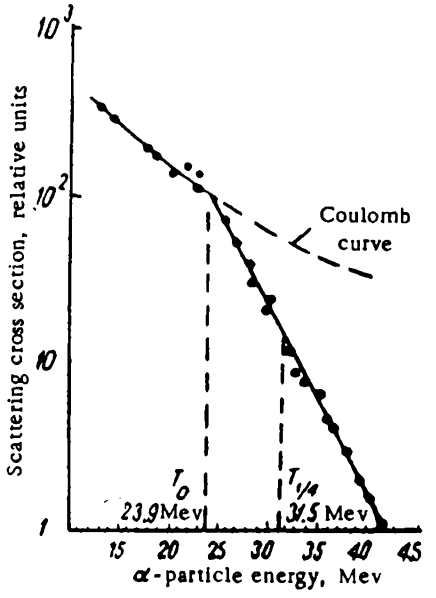

FIGURE 7. Energy dependence of the cross sections of elastic scattering of α-particles by tantalum for $\theta = 60°$ /267/:

T_0 is the critical energy; $T_{1/4}$ is the energy at which the experimental scattering cross section is 1/4 of the theoretical value calculated for a pure Coulomb field

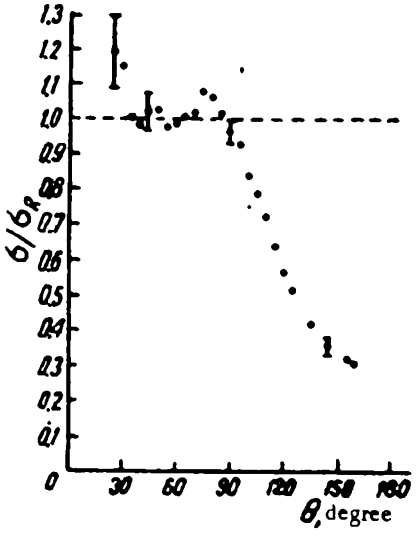

FIGURE 8. Angular dependence of the differential cross section of elastic scattering of α-particles by gold for $T = 22$ Mev, measured and calculated by the Rutherford formula

* These deviations, or so-called anomalies, are also observed in the elastic scattering of high-energy protons, deuterons and tritons /27, 61, 224, 280/. However, the anomalous scattering of α-particles is of greatest interest. Since α-particles have no spin, an unambiguous analysis is possible, as spin-orbital forces may be neglected. A complete review of the investigations of elastic scattering of fast α-particles by nuclei is contained in Elsberg and Porter. — Rev. Mod. Phys., Vol. 33:190, 1961.

Up to the present the scattering of 10—40 Mev α-particles by heavy and light elements has been studied in some detail. The main results of the experimental investigations (see for example, /257, 357, 280, 205, 60, 315/) can be formulated as follows:

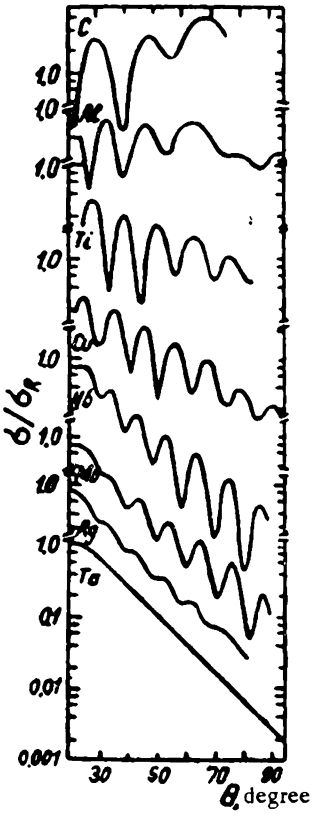

FIGURE 9. Angular dependence of the ratio of the experimental to the Coulomb scattering cross sections of 40.2 Mev α-particles on various nuclei

1) The energy dependence of the scattering cross section of α-particles by heavy nuclei (silver, gold, lead) for a fixed scattering angle follows expression (2.29) up to some critical energy T_0. For example, in the scattering of α-particles by gold at an angle of $\theta = 60°$, $T_0 = 27$ Mev /257/. As the energy is further increased, a rapid (almost exponential) fall-off in the scattering cross sections is observed, and the absolute values of the cross sections are much smaller than the Rutherford cross sections (see, for example, Figure 7). The critical energy T_0 increases with the charge of the scattering nuclei and with the scattering angle.

2) The angular distribution of elastically scattered α-particles for a given energy follows the Rutherford formula up to some critical angle θ_0; then the measured scattering cross section falls rapidly and becomes much smaller than the Rutherford cross section. One of the experimental angular distributions is shown in Figure 8.

3) The angular distribution of α-particles in elastic scattering by light and medium nuclei (carbon, aluminum, magnesium) has a pronounced oscillatory character (presence of maxima and minima), which varies for different scattering elements (Figure 9) and for different energies.

When fast α-particles are scattered by heavy nuclei, the condition $(\lambda/2\pi) < R_{A\alpha}$ is satisfied, and therefore the basic features of the angular and energy distributions in elastic scattering can be explained by the semi-classical theory (see, for example, /9, 206/), according to which the di-emergent l-partial wave disappears, if the distance of closest approach for the corresponding classical trajectory is smaller than the sum of the radii of the nucleus and of the α-particle. In all other cases there is a phase which is characteristic of pure Coulomb scattering. In this theory, the classical distance of closest approach corresponding to the energy at which the experimental cross section is 1/4 of the Rutherford cross section (see Figure 7) is equal to the sum of the radii of the nucleus and of the α-particle. An analysis of the experimental data based on this theory provided the following expression for the interaction radius /357/:

$$R_{A\alpha} = r_0 A^{1/3} + b,$$

where

$$r_0 = (1.414 \pm 0.042) \cdot 10^{-13} \text{ cm},$$

$$b = (2.19 \pm 0.20) \cdot 10^{-13} \text{ cm}.$$

The nuclear radius obtained from such measurements is the distance at which an α-particle begins to "feel" the tail of the nuclear potential, i.e., it is considerably larger than the so-called "electron" radius of the nucleus, determined from experiments on the scattering of electrons (§ 12) or on transitions in mesoatoms.

A more rigorous analysis of the same experimental data on the elastic scattering of charged particles based on the optical model (see, for example, /314/) provides data on the interaction radius, as well as on the parameters of the interaction potential in question, and also explains the features of the angular distribution of α-particles elastically scattered on light nuclei. However, a much simpler method is based on an analogy with diffraction of light on a sphere, whence the radius of the nuclear interaction may be determined. In this method a comparison is made between the maxima and minima on the experimental curve and the zeros of the function

$$j_1(qR) = j_1(2kR\sin\theta/2),$$

where k and q are the wave numbers of the α-particle and of the recoil nucleus;

R is the interaction radius;

j_1 is the spherical Bessel function.

An even simpler method consists of the determination of the differences of the quantity qR for neighboring maxima (minima) of the experimental curve. These differences satisfy the empirical relation

$$\Delta(qR) = 2kR\,\Delta\left(\sin\frac{\theta}{2}\right) = \pi.$$

Effective cross section for the energy loss in elastic scattering. The energy Q acquired in elastic scattering by the scattering particle (recoil energy) is equal to the energy lost by the scattered particle. It is determined by expression (2.2) or, when using (2.5) and (2.7), by the relation

$$Q = 4\left(\frac{m_1}{m_2}\right) T_c^2 \sin^2\frac{\theta}{2}.$$

Expressing $\sin\frac{\theta}{2}$ in terms of Q and substituting it in formula (2.23), we obtain the expression

$$d\sigma_n = B_n\frac{dQ}{Q^2}, \tag{2.48}$$

determining the effective scattering cross section as a function of the energy loss Q of the scattered particle.

B_n denotes here

$$B_n = \pi\frac{Z_1^2Z_2^2e^4}{T}\left(\frac{m_1}{m_2}\right) = 2\pi\frac{Z_1^2Z_2^2e^4}{m_2v^2}. \tag{2.49}$$

It follows from (2.49) that the cross section for energy transfer decreases rapidly with the increase of transferred energy.

The integral cross section for collisions with energy transfer between Q_1 and Q_2 is

$$\sigma_n = B_n\left(\frac{1}{Q_1} - \frac{1}{Q_2}\right), \tag{2.50}$$

where $Q_2 \leqslant Q_{max}$, as defined by (2.3), and $Q_1 > Q_a^*$ (Q_a^{**}). The quantity Q_a of the energy transferred at the limiting screening angle θ_a^* or θ_a^{**} is calculated from (2.38) or (2.44). Q_a^* is determined, for example, by (2.38a).

In spherically-symmetric scattering (hard-sphere collisions) all energy transfers from 0 to Q_{max} are equally probable. In this case

$$d\sigma \approx \pi a'^2 \frac{dQ}{Q_{max}}, \tag{2.51}$$

where a' is of the order of the screening length.

Energy losses in elastic nuclear collisions. The mean energy loss for unit path length is given by

$$-\frac{dE}{dx} = n \int Q \, d\sigma, \tag{2.52}$$

where n is the number of scattering particles per 1 cm^3 of the retarding medium;

Q is the energy transferred in a single collision;

$d\sigma$ is the cross section for collisions accompanied by energy transfer Q.

If we assume that the number of collisions per unit path length is given by the Poisson distribution about the mean value, which corresponds to the mean energy losses $d\bar{E}$ determined by (2.52), then the mean square deviation of the energy losses

$$\sigma_E^2 = \left(dE - d\bar{E}\right)^2_{\text{mean}}$$

can be claculated /12/ by

$$\sigma_E^2 = n dx \int Q^2 d\sigma. \tag{2.53}$$

As was mentioned above, the condition of weak screening is usually fulfilled for fast particles; for most angles the scattering cross sections are determined by (2.48). Substituting (2.48) in (2.52) and (2.53) and neglecting the energy losses in collisions with $Q < Q_a^*$ (Q_a^{**}) we obtain

$$\left(-\frac{dE}{dx}\right)_n = nB_n \ln \frac{Q_{max}}{Q_a}. \tag{2.54}$$

$$\sigma_n^2 \cong nB_n Q_{max} \Delta x. \tag{2.55}$$

Using expressions (2.10), (2.38) and (2.42) we have

$$\begin{aligned} &\frac{Q_{max}}{Q_a} \cong \left(\frac{2}{\theta^*}\right)^2 = \left(\frac{4a}{b}\right)^2 \quad \text{for } a > 1, \\ &\frac{Q_{max}}{Q_a} \cong \left(\frac{2}{\theta^{**}}\right)^2 = \left(\frac{4\pi a}{\lambda}\right)^2 \quad \text{for } \begin{cases} a < 1 \\ \dfrac{\lambda}{2\pi a} \ll 1. \end{cases} \end{aligned} \tag{2.56}$$

When the condition of weak screening (2.37) is fulfilled, these quantities are always much greater than 1. For example, in the collision of a 1 Mev α-particle with aluminum, $\frac{Q_{max}}{Q^*} \sim 10^6$; in the collision of a neon ion with an argon atom (T= 200 kev), $\frac{Q_{max}}{Q^*} \sim 250$ and so on; therefore, the logarithm in (2.54) does not depend much on the velocity (energy) of the incident particle.

Thus, the energy losses in elastic atomic (nuclear) collisions are approximately proportional to the product of the squares of the charges of the colliding particles and inversely proportional to the squares of the

velocities of the incident particles and to the mass of the scattering particle. As the velocity decreases, when $\xi \approx 1$, the argument of the logarithm in (2.54) becomes small; the dependence of the logarithmic term in (2.54) on the velocity should also be taken into account. The mean energy losses then vary more slowly than v^{-2}.

TABLE 4

Mass stopping powers of some metals for helium ions due to nuclear* and electron** collisions

Ion energy, Mev	Aluminum		Nickel		Silver		Gold	
	$\frac{1}{\rho}\left(\frac{dE}{dx}\right)_n$, kev·cm²/g	$\frac{1}{\rho}\left(\frac{dE}{dx}\right)_e$, Mev·cm²/g	$\frac{1}{\rho}\left(\frac{dE}{dx}\right)_n$, kev·cm²/g	$\frac{1}{\rho}\left(\frac{dE}{dx}\right)_e$, Mev·cm²/g	$\frac{1}{\rho}\left(\frac{dE}{dx}\right)_n$, kev·cm²/g	$\frac{1}{\rho}\left(\frac{dE}{dx}\right)_e$, Mev·cm²/g	$\frac{1}{\rho}\left(\frac{dE}{dx}\right)_n$, kev·cm²/g	$\frac{1}{\rho}\left(\frac{dE}{dx}\right)_e$, Mev·cm²/g
0.2	7.4	—	5.7	—	4.28	—	3.0	—
0.5	3.5	—	2.75	0.709	2.12	0.544	1.56	0.315
1.0	1.94	1.31	1.54	0.82	1.22	0.64	0.92	0.42
2.0	1.06	—	0.87	—	0.70	—	0.53	—

* Calculated by (2.54).

** Experimental values /416/.

For fast charged particles, when $\xi < 1$, the electron collisions (§ 4—5) are of greater importance in the energy loss than the atomic (nuclear) collisions. The latter affect the stopping mainly for relatively low velocities and large charges of the incident particles.

Let us consider some examples. Table 4 gives the mass nuclear stopping powers $\frac{1}{\rho}\left(\frac{dE}{dx}\right)_n$ calculated for helium ions and various stopping materials from (2.54). The table also gives the experimental values of the mass stopping powers due to collisions with electrons (§ 5). The total mass stopping power is made up of the losses in both the nuclear and the electron collisions. It can be seen from the table that for helium ions with $T \geqslant 0.5$ Mev even in heavy materials the nuclear collisions do not contribute more than 0.5% of the total energy losses.

For heavy ions with relatively low velocities the stopping due to nuclear collisions is more important than for helium ions. However, in this case too, the stopping due to electron collisions is the most important. For example, the energy losses in nuclear collisions of quadruply charged carbon and oxygen ions in metals amount to only a few percent of the losses in electron collisions (Tables 5 and 6). The situation is different for slow particles with a large effective charge; in this case, for strong screening ($\xi > 1$), the scattering is almost spherically symmetric and the substitution of (2.51) in (2.52) and (2.53) leads to the following results:

$$\left(\frac{dE}{dx}\right)_n = \frac{1}{2} n\pi a'^2 Q_{max}, \tag{2.57}$$

$$\sigma_E^2 = \frac{1}{3} n\Delta x \pi a'^2 Q_{max}. \tag{2.58}$$

For $\xi \approx 1$, the cross section σ for energy transfer is inversely proportional to the square of the particle velocity and $\left(\frac{dE}{dx}\right)_n$ is almost independent of the velocity. This case, for example, corresponds to the stopping of the

recoil atoms in alpha decay. In the velocity range where $\xi > 1$, nuclear collisions are the most important in stopping, in contrast to the case $\xi < 1$.

TABLE 5

Mass stopping powers of metals for quadruply charged carbon ions $\frac{1}{\rho}\left(\frac{dE}{dx}\right)$, Mev·cm²/g

T, kev	$\frac{v}{u_0}$	Carbon		Aluminum		Nickel		Silver		Gold	
		a	b	a	b	a	b	a	b	a	b
360	1.10	3.42	0.113	2.36	0.097	1.24	0.078	1.01	0.055	0.475	0.037
400	1.16	3.56	0.108	2.56	0.088	1.34	0.071	1.06	0.051	0.496	0.035
600	1.42	4.17	0.078	3.27	0.064	1.69	0.053	1.32	0.038	0.650	0.027
800	1.64	4.67	0.061	3.68	0.051	1.98	0.042	1.54	0.031	0.773	0.022
1000	1.83	5.08	0.051	3.93	0.043	2.21	0.036	1.71	0.026	0.882	0.019
1200	2.00	5.43	0.043	4.11	0.036	2.40	0.030	1.85	0.022	0.970	0.016
1400	2.16	5.76	0.038	4.24	0.032	2.57	0.027	1.98	0.020	1.06	0.014
1600	2.32	6.04	0.034	4.36	0.029	2.70	0.024	2.08	0.013	1.13	0.013
1800	2.46	6.30	0.031	4.42	0.026	2.83	0.022	2.17	0.016	1.20	0.012
2000	2.58	6.50	0.028	4.48	0.024	2.93	0.020	2.25	0.015	1.26	0.011
2200	2.71	6.64	0.026	4.51	0.022	2.97	0.018	2.33	0.014	1.32	0.010
2400	2.83	6.76	0.024	4.58	0.020	3.01	0.017	2.40	0.013	1.36	0.010
2600	2.94	6.81	0.023	4.60	0.019	3.05	0.016	2.46	0.012	1.40	0.009
2800	3.06	6.87	0.022	4.62	0.012	3.09	0.015	2.50	0.012	1.42	0.009
3000	3.16	6.87	0.020	4.65	0.017	3.11	0.015	2.54	0.011	1.44	0.008
3200	3.27	6.88	0.019	4.68	0.016	3.14	0.014	2.57	0.010	1.45	0.008

Note. a — experimental values /422/ of the mass stopping power $\frac{1}{\rho}\left(\frac{dE}{dx}\right)_e$ due to electron collisions; b — mass stopping power $\frac{1}{\rho}\left(\frac{dE}{dx}\right)_n$ due to nuclear collisions calculated from (2.54).

TABLE 6

Mass stopping powers of metals for quadruply charged oxygen ions $\frac{1}{\rho}\left(\frac{dE}{dx}\right)$, Mev·cm/g*

T, kev	$\frac{v}{u_0}$	Carbon		Aluminum		Nickel		Silver		Gold	
		a	b	a	b	a	b	a	b	a	b
360	0.949	3.43	0.257	2.30	0.205	1.35	0.164	1.02	0.116	—	—
400	1.00	3.53	0.230	2.52	0.189	1.42	0.152	1.10	0.107	0.517	0.072
600	1.23	4.43	0.167	3.32	0.139	1.79	0.113	1.40	0.082	0.707	0.056
800	1.42	5.11	0.133	3.91	0.111	2.13	0.092	1.68	0.067	0.833	0.047
1000	1.58	5.72	0.111	4.35	0.093	2.41	0.077	1.89	0.057	0.935	0.041
1200	1.73	6.22	0.094	4.72	0.078	2.64	0.066	2.09	0.049	1.05	0.035
1400	1.87	6.78	0.082	4.96	0.070	2.87	0.059	2.24	0.044	1.16	0.031
1600	2.00	7.13	0.074	5.18	0.062	3.09	0.053	2.39	0.039	1.28	0.028
1800	2.12	7.62	0.067	5.37	0.056	3.27	0.048	2.53	0.036	1.38	0.026
2000	2.24	8.02	0.062	5.54	0.053	3.39	0.045	2.67	0.034	1.46	0.025
2200	2.35	8.45	0.057	5.66	0.048	3.51	0.041	2.79	0.031	1.53	0.023
2400	2.45	8.79	0.053	5.73	0.045	3.61	0.039	2.89	0.029	1.61	0.021
2600	2.55	9.02	0.050	5.80	0.042	3.69	0.036	2.98	0.027	1.67	0.020
2800	2.65	9.27	0.046	5.87	0.040	3.78	0.034	3.08	0.026	1.73	0.019
3000	2.74	9.50	0.044	5.92	0.038	3.85	0.037	3.17	0.025	1.79	0.018
3200	2.83	9.70	0.042	5.98	0.036	3.86	0.031	3.22	0.023	1.84	0.017

* See note to Table 5.

Multiple scattering of charged particles. The preceding relations are valid for the calculation of the angular distributions of particles undergoing

an average of one collision when passing through a foil (single scattering). In many cases, however, the final deflection of a particle is the total effect not of a single, but of many elementary events of close scattering. Depending on the mean number of collisions Ω of a particle in a foil of thickness t, we distinguish between single ($\Omega < 1$), plural ($\Omega = 1 - 20$), and multiple ($\Omega > 20$) scattering events.

The actual path length traversed by a particle, considering multiple scattering, is larger than the foil thickness. This fact is important in the study of the range—energy relations of particles (see § 6, 15), in the interpretation of track distortion in cloud chambers or in photoemulsions (§ 10), etc.

Multiple scattering of ultra-fast charged particles is widely used at present in nuclear and in elementary-particle physics as a method for determining the energy of the particles (§ 10). The method is based on the fact that after multiple scattering the deflection angle of a particle is directly proportional to its charge and inversely proportional to its energy.

The theory of multiple scattering is developed in /52, 505, 262, 389, 460, 404, 407/.

The earliest and simplest theory is by Williams /505/. He assumed that the deflection of a particle after multiple scattering is the sum of a multiplicity of single deflections, whose probability is determined by Rutherford's formula. The angular distribution of particles which pass a foil possesses azimuthal symmetry with respect to the direction of the incident beam, so that the probability of their emergence from the foil in the angular range $(\theta, \theta + d\theta)$ is given by a Gaussian distribution:

$$p(\theta)d\theta = \frac{2\theta}{<\theta^2>_{mean}} \exp\left(-\frac{\theta^2}{<\theta^2>_{mean}}\right) d\theta, \qquad (2.59)$$

where $<\vartheta^2>_{mean}$ is the mean square deflection, which is the sum of the mean square deflections along orthogonal axes in a plane perpendicular to the direction of the incident particles (Figure 10).

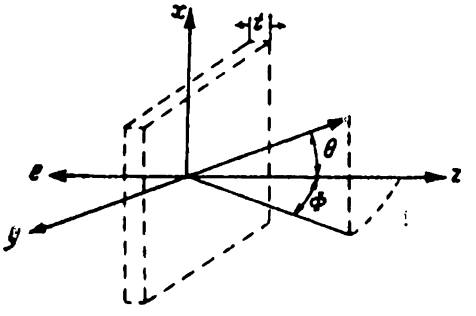

FIGURE 10. Geometry of multiple scattering

According to Rutherford's formula (2.23), the probability that a particle passing a layer of thickness dx is deflected as a result of a single collision by a small angle θ in the interval $(\theta, \theta + d\theta)$ is

$$ndx \frac{8\pi Z_1^2 Z_2^2 e^4}{p^2v^2} \frac{d\theta}{\theta^3}, \qquad (2.60)$$

where n is the number of atoms in 1 cm^3 of the substance;

Z_1e, p and v are the charge, the momentum, and the velocity of the incident particle;

Z_2e is the charge of the scattering nuclei.

The product pv is equal to twice the kinetic energy of the particles at low velocities ($v \ll c$) or to the kinetic energy at relativistic ($v \approx c$) velocities.

Multiplying this probability by θ^2 and integrating over θ from θ_{min} to θ_{max} and over x from 0 to t, we obtain the mean square angle of deflection in passing a layer t (the energy losses in it are assumed sufficiently small so that p and v remain unchanged):

$$\langle \theta^2 \rangle_{mean} = \frac{8\pi Z_1^2 Z_2^2 e^4}{p^2 v^2} nt \ln \frac{\theta_{max}}{\theta_{min}}. \qquad (2.61)$$

The choice of the angle θ_{max} is somewhat arbitrary (this is the largest of the small scattering angles). Williams takes for θ_{max} an angle θ_1 for which an average of one collision with a deflection angle θ greater than θ_1 occurs in the foil. The total probability of a single scattering by an angle larger than θ_1 is taken equal to one, so that

$$\theta^2_{max} = \theta_1^2 = \frac{4\pi Z_1^2 Z_2^2 e^4}{p^2 v^2} nt. \qquad (2.62)$$

The minimum angle θ_{min} is determined by the screening of the nucleus by the atomic electrons (see above). Williams considered separately the classical case ($\alpha = \frac{Z_1 Z_2}{137\beta} \gg 1$) when the anlge θ_{min} is equal to θ_a^*, and the case when the Born approximation applies ($\alpha \ll 1$), with the anlge θ_{min} equal to θ_a^{**}. The values of the screening angles θ_a^* and θ_a^{**} are determined by (2.38) and (2.44).

Substituting $\theta_{max} = \theta_1$ and $\theta_{min} = \theta_a^{**}$ in (2.61), the following expression for the mean square angle of deflection is obtained:

$$\langle \theta^2 \rangle_{mean} = 2\theta_1^2 \ln \frac{\theta_1}{\theta_a^{**}} = \frac{4\pi Z_1^2 Z_2^2 e^4}{p^2 v^2} nt \ln \left[4\pi Z_1^2 Z_2^{4/3} nt \left(\frac{h}{2\pi m_e v} \right)^2 \right], \qquad (2.63)$$

where m_e is the electron mass.

The quantity $\frac{\theta_1}{\theta_a^{**}}$ is of the same order of magnitude as the mean number of collisions Ω experienced by the particle in passing the foil. Since in multiple scattering $\Omega > 20$, the logarithm in (2.63) does not depend much on the argument. The dependence of $\langle \theta^2 \rangle_{mean}$ on the parameters of the scattered particle is mainly determined by the factor in front of the logarithm.

Thus, already from Williams' simple theory the basic features of multiple scattering may be deduced: the mean scattering angle is proportional to the charge of the scattering nuclei, inversely proportional to the energy of the incident particles, and depends on the thickness of the scatterer as $t^{1/2}$.

The problem of multiple scattering was studied more rigorously by Kompaneets /52/, Goudsmith and Saunderson /262/, Moliere /389/, and Snyder and Scott /460/*. The most comprehensive, as far as experimental verification is concerned, is Moliere's non-relativistic theory, which is based on the results described above of the investigation of a single scattering event in the screened atomic field.

* See also /148, 404, 256/, where the connection between these theories was studied and their range of applicability established.

Bethe /148/ considers these theoretical calculations and introduces some corrections. Finally, in recent papers /256, 404, 407/ the range of applicability of Moliere's calculations is discussed and exact formulas in the second Born approximation are given.

According to Moliere, the function $f(\Theta t)\,\Theta d\Theta$, giving the number of particles deflected in the interval $(\Theta,\ \Theta + d\Theta)$ when passing through a foil of thickness t, depends mainly on the angle Θ_1, which is determined by (2.62) and takes into account the foil thickness, and on the screening angle Θ_a, which is determined by (2.45) and represents the screening of the Coulomb field of the scattering nuclei. On the other hand, according to Moliere, the dependence of $f\ (\Theta,\ t)$ on the differential cross section for a single scattering event is not significant if this cross section is equal to the Rutherford cross section for large scattering angles. Thus, the screening function $q\ (\Theta)$, which Moliere uses in her theory of multiple scattering, has the form:

$$q_1\ (\Theta) = \frac{\Theta^4}{(\Theta^2+\Theta_a^2)^2}.$$

For large values of the parameter

$$a = \frac{Z_1 Z_2 e^2}{137\beta} \gg 1$$

$q_1(\Theta)$differs appreciably from $q_0(\Theta)$ (Figure 6).

According to (2.62) and (2.45), the mean number of scattering events of a particle passing a layer of thickness t is

$$\Omega \cong \frac{\Theta_1^2}{\Theta_a^2} = 4\pi N_A\, t \left(\frac{\hbar}{2\pi m_e c}\right)^2 \frac{Z_1^2 Z_2^{4/3}}{\beta^2 A} \frac{0.885^2}{1.13+3.76a^2} = \frac{7800t\,(\text{g/cm}^2)\,Z_1^2\,Z_2^{4/3}}{\beta^2 A\,(1+3.35a^2)}, \qquad (2.64)$$

where N_A is Avogadro's number;

A is the atomic number of the scattering element, $\beta = \frac{v}{c}$;

m_e is the electron mass.

The corrections introduced by Bethe /148/ require the substitution of 6680 for the numerical coefficient in expression (2.64) and of $(Z_2+1)\,Z_2^{1/3}$ for Z_2^2. This takes into account the additional effect of scattering by electrons /58/.

The determination of the mean angle of deflection resulting from numerous individual deflections is reduced, according to Moliere, to the solution of the transcendental equation

$$B - \ln B = \ln \Omega - 0.115$$

and to the expansion of the distribution function $f(\Theta, t)$ in a series of negative powers of the parameter B:

$$f(\Theta, t)\,\Theta d\Theta = \left[f^{(0)} + f^{(1)}(\delta)\,B^{-1} + f^{(2)}(\delta)\,B^{-2} + \cdots\right]\Theta d\Theta, \qquad (2.65)$$

where

$$\delta = \frac{\Theta}{\Theta_1\sqrt{B}},\quad f^{(0)} = 2\exp(-\delta^2).$$

The first term in expression (2.65) gives the usual Gaussian distribution, the second term takes into account the corrections for distant scattering.

For close scattering and sufficiently large values of B ($\delta < 1$), the angular distribution of particles is essentially Gaussian; the corrections are $\sim 1/B$, i.e., of the order of 10%. The numerical values of the parameter B in expressions (2.65) and (2.66) are given below:

$\log \frac{\theta_1^2}{\theta_a^2}$	1	2	3	4	5	6	7	8	9
B	3.36	6.29	8.93	11.49	13.99	16.46	18.90	21.32	23.71

The quantities $f^{(1)}$ and $f^{(2)}$ were calculated and tabulated by Moliere /389/ and Bethe /138/. Bethe's results are more accurate and include a larger range of values of δ. They are given in Table 7 which also tabulates the

TABLE 7

Numerical values of the coefficients of the distribution function $f(\theta,t)$ (2.65)

δ	$f^{(0)}$	$f^{(1)}$	$f^{(2)}$	$\frac{1}{2}\delta^4 f^{(1)}$	$\frac{1}{2}\delta^4 f^{(2)}$
0	2	0.8456	2.4929	0	0
0.2	1.9216	0.7038	2.0694	0.0006	0.0008
0.4	1.7214	0.3437	1.0488	0.0044	0.0034
0.6	1.4094	−0.0777	−0.0044	−0.0050	−0.0003
0.8	1.0546	−0.3981	−0.6068	−0.0815	−0.1246
1	0.7338	−0.5285	−0.6359	−0.2642	−0.318
1.2	0.4738	−0.4770	−0.3086	−0.4946	−0.320
1.4	0.2817	−0.3183	0.0525	−0.6113	0.101
1.6	0.1546	−0.1396	0.2423	−0.4573	0.669
1.8	0.0783	−0.0006	0.2386	−0.0032	1.251
2	0.0366	0.0782	0.1316	0.6258	1.053
2.2	0.01581	0.1054	0.0196	1.2347	0.475
2.4	0.00630	0.1008	−0.0467	1.6718	−0.775
2.6	0.00232	0.08262	−0.0649	1.8877	−1.483
2.8	0.00079	0.06247	−0.0546	1.9200	−1.676
3	0.000250	0.04550	−0.03568	1.8429	−1.448
3.2	$7.3\cdot10^{-5}$	0.03288	−0.01923	1.7240	−1.008
3.4	$1.9\cdot10^{-5}$	0.02402	−0.00847	1.6050	−0.566
3.6	$4.7\cdot10^{-6}$	0.01791	−0.00264	1.5038	−0.222
3.8	$1.1\cdot10^{-6}$	0.01366	0.00005	1.4237	0.005
	$1000\ f^{(0)}$	$1000\ f^{(1)}$	$1000\ f^{(2)}$		
4.0	$2.3\cdot10^{-4}$	10.638	1.0741	1.3617	0.1375
4.5	$3\cdot10^{-6}$	6.140	1.2294	1.2588	0.2521
5	$2\cdot10^{-8}$	3.831	0.8326	1.1972	0.2602
5.5	$2\cdot10^{-10}$	2.527	0.5368	1.1563	0.2456
6	$5\cdot10^{-13}$	1.739	0.3495	1.1275	0.2264
7	$1\cdot10^{-18}$	0.9080	0.1584	1.0901	0.1901
8	$3\cdot10^{-25}$	0.5211	0.0783	1.0679	0.1604
9	$1\cdot10^{-32}$	0.3208	0.0417	1.0523	0.1369
10	$1\cdot10^{-40}$	0.2084	0.0237	1.0419	0.1186

numerical values of the functions $\frac{1}{2}\delta^4 f^{(1)}$ and $\frac{1}{2}\delta^4 f^{(2)}$, determining the ratio of the corresponding cross sections to the Rutherford cross section for large scattering angles.

The distribution of the projections of the scattering angles on a plane parallel to the direction of the beam of scattered particles is given by the

distribution function

$$f(\varphi, t)\,d\varphi = \left[2\pi^{-1/2}\exp(-\varphi^2) + f^{(1)}(\varphi)\,B^{-1} + f^{(2)}(\varphi)\,B^{-2} + \cdots\right] d\varphi, \quad (2.66)$$

where $\varphi = \frac{\Phi}{\theta_1\sqrt{B}}$, and Φ is the projection of the scattering angle (Figure 10).

The mean value $\bar{\alpha}_t$ of the multiple-scattering angle is determined from the expression

$$\frac{2}{\pi}\bar{\alpha}_t = \bar{\Phi} = \theta_1\sqrt{B}\left(1 + \frac{0.982}{B} - \frac{0.117}{B^2} + \cdots\right). \quad (2.67)$$

Nigam et al. /404, 407/ show that Moliere's calculations are insufficiently accurate, since they are based on expression (2.45), which is only correct when condition (2.42) is fulfilled, i.e., in the first Born approximation.

Using the formulas of Goudsmith and Saunderson /262/ for the expansion coefficients of the distribution function of multiple scattering in Legendre polynomials and Dalitts' relativistic formula (2.45a) for single-scattering angle, Nigam et al. obtained the following expression for the distribution function of multiple scattering:

$$f(\Theta, t) \simeq C\left(\theta_1^2 B\right)^{-1}\left\{f^{(0)} + B^{-1}\left(f^{(1)'} + f^{(1)}\right) + \frac{1}{2!B^2}\left(f^{(2)'} + f^{(2)} + \cdots\right)\right\}, \quad (2.68)$$

where

$$C = \exp\left\{\frac{B\theta_1^2}{16}\left[1 + \frac{8\pi\alpha}{B} + 2\xi\frac{\ln 2}{B} + \frac{8(\beta^2 + \pi\alpha)}{B} \times (0.577 - \ln\theta_1\sqrt{B})\right]\right\};$$

$$\xi = 1 + 2\alpha\theta_0(1 - \beta^2).$$

The numerical values of $f^{(0)}$ and $f^{(1)}$ should be taken from Table 7. The values of $f^{(1)'}$ were calculated for a number of special cases in /404, 256/; we give the numerical values of $f^{(1)'}/\alpha\theta_1\sqrt{B}$:

δ	0	0.2	0.4	0.6	0.8
$f^{(1)'}/\alpha\theta_1\sqrt{B}$	−11.123	−9.085	−6.848	−4.952	−3.254

δ	1.0	1.2	1.4	1.6	1.8	2.0	3.0
$f^{(1)'}/\alpha\theta_1\sqrt{B}$	− 1.740	−0.371	+0.908	2.179	3.569	0.716	0.170

The contribution of $f^{(2)}$ and $f^{(2)'}$, as mentioned above, can be neglected in most cases.

The experimental verification of the theory of multiple scattering was done mainly in the study of electron scattering (see § 12). Only a few investigations are available which use non-relativistic heavy charged particles to verify the theory.

Maurer /394/ and Fleischmann /256/ studied the multiple scattering of α-particles from natural radioactive substances. Bichsel /173/ experimentally studied the multiple scattering of 0.7—4.8 Mev protons in metal

foils. Ashmore and Crewe /141/ investigated multiple scattering of 7.5 Mev deuterons in metals.

A satisfactory agreement with the results of Moliere's calculations was found in all these studies. An example is shown in Figure 11 which gives the angular distribution of 8.78 Mev α-particles after passing through 2.6 mg/cm^2 of lead (dots) /256/. The dashed line shows the theoretical distribution.

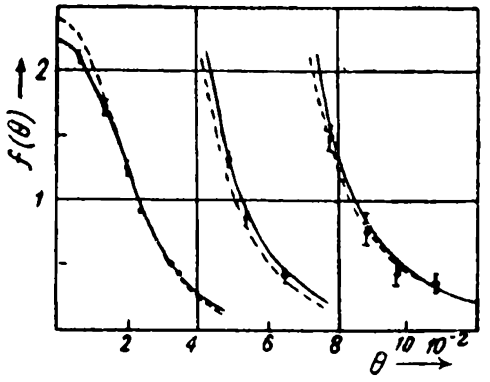

FIGURE 11. Angular distribution of α-particles with an initial energy of 8.78 Mev after passing a lead layer of 2.6 mg/cm^2 /256/. The dashed curve was calculated according to Moliere's theory, the solid curve takes into account the corrections of Nigam et al. /404/

Arutyunyan /10/ investigated the angular distribution of 40 — 200 Mev protons after multiple scattering in copper and lead. In this energy range the finite dimensions of the nucleus and the influence of the nuclear force field should be taken into account.

Plural scattering. The angular distribution of particles in plural ($\Omega < 20$) scattering can only be obtained by numerical methods. Table 8 gives the numerical results of the angular distribution function of particles in single and plural scattering /356/.

In order to use the data of Table 8 in practice it is necessary to determine the experimental ratio $\frac{I'(0)}{I(0)}$, where $I'(0)$ is the forward particle flux without the foil, and $I(0)$ the flux with the scattering foil imposed. If the incident flux is normalized to unity, and in accordance with the conditions of the experiment

$$I(\gamma) = \begin{cases} 2/\gamma_H^2 & \text{for } \gamma = \gamma_H = \dfrac{\theta_a}{\theta_s} \\ 0 & \text{for } \gamma > \gamma_H, \end{cases}$$

then the measured ratio is

$$\frac{I'(0)}{I(0)} = 1 - G(\Omega, \gamma_H). \qquad (2.69)$$

From Table 8 a pair of values of Ω and γ_H is chosen which satisfies formulas (2.69) and (2.64) simultaneously.

§ 3. Excitation of nuclei and nuclear reactions induced by fast charged particles

Most interaction events of fast charged particles with the nuclei of the stopping medium are of an elastic nature. However, some events may lead to nuclear excitation (inelastic scattering) or to nuclear reactions. The relative number of inelastic collisions with nuclei generally increases with increasing energy although, as shown below, inelastic scattering and nuclear reactions are insignificant in attenuating the beam of fast charged particles at nonrelativistic energies. At high energies the contributions of elastic and inelastic interactions become approximately equal.

In this section we shall consider the most general problems connected with nuclear reactions.

Kinematics of nuclear reactions. In the nonrelativistic case, the kinetic energy of a particle b, emerging as a result of a nuclear reaction $A(a, b)B$ and escaping at an angle ϑ_a (LS) to the direction of motion of a, is given by the formula:

$$T_b^{1/2} = \frac{(m_a m_b T_a)^{1/2}\cos\vartheta_a}{m_b + m_B} \pm \left\{\left[\frac{m_B - m_a}{m_b + m_B} + \frac{m_a m_b \cos^2\vartheta_a}{(m_a + m_b)^2}\right] T_a + \frac{m_B}{m_b + m_B} Q\right\}^{1/2}, \tag{3.1}$$

where T_a is the kinetic energy of the particle a, caused by the reaction in LS;

m_a, m_A, m_b, m_B are the masses of the incident particle, target nucleus, emerging light particle and recoil nucleus respectively;

Q is the reaction energy.

The expression for the recoil energy T_B as a function of the escape angle ϑ_B of the recoil nucleus (LS) has the same form, only that the index a should everywhere be replaced by B.

The difference in the kinetic energies of the particles before and after the reaction is given by Q. It can also be expressed in terms of the masses of the particles in the reaction

$$Q = T_B + T_b - T_a = \frac{1}{c^2}\left[(m_a + m_A) - (m_b + m_B)\right], \tag{3.2}$$

where c is the velocity of light.

In practice the following expression is convenient

$$Q = \frac{m_a + m_A}{m_B} T_a - \frac{(m_B - m_b)}{m_B} T_a - \frac{2\sqrt{m_a m_b T_a T_b}}{m_B}\cos\vartheta_a. \tag{3.2a}$$

Reactions for which $Q > 0$ are called exothermic. For $Q > 0$ and $m_B > m_a$, the positive sign is valid in front of the brackets in (3.1).

For endothermic reactions ($Q < 0$), the energy of the particle has a single value only if

$$T_a > \left(-\frac{m_B}{m_B - m_a}\right) Q.$$

For example, in the reaction $H^3(p, n)He^3$ ($Q = -0.764$ Mev) for $T_a < 1.148$ Mev, T_b has two values. Endothermic reactions are energetically possible only

TABLE 8

Numerical values of the function $G\ (\Omega,\ \theta/\theta_a)$

θ/θ_a \ Ω	0.2	0.4	0.6	1	2	3	4	5	6	7	8
0.0	0.338(−0)	0.572(−0)	0.725 (−0)	0.8808 (−0)	0.8137 (−0)	0.5945 (−0)	0.4114 (−0)	0.2866 (−0)	0.2062 (−0)	0.1547 (−0)	0.1210 (−0)
0.1	0.336(−0)	0.569(−0)	0.721 (−0)	0.8658 (−0)	0.8020 (−0)	0.5875 (−0)	0.4076 (−0)	0.2846 (−0)	0.2052 (−0)	0.1542 (−0)	0.1207 (−0)
0.2	0.313(−0)	0.531(−0)	0.673 (−0)	0.8233 (−0)	0.7685 (−0)	0.5675 (−0)	0.3969 (−0)	0.2791 (−0)	0.2024 (−0)	0.1527 (−0)	0.1199 (−0)
0.4	0.253(−0)	0.431(−0)	0.549 (−0)	0.6833 (−0)	0.6573 (−0)	0.5004 (−0)	0.3601 (−0)	0.2597 (−0)	0.1923 (−0)	0.1474 (−0)	0.1170 (−0)
0.6	0.186(−0)	0.319(−0)	0.414 (−0)	0.5229 (−0)	0.5270 (−0)	0.4196 (−0)	0.3147 (−0)	0.2351 (−0)	0.1790 (−0)	0.1400 (−0)	0.1128 (−0)
0.8	0.129(−0)	0.224(−0	0.294 (−0)	0.3834 (−0)	0.4096 (−0)	0.3441 (−0)	0.2703 (−0)	0.2099 (−0)	0.1647 (−0)	0.1318 (−0)	0.1079 (−0)
1.0	0.883(−1)	0.155(−0)	0.207 (−0)	0.2770 (−0)	0.3158 (−0)	0.2806 (- 0)	0.2311 (−0)	0.1864 (−0)	0.1506 (−0)	0.1233 (−0)	0.1025 (−0)
1.25	0.550(−1)	0.995(−1)	0.134 (−0)	0.1853 (−0)	0.2293 (−0)	0.2181 (−0)	0.1900 (−0)	0.1602 (−0)	0.1340 (−0)	0.1126 (−0)	0.9554 (−1)
1.5	0.348(−1)	0.655(−1)	0.905 (−1)	0.1262 (−0)	0.1688 (−0)	0.1709 (−0)	0.1566 (−0)	0.1374 (−0)	0.1187 (−0)	0.1023 (−0)	0.8844 (−1)
2.0	0.152(−1)	0.288(−1)	0.415 (−1)	0.6276 (−1)	0.9574 (−1)	0.1076 (−0)	0.1073 (−0)	0.1010 (−0)	0.9229 (−1)	0.8316 (−1)	0.7456 (−1)
2.5	0.741(−2)	0.147(−1)	0.215 (−1)	0.3402 (−1)	0.5720 (−1)	0.6976 (−1)	0.7449 (−1)	0.7243 (−1)	0.7116 (−1)	0.6673 (−1)	0.6183 (−1)
3.0	0.396(−2)	0.800(−2)	0.120 (−1)	0.1975 (−1)	0.3567 (−1)	0.4634 (−1)	0.5229 (−1)	0.5467 (−1)	0.5462 (−1)	0.5307 (−1)	0.5067 (−1)
4.0	0.139(−2)	0.285(−2)	0.442 (−2)	0.7733 (−2)	0.1531 (−1)	0.2176 (−1)	0.2667 (−1)	0.3006 (−1)	0.3211 (−1)	0.3310 (−1)	0.3329 (−1)
6.0	0.291(−3)	0.605(−3)	0.950 (−3)	0.1737 (−2)	0.3745 (−2)	0.5848 (−2)	0.7894 (−2)	0.9774 (−2)	0.1142 (−1)	0.1279 (−1)	0.1390 (−1)
8.0	0.948(−4)	0.195(−3)	0.300 (−3)	0.5359 (−3)	0.1187 (−2)	0.1927 (−2)	0.2723 (−2)	0.3543 (−2)	0.4357 (−2)	0.5138 (−2)	0.5869 (−2)
10	0.381(−4)	0.780(−4)	0.117 (−3)	0.2040 (−3)	0.4531 (−3)	0.7444 (−3)	0.1072 (−2)	0.1429 (−2)	0.1806 (−2)	0.2195 (−2)	0.2587 (−2)
15	—	—	—	0.3273 (−4)	0.7099 (−4)	0.1152 (−3)	0.1656 (−3)	0.2225 (−3)	0.2856 (−3)	0.3550 (−3)	0.4303 (−3)
20	—	—	—	0.8744 (−5)	0.1851 (−4)	0.2938 (−4)	0.4146 (−4)	0.5484 (−4)	0.6958 (−4)	0.8577 (−4)	0.1034 (−3)

TABLE 8 (continued)

ϱ / θ/θ_a	9	10	11	12	13	14	15	16	18	20
0.0	0.9806 (−1)	0.8188 (−1)	0.7001 (−1)	0.6098 (−1)	0.5392 (−1)	0.4825 (−1)	0.4360 (−1)	0.3973 (−1)	0.3365 (−1)	0.2911 (−1)
0.1	0.9791 (−1)	0.8179 (−1)	0.6995 (−1)	0.6094 (−1)	0.5389 (−1)	0.4822 (−1)	0.4358 (−1)	0.3971 (−1)	0.3364 (−1)	0.2911 (−1)
0.2	0.9746 (−1)	0.8152 (−1)	0.6978 (−1)	0.6082 (−1)	0.5380 (−1)	0.4816 (−1)	0.4353 (−1)	0.3967 (−1)	0.3362 (−1)	0.2909 (−1)
0.4	0.9577 (−1)	0.8049 (−1)	0.6911 (−1)	0.6037 (−1)	0.5347 (−1)	0.4791 (−1)	0.4334 (−1)	0.3952 (−1)	0.3351 (−1)	0.2901 (−1)
0.6	0.9328 (−1)	0.7892 (−1)	0.6806 (−1)	0.5963 (−1)	0.5294 (−4)	0.4750 (−1)	0.4302 (−1)	0.3926 (−1)	0.3334 (−1)	0.2888 (−1)
0.8	0.9022 (−1)	0.7692 (−1)	0.6670 (−1)	0.5866 (−1)	0.5221 (−1)	0.4695 (−1)	0.4258 (−1)	0.3891 (−1)	0.3309 (−1)	0.2871 (−1)
1.0	0.8675 (−1)	0.7459 (−1)	0.6506 (−1)	0.5746 (−1)	0.5131 (−1)	0.4625 (−1)	0.4203 (−1)	0.3847 (−1)	0.3279 (−1)	0.2849 (−1)
1.25	0.8203 (−1)	0.7130 (−1)	0.6269 (−1)	0.5571 (−1)	0.4998 (−1)	0.4521 (−1)	0.4120 (−1)	0.3779 (−1)	0.3232 (−1)	0.2814 (−1)
1.5	0.7705 (−1)	0.6771 (−1)	0.6005 (−1)	0.5371 (−1)	0.4843 (−1)	0.4399 (−1)	0.4022 (−1)	0.3698 (−1)	0.3176 (−1)	0.2773 (−1)
2.0	0.6683 (−1)	0.6008 (−1)	0.5423 (−1)	0.4920 (−1)	0.4487 (−1)	0.4113 (−1)	0.3789 (−1)	0.3506 (−1)	0.3039 (−1)	0.2673 (−1)
2.5	0.5694 (−1)	0.5234 (−1)	0.4812 (−1)	0.4432 (−1)	0.4071 (−1)	0.3789 (−1)	0.3520 (−1)	0.3281 (−1)	0.2787 (−1)	0.2551 (−1)
3.0	0.4787 (−1)	0.4495 (−1)	0.4208 (−1)	0.3935 (−1)	0.3680 (−1)	0.3445 (−1)	0.3231 (−1)	0.3030 (−1)	0.2695 (−1)	0.2412 (−1)
4.0	0.3291 (−1)	0.3215 (−1)	0.3115 (−1)	0.3001 (−1)	0.2880 (−1)	0.2757 (−1)	0.2636 (−1)	0.2519 (−1)	0.2300 (−1)	0.2104 (−1)
6.0	0.1475 (−1)	0.1536 (−1)	0.1578 (−1)	0.1602 (−1)	0.1612 (−1)	0.1611 (−1)	0.1600 (−1)	0.1583 (−1)	0.1533 (−1)	0.1473 (−1)
8.0	0.6537 (−2)	0.7132 (−2)	0.7652 (−2)	0.8097 (−2)	0.8470 (−2)	0.8775 (−2)	0.9018 (−2)	0.9204 (−2)	0.9432 (−2)	0.9506 (−2)
10	0.2974 (−2)	0.3349 (−2)	0.3708 (−2)	0.4045 (−2)	0.4359 (−2)	0.4647 (−2)	0.4908 (−2)	0.5142 (−2)	0.5532 (−2)	0.5824 (−2)
15	0.5109 (−3)	0.5964 (−3)	0.6860 (−3)	0.7791 (−3)	0.8748 (−3)	0.9725 (−3)	0.1071 (−2)	0.1171 (−2)	0.1368 (−2)	0.1559 (−2)
20	0.1227 (−3)	0.1434 (−3)	0.1658 (−3)	0.1896 (−3)	0.2150 (−3)	0.2418 (−3)	0.2701 (−3)	0.2996 (−3)	0.3622 (−3)	0.4289 (−3)

Note. In the table 0.800 (−2) denotes $0.800 \cdot 10^{-2}$ etc.

the energy of the incident particles exceeds the threshold value

$$T_{a\ \text{thresh}} = Q\left(\frac{m_a + m_A}{m_A}\right). \tag{3.3}$$

For the reaction $H^3(p, n)He^3$, the threshold value of the energy is 1.019 Mev. For incident proton energies of from 1.019 to 1.148 Mev, neutrons of two energy groups are formed.

In the notation used here, the elastic scattering on nuclei is written thus: $A(a, a)A$. For elastic scattering $Q = 0$ and expression (3.1) is identical with expression (2.2).

In inelastic scattering, $A(a, a)A^*$, the nucleus remains in an excited state after the collision. The reaction energy in this case is the excitation energy of A, taken with negative sign:

$$Q = -W_{A^*}.$$

The relation between the escape angles of the particles in LS and in CMS is given by (2.6) and (2.8). However, in contrast to elastic scattering, k is now defined thus:

$$k = \left(\frac{m_a m_b}{m_A m_B}\frac{T_{ac}}{T_{ac} + Q}\right)^{1/2} = \left[\frac{m_a m_b}{m_A m_B}\frac{T_a}{T_a + Q\left(1 + \frac{m_a}{m_A}\right)}\right]^{1/2}; \tag{3.4}$$

where T_a and T_{ac} are the kinetic energies of the incident particles in LS and CMS respectively.

Nuclear reaction cross sections and their relation to the attenuation of a beam of charged particles. According to the general definition (§ 1), the cross section for a nuclear reaction is defined as its probability, if the incident beam is a single particle, and the target contains one nucleus per unit area of the beam cross section.

The total number of nuclear reactions of a given type, occuring when particles pass through a layer of thickness dx, is determined by (1.1), where σ is the total reaction cross section for the energy E of the particles. As a result of the inelastic nuclear interaction, the bombarding particle either vanishes or its energy and direction of motion are considerably changed. This results in an attenuation of the intensity of the incident beam. For a thin target, the decrease in flux is, according to (1.1),

$$\Delta N = N_0\left[1 - \exp(-\sigma n x)\right] \approx N_0 \sigma n x, \tag{3.5}$$

where x is the target thickness;

n is the number of nuclei of a given kind in 1 cm^3;

σ is the sum of the cross sections of the reactions caused by a particle of given energy.

The absolute reaction cross sections and their dependence on the energy (excitation function) can be theoretically calculated only in a small number of cases. We shall confine ourselves only to the most general data referring to nuclear reactions with fast charged particles.

When the energy of the charged particles is lower than the height of the coulomb barrier

$$B = \frac{Z_1 Z_2 e^2}{R}\ (R - \text{nuclear radius})$$

the reaction cross section increases exponentially with T_a. If the energy exceeds the height of the barrier, the cross section is determined by other factors. For rough estimates, $\sigma \approx 10^{-25}-10^{-24}$ cm^2 should be substituted in (3.5). Note that reactions induced by deuterons have a higher yield than reactions induced by protons and α-particles of the same energy.

If we take $\sigma = 10^{-25}$ cm^2 and $n = 10^{22}$ cm^{-3} in (3.5) then the decrease in the flux passing through a layer 10 microns thick (10^{-5} cm) is 10^{-4}%.

Due to the large energy losses on ionization in thick targets ($\sigma nx \sim 1$) (§ 5—6) the particles are rapidly slowed down. Approximately 10^5-10^6 fast charged particles, hitting a target, cause one nuclear reaction.

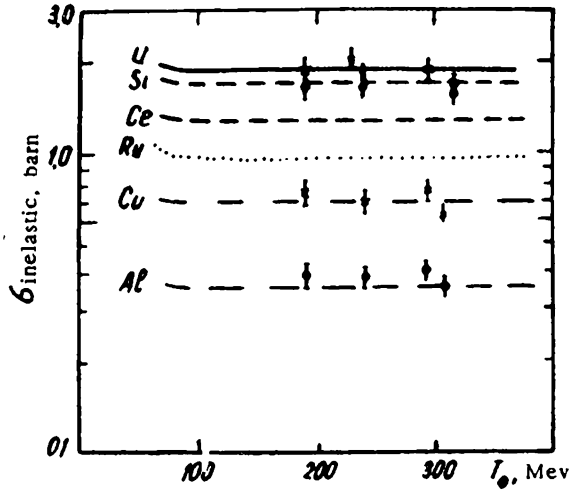

FIGURE 12. Comparison of experimental cross sections /378/ of inelastic interaction of protons with nuclei (points) with the theoretical cross sections (solid curves), taken from /377/

Figure 12 gives the calculated /377/ curves of the total cross sections for the inelastic interaction of fast protons with nuclei of various elements. The figure also shows the experimental results /378/. From these curves the cross sections of inelastic scattering of fast charged particles can be estimated.

The attenuation of the beam due to particle absorption by nuclei has to be taken into account, for example, in analyzing transmission curves for the determination of the mean range of particles in a medium (see § 6).

Measurement of particle energies and energy calibration standards. In practice it is often necessary to determine the energy of the particles accurately; For example, when the energy losses in the passage of particles through matter are investigated (§ 5). The most accurate methods for energy determination are the electrostatic and the magnetic analyses, and for ultra-fast particles, in addition, the measurement of the emission angle of the Cerenkov radiation (see § 9).

The magnetic rigidity $B\rho$, where B is the magnetic flux density and ρ is the radius of curvature of the trajectory of a particle in a transverse magnetic field, is a measure of the ratio of the particle momentum p to its charge Ze

$$B\rho = \frac{pc}{Ze} = \frac{m\beta c^2}{Ze(1-\beta^2)^{1/2}}.$$

Using the well-known relativistic energy momentum relation

$$\left.\begin{aligned} E &= mc^2\left\{1+\left(\frac{ZeB\rho}{mc^2}\right)^2\right\}^{1/2} \\ T &= mc^2\left\{\left[1+\left(\frac{ZeB\rho}{mc^2}\right)^2\right]^{1/2}-1\right\} \end{aligned}\right\}, \tag{3.6}$$

where T is the kinetic energy of the particle;

m is its rest mass.

At very high particle velocities when the total and the kinetic energies are equal, $B\rho$ is connected with E (ev) by

$$E(\text{ev}) = 300\, B\rho\,(\text{gauss}\cdot\text{cm}). \tag{3.7}$$

At small (nonrelativistic) velocities

$$T \cong \frac{(ZeB\rho)^2}{2mc^2}. \tag{3.8}$$

Expressing $B\rho$ in gauss-centimeters, the mass of the particle in atomic mass units (1 amu $= 1.6\cdot10^{-24}$ g) and its energy in electronvolts, we have

$$B\rho(\text{gauss}\cdot\text{cm}) = \frac{144}{Z}\sqrt{M\,(\text{amu})\,T\,(\text{ev})}. \tag{3.8a}$$

Another convenient expression for calculations, relating $B\rho$ and the electron velocity, is

$$B\rho\,(\text{gauss}\cdot\text{cm}) = 1704.5\,\beta\,(1-\beta^2)^{-1/2}. \tag{3.9}$$

The radius of deflection of a particle in an electrostatic field is dependent on its charge to energy ratio. For the most common case of a cylindrical analyzer, the relation between the energy V of a particle, moving on an average radius ρ, and the voltage V' between the plates of a condenser is given approximately by

$$V' = \frac{2d}{\rho}V, \tag{3.10}$$

where d is the distance between the plates of the condenser.

TABLE 9

Energies and magnetic rigidities of alpha-particles from natural sources used as standards

Isotope	Group of particles	Energy T_α, Mev	Magnetic rigidity $B\rho$ (10^5 G·cm)
Po^{210}	—	5.307 ±0.0026	3.31649±0.0008
Bi^{212} (ThC)	α_1 (70%)	6.0861±0.0024	3.55389±0.0007
	α_0 (23%)	6.0466±0.0027	3.51232±0.0008
Po^{214} (RaC′)	—	7.6802±0.0009	3.99274±0.00022
Po^{212} (ThC′)	—	8.7801±0.004	4.26934±0.0009

TABLE 10

Resonance and threshold energies of protons used as absolute calibration standards

Reaction	Energy (kev), determined by the method of		Remarks
	Electrostatic analysis	magnetic analysis	
$F^{19}(p, \alpha\gamma)O^{16}$	340.4±0.4 483.6±0.3 872.4±0.4	340.5±0.3 — 871.3±0.4	Resonance " "
$Al^{27}(p, \gamma)Si^{28}$	992.4±0.5	990.8±0.2	"
$Ni^{58}(p, \gamma)Cu^{59}$	1424.1±0.7 1843.7±0.9	— —	" "
$C^{13}(p, \gamma)N^{14}$	1747.6±0.9 3237.2±1.6	— —	" "
$Li^{7}(p, n)Be^{7}$	1881.2±0.9	1881.3±0.7	Threshold
$C^{13}(p, \gamma)N^{14}$	3237.2±1.6	—	"
$F^{19}(p, n)Ne^{19}$	4223.2±2.0	—	"

When working with beams of charged particles, the problem of monochromatization of the beam is usually more simple than the measurement of the absolute energy of the particles. Therefore, energy calibration standards are widely used in practice.

Table 9 gives the values of $B\rho$ and the absolute energies of the spectra of some α-radioactive natural isotopes, often used as standard reference points.

The resonance and threshold energies of some reactions, used as energy standards, are given in Table 10.

§ 4. Theory of energy loss of particles in inelastic collisions with atomic electrons

Classical theory of ionization energy losses (Bohr). Suppose a particle with charge ze^* moves with the velocity v relative to a stationary free electron in a trajectory with the impact parameter ρ. If the impact parameter is sufficiently large, it may be assumed that it remains practically unchanged in the collision with the electron; the velocity of the incident particle also remains unchanged. As a result of the collision the electron acquires a recoil momentum $P_\perp$ in a direction perpendicular to the motion of the particle

$$p_\perp = \int_{-\infty}^{\infty} F_\perp \frac{dx}{v} = \frac{z^2e^2\rho}{v}\int_{-\infty}^{\infty}\frac{dx}{(x^2+\rho^2)^{3/2}} = \frac{2ze^2}{\rho v} \qquad (4.1)$$

* Here and in what follows the effective charge of the moving particle is meant, which coincides with the nuclear charge only at velocities much higher than the velocity of electrons of stronger couplings.

and an energy

$$Q = \frac{p_\perp^2}{2m} = \frac{2z^2e^4}{mv^2\rho^2}. \tag{4.2}$$

In a more accurate form (see § 2)

$$Q = \frac{2z^2e^4}{mv^2} \frac{1}{\rho^2 + (b/2)^2}. \tag{4.2a}$$

In (4.2), (4.3), and in all the following expressions m is the electron mass, b is the collision diameter, as determined by (2.22).

Passing through a layer of thickness dx, the particle suffers $2\pi\rho d\rho dx n$ collisions whose impact parameters lie within the limits from ρ to $\rho + d\rho$ (n is the number of electrons in 1 cm^3 of the medium).

Using the impact parameter obtained from (4.1), the number of collisions for which the transferred momentum lies between p and $p + dp$ is found to be $\frac{8\pi n dx z^2e^4 dp}{p^3}$. Dividing by ndx gives the mean number of collisions with the momentum transfer between p and $p + dp$ per electron

$$\sigma(p)dp = \frac{8\pi z^2e^4}{v^2} \frac{dp}{p^3}. \tag{4.3}$$

According to § 1, this is the differential cross section for the transfer of momentum p to the electron.

The differential cross section for the energy loss of the incident particle (energy transfer to a free electron) is

$$d\sigma_{cl}(Q) = \sigma(Q)\,dQ = B_e \frac{dQ}{Q^2}, \tag{4.4}$$

where

$$B_e = \frac{2\pi z^2e^4}{mv^2} \tag{4.5}$$

is analogous to B_n (see § 2) for electron collisions. This expression can also be derived from (2.48), if we set $m_2 = m$, $z_2 = 1$ and $Z_1 = z$.

Substituting (4.5) in (2.52) and using (4.3) and (4.4) we obtain:

$$-\frac{dE}{dx} = \frac{4\pi z^2e^4}{mv^2} n \int \frac{\rho d\rho}{\rho^2 + \left(\frac{b}{2}\right)^2}. \tag{4.6}$$

Integration of (4.6) over all values of ρ from 0 to ∞ leads to an absurd result (infinite energy transfer). Therefore it is necessary to take into account the electron binding in the atoms of the stopping medium. Bohr /149/, using the harmonic oscillator model of the atom, i.e., considering the electrons bound by elastic forces with the eigenfrequencies ν_i ($i = 1, 2, 3...$), showed that the electrons may be regarded as free for small impact parameters (close collisions), if the impact time $\tau \simeq \frac{\rho}{v}$ is shorter than the oscillation period of the electrons $\frac{1}{\nu_i}$. Conversely, for distant collisions $\left(\tau \gg \frac{1}{\nu_i}\right)$, the energy transferred to the bound electrons is considerably smaller than the energy received by free electrons for the same value of ρ. According to Bohr we may assume that for

$$\rho > \rho_s = \frac{1.123v}{\omega_s}$$

the electrons are adiabatically perturbed by the field of the charged particle ($Q = 0$). The quantity ρ_s is called the adiabatic limit.

Integration of (4.6) from 0 to ρ_s with the condition $\rho_s \gg b$ (b being the collision diameter, see (2.22)), gives an expression for the mean energy loss per unit path length, due to electron collisions

$$-\left(\frac{dE}{dx}\right)_e = \frac{4\pi z^2 e^4}{mv^2} n \sum \ln \frac{1{,}123\, Mmv^3}{\omega_i\, ze^2 (M+m)} \text{ erg/cm},$$

where M is the mass of the incident particle; and

$$\omega_i = 2\pi\nu_i.$$

If the oscillation frequencies of the electrons are given by

$$\ln \bar{\omega} = \sum_i f_i \ln \omega_i, \tag{4.7}$$

where f_i are the oscillator strengths corresponding to transitions with frequencies ω_i*, then the expression for the ionization losses is as follows (omitting the index e of dE/dx in the following):

$$-\frac{dE}{dx} = \frac{4\pi z^2 e^4}{mv^2} n \ln \frac{1{,}123\, Mmv^3}{\bar{\omega}\, ze^2 (M+m)}. \tag{4.8}$$

Introducing the relativistic correction /149/, formula (4.8) has the form

$$-\frac{dE}{dx} = \frac{4\pi z^2 e^4}{mv^2} n \left\{ \ln \frac{1{,}123\, Mmv^3}{\bar{\omega}\, ze^2 (M+m)} - \ln (1-\beta^2) - \beta^2 \right\}; \qquad \beta = v/c. \tag{4.9}$$

Formulas (4.8) and (4.9) are known as Bohr's formulas.

Bohr's formulas are used for a limited range of particle velocities and charges. Since the classical methods of calculation are only applicable if inequality (2.36) is fulfilled, a necessary condition for the applicability of Bohr's formulas is

$$v \ll zu_0 = \frac{ze^2}{2\pi\hbar},$$

where ze is the effective charge of the incident particle;

v is the velocity of the electron in the hydrogen atom.

The restriction to small velocities is due to the separation of the impacts into close and distant, requiring that

$$v > u_s, \text{ or } \eta_s = \frac{v}{u_s} > 1; \tag{4.10}$$

where u_s is the orbital velocity of the electron in the atom of the stopping medium. If these conditions are satisfied, the distribution of the energy transfer is determined by the classical theory (Figure 13a).

Strictly speaking, Bohr's formula (4.8) is suitable for calculations,

$$\frac{\alpha}{\eta_0} < 1 \text{ and } \eta_s > \alpha > 1, \tag{4.11}$$

where α is determined by (2.36), and η_s —by (4.10).

Under this condition, the adiabatic limit ρ_s is larger than a certain value of the impact parameter ρ_i, for which the energy Q transferred to the

* The oscillator strength for a given transition is equal to the number of electrons in the corresponding level, divided by the number of electrons Z in the atom.

electron is equal to I_s, which is the energy necessary for removing an electron from the s-orbit $\left(I_s = \frac{\hbar\omega_s}{2\pi} = \frac{mu_s^2}{2} \right)$. Collisions with $\rho < \rho_i$ are "free", since the energy transferred to the electron exceeds I_s, and collisions with $\rho > \rho_i$ belong to the so-called resonance collisions. In the latter case, the field created by the moving particle in the region of the atom is small and practically the same throughout the atom. There is only a small probability of ionization or excitation of the atom in a single collision. The statistical distribution of the transitions caused by resonance collisions should be calculated by the methods of quantum mechanics. However, as was shown by Bohr /12/, expression (4.8) for the total energy loss as the sum of the energies transferred in individual collisions up to Q_s gives a correct result if (4.11) is fulfilled. This is illustrated by Figure 13b,

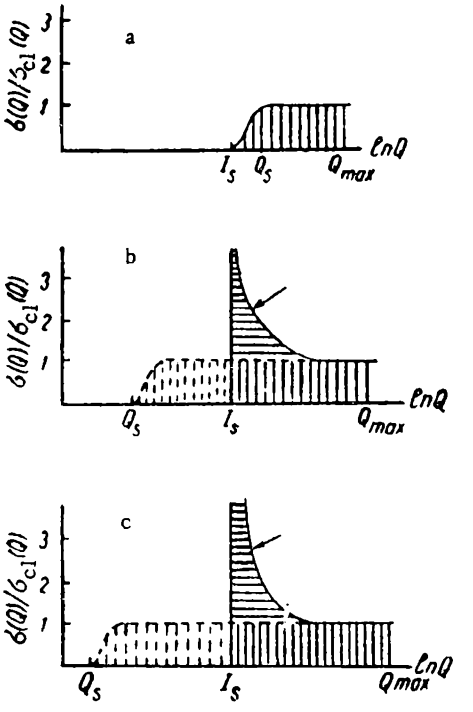

FIGURE 13. Statistical distribution of the energy transfer in collisions with electrons. The arrows indicate the maxima of quantum-mechanical resonances

where the area crosshatched by the horizontal lines showing the energy loss in quantum resonance collisions* is equal to the area crosshatched by the vertical broken lines (the calculation was performed by classical methods).

The contribution of resonance effects to the stopping under condition (4.11) is always smaller than the contribution of the free collisions. This difference increases with the parameter α; when

$$\frac{Zz}{(137\beta)^2} \approx 1,$$

resonance effects are unimportant in the stopping by the K-electrons of a medium with atomic number Z.

* This area conditionally expresses the total cross section of energy transfer in resonance transitions occurring with $\rho > \rho_i$.

If the stopping occurs when

$$\alpha > \eta_s > 1; \left(\frac{\alpha}{\eta_s} > 1\right) \tag{4.12}$$

or

$$\frac{Zz}{(137\beta)^2} > 1,$$

then the energy losses should be evaluated by another expression, proposed by Bohr in 1948 /12/:

$$-\frac{dE}{dx} = B_e n \ln\left[\frac{2^{3/2} m^{3/2} v^4}{h^{1/2} \omega^{3/2} z e^4}\right], \tag{4.13}$$

where B_e is determined as before by (4.5); the notation is the same as in (4.8). In this case $\rho_i > \rho_s$, but collisions with $\rho_i > \rho_s$ will not be adiabatic, since the duration of a collision exceeds $\frac{1}{\nu_s}$. According to Lamb /374/, the ionization when $\rho > \rho_s$ is due to the tearing away of electrons from the atom by the static force field.

A detailed analysis of other possible applications of Bohr's classical theory can be found in /12/ and /401/.

We only point out that Bohr's classical theory can be successfully applied to calculate the ionization energy losses of heavy particles with large effective charges. Let us consider the passage of fission fragments through hydrogen. At the beginning of motion the effective charge z of the fragments is approximately 20, and the velocity is $1.4 \cdot 10^9$ cm/sec /89, 364/, so that $\alpha \approx 3.2$ and $\eta = 6.6$. The ionization energy losses shold be calculated by (4.8). At the end of the range of the fragments, when $z \sim 2$ and $v \sim \sim 2.2 \cdot 10^8$ cm/sec, $\alpha = 2$ and $\eta = 1$, the energy losses are calculated by (4.13).

The ionization energy losses of fast particles with a small effective charge (protons, alpha-particles), as determined by Bohr's formulas, exceed the experimental values considerably. This is due to the fact that with an increase in the velocity of the particles the adiabatic limit Q_s becomes much smaller than I_s (Figure 13c). At the same time, the energy losses in the range of the quantum-mechanical resonance effects are considerably smaller than the energy losses for $Q_s < I_s$, as calculated by the classical theory (the vertical broken lines in Figure 13c).

Quantum-mechanical theory of ionization energy losses, (Bethe, Bloch).

In quantum theory it is also useful to separate the collisions into distant and close. A close collision /92, 480/ is one in which the particle transmits an energy $Q > H$ to the electron; collisions for which $Q < H$ are considered distant. The quantity H should satisfy two conditions: it should be large compared with the binding energy of the electron, and it should be small enough so that the effective collision diameter is larger than the atomic dimensions. In most practical cases, $H \approx 10^4 - 10^5$ ev.

The separation of collisions into close and distant is necessary because in close collisions typical quantum-mechanical effects have to be considered such as the spin and the magnetic moment, as well as the charge exchange effect in collisions of identical particles. In distant collisions, these effects are unimportant in the determination of the energy losses.

If condition (2.42) is satisfied, the ionization energy losses due to distant collisions are calculated by the method of partial waves in the Born approximation of the perturbation theory (see, for example, /64, 71/). According

to calculations performed by Bethe /150/,

$$-\left(\frac{dE}{dx}\right)_{Q<H}=\frac{2\pi z^2e^4}{mv^2}n\left[\ln\frac{2mv^2H}{I^2(1-\beta^2)}-\beta^2\right], \tag{4.14}$$

which is valid both for heavy and for light incident particles.

In (4.14) I is the mean excitation potential of the atoms of the stopping medium, which is determined by an expression similar to (4.7):

$$Z\ln I=\sum f_{nk}\ln I_{nk},$$

where f_{nk} are the oscillator strengths for transitions between the optical levels n and k;

I_{nk} are the energies corresponding to these transitions.

The cross sections for energy losses in close collisions ($H<Q<Q_{max}$) depend on the quantum-mechanical spin and charge-exchange effects.

The corresponding calculations (Bhabha, Massey, Oppenheimer, Snyder and Serber) for heavy particles with spin 0, $\frac{1}{2}$ and 1 led to the following results:

For particles with zero spin (α-particles, π-mesons) the differential cross section for energy transfer (loss) is equal to /152/

$$d\sigma(Q)=d\sigma_{cl}(Q)\left[1-\beta^2\frac{Q}{Q_{max}}\right]\ \text{cm}^2/\text{electron}. \tag{4.15}$$

For particles with spin $\frac{1}{2}$ (protons, μ-mesons)

$$d\sigma(Q)=d\sigma_{cl}(Q)\left[1-\beta^2\frac{Q}{Q_{max}}+\frac{Q}{2E^2}\right],$$

and for particles of spin 1 (deuterons, Li^6 nuclei)

$$d\sigma(Q)=d\sigma_{cl}(Q)\left[\left(1-\beta^2\frac{Q}{Q_{max}}\right)\left(1+\frac{Q}{3Q_c}\right)+\frac{Q}{3E^2}\left(1+\frac{Q^2}{2Q_c}\right)\right].$$

Here $d\sigma_{cl}(Q)$ is the classical cross section for energy transfer to a free electron, given by (4.4);

$E=T+Mc^2$ is the total energy of the incident particle;

$$Q_c=\frac{M^2c^2}{m};$$

Q_{max} is the maximum possible energy transfer in a collision with an electron, which according to the law of conservation, is equal to /152/

$$Q_{max}=Mc^2\frac{\left(\frac{E}{mc^2}\right)^2-1}{\left(\frac{M}{2m}\right)+\left(\frac{m}{2M}\right)+\left(\frac{E}{Mc^2}\right)}. \tag{4.16}$$

The difference in the cross sections appears only in the extreme relativistic case, when the cross section for energy losses for particles with spin 1 exceeds the cross section for losses for particles with spin 1/2 and 0.

For $T\ll\left(\frac{M}{2m}\right)Mc^2$ ($\sim 10^{10}$ ev for μ-mesons, $\sim 10^{12}$ ev for protons) (4.16) is simplified:

$$Q_{max}=\frac{2mv^2}{1-\beta^2}. \tag{4.16a}$$

For $E \gg \left(\frac{M}{m}\right) Mc^2$, as in § 2, $Q_{max} = E$. In this case, the conditions $\frac{Q_{max}}{E} \ll 1$ and $\frac{Q}{Q_c} \ll 1$ are also satisfied, so that the difference in the cross sections, due to the spin effect, disappears, and (4.15) should be used in calculations of energy loss cross sections for all heavy incident particles.

Substitution of (4.15) in (2.52) gives

$$-\left(\frac{dE}{dx}\right)_{Q>H} = \\ = \frac{2\pi z^2 e^4}{mv^2} n \left[\ln \frac{Q_{max}}{H} - \beta^2\right]. \tag{4.17}$$

The mean total energy loss per unit path length is equal to the sum of the losses of close and distant collisions with electrons:

$$-\frac{dE}{dx} = \frac{2\pi z^2 e^4}{mv^2} n \left[\ln \frac{2mv^2 Q_{max}}{I^2(1-\beta^2)} - 2\beta^2\right]. \tag{4.18}$$

Substitution of Q_{max} from (4.16a) leads to the commonly used expression:

$$-\frac{dE}{dx} = \frac{4\pi z^2 e^4}{mv^2} n \left\{\ln\left(\frac{2mv^2}{I}\right) - \ln(1-\beta^2) - \beta^2\right\}. \tag{4.19}$$

Expressions (4.18) and (4.19) are called the Bethe-Bloch formulas for the mean ionization energy losses, $\frac{dE}{dx}$ is the stopping power of the substance for particles of a given kind (see § 5).

As a rule, when determining energy losses, no detailed calculations of $\left(\frac{dE}{dx}\right)_{Q>H}$ (close collisions) are performed. Formula (4.14) is usually applied and instead of H the value of Q_{max}, determined by (4.16a), is used. In fact, since $d\sigma(Q) \sim \frac{1}{Q^2}$ close collisions with large energy transfer are relatively rare. They are important when determining the probable, and not the mean energy losses (see below).

For small values of β, the total contribution of the relativistic terms in (4.19) is equal to $+\beta^4/4$. For $\beta \approx 0.96$ ($E \sim 3Mc^2$), the energy losses are a minimum, consequently, according to (4.19), a continuous logarithmic increase in the losses should be observed. In practice, as we see below, at a certain value of the energy this increase is compensated by a decrease in the losses due to the polarization of the medium.

Expression (4.19) for non-relativistic velocities of the incident particles has the form

$$-\frac{dE}{dx} = \frac{4\pi z^2 e^4}{mv^2} NB = \frac{2\pi z^2 e^4}{T}\left(\frac{M}{m}\right) NB, \tag{4.20}$$

where N is the number of atoms in 1 cm^3 of the stopping medium; M and T are the mass and kinetic energy of the incident particles;

$$B = Z \ln \frac{2mv^2}{I} = Z \ln\left[4\left(\frac{M}{m}\right)\frac{T}{I}\right]; \tag{4.21}$$

B is the stopping coefficient, a dimensionless quantity dependent on the characteristics of the stopping medium.

The logarithmic factor in (4.21) varies from 5 (uranium) to 11 (hydrogen).

Ionization energy losses are the main source of losses, therefore, the Bethe-Bloch formula can be used to calculate the stopping powers of materials for fast charged particles. It is then assumed that the following conditions are fulfilled:

1) The de Broglie wavelength $\frac{\lambda}{2\pi}$ of the incident particle is large in comparison with the collision diameter s, and condition (2.42) for electron collision is of the form:

$$\left.\begin{aligned} &\frac{2\pi ze^2}{hv} = \left(\frac{2\pi Ze^2}{hv}\right)\frac{z}{Z} \ll 1 \\ &\text{or } v > 2zu_0 \end{aligned}\right\}, \qquad (4.22)$$

where ze is the charge of the incident particle;

Z is the atomic number of the stopping medium;

u_0 is the velocity of the hydrogen electron.

2) The velocity of the incident particle is sufficiently large in comparison with the velocities of the electrons in the atoms of the stopping medium, so that

$$T > \frac{M}{m} I_s; \qquad (4.23)$$

where I_s is the ionization energy of the s-electron.

3) The charge of the incident particle is small $\left(\frac{z}{Z} \leqslant 1\right)$ and does not change (no charge exchange).

4) The ratio $\frac{ze}{T}$ is small (the contribution to the energy lossed due to elastic scattering on the nuclei can be neglected, see § 2).

Investigations have proved that the Bethe-Bloch formula (4.19) is satisfactory for the ionization and total losses of protons with energies $T \geqslant$ $\geqslant 1.5$ Mev and of α-particles with energies $T > 5$ Mev, in light materials. At energies close to these limits, as well as in the stopping in heavy materials, it is necessary to take into account the unequal effectiveness of the excitation of different electronic shells (binding effect of the electrons). At high energies, the effects connected with the polarization of the atoms of the stopping medium and the Cerenkov radiation should also be considered.

Expressions (4.9) and (4.19) are the limiting cases of the Bloch formulas /151/, obtained by the generalized quantum-mechanical method of impact parameters. The corresponding expression has the form

$$-\frac{dE}{dx} = \frac{2\pi z^2 e^4}{mv^2} n \left[\ln \frac{mv^2 Q_{max}}{(1-\beta^2) I^2} - \beta^2 + 0{,}423 - \mathrm{Re}\psi\left(i\frac{2\pi ze^2}{hv}\right)\right], \qquad (4.24)$$

where ψ is the logarithmic derivative of the Γ-function and $\mathrm{Re}\psi$ is the real part of ψ.

For

$$\frac{2\pi ze^2}{hv} \gg 1$$

$$\mathrm{Re}\psi\left(i\frac{2\pi ze^2}{hv}\right) \approx \ln \frac{ze2\pi}{hv}$$

and, since $\bar{\omega} = \frac{2\pi I}{h}$, expression (4.24) reduces to Bohr's formula (4.9). When $\frac{2\pi z e^2}{hv} \ll 1$, the Bethe-Bloch formula (4.18) follows directly from (4.24), since for small values of the argument

$$\psi(x) \approx \psi(0) = -0.577.$$

Corrections to the Bethe-Bloch formula, taking into account the binding of the electrons. As was mentioned above, the Bethe-Bloch formula is valid if (4.23) is satisfied, that is, if the velocity of the incident particle is higher than the velocities of the K-electrons of the atoms of the stopping medium. Only in this case all electrons participate equally in the energy absorption and the value of I, in (4.19) and (4.21), is then independent of the energy of the incident particles.

When the velocity decreases to $v \sim v_K$, where v_K is the velocity of the K-electrons of the stopping medium, their contribution to the stopping decreases, and when $v \sim v_L$ that of the L-electrons decreases, and so on.

In order that these conditions will be satisfied the quantity I in the Bethe-Bloch formula should be equal to the mean excitation potential of the atoms of the medium, i.e., they would only depend on the properties of the medium and not on the velocity of the incident particles. It is necessary to introduce the appropriate corrections for the binding effect of the electrons which were calculated in /295, 359, 493, 494/.

Bethe /150, 259/ and Walske /493, 494/ determined the contribution to the stopping from the K-, L-electrons separately. In this case, the corresponding partial stopping coefficients in (4.20) can be expressed according to Walske as follows:

$$B_i(\theta_i, \eta_i) = S_i(\theta_i) \ln \frac{4n_i^2 \eta_i}{\lambda_i} - C_i(\theta_i, \eta_i), \qquad (4.25)$$

where

$$S_i = \frac{N_i}{2}\left[1 + f_i(\theta_i)\right];$$

N_i is the number of electrons in the i-th shell of the stopping atom;

f_i is the oscillator strength for all optical electron transitions from the i-th shell to the continuous spectrum or to the vacant levels of the discrete spectrum.

In (4.25) the parameter θ_i is the observed ionization energy of the electrons of the i-th shell in units of $Z_i^* \mathrm{Ry}/n_i^2$ (Z_i^* is the effective charge of the nucleus at the i-th shell, n_i is the principal quantum number and Ry = = 13.6 ev). Thus, for example, for the electrons of the K-shell

$$\theta_K = \frac{E_K}{(Z - 0.3)\,\mathrm{Ry}}.$$

According to /494/, the quantities θ_K and θ_L may be determined from the curves given in Figure 14.

The parameter η_i determines the energy of the incident particle, expressed in units of MZ_i^{*2} Ry/m, where M is the mass of the incident particle, and m is the mass of the electron. Its value depends on the ratio of the velocity of the incident particle to the velocity of the electrons in the i-th shell:

$$\eta_i = \frac{m}{M}\left(\frac{E}{Z_i^{*2}\mathrm{Ry}}\right) = \frac{mv^2}{2Z_i^{*2}\,\mathrm{Ry}} = \left(\frac{v}{u_0 Z_i^*}\right)^2,$$

where $u_0 = \frac{2\pi e^2}{h}$ is the Bohr electron velocity.

Finally, the parameter λ_i represents the mean excitation energy I_i of the i-th shell in units of $Z_i^{*2}\,\mathrm{Ry}/n_i^2$

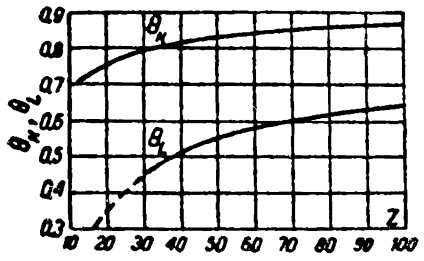

FIGURE 14. Theoretical dependence of the screening parameters θ_K and θ_L on the nuclear charge /494/

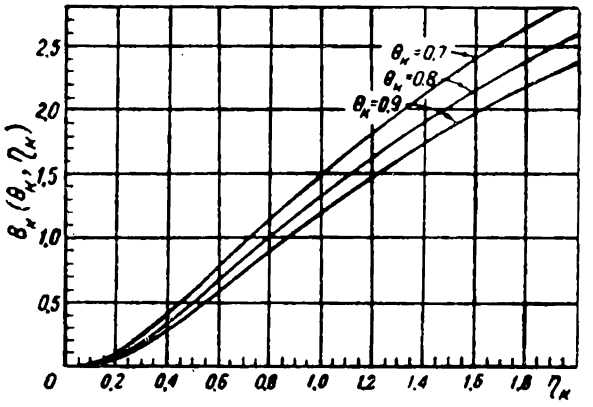

FIGURE 15. Theoretical dependence of the stopping coefficient on the parameter η_K /493/

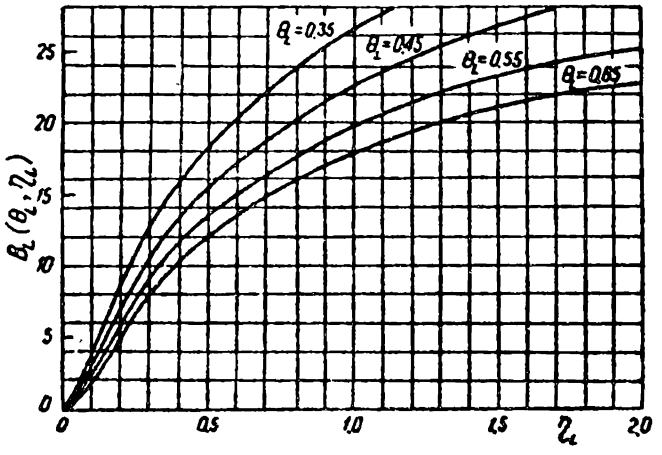

FIGURE 16. Theoretical dependence of the stopping coefficient B_L on the parameter η_L /494/

Figures 15 and 16 give the graphs of

$$B_K(\theta_K, \eta_K) \text{ and } B_L(\theta_L, \eta_L),$$

obtained by /493, 494/, in which hydrogen-like atomic wave functions were applied.

The stopping coefficient B, appearing in (4.20) is determined by the sum of B_i according to expression (4.25) and summed over all the shells. This

TABLE 11

Values of the stopping coefficients $B_K(\theta_K, \eta_K)$

η_K	$\theta_K=0.7$	$\theta_K=0.8$	$\theta_K=0.9$
1.50	2.249	2.031	1.857
1.75	2.573	2.337	2.142
2.00	2.851	2.595	2.385
2.50	3.366	3.077	2.841
3.50	4.122	3.782	3.508
5.0	4.931	4.537	4.221
10.0	6.406	5.900	5.496

can also be written according to the definition of the parameters η and λ, in the form

$$B = \sum_i B_i(\theta_i, \eta_i) = \sum_i \left[S_i(\theta) \ln \frac{2mv^2}{I_i} - C_i(\theta_i, \eta_i) \right].$$

Since $\sum S_i(\theta) = Z$,

$$B = Z \ln \frac{2mv^2}{I} - \sum C_i(\theta_i, \eta_i), \qquad (4.26)$$

where

$$Z \ln I = \sum_i S_i(\theta_i) \ln I_i = \sum_i S_i(\theta_i) \ln \left(\frac{Z_i^{*2} \lambda_i \mathrm{Ry}}{n_i^2} \right).$$

It is convenient to use the coefficient B in the form of (4.26), as the mean excitation potential I is independent of the velocity of the incident particles,

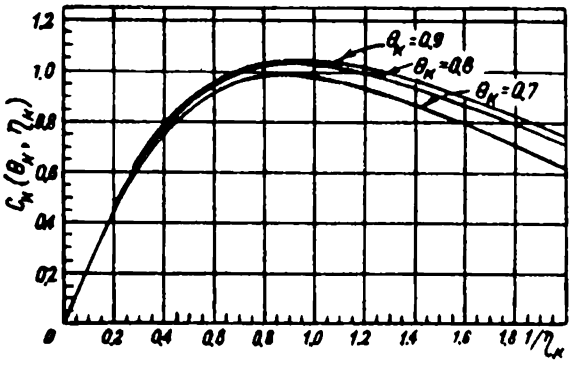

FIGURE 17. Dependence of the corrections C_K on the parameter η_K, according to Walske /493/

even if condition (4.23) is not satisfied. The reduction of the stopping power of the electrons of the i-th shell is given by the quantity C_i.

Using the calculated curves of Figure 17 or the data of Table 11, C_K may be determined for values of η_K from 0.5 to 10 (20) for various θ_K. The calculated results with $\theta_K \approx 0.7$ are suitable for light elements (from carbon to aluminum),

with $\theta_K \approx 0.8$ — for elements with intermediate values of Z ($Z \sim 30$), and with $\theta_K \approx 0.9$ — for heavy elements ($Z \sim 80$).

TABLE 12

Values of $S_K(\theta_K)$ and $T_K(\theta_K)$

θ_K	$S_K(\theta_K)$	$T_K(\theta_K)$
0.70	1.8133	2.4603
0.75	1.7223	2.4044
0.80	1.6457	2.3462
0.85	1.5807	2.2868
0.90	1.5250	2.2273

TABLE 13

Values of the coefficients in (4.28)

θ_K	U_K	V_K	W_K
0.70	2.0662	7.3246	−45.0 (approx-
0.75	2.0999	7.3194	imately for all θ_K)
0.80	2.1196	7.3191	
0.85	2.1290	7.3218	
0.90	2.1309	7.3263	

In order to calculate the corrections C_K for low-energy particles ($\eta_K < 0.5$) it is necessary to use an asymptotic expression

$$B_K(\theta_K, \eta_K) = S_K(\theta_K) \ln \eta_K + T_K(\theta_K) - C_K(\theta_K, \eta_K). \quad (4.27)$$

The values of B_K are determined from Figure 15, and the values of S_K and T_K are given in Table 12. For $\eta_K > 10$, the corrections C_K are found by means of (see also Table 13):

$$C_K(\theta_K, \eta_K) = U_K(\theta_K)\,\eta_K^{-1} + V_K(\theta_K)\,\eta_K^{-2} + W_K(\theta_K)\,\eta_K^{-3} + \cdots \quad (4.28)$$

The hydrogen-like wave functions used in the calculation of B_K and C_K are justified to a certain extent by the small screening of the K-electrons

TABLE 14

Values of the corrections $C_L(\theta_L, \eta_L)$ according to Walske /494/

θ_L \ η_L	1	3.5	10	25	100	1000
0.35	1.6934	0.4917	0.1619	0.06235	0.01516	0.001505
0.45	2.0298	0.5950	0.1988	0.07719	0.01888	0.001877
0.55	2.1358	0.6268	0.2100	0.08171	0.02001	0.001991
0.65	2.1519	0.6312	0.2116	0.08232	0.02016	0.002006

by the external electrons. However, the calculation of C_L, and moreover, of C_M, introduces an error which is large for strong screening. Moreover, the use of Hartree's functions is not always possible, and involves laborious calculations.

TABLE 15

Values of the stopping coefficient B_L

η_L \ θ_L	0.35	0.45	0.55	0.65
1.0	26.52	22.48	19.80	17.89
1.1	27.70	23.48	20.70	18.71
1.25	29.32	24.86	21.95	19.87
1.50	31.48	26.68	23.56	21.36
1.75	32.89	27.79	24.51	22.20
2.00	34.09	28.74	25.31	22.90
2.5	36.88	31.09	27.40	22.84
3.5	40.34	33.87	29.81	27.01

The values of the contribution of the L-electrons to the stopping coefficient B_L and to the corrections C_L were obtained by Walske /494/ using hydrogen-like wave functions. The results are plotted in Figure 9 and in Tables 14—17. These tables are used in the same way as that for the K-shell.

TABLE 16

Values of the coefficients S_L, T_L and U_L in (4.29)

θ_L	S_L	T_L	U_L
0.35	10.0371	28.1449	−1.5032
0.45	7.9116	24.4501	−1.8756
0.55	6.7454	21.9061	−1.9890
0.65	6.0345	20.0154	−2.0040

TABLE 17

Values of the coefficients U_L, M_L, N_L, O_L in (4.30)

θ_L	U_L	M_L	N_L	O_L
0.35	1.503	1.543	−4.00	+4.43
0.45	1.876	1.506	−4.00	+4.43
0.55	1.989	1.498	−4.00	+4.43
0.65	2.004	1.500	−4.00	+4.43

The calculated values of the coefficients B_L and of the corrections C_L for some values of θ_L and η_L are given in Tables 14 and 15. For relatively low energies of the incident particles, $\eta_L < 1$ (3.5), the contribution of the L-electrons to the stopping coefficient can be calculated by the asymptotic formula

$$B_L(\theta_L, \eta_L) = S_L(\theta_L) \ln \eta_L + T_L(\theta_L) + U_L \eta_L^{-1}, \tag{4.29}$$

the numerical values of S_L, T_L and U_L are given in Table 16.

For $\eta_L > 3.5$ (10), the corrections C_L are given by

$$C_L(\theta_L, \eta_L) = U_L \eta_L^{-1} + M_L \eta_L^{-2} + N_L \eta_L^{-3} + O_L \eta_L^{-4}. \tag{4.30}$$

The coefficients U_L, M_L, N_L and O_L are given in Table 17.

In order to form an idea on the order of magnitude of the corrections to (4.20), Table 18 shows the total corrections (in percent of $\frac{dE}{dx}$ calculated

TABLE 18

Corrections (%) to $\frac{dE}{dx}$ for the binding effect of the K- and L-electrons, calculated by (4.20)

T_p, Mev	Zinc $Z = 30$	Tin $Z = 50$	Ytterbium $Z = 70$	Thorium $Z = 90$
1	+4.3*	+14*	+21**	+26**
5	−3.9*	−1.4*	+1.4*	+2.6**
10	−3.0	−2.3	−0.7*	+0.4**
20	−1.7	−2.0	−1.5*	−0.9*
50	−0.9	−1.2	−1.3	−1.1*
100	−0.4	−0.7	−0.8	−0.9
200	−0.2	−0.4	−0.5	−0.6
500	−0.07	−0.14	−0.2	−0.3
1000	−0.03	−0.06	−0.09	−0.13

* The value of C_K is negative

** The values of C_K and C_L are negative

by (4.20)) for the binding effect of the K-and L-electrons in various elements and for various proton energies. Since the first two terms in the asymptotic expression (4.72) can be written as $S_K \ln\left(\eta_K \frac{T_K}{S_K}\right)$, it is obvious that for $\eta_K < \exp\left(-\frac{T_K}{S_K}\right)$ the value of C_K is negative (B_K is always positive). For this reason, C_L may be negative (see Table 18).

It follows from Table 18 that the total correction $(C_K + C_L)$ reduces the calculated values of the energy losses in zinc ($Z = 30$) by $\sim 4\%$ for $T_p = 5$ Mev, by 0.2% for $T_p = 260$ Mev, and by 0.07% for $T_p = 500$ Mev.

For beryllium, the introduction of the corrections C_K reduces the energy losses by 8% for $T_p = 0.6$ Mev, by 3% for $T_p = 1$ Mev, and by 1.5% for $T_p = 2$ Mev.

The correction C_L for light elements can be approximately calculated by expression (4.30) for large η_L:

$$C_L \cong \frac{A}{T_p\,(\text{Mev})}. \tag{4.31}$$

For aluminum, for example, $A = 1.5$ for $T_p > 2$ Mev /171/, which is in agreement with Walske's theory.

The maximum value of the correction C_L for aluminum is attained at the energy $T_p = 4.6$ Mev. C_L has a maximum value at $T_p \approx 0{,}2$—$0{,}3$ Mev.

The mean potentials of the atoms of the stopping medium. The mean excitation potential of the atoms of the stopping medium, appearing in the Bethe-Bloch formula, cannot be exactly evaluated, with the exception of the lightest elements (hydrogen, helium).

Bloch /151/, using the statistical Thomas-Fermi model, showed that the dependence of I on the atomic number should, at least for heavy materials, have the form

$$I = I_0 Z, \tag{4.32}$$

where I_0 is an experimental constant approximately equal to the Rydberg constant (13.5 ev).

In the theory of ionization energy losses, I is a parameter representing the properties of the stopping medium, but is independent of the velocity of the passing particles. Thus assuming the theory to be correct and taking into account the corrections for the electron binding and the polarization, then all the experiments for determining $\frac{dE}{dx}$ and R should lead to the same value of I for a given medium, independent of the energy and kind of particles used. If the experiment shows a dependence of I on the energy this will indicate fundamental errors in the theory described above. Table 19 gives all the experimental data on I available at present.

Examination of Table 19 shows that the data on I are contradictory and are not always in agreement with the Bloch relation. There is, for example, a tendency for a decrease in the experimental values of I with increasing energy of the incident particles. The introduction of corrections C_l for the electron binding reduces this effect, but does not remove the discrepancies completely. Thus, there are strong indications /171, 492/ that either the experiments are not sufficiently accurate, or that some of the corrections to the experimental values of $\frac{dE}{dx}$ and R, used for the determination of I, are not applied (for further details, see § 6).

TABLE 19

Experimental values of the mean excitation potentials of the atoms of stopping media

Element	Experimental value of I, ev	$I_0 = \frac{I}{Z}$	Method of determination of I*	Particle energy T_p, Mev	Reference
$_1$H	15.6	15.6	S_m (I_{Al} = 150)	340	/ 58/
	15	15	S_m (I_{Cu} =305)	635	/49/
	18.0	18.0	S_m (I_{Al} = 150)	270	/476/
$_2$He	44	22	—	2	/137/
$_3$Li	34.0	11.3	S_m (I_{Al} = 150)	340	/158/
$_4$Be	64±5	16	S_m		/383/
	59.0	14.75	R_l	339.7	/384/
	64	16.0	S_m (I_{Al} = 166,4)	19.8	/155/
	63.4±0.5	15.8	R, multiple scattering taken into account	6—18	/156/
	61±6	15.3	S_m (I_{Cu} =305)	635	/158/
	60.4	15.1	S_m (I_{Al} = 150)	340	/158/
$_6$C	69.7	11.6	S_m (I_{Al} = 150)	270	/476/
	85±8	14.2	S_m (I_{Cu} =305)	635	/49/
	74.4	12.91	R_l	339.7	/384/
	76.4	12.7	S_m (I_{Al} = 150)	340	/158/
$_7$N	75.9	10.85	S_m (I_{Al} = 150)	270	/476/
air	80.5	11.5	R_l	5—8	/359/
(Z=7.22)	94	13.5	—	2	/447/
$_8$O	87.6	11	S_m (I_{Al} = 150)	270	/476/
$_{13}$Al	155±3	12	R	—	/456/
	172±5	12.2	R	35—120	/161/
	166.4	12.8	$\frac{dE}{dx}$	19.8	/155/
	150	11.5	S_m (I_{Al} = 150)	340	/158/
	150.3	11.56	R_l	1.5—4	/502/
	167	12.82	R_n	333.7	/374/
	166.45±1	12.8	R_n, multiple scattering taken into account	18	/291/
	163	12.6	R	6—18	/156/
	163±3	12.6	$\frac{dE}{dx}$ (absolute)	6—18	/171/
$_{26}$Fe	328.8	12.6	S_m (I_{Al} = 166.4)	18	/216, 451/
	273±22	10.5	S_m (I_{Al} = 305)	19.8	/155/
	243	9.3	S_m (I_{Al} = 150)	635	/49/
$_{28}$Ni	363.18	13.0	$\frac{dE}{dx}$	340	/158/
$_{29}$Cu	323	11.5	R	18	/216/
	370	12.2	S_m	752	/451/
	377.5±8	13.0	$\frac{dE}{dx}$	35—120	/177/
	309.9±3	10.7	R_l	18	/161/
	366.0	12.6	S_m (I_{Al} = 166.4)	337.9	/216, 451/
	375.6±20	12.9	R_n, multiple scattering taken into account	19.8	/384/
	305±10	10.5	S_m (I_{Al} = 305)	6—18	/155/
	278	9.5	S_m (I_{Al} = 15)	635	/156/
Rh	645±45	14.6	$\frac{dE}{dx}$	340	/49/
$_{47}$Ag	428	8.9	S_m (I_{Al} = 150)	18	/216, 451/
				340	/158/

TABLE 19 (continued)

Element	Experimental value of I, ev	$I_0 = \frac{I}{Z}$	Method of determination of I*	Particle energy T_p, mev	Reference
$_{47}$Ag	587.0	12.5	S_m ($I_{Al} = 166.4$)	19.8	/155/
	585±40	12.5	R_n, multiple scattering was taken into account	6—18	/156/
	659±50	14.0	$\frac{dE}{dx}$	18	/216, 451/
$_{50}$Sn	708±59	14.2	$\frac{dE}{dx}$	18	/216, 451/
	479	9.2	S_m ($I_{Al} = 150$)	340	/158/
$_{73}$Ta	962±54	13.2	$\frac{dE}{dx}$	18	/216, 451/
$_{74}$W	920.5	12.4	S_m ($I_{Al} = 166.4$)	19.8	/155/
	680±50	9.2	S_m ($I_{Cu} = 305$)	635	/49/
	656	9.2	S_m ($I_{Al} = 150$)	340	/158/
$_{79}$Au	1136±100	14.4	$\frac{dE}{dx}$	18	/216, 451/
	997	12.7	$\frac{dE}{dx}$	19.8	/155/
	1037±100	13.1	R_n, multiple scattering taken into account	6—18	/156/
$_{82}$Pb	810.7±12	9.9	R_l	340	/384/
	970	11.8	R_l	35—120	/161/
	1070	13.0	S_m ($I_{Al} = 166.4$)	19.8	/155/
	758	8.6	S_m ($I_{Al} = 150$)	340	/158/
	826	10.1	R	752	/510/
$_{92}$U	821	8.8	S_m ($I_{Al} = 150$)	340	/158/
	917	10	R	752	/177/

* In this column S_m is the mean potential, determined from experimental data on the relative mass stopping power of the medium, dE/dx was determined from absolute measurements of the stopping power, R was determined from measurements of the mean range, R_l was determined from measurements of the extrapolated range with respect to ionization, R_n was determined from the transmission curve; see § 5—6.

Another explanation to the variation of I with velocity is that in actuality I is not fully velocity-independent. In this connection, Lindhard and Scharff /360/, using statistical arguments, proposed for the calculation of the ionization energy losses a universal function $L(x)$, equal (see § 5) to the stopping power of one electron

$$L(x) = \frac{mv^2}{4\pi z^2 e^4}\left(\frac{1}{NZ}\right)\left(-\frac{dE}{dx}\right). \qquad (4.33)$$

Here x is a dimensionless parameter (assuming that the atoms of the stopping medium are sufficiently well represented by the Thomas-Fermi model), depending only on the velocity v of the particles and on the atomic number of the stopping medium:

$$x = \frac{1}{Z}\left(\frac{v}{u_0}\right)^2, \quad \left(u_0 = \frac{2\pi e^2}{h}\right). \qquad (4.34)$$

The function $L(x)$ should behave as $\ln x$ for large values of the parameter x ($x > 100$), i.e., as the logarithmic term in the Bethe-Bloch formula.

The function $L(x)$, which is empirically determined, has a sufficiently universal character. For all charged particles and energies, the data on ionization losses, expressed as a dependence of $L(x)$ on the parameter x, should fit along a curve; only slight deviations from this curve are allowed

for light stopping elements, which are explained by deviations from the Thomas-Fermi model.

From experimental data obtained until 1953, Lindhard and Scharff /360/ established the analytic form of $L(x)$:

$$L(x) = 1.36x^{1/2} - 0.016x^{3/2}. \qquad (4.35)$$

The use of this empirical function $L(x)$ eliminates the need to introduce the corrections C_i in calculating ionization energy losses.

Definite conclusions concerning the dependence of I on the velocity of the particles, and on whether the function $L(x)$ should be used can only be made on the basis of experimental results.

Polarization effect (density effect). At high energies of the incident particles, the density and the dielectric properties of the stopping medium influence the ionization energy losses. Thus, the polarization effect provides a partial compensation for the unlimited increase of the energy losses according to the Bethe-Bloch formula for $\beta \to 1$. In the theory which neglects this effect, the atoms of the stopping medium are considered separately. The energy losses are calculated as resulting from the independent interactions of the particle with the individual atoms. This is only correct for close collisions, in which the impact parameter is equal to, or smaller than, the atomic dimensions. However, in distant collisions (the impact parameter exceeds the atomic dimensions) the influence of the electric field of the incident particle is reduced due to the polarization of the intermediate atoms of the medium. This reduces the energy losses and the reduction depends on the dispersion properties of the medium, but not on the identity of the passing particles. Since in dense media the importance of distant collisions increases with increasing velocity of the particles, the corrections for the polarization should also increase.

In the early works of Tamm and Frank /106/ dealing with the Vavilov-Cerenkov effect (see § 9), it was already noted that in distant collisions the macroscopic properties of the medium are significant. Fermi /242/ made the first theoretical investigation of the effects of the density of the medium. He used the simplified assumption that the quasi-elastic binding of the electrons is represented by oscillations with a single eigenfrequency, and the energy lost by the particle is transferred to the oscillators. Calculations showed that the energy losses depend on the density of the electrons in the medium and on its dielectric properties. The maximum effect is shown for $v > c/\sqrt{\varepsilon}$, where $\varepsilon = 1 + \frac{4\pi ne^2}{mv^2}$ is the dielectric constant; the energy losses then tend to a finite limit, independent of the particle energy.

In the works of Wick /497/, Halpern and Hall /286/, Fermi's calculations were generalized to the case of an arbitrary number of dispersion oscillators, i.e., they considered the dependence of the dielectric constant ε on a large number of eigenfrequencies. The influence of the conduction electrons was also taken into account. The allowance for the dependence of $\varepsilon(\nu_i)$ led to important refinements. Thus, contrary to Fermi's calculations, the density effect was found to be larger for water than for lead; the saturation of the ionization losses is weaker than what follows from Fermi's calculations, and so on.

The most comprehensive calculations of the density effect were carried out by Swenheimer /446/*. The main results of these calculations are given below.

The correction δ for the density effect is determined from

$$\Delta\left(\frac{dE}{dx}\right) = \frac{2\pi n e^4}{mv^2}\delta, \tag{4.36}$$

where

$$\delta = \sum f_i \ln\left(\frac{l_i^2 + l^2}{\nu_i^2}\right) - l^2(1-\beta^2). \tag{4.37}$$

Here f_i is the oscillator strength for transitions with frequencies ν_i; is measured in units of the plasma frequency $\left(\frac{ne^2}{\pi m}\right)^{1/2}$;

n is the number of electrons per 1 cm^3;

$l_i = (\nu_i + f_i)^{1/2}$;

l is determined from

$$\frac{1}{\beta^2} - 1 = \sum \frac{f_i}{\nu_i^2 + l^2}. \tag{4.38}$$

At a certain velocity $\beta = \beta_0$, $l = 0$, and then

$$\frac{1}{\beta_0^2} = 1 + \sum \frac{f_i}{\nu_i^2} = \varepsilon$$

(ε is the static dielectric constant).

For $\beta < \beta_0$, the corrections for the density effect vanish. This is only correct if the experimental values of I, which already include the correction for the density effect at low particle energies, are used in the calculations of the energy losses by the Bethe formula. If, however, I is determined from spectral data on the frequency and energy of the optical transitions, then the corrections for the density are also important at low energies. For example, Sternheimer determined the frequencies ν_i from the ionization potentials of the electrons of the K-, L, etc, shells, and assumed f_i equal to the occupation numbers of the corresponding shells divided by Z. The calculated values of I were then 30—40% lower than the experimental values, which is due to the density and polarization.

When $\beta \ll \beta_0$, and $l = 0$, it follows from (4.37) that

$$\delta = \sum_i f_i \ln \frac{l_i^2}{\nu_i^2} = \sum_i f_i \ln\left(1 + \frac{f_i}{\nu_i^2}\right). \tag{4.39}$$

For a medium whose dispersion properties are represented by a single type of oscillators, expression (4.39) is simplified:

$$\delta = \ln\left(1 + \frac{1}{\nu_i^2}\right) = \ln\varepsilon,$$

which is the same as the result obtained by Fermi /242/.

An approximate analytic expression for δ can be written in the form /446/

$$\left.\begin{aligned} \delta &= 4.606X + C + a(X_1 - X)^r, \quad (X_0 < X < X_1) \\ \delta &= 4.606X + C, \qquad\qquad\qquad (X > X_1) \end{aligned}\right\}, \tag{4.40}$$

* See also the works of Budini and Taffara /211/, Avak'yants /11/ and Shakhbazyan /131/.

where $X = \log_{10}\left(\frac{p}{Mc}\right)$;

p is the momentum;

M is the mass of the charged particles;

a, r and X_1 are constants characteristic of the medium;

X_0 is the value of X, below which $\delta = 0$;

$$C = -2\ln(I/h\nu_p) - 1. \qquad (4.41)$$

Values of C, a, r, X, and X_0 for various substances are given in Table 20 /446/.

TABLE 20

Calculated ionization potentials (Ry) and coefficients in (4.40) and (4.42) according to Sternheimer /446/

Medium	I	G	$-C$	a	m	X_1	X_0
Lithium, Li	2.87	0.0664	3.07	0.374	3.05	2	−0.05
Beryllium, Be	4.71	0.0681	2.83	0.413	2.82	2	−0.10
Graphite,	5.74	0.0768	3.22	0.531	2.63	2	−0.05
Magnesium, Mg	11.5	0.0758	4.54	0.0938	3.56	3	0.10
Aluminum, Al	12.0	0.0740	4.21	0.0906	3.51	3	0.05
Iron, Fe	24.8	0.0715	4.62	0.127	3.29	3	0.10
Copper, Cu	27.7	0.0701	4.74	0.119	3.38	3	0.20
Silver, Ag	48.5	0.669	5.75	0.251	2.88	3	0.20
Tin, Sn	52.1	0.0647	6.28	0.104	2.52	3	0.20
Tungsten, W	72.9	0.0618	6.03	0.0283	3.91	4	0.30
Gold, Au	83.5	0.0615	6.31	0.0436	3.62	4	0.30
Lead, Pb	86.8	0.0608	6.93	0.0652	3.41	4	0.40
Uranium, U	97.4	0.0594	6.69	0.0652	3.37	4	0.30
Anthracene	4.94	0.0810	3.11	0.420	2.86	2	0.11
Stilbene	4.81	0.0818	3.12	0.423	2.86	2	0.12
Polystyrene	4.69	0.0826	3.15	0.429	2.85	2	0.13
Polyethylene	4.04	0.0876	2.94	0.393	2.86	2	0.12
Lucite	5.08	0.0829	3.21	0.456	2.78	2	0.14
Toluene	4.58	0.0834	3.30	0.454	2.83	2	0.17
Xylene	4.50	0.0839	3.25	0.444	2.84	2	0.16
Water, H_2O	5.45	0.0853	3.47	0.519	2.69	2	0.23
Silver chloride, AgCl	36.1	0.0686	5.77	0.177	4.21	4	0.33
Silver bromide, AgBr	42.2	0.0671	5.95	0.0235	4.03	4	0.30
Emulsion	27.4	0.0698	5.55	0.0220	4.01	4	0.23
Lithium iodide, LiI	46.3	0.0643	6.66	0.525	2.32	3	0.08
Sodium iodide, NaI	41.3	0.0656	6.49	0.452	2.44	3	0.18
Hydrogen, H_2	1.40	0.1524	9.50	0.505	4.72	3	1.85
Helium, He	3.24	0.0767	11.18	2.13	3.22	3	2.21
Nitrogen, N_2	6.69	0.0768	10.68	0.125	3.72	4	1.86
Oxygen, O_2	7.65	0.0768	10.80	0.130	3.72	4	1.90
Neon, Ne	9.56	0.0761	11.72	0.258	3.18	4	2.14
Argon, A	16.8	0.0692	12.27	0.0255	4.36	5	2.02
Krypton, Kr	36.3	0.0661	13.12	0.0771	3.57	5	2.12
Xenon, Xe	55.7	0.0632	13.57	0.150	3.07	5	1.90
Methane, CH_4	3.27	0.0958	9.56	0.0552	4.22	4	1.55
Ethylene, $(CH_2)_2$	4.04	0.0876	9.52	0.0700	3.94	4	1.54
Acetylene, $(CH)_2$	4.69	0.0826	9.95	0.0841	3.91	4	1.62
Carbon dioxide, CO_2	7.08	0.0768	10.32	0.0865	4.03	4	1.72

The experimental values of I, determined by Coldwell, Sachs and Richardson /216, 451/ (see Table 19) were used in the calculation. The coefficients are given for gases under normal pressure. If the gases are used at P atmospheres, then we have the correction factor for $\delta_p(p) = \delta_1(pP^{1/2})$.

Theoretical values of the ionization energy losses for fast protons. The Bethe-Bloch formula, including the corrections considered above $C = \sum C_i$ for the electron binding and δ for the density effect, can be written

in a form convenient for calculations

$$-\frac{1}{\rho}\frac{dE}{dx}\left(\frac{\text{Mev}\cdot\text{cm}^2}{\text{g}}\right)=\frac{Gz^2}{\beta^2}\left[\ln\frac{2mv^2Q_{max}}{(1-\beta)^2I^2}-2\beta^2-\delta-\frac{2C}{Z}\right], \qquad (4.42)$$

where $G=0.1536\frac{Z}{A}$ (the values of G for various substances are given in Table 20);

ρ is the density of the stopping medium, g/cm^3;

Z and A are the atomic charge and mass number of the atoms of the medium;

z and $v=\beta c$ are the charge and velocity of the passing particle;

Q_{max} is the maximum energy transferred to the electron, as determined by (4.16).

The accuracy of the calculations obtained by formula (4.42) depends mainly on the accuracy of the values of I, and of the corrections C and δ. Substituting in (4.42) the overestimated values of I lowers the values of $\frac{dE}{dx}$, and conversely, neglecting the corrections C and δ gives too large values of $\frac{dE}{dx}$. The results obtained by Sternheimer /447/ for protons with $T_p > 2$ Mev are represented by the solid curves in Figures 18 — 23. The following values of the mean ionization potentials were used: $I_{(Be)}=64$ ev, $I_{(C)}=78$ ev, $I_{(Al)}=166$ ev, $I_{(Cu)}=371$ ev, $I_{(Pb)}=1070$ ev, $I_{air}=94$ ev. They were the average values of I found in /155, 156/ (see Table 19).

The density corrections were calculated by the method described above (see also Table 20), and the binding corrections of the K-and L-electrons were obtained from Walske's calculations (for beryllium, carbon and air only the C_K corrections were introduced); the C_L corrections for these media were neglected.

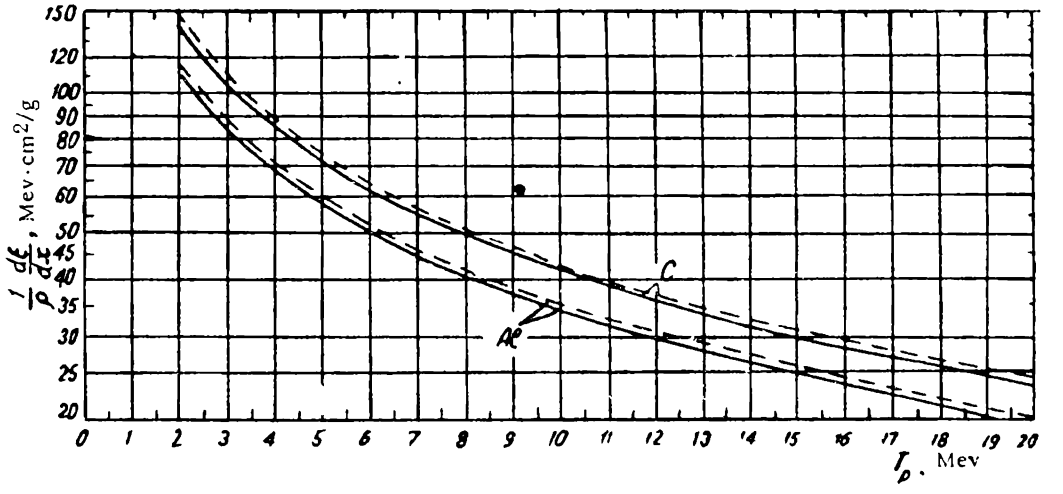

FIGURE 18. Mass stopping power of carbon and aluminum for protons /447/; $T_p = 0-20$ Mev

The results of Sternheimer's calculations differ somewhat from the results obtained earlier by Smith /449/, Aron et al. /137/ and Rich et al. /432/, particularly at high proton energies. The difference is due to two reasons:

1) the values of I, used by Sternheimer, are larger than the corresponding values of I, used in /449, 137, 432/*, which leads to a decrease in the values of $\frac{dE}{dx}$, and to an increase in R for the same energy;

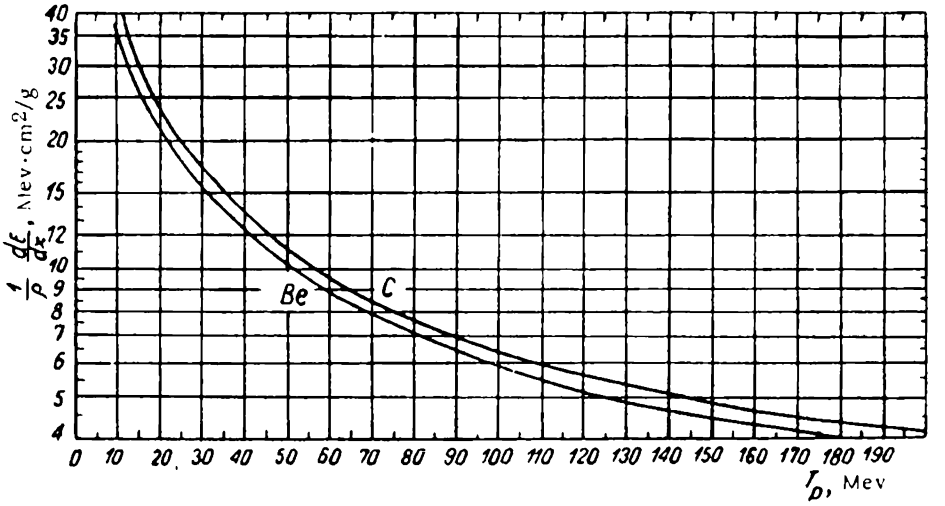

FIGURE 19. Mass stopping power of carbon and beryllium for protons /447/; $T_p = 0-200$ Mev

2) Sternheimer considered the density effect which further decreases $\frac{dE}{dx}$ and increases R in the range $T_p > 10^9$ ev.

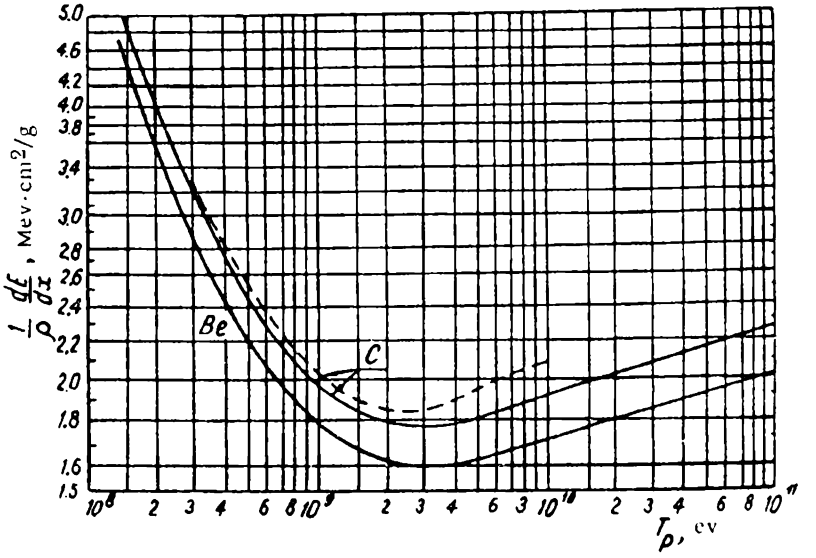

FIGURE 20. Mass stopping power of carbon and beryllium for protons /447/; $T_p = 10^8$ ev $- 10^{11}$ ev

* In his calculations, Smith /449/ assumed $I_{(Al)} = 150$ ev, $I_{(air)} = 80.5$ ev. The authors of /137, 432/, using the experimental data of Wilson /502/, took the constant in Bloch's relation (432) as equal to 11.5 ev.

The character of the differences and their magnitudes can be seen in Figures 18, 20, 21 — 23, in which the broken curves represent the results

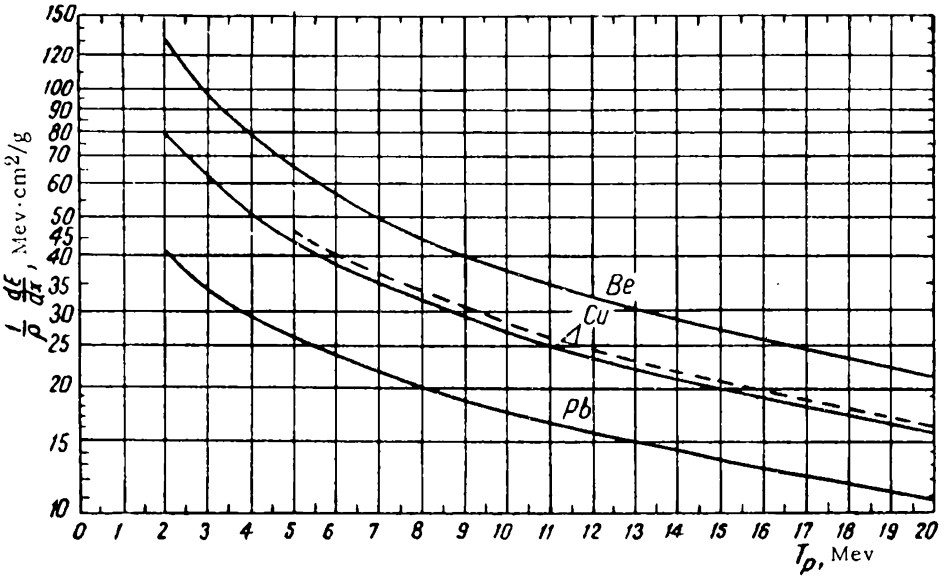

FIGURE 21. Mass stopping power of beryllium, copper and lead for protons /447/; $T_p = 0—20$ Mev

of Rich and Madey /432/; the values of $\frac{dE}{dx}$ for deuterium, hydrogen, and air (Figures 24 — 27) are also taken from /432/.

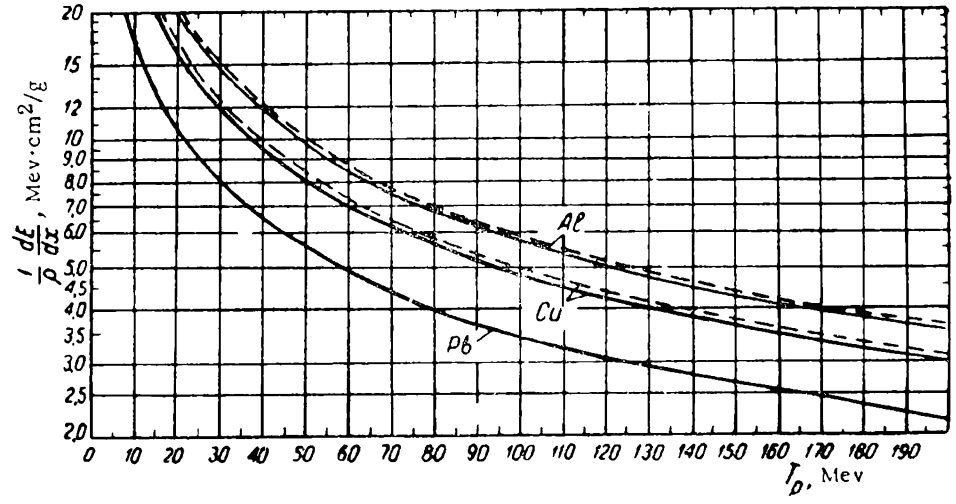

FIGURE 22. Mass stopping power of aluminum, copper and lead for protons /447/; $T_p = 0—200$ Mev

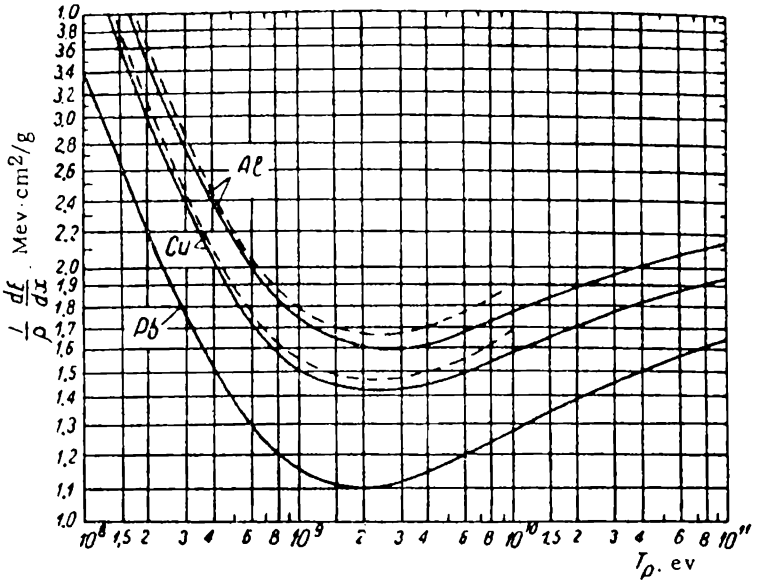

FIGURE 23. Mass stopping power of aluminum, copper and lead for protons; $T_p = 10^8$ ev -10^{11} ev

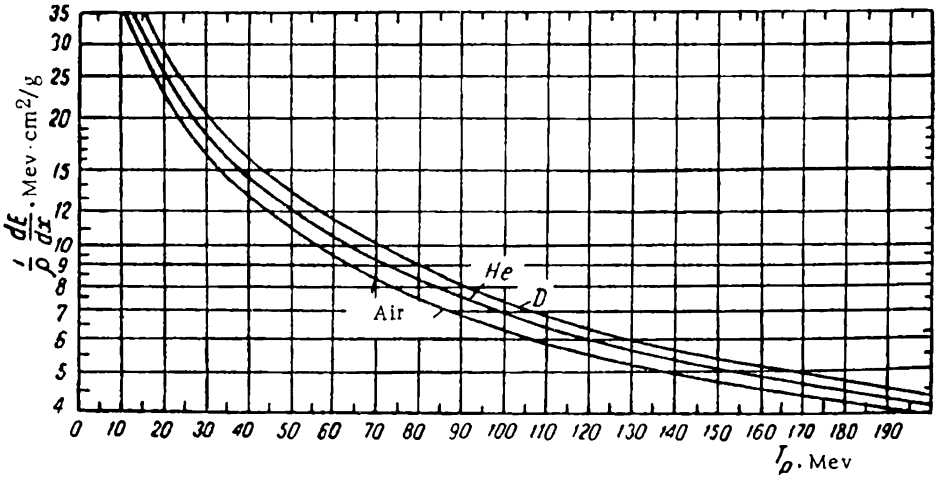

FIGURE 24. Mass stopping power of air, helium and deuterium for protons /137/; $T_p = 0-20$ Mev

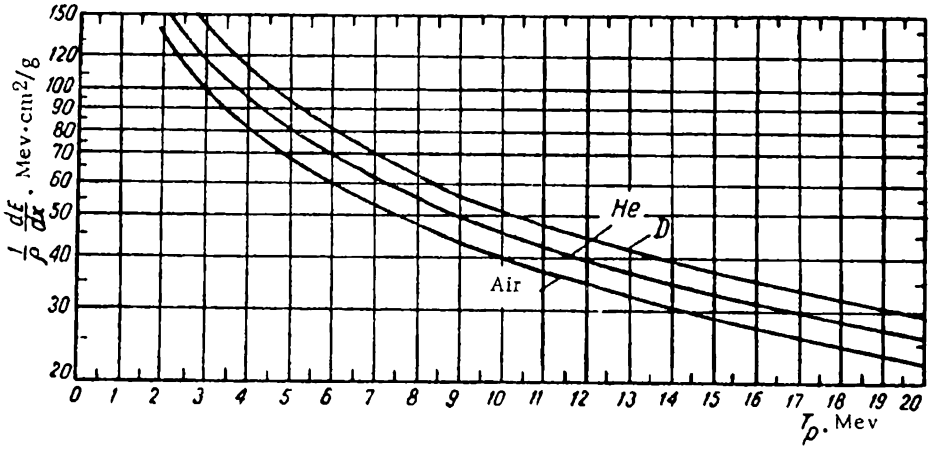

FIGURE 25. Mass stopping power of air, helium and deuterium for protons /137/; $T_p = 0-200$ Mev

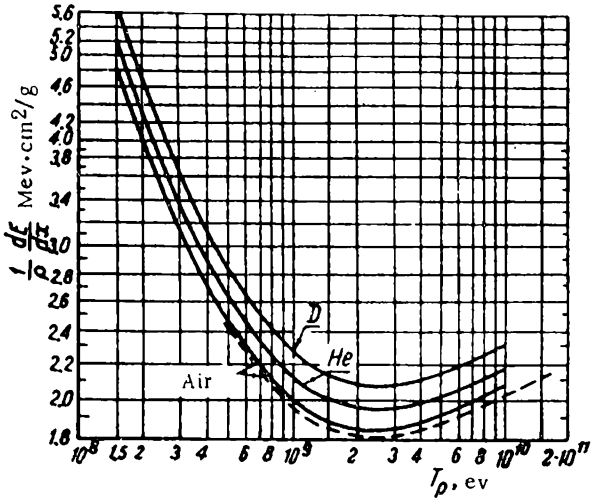

FIGURE 26. Mass stopping power of air, helium, and deuterium for protons /137/; $T_p = 10^8$ ev—$2 \cdot 10^{11}$ ev

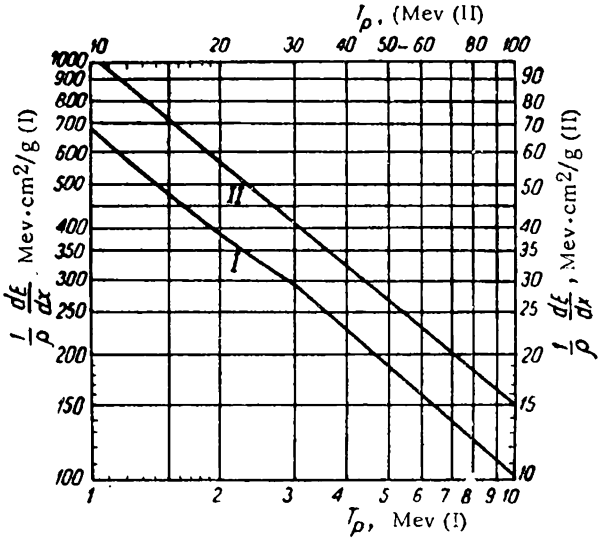

FIGURE 27. Mass stopping power of hydrogen for protons /432/

Table 21 gives the calculated values of the energy loss in polystyrene and polyethylene for proton energies from 1 Mev to 10 Bev /432/.

The relation between the ionization energy losses of protons and of heavy charged particles. According to the Bethe-Bloch equation the mean ionization energy loss in a given medium depends only on the charge and the velocity of the incident particle, and not on its mass. Thus the ionization losses of protons, deuterons, and tritons are the same, if they all have the same velocities and pass through the same thickness of stopping medium. In other words, protons with an energy T lose the same energy upon ionization as deuterons with an equivalent energy $\frac{M_d}{M_p} T$ or as tritons with an energy $\frac{M_t}{M_p} T$ (this is verified experimentally, see § 5).

When α-particles with an energy $\frac{M_\alpha}{M_p} T$ and protons with an energy T pass through the same thickness, the ionization losses of the former are four

times as large as those of the latter, etc. This is only valid if the charge of the particles remains constant. The tabulated data on ionization energy losses of protons and the curves describing them can therefore be used for the evaluation of the mean energy losses of deuterons, tritons, α-particles, etc. Therefore, the values on the energy axis in Figures 18—27 should be

TABLE 21

Calculated values of the stopping power of polystyrene (CH) and of polyethylene (CH_2) for protons /432/

T_p, Mev	$\frac{1}{\rho}\frac{dE}{dx}$, Mev·cm²/g		T_p, Mev	$\frac{1}{\rho}\frac{dE}{dx}$, Mev·cm²/g	
	$(CH)_n$	$(CH_2)_n$		$(CH)_n$	$(CH_2)_n$
1	276	306	60	10.9	11.7
2	169	185	80	8.67	9.36
3	123	135	100	7.32	7.90
4	98.0	107	150	5.46	5.89
5	82.0	89.4	200	4.50	4.85
6	70.8	77.1	300	3.52	3.79
7	62.5	68.0	400	3.03	3.26
8	56.1	61.0	500	2.74	2.95
9	50.9	55.4	700	2.42	2.60
10	46.7	50.8	1000	2.20	2.37
12	40.2	43.7	2000	2.04	2.19
16	31.9	34.4	3000	2.04	2.19
20	26.4	28.7	4000	2.08	2.23
30	19.0	20.5	5000	2.12	2.27
40	15.0	16.2	10000	2.28	2.45
50	12.5	13.6	—	—	—

multiplied by two, three, and four respectively for deuterons, tritons, and α-particles (reduction to "equivalent" energies; see above). Moreover, for π-particles the respective values of the energy losses have to be increased fourfold (quadratic dependence of the ionization losses on the charge of the incident particle).

Statistical distribution of energy losses. Most probable energy losses. As a result of the statistical fluctuations in the number of ionizing collisions, as well as of the fluctuations in the energy losses in individual collisions, a monochromatic beam of particles, after passing some homogeneous layer, becomes nonmonochromatic. The function describing the distribution of the energy losses depends in general on the kind of particles, on their energy, and on the thickness t of the layer.

For heavy charged particles passing through a sufficiently thick layer, the distribution of the energy losses can be represented by a Gaussian function with half-width T, where

$$\sigma_E^2 = Pt = T^2. \tag{4.43}$$

According to Bohr /149/, the quantity P is independent of the velocity of the particles and is given by

$$P = 4\pi z^2 e^4 n = 4\pi z^2 e^4 NZ, \tag{4.44}$$

which follows directly from (2.53), (4.4) and (2.3) for $Q_{max} \gg Q_{min}$ (Q is the energy transferred to the electron).

A more exact expression was given by Livingston and Bethe /359/

$$P = 4\pi z^2 e^4 n K, \tag{4.45}$$

where the factor K allows for electron binding in the atom

$$K = \frac{Z^*}{Z} + \sum_n \frac{K_n I_n Z_n}{mv^2} \ln \frac{2mv^2}{I_n}, \tag{4.46}$$

where Z_n is the number of electrons in the n-th shell of the atoms of the stopping medium;

I_n is the corresponding effective excitation potential of the n-th shell;

$K_n \sim \frac{4}{3}$ is for all the shells;

Z^* is the number of effective electrons upon stopping; summation over n is carried out for shells where

$$I_n < 2\ mv^2.$$

For beryllium, K is 1.37 with $T_p = 1$ Mev, 1.12 with $T_p = 5$ Mev, 1.02 with $T_p = 50$ Mev. For lead the value decreases from 1.33 with $T_p = 5$ Mev to 1.11 with = 200 Mev. Thus, if the charged particles have low energies, then Bohr's formula gives σ_E^2 low by 10—30%. At high energies, formulas (4.44) and (4.45) give similar results.

In the general case, the distribution of the energy losses is asymmetric about the mean value, and the most probable energy loss is not equal to the mean loss given by the Bethe-Bloch equation. This is particularly important for electrons. For heavy charged particles and thin absorbers, one should also distinguish between the most probable and the mean energy losses. This problem was theoretically investigated by Williams /511/, Landau /63/, Vavilov /25/, Blunck et al. /191, 192/.

A more rigorous solution of the problem for thin ($\Delta E \ll E$) absorbers, from which Landau's results follow as a particular case, was given by Vavilov /25/ and others /174, 94/. The probability that a particle loses an energy lying in the interval from Δ to $\Delta + d\Delta$ in passing a layer t is, according to Landau,

$$f(\Delta, t) = \varphi\left(\frac{\Delta - \Delta_0}{\xi}\right) d\left(\frac{\Delta - \Delta_0}{\xi}\right), \tag{4.47}$$

where the parameter ξ is equal to the energy loss in a single collision, which occurs only once along the path t:

$$\xi = \frac{2\pi z^2 e^4}{mv^2} nt, \tag{4.48}$$

$$\xi_{(ev)} = \frac{1.53 \cdot 10^5 \rho(\text{g/cm}^3) t\,(\text{g/cm}^2)}{\beta^2} z^2 \left(\frac{Z}{A}\right). \tag{4.48a}$$

The quantity Δ_0 is called the most probable energy loss and is defined by

$$\Delta_0 = \xi\left[\ln \frac{2mv^2\xi}{I^2(1-\beta^2)} - \beta^2 + 0.373\right]. \tag{4.49}$$

It can be seen that the most probable energy loss is not equal to the mean loss. The quantity 0.373 in expression (4.49) is the contribution to the most probable energy losses of those single collisions in which the energy transfer is larger than or of the order of ξ.

Contrary to the mean energy loss, the quantity Δ_0 is not a linear function of the thickness of the absorber. Its value increases somewhat faster, owing to the factor $\ln\xi$.

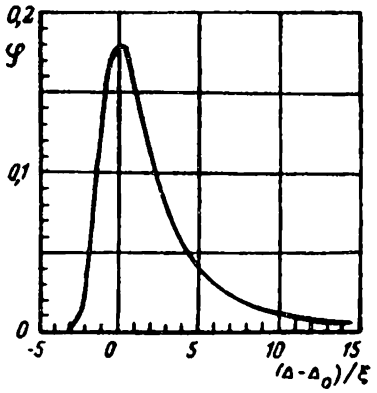

FIGURE 28. Probability of energy loss Δ in an ionizing collision of a charged particle with an electron as a function of the most probable energy loss Δ_0 and the parameter ξ, according to Landau /63/. The area under the curve is normalized to unity

Figure 28 shows the function φ of (4.47) and gives the distribution of the energy losses in a thin absorber. The width of this distribution at half the peak height is $T = 3.98\xi$.

The results are correct if the energy losses Δ in passing a layer t are small as compared with the initial energy of the particle, and if ξ is larger than the mean excitation potential I of the atoms of the stopping medium.

The question arises, in which cases one should expect differences between the mean and most probable energy losses. Hanson showed that the answer to this question can be obtained by comparing ξ determined by (4.48) with the maximum energy Q_{max} transferred to the electron in a collision (Q_{max} is given by (4.16a)). If $\xi > Q_{max}$, the most probable and the mean energy losses are practically equal. In the opposite case, the Landau distribution function given above should be used.

Simon considered the case of absorbers in which the energy losses constitute a considerable fraction of the initial energy of the particle. * The results of his calculations are given by Rossi /92/, and the corrections to these calculations taking into account the electron binding are given in /439/.

According to Simon, the distribution of the energy losses in layers of intermediate thickness is represented by a set of curves with differently pronounced asymmetries. A smooth transition obtains from the symmetric Gaussian curve (thick absorbers) to Landau's curve (thin absorbers).

§ 5. Experimental verification of the stopping theory and data on the ionization energy losses of fast protons and α-particles

It was shown in the previous sections that particles with a small charge and high velocity lose energy mainly by inelastic collisions with atomic electrons.

It is known from theory (4) that the ionization energy losses depend on the properties of the incident particles and on the properties of the stopping medium.

In special experiments /214, 296/ and in numerous other investigations considered in this section, it was established that the ionization energy losses are independent of the mass of the incident particles and are proportional to the square of the charge of the incident particles, rapidly increasing when their velocity decreases.

Thus, for example, it was discovered that, within the experimental margin of error, in passing through layers of the same thickness, protons,

* The fluctuations of the energy losses in thick absorbers with an allowance for scattering were studied earlier by Pomeranchuk /88/; see § 6.

deuterons, and tritons having the same velocity lose the same amount of energy. The ratio of the thicknesses Δx_α and Δx_p in the passing of which the velocities of α-particles and protons were reduced from v_1 to v_2 was found to be $\frac{M_\alpha}{M_p}\left(\frac{z_p}{z_\alpha}\right)^2$, which fits the theory in § 4).

The stopping of the particles depends on the atomic number Z and on the mean excitation potential $I(Z)$ (see formula (4.21)). Since the theory cannot determine the numerical values of I, the latter are obtained from measurements of ionization energy losses and ranges (§ 6).

Let us consider the methods of measuring the absolute and relative energy losses of charged particles, as well as some of the experimental results which are important for the verification of the stopping theory (§ 2, 4) and for the plotting of the stopping power vs. energy and range vs. energy relations (§ 6). These results are particularly important for the range of relatively low energies ($T_p < 2$Mev, $T_\alpha < 5$ Mev), in which the theory considered in § 4 is inadequate.

TABLE 22

Numerical values of the coefficients A and B (for gases B is given at 15°, 760 mm of mercury)

Medium	A	B	Remarks	Medium	A	B	Remarks
Hydrogen, H_2	598	0.0509		Cobalt, Co	10.2	90.9	
Helium, He	150	0.02547		Nickel, Ni	10.3	91.3	
Lithium, Li	86.8	46.3		Copper, Cu	9.48	84.7	
Beryllium, Be	66.8	124		Zinc, Zn	9.21	65.8	
Boron, B	55.7	130	Amorphous	Germanium, Ge	8.30	44.5	
Carbon, C	50.1	113	Graphite	Krypton, Kr	7.19	0.02547	
				Molybdenum, Mo	6.28	64.0	
				Palladium, Pd	5.64	68.6	
Nitrogen, N_2	43.0	0.0509		Silver, Ag	5.58	58.6	
Oxygen, O_2	38.8	0.0509				29.2	Cubic
Fluorine, F	31.7	0.02547		Tin, Sn	5.07	33.2	Rhombic
						37.1	Tetragonal
Neon, Ne	29.8	0.02547					
Sodium, Na	26.2	25.4					
Magnesium, Mg	24.8	43.1		Antimony, Sb	4.95	33.1	
Aluminum, Al	22.3	60.3		Xenon, Xe	4.59	0.02547	
Silicon, Si	21.5	51.9					
Phosphorus, P	19.4	42.8	Red phosphorus	Tantalum, Ta	3.33	55.3	
				Tungsten, W	3.27	63.2	
				Platinum, Pt	3.09	65.9	
Sulfur, S	18.8	38.9	Rhombic	Gold, Au	3.05	59.0	
				Mercury, Hg	2.99	40.5	
Chlorine, Cl	17.0	0.02547		Lead, Pb	2.91	33.0	
Argon, A	15.1	0.02547		Bismuth, Bi	2.88	28.2	
Potassium, K	15.4	13.4		Air	20.79	0.0509	
Calcium, Ca	15.0	23.3		Water, H_2O	33.42	0.0764	Vapor
Vanadium, V	11.8	70.5		Carbon dioxide, CO_2	13.68	0.0764	
Germanium, Ge	11.6	82.2		Methane, CH_4	37.55	0.1283	
Manganese, Mn	11.0	78.9					
Iron, Fe	10.8	84.8					

The following terminology and notation will be used.

The quantity

$$\varepsilon = \frac{dE}{dx}$$

will be called the linear stopping power of the medium in Mev or kev per centimeter.

The quantity

$$\varepsilon_m = \frac{1}{\rho}\frac{dE}{dx}, \tag{5.1}$$

where ρ is the density of the medium (g/cm^3), is called the mass stopping power ($Mev \cdot cm^2/g$ or $kev \cdot cm^2/g$).

Finally, the quantities

$$\varepsilon_a = \frac{1}{N}\frac{dE}{dx} \tag{5.2}$$

and

$$\varepsilon_e = \frac{1}{n}\frac{dE}{dx} = \frac{1}{NZ}\frac{dE}{dx} \tag{5.3}$$

are the atomic and electronic stopping powers of the medium respectively (N and n are the numbers of atoms and electrons in 1 cm^3 of the stopping medium). The quantity ε_a has the dimensions of [ev. cm^2/atom]; it is sometimes called stopping cross section.

Table 22 gives the numerical coefficients relating the atomic, mass, and linear stopping powers of materials, expressed in the following units /491/:

$$\varepsilon_a\,(10^{-15}\ \text{ev}\cdot\text{cm}^2) = A\varepsilon_m\left(\frac{\text{Mev}\cdot\text{cm}^2}{\text{g}}\right) = B\varepsilon\ (\text{Mev/cm}).$$

Experimental methods for measuring stopping powers. The stopping theory provides formulas for the ionization losses due to the ionization, as well as to the excitation of the atoms of the stopping medium. Therefore, it is not sufficient to verify the theory by the measurements of the number of ion pairs formed by a particle along its path, although there is a satisfactory correlation between the energy of a particle and the ionization produced by it (§ 8).

Experiments on the determination of the stopping power should include the measurements of the energies of the particles before and after the absorber, as well as the determination of the thickness of the absorber or of the number of atoms per $1 cm^2$. The energy loss in the absorber should be sufficiently small and negligible in comparison to the initial energy of the particles.

The main methods of studying the stopping power are examined below.

1. Magnetic or electric analysis of beams of particles before and after passing through a known thickness of the medium (the energy scales of the analyzers are calibrated by known standards; see § 3).

A typical arrangement for the measurement of the stopping powers of solid targets /500, 296, 495, 340/ is shown in Figure 29. Protons, deuterons, or helium ions accelerated in a Cockroft-Walton or Van de Graaf generator hit after a magnetic analysis a gold foil or a target in which new particles are formed in nuclear reactions. The spectrum of the particles scattered by the gold, or of the products of the nuclear reactions escaping at 90° to the target was determined by an electric analyzer. After this, the displacement in the energy scale of the maximum of the line corresponding

to the given kind of particles was measured. This displacement $(T_0 - T_x)$ divided by the thickness Δx of the foil gives $\frac{dE}{dx}$ for the energy

$$T = \frac{1}{2}(T_0 + T_x)^*.$$

For beam energies $T_p > 1$ Mev, magnetic analysis is always used.

The authors of /161, 291, 451/ measured the stopping powers and ranges in solid targets on internal (non-emergent) beams of charged particles in a cyclotron. The magnitude of the magnetic field of the cyclotron and the radial displacement of the slits of the detector when the stopping foil was introduced in the path of the beam made it possible to determine $\frac{dE}{dx}$. Modifications and improvements of the method /157, 263/ reduce errors in the measurement to 1%.

Equipment similar to that shown in Figure 29 is used for the measurement of the stopping power of gases /498/. In this case one has to use an

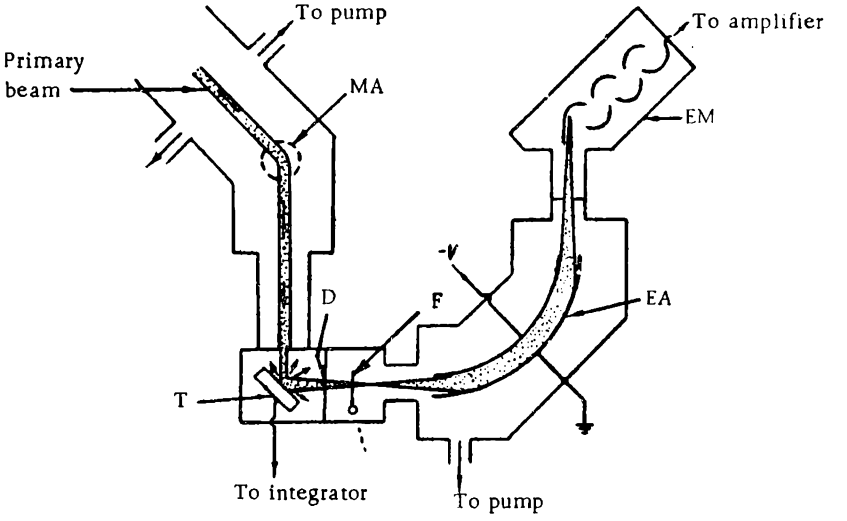

FIGURE 29. The experimental arrangement /340/ for the study of the stopping of protons in a medium

MA—magnetic analyzer; T—target; D—slit; F—foil; EA—electrostatic analyzer; EM—electron-multiplier.

extended gas target, which imposes additional stringent requirements on the collimation of the particle beam before and after the target.

2. The method of displacement of resonance peaks is based on the well-known phenomenon of the resonance dependence of the gamma-quantum yield in certain (p,γ) reactions on the proton energy. Depending on the proton energy, a suitable (p,γ) reaction is chosen (see Table 10). The experiment consists in measuring the excitation curves of the reaction first without interposing a stopping foil in the path of a beam of monoenergetic protons, and then with a foil interposed. The resonance energy of the protons, which is compared with the calibration standard (Table 10), is determined by means of a gamma-counter. After this, the foil is placed in the path of the beam and the proton energy is increased until a new maximum occurs

* When $\frac{dE}{dx}$ varies rapidly with the thickness, the effective value of the mean energy of the particles should be used, which can be calculated /132/.

in the gamma-quantum yield (resonance). The energy loss in the foil is determined from the displacement of the position of the maximum of the differential yield curves on the energy scale. The broadening of the displaced yield curve gives the σ_E of the energy losses.

The method was used for measurements on solid /382, 383, 290, 85/ and gaseous targets /212/. The accuracy of $\frac{dE}{dx}$ by this method reaches 99%. As an example, Table 23 gives the measurements /290/ of the stopping power of gold for protons energies of 364 — 1003 kev.

TABLE 23

Measurements of the stopping power of gold for protons by the method of displacement of the (p,γ) reaction resonances /290/

Indicator	Foil thickness, mg/cm2	Displacement of maxima	Mean proton energy, T_p	ε_m, kev·cm2/mg
		kev		
Fluorine-339*	0.46	39	364	85
Fluorine-339	0.52	42	366	81
Aluminum-986	0.46	27	1001	59
Aluminum-986	0.51	30	1002	59
Aluminum-986	0.52	31	1003	60

* Fluorine-339 is indicatory of the resonance of the reaction $F^{19}(p,\gamma)Ne^{20}$ with T_p = 339 Mev. The resonance proton energies given by the authors of /290/ differ somewhat from the accepted values at present (Table 10). Aluminum-986 respectively denotes the resonance in the reaction $Al^{27}(p,\gamma)Si^{28}$ with T_p = = 986 Mev.

3. The scintillation counter method. The energy losses are measured by a comparison of the amplitudes of the pulses produced in a scintillation counter by particles which have passed through the foil with those obtained in the absence of the foil /159/. The energy loss in the foil is

$$\Delta E = T_0 \frac{\Delta h}{h},$$

where T_0 is the kinetic energy of the particles before hitting the foil;

h_0 is the amplitude of the pulses caused by the particles. A linear dependence of the light yield of the crystal on the particle energy is assumed in this case (see below).

4. Phillips method. To measure the energy losses of hydrogen ions in gases, Phillips /414/ used the equipment shown schematically in Figure 30. Hydrogen ions were accelerated by a source-earth potential and passed through a gaseous target, which was confined by very thin SiO_2 plates; they were then slowed down by entering into the space between the collimator and a Faraday cylinder having the same potential as the source. Analysis of the energy of the particles after deceleration was performed by means of an adjustable decelerating voltage. If the particles lost energy in the target, the potential of the collector was reduced in order to collect the particle beam. This variation in the collector potential was measured. By means of this device, Phillips measured values of ΔE from 1 to 25 kev for proton energies of 10—80 kev.

The accuracy of the experiments on the stopping powers of materials is mainly dependent on the accuracy of the measured target thickness.

In the case of gaseous targets, their length sould be determined, as well as the gas pressure and temperature and the energy absorption in the windows. Then the error in Ndx atoms/cm^2 may be within 1 — 2%.

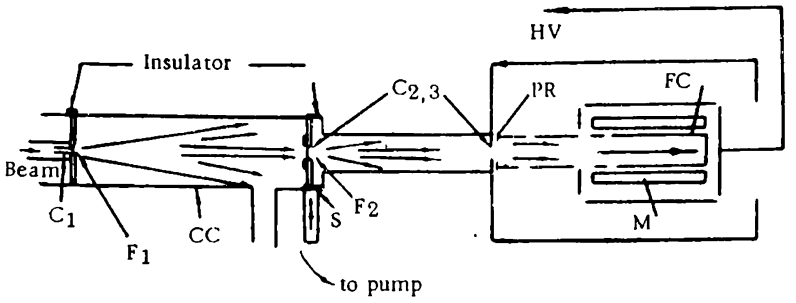

FIGURE 30. The experimental setup of Phillips /414/ for the study of the stopping of charged particles in gases:

CC — collision chamber; C_1, C_2, C_3 — collimators; F_1, F_2 — foils; S — shutter; PR — protective rings; FC — Faraday cylinder; M — magnet; HV — high voltage

The thickness of solid targets is determined by weighing or by chemical analysis of the material deposited on a known area. The error in Ndx is then 3 — 5%.

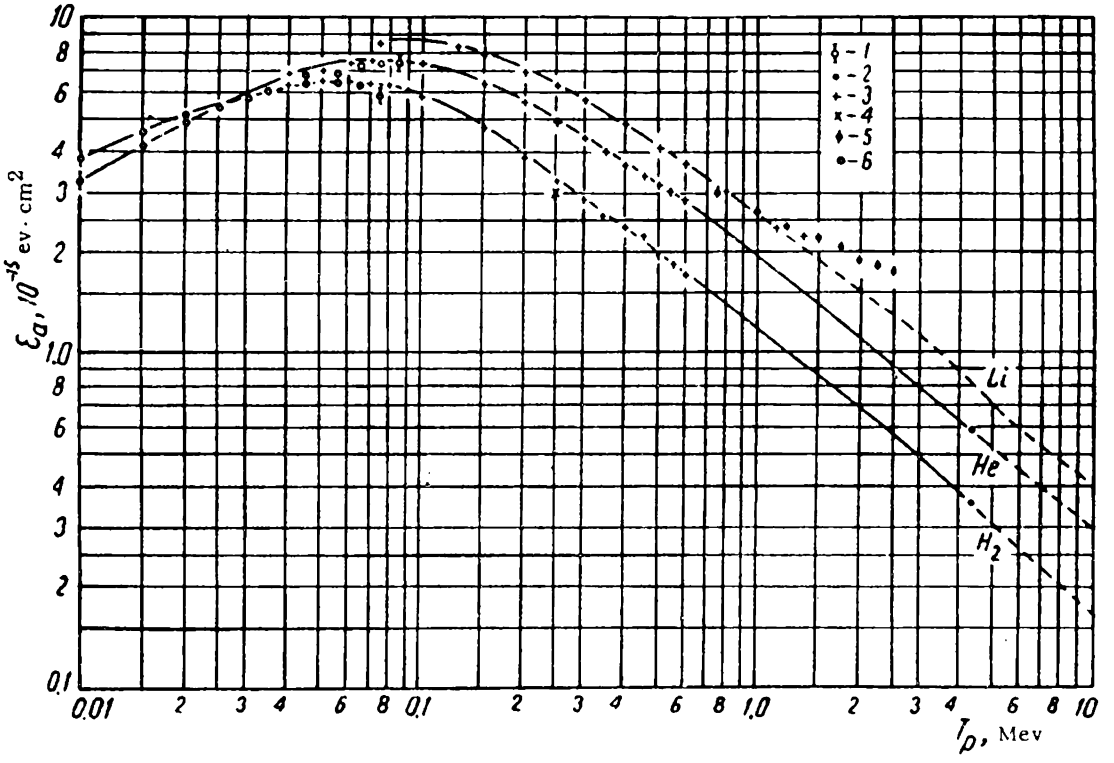

FIGURE 31. Atomic stopping power of hydrogen, helium, and lithium for protons:

1 — Phillips /414/; 2 — Brolley and Ribe /159/; 3 — Reynolds et al. /434/ (helium and lithium); 4 — Bader et al. /157/ (lithium); 5 — Weyl /498/; 6 — investigation of the stopping of α-particles, Rosenblum /433/

Experimental data on the stopping powers of various media for protons. The most comprehensive summary of the experimental data (up to 1953) on

the stopping powers of various media for protons is contained in the review of Allison and Warshaw /132/. More recent data are given in Whalling /491, 492/.

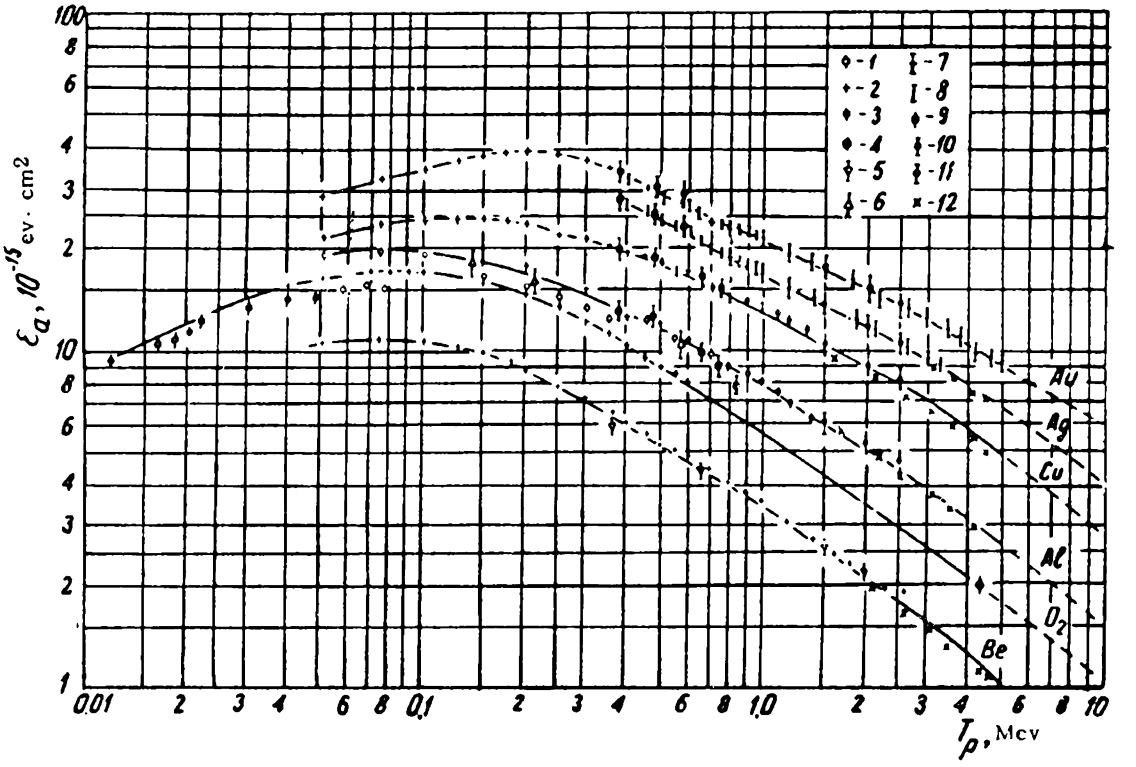
$\varepsilon_a, 10^{-15}$ ev · cm²
T_p, Mev
1-Phillips /414/; 2-Reynolds et al. /434/ (oxygen); 3-Bader et al. /157/ (beryllium, copper, aluminum, gold); 4-Kahn /340/ (copper); 5-Madsen /382/; 6-Parkinson et al. /413/; 7-Stelson and McCowan /472/; 8-Green et al. /263/; 9-Brolley, and Ribe /159/; 10-investigation of the stopping of α-particles, Rosenblum /433/; 11-Gobeli /266/; 12-Nielsen /410/.
Au
Ag
Cu
Al
O₂
Be

FIGURE 32. Atomic stopping power of gold, silver, copper, aluminum, oxygen, and beryllium for protons:

Figures 31-35 give the dependence of the atomic stopping powers of various materials on the proton energy (the solid lines). These were obtained by averaging over a large number of experimental data /491/. The points in these figures represent the experimental data of various authors with the measurement methods listed. Although the experimental data extend, as a rule, only over proton energies from $T_p \sim 0.1$ to 4-5 Mev, they can be used for extrapolation to higher energies (the broken lines in Figures 31-35). To pass from atomic stopping powers, expressed in units of 10^{-15} ev·cm²/atoms, to mass stopping powers (Mev·cm²/g) or to linear stopping powers (Mev/cm), the table of conversion coefficients (Table 22) should be used.

The curves given in Figures 31-35 can also be used in calculating the stopping powers of various materials for deuterons and tritons, as well as for α-particles and He^3 ions with $T > 2$ Mev. For this purpose it is necessary to use on the energy scale the value $T_x = \frac{M_x}{M_p} T_p$ of the equivalent energy for the given type of particles, and to determine the corresponding value of the stopping power by

$$\varepsilon_a^{(x)} = \varepsilon_a^{(p)} \left(\frac{z_x}{z_p}\right)^2.$$

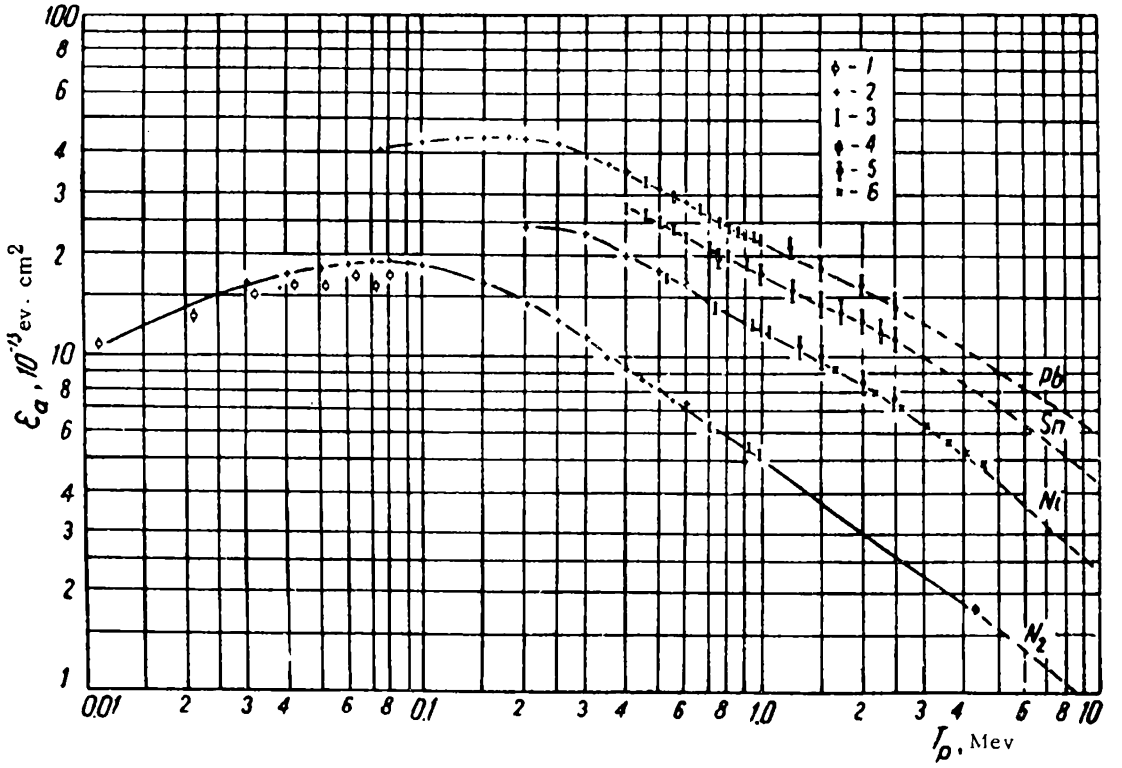

FIGURE 33. Atomic stopping power of lead, tin, nickel, and nitrogen for protons:

1—Phillips /412, 414/; 2—Reynolds et al. /434/ (nitrogen); Bader et al. /157/ (nickel, lead); 3—Green et al. /263/ (lead, tin); Milani et al. /395/ (nitrogen); Chilton et al. /212/ (nickel); 4—Brolley and Ribe /159/; 5—investigation of the stopping of α-particles by Rosenblum /433/; 6—Nielsen /410/.

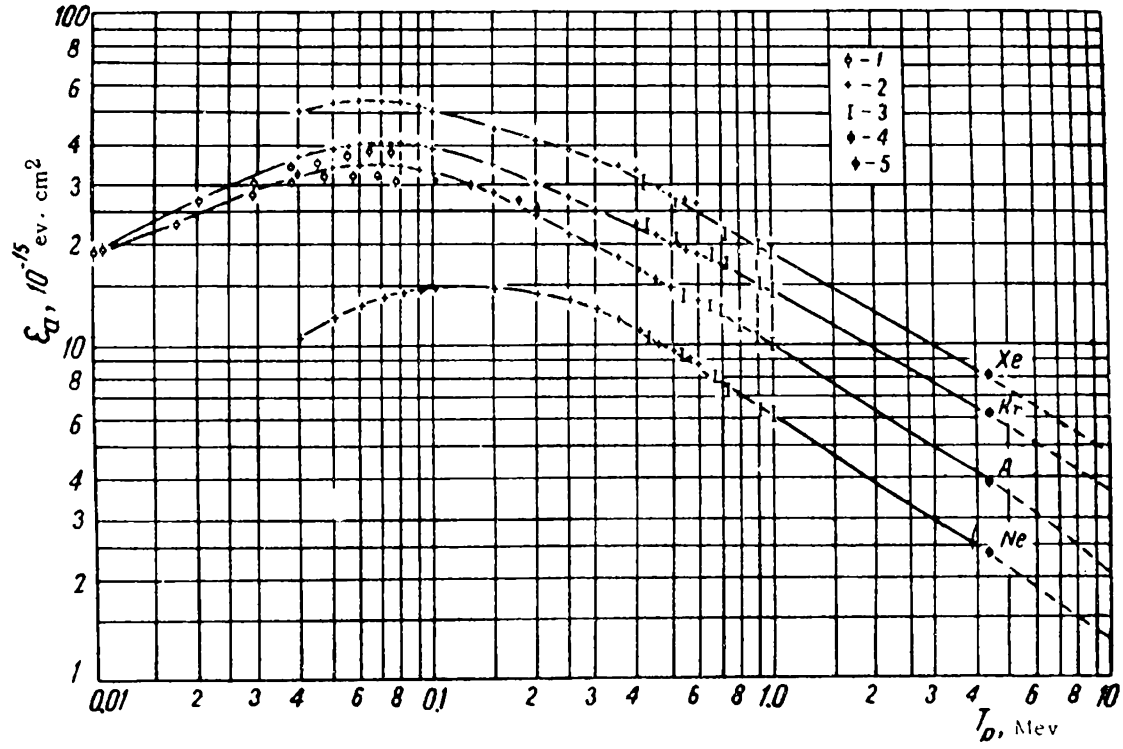

FIGURE 34. Atomic stopping power of neon, argon, krypton, and xenon;

1—Phillips /412, 414/; 2—Reynolds et al. /434/; 3—Milani et al. /395/ (xenon); Chilton et al. /212/ (neon, argon, krypton); 4—Brolley and Ribe /159/; 5—Weyl /498/.

For example, the stopping power for a 9-Mev triton is equal to the stopping power for a 3 Mev proton, and the stopping power for a 5 Mev α-particle is four times the stopping power for a 2 Mev proton, and so on.

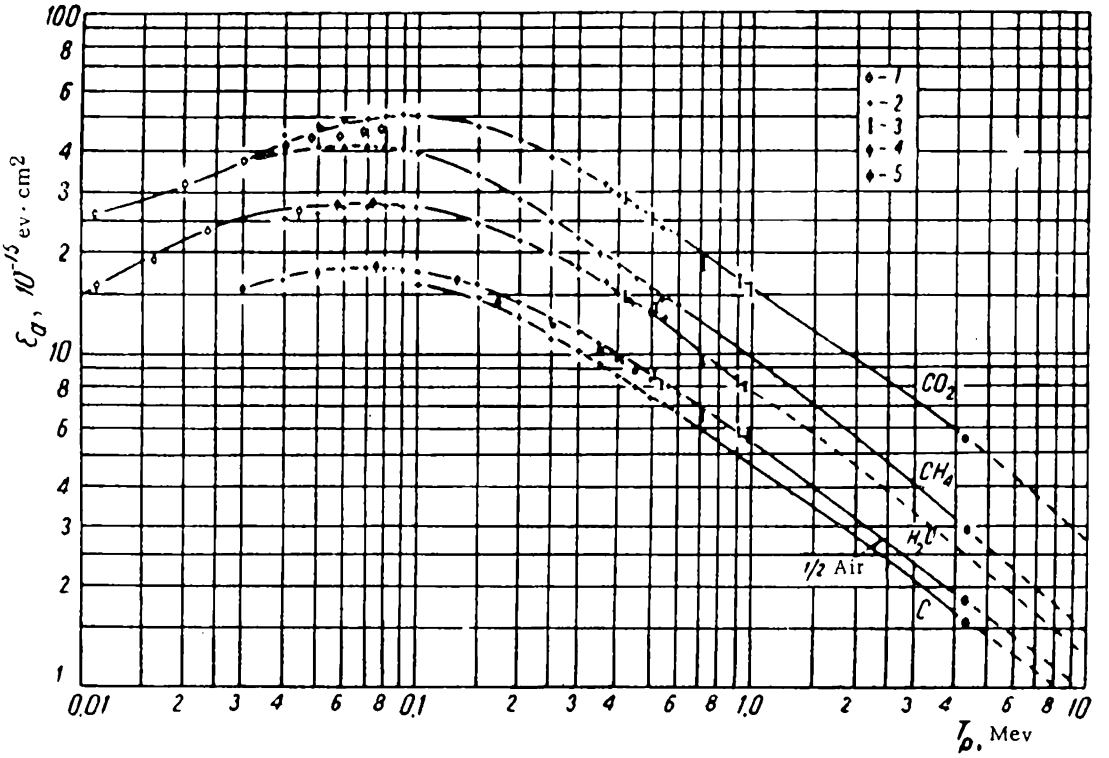

FIGURE 35. Molecular stopping power of water vapor, methane, carbon dioxide gas, and air (per 1/2 molecule) for protons:

1—Phillips /412/; 2—Reynolds et al. /434/; 3—Milani et al. /394/; 4—Weyl /498/; 5—Brolley and Ribe /159/.

Figures 31—35 and Tables 24—25 may be used to determine the values of the stopping powers of various substances for protons with energies from

TABLE 24

Experimental values /263/ of atomic stopping power of some elements for protons (in units of 10^{-15} ev·cm²/atoms)

T_p, kev	Manganese Mn	Germanium Ge	Selenium Se	Antimony Sb	Bismuth Bi
400	19.9	21.3	22.0	29.5	36.1
450	18.8	20.2	21.0	27.9	34.4
500	17.9	19.2	20.2	26.7	32.7
550	17.0	18.4	19.4	25.2	31.3
600	16.1	17.7	18.7	24.1	29.9
650	15.4	17.1	18.1	22.8	28.5
700	14.8	16.6	17.6	21.8	27.4
750	14.2	16.0	17.0	21.0	26.1
800	13.8	15.7	16.5	20.4	25.4
850	13.4	15.2	16.0	19.8	24.3
900	13.1	14.8	15.7	19.4	24.0
950	12.8	14.3	15.3	18.8	23.3
1000	12.4	14.0	15.1	18.4	23.0

0.1 to 4 Mev and for α-particles with energies from 2 to 16 Mev. For higher energies, the theoretical curves of Figures 18—27 should be used.

TABLE 25

Experimental values of the stopping power of some metals for protons /157/ (in units of 10^{-15} ev·cm²/atoms)

T_p, Mev	Calcium Ca	Vanadium V	Chromium Cr	Iron Fe	Cobalt Co	Zinc Zn
0.2	25.9	29.9	29.2	27.4	25.7	24.3
0.3	21.3	25.3	24.9	24.4	22.7	23.0
0.4	17.6	21.4	21.4	21.1	19.7	20.4
0.5	15.3	18.5	18.4	18.1	17.2	18.6
0.6	14.3	16.6	17.1	16.8	16.7	17.6

For a rough estimate in the non-relativistic energy range, Whaling's semi-empirical formula /491/, based on (4.21), may be applied,

$$\varepsilon_a(T) = \frac{0.24zZ}{T_{(\text{Mev})}}\left[\ln\frac{T_{(\text{Mev})}}{Z} + a\right]\cdot 10^{-15}\ \text{ev}\cdot\text{cm}^2, \qquad (5.4)$$

where a varies from 5.1 to 5.3 with Z from 10 to 60.

Expression (5.4) is suitable for $T_p > 0.5$ Mev and $T_\alpha > 2$ Mev.

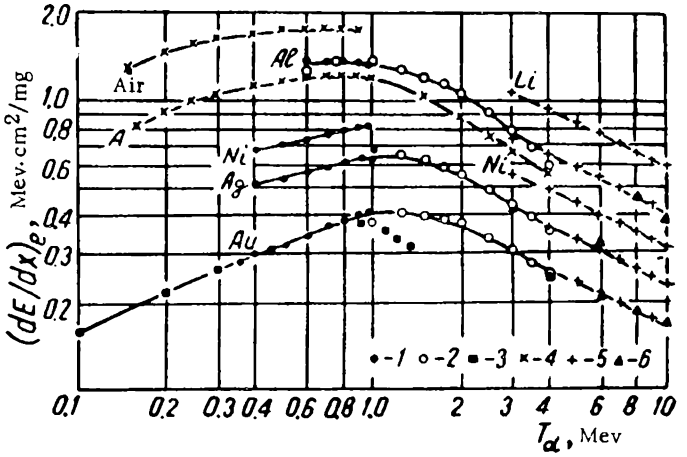

FIGURE 36. Mass stopping power of aluminum, nickel, silver and gold for α-particles. Experimental data:

1—Porat and Ramavataram /416/; 2—Gobeli /266/; 3—Wilcox /500/; 4—Weyl /498/; 5—Rosenblum /433/; 6—calculated results from Aron /137/.

Experimental data on the stopping powers of materials for α-particles. For $T_\alpha < 2$ Mev (Figure 36), the difference in electron capture by α-particles and protons begins to be noticeable (see § 8), and the effective charge of the α-particles decreases rapidly with the velocity. In this case the above method of calculating the stopping powers of α-particles from the curves for protons of equivalent energies (Figures 31—35) is unsuitable.

However, ε_a for α-particles can be obtained from the experimental values of ε_a for protons in the same medium, if the experimental dependence of the ratio of the effective charges of the α-particle and the proton on the velocity (see § 7) is used.

TABLE 26

Experimental values of the atomic stopping power of some materials for α-particles /133/ (in units of 10^{-15} ev·cm²/atoms)

T_a, Mev	Iron Fe	Zinc Zn	Molybdenum Mo	Palladium Pd	Cadmium Cd	Platinum Pt
3	53.4	57.1	68.7	72.5	76.3	[illegible]
4	47.0	50.3	60.4	63.8	67.2	83.7
5	42.4	45.4	54.5	57.6	60.6	75.5
6	38.8	41.6	49.9	52.6	55.4	69.2
7	36.1	38.7	46.4	48.9	51.5	64.3
8	33.7	36.1	43.3	45.7	48.1	60.1
9	—	34.0	40.8	43.1	45.3	56.6
10	—	32.3	38.8	40.9	43.1	53.8

Table 26 gives experimental data from Rosenblum /433/ on the stopping power of some materials for α-particles of 3—10 Mev (Rosenblum's data for other materials were incorporated in the curves of Figures 31—35).

In practice it is often necessary to deal with relative stopping powers.

The relative stopping power of a material with respect to a standard material is the ratio of the amount of standard material to that of the given material which produces in both the same energy losses. Depending on the basic quantities characterizing the amount of substance, we may define linear, mass, atomic and electronic relative stopping powers (denoted respectively by S, S_m, S_a and S_e).

The linear relative stopping power of a material is defined as the thickness in centimeters which results in the same energy loss along 1 cm of path as in the standard material:

$$S = \frac{\Delta x_{st}}{\Delta x} = \frac{NB}{N_{st} B_{st}}, \tag{5.5}$$

where N is the number of atoms in 1 cm³ of the material;

B is the stopping coefficient (§ 4).

Similarly, the atomic relative stopping power is the thickness of a given material (expressed by the number of atoms per 1 cm²), which corresponds to the same energy loss as in a thickness of the standard material containing 1 atom per 1 cm²:

$$S_a = \frac{N_{st} \Delta x_{st}}{N \Delta x} = \frac{B}{B_{st}}. \tag{5.6}$$

Similarly

$$S_e = \frac{N_{st} Z_{st} \Delta x_{st}}{N z \Delta x} = \frac{(B/Z)}{(B/Z)_{st}}, \tag{5.7}$$

$$S_m = \frac{(\rho \Delta x)_{st}}{\rho \Delta x} = S_e \frac{(A/Z)_{st}}{(A/Z)}. \tag{5.8}$$

TABLE 27

Relative stopping powers of metals for protons on aluminum

Element	Burkig /155/, T_p = 19.8 Mev		Sonett /452/ T_p = 20.6 Mev		Bakker-Segre /158/, T_p = 340 Mev		Thompson /476/, T_p = 270 Mev	Warshaw /495/, T_p = 0.1 Mev	Wilson /502/, T_p = 2-4 Mev
	S_m	S_e	S_m	S_e	S_m	S_e	S_m	S_m	S_m
3 Li	—	—	—	—	1.062	1.18	—	—	—
4 Be	1.166∓0.005	1.073±0.005	—	—	1.024	1.11	—	1.5	—
6 C	—	—	—	—	1.124	1.08	1.137	—	—
13 Al	1.000	1.000	1.000	1.000	1.000	1.000	1.000	1.000	1.000
20 Ca	0.970±0.020	0.008±0.090	—	—	—	—	—	—	—
22 Ti	0.936±0.006	0.888±0.006	—	—	—	—	—	—	—
26 Fe	0.886±0.002	0.856±0.002	—	—	0.906	0.94	—	—	—
28 Ni	0.872±0.002	0.863±0.002	0.859±0.004	0.868±0.004	—	—	—	—	—
29 Cu	0.867±0.002	0.819±0.002	0.836±0.006	0.883±0.003	0 875	0.92	—	0.54	0.735
30 Zn	0.866±0.002	0.819±0.002	—	—	—	—	—	—	—
41 Nb	0.816±0.002	0.746±0.002	—	—	—	—	—	—	—
42 Mo	0.809±0.005	0.735±0.005	—	—	—	—	—	—	—
45 Rh	0.809±0.005	0.735±0.005	—	—	—	—	—	—	—
46 Pd	0.793±0.003	0.710±0.003	0.720∓0.006	0.805±0.006	—	—	—	—	—
47 Ag	0.791±0.003	0.715±0.003	0.717±0.006	0.793±0.006	0.789	0.87	—	0.328	—
48 Cd	0.789±0.002	0.700±0.002	0.714±0.004	0.806±0.004	—	—	—	—	—
49 In	0.782±0.002	0.693±0.002	0.707±0.010	0.798±0.010	—	—	—	—	—
50 Sn	0.782±0.002	0.680±0.002	—	—	0.751	0.85	—	—	—
73 Ta	0.716±0.005	0.597±0.005	0.607±0.006	0.725±0.006	—	—	—	—	0.462
74 W	0.706±0.002	0.590±0.002	—	—	0.680	0.81	—	—	—
77 Ir	0.703±0.002	0.581±0.002	—	—	—	—	—	—	—
78 Pt	0.695±0.002	0.576±0.002	0.590±0.062	0.712±0.012	—	—	—	—	—
79 Au	0.692±0.003	0.576±0.003	0.588±0.006	0.708±0.006	—	—	—	0.21	0.458
82 Pb	0.677±0.003	0.556±0.003	—	—	0.660	0.80	—	—	—
90 Th	0.691±0.002	0.556±0.002	0.581±0.006	0.7123±0.006	—	—	—	—	—
92 U	—	—	—	—	0.630	0.78	—	—	—

From the definition of the stopping coefficient B (§ 4), we can see that the relative stopping powers will be either increasing, or decreasing functions of the energy of the incident particles, depending on whether I is larger or smaller than I_{st}.

The relative stopping powers are more accurately determined than the absolute stopping powers. Usually /93, 158, 476, 177/ the mean range of the particles in the standard material is determined from the transmission or specific-ionization curves (see § 6). Then, the front surface of the standard facing the incident particles is replaced by the sample to be investigated. By means of thin shims of the standard material the readings of the recording instrument are made to correspond with the same values of R_n or R_l (see § 6). The ratio of the thickness of the standard material

TABLE 28

Stopping powers of materials relative to copper for high energy protons

Material	Zrelov/49/ $S_m(T_p =$ = 635 Mev)	Barkas /177/			Bloembergen/161/ $S_m(T_p =$ = 70 Mev)	Heinz/297/ $S_m(T_p =$ = 342 Mev)	Carvalho /221/ $S_m(T_p =$ = 208 Mev)
		$S_m(T_p =$ = 750 - - 600 Mev)	$S_m(T_p =$ = 600 - - 450 Mev)	$S_m(T_p =$ = 450 - - 300 Mev)			
Hydrogen, H	3.016	—	—	—	—	—	—
Beryllium, Be	1.167	—	—	—	—	—	—
Carbon, C	1.268	—	—	—	—	—	—
Aluminum, Al	—	1.14	1.14	1.136	1.22	—	—
Copper, Cu	1.000	1.100	1.000	1.000	1.000	—	—
Cadmium, Cd	0.887	—	—	—	—	—	—
Tungsten, W	0.794	—	—	—	—	—	—
Lead, Pb	—	0.76	0.758	0.756	0.748	—	—
Uranium, U	—	0.738	0.736	0.728	—	—	—
Photoemulsion	—	0.999	0.994	0.989	—	0.89	1.005

to that of the investigated material in these two experiments gives the equivalent stopping power of the sample for a given energy of the particles. If, for example, in 1 g/cm^2 of aluminum, a proton loses the same amount of energy as in 1.25 g/cm^2 of the investigated material, then the relative mass stopping power of the latter is equal to 0.8. Aluminum, copper or air, and recently also argon, are usually chosen as standards.

The relative stopping powers of various materials for protons, deuterons and α-particles are given in Tables 27—30 and are also partly used for the curves in Figures 31— 35. Figure 37 shows experimental curves of the dependence of the relative electronic stopping powers on log Z (the charge of the stopping atoms) for three proton energies.

It follows from Tables 27—30 that in agreement with the theory the thickness of a material with $Z > 13$, whose stopping power is equivalent to 1 g/cm^2 of aluminum, decreases with increasing energy. For example, the thickness of silver, with an equivalent stopping power of 1 g/cm^2 of aluminum, varies from 3.05 mg/cm^2 for $T_p \approx 0.1$ Mev to 1.27 g/cm^2 for $T_p = 340$ Mev. Different thicknesses of gold and aluminum are required to produce the same stopping of protons and α-particles in all energy ranges.

TABLE 29

Relative stopping powers for deuterons

Material	Brolley /159/ S_a (relative to air) T_d = 8.86 Mev	Tobnas /132/ S_m (relative to aluminum) T_d = 180 Mev	Stefan-Thornton /132/ S_m (relative to aluminum) T_d = 190 Mev
Hydrogen, H	0.185	2.57	—
Helium, He	0.321	—	—
Lithium, Li	—	—	—
Beryllium, Be	—	1.02	1.08
Carbon, C	—	1.12	1.14
Nitrogen, N	0.966	1.10	—
Air	1.000	—	—
Oxygen, O	1.088	1.08	—
Neon, Ne	1.258	—	—
Aluminum, Al	—	1.00	1.00
Argon, A	2.042	—	—
Iron, Fe	—	0.889	—
Copper, Cu	—	0.867	0.86
Krypton, Kr	3.393	—	—
Silver, Ag	—	—	0.752
Tantalum, Ta	—	—	0.658
Xenon, Xe	4.425	—	—
Methane, CH_4	1.598	—	—
Carbon dioxide, CO_2	3.037	—	—
Gold, Au	—	—	0.627
Lead, Pb	—	0.613	—
Uranium, U	—	—	0.602

TABLE 30

Relative stopping powers for α-particles

Material	Kelly /339/ S_m (relative to aluminum)		Rosenblum, Mano /433, 381/ S_m (relative to aluminum)	Porat /416/ S_m (relative to air)	
	T_α, Mev				
	33	21	6	3.72	4.33
Carbon, C	—	—	1.35	—	—
Aluminum, Al	1.000	1.000	1.000	0.777	0.806
Copper, Cu	0.799	0.782	0.724	—	—
Nickel, Ni	—	—	—	0.573	0.585
Silver, Ag	0.671	0.551	0.56	0.415	0.439
Tantalum, Ta	0.546	0.517	—	—	—
Gold, Au	—	—	0.41	0.296	0.306
Bismuth, Bi	0.520	0.494	0.387	—	—
Thorium, Th	0.503	0.475	—	—	—

For light materials ($Z < 13$), the stopping power relative to aluminum decreases with increasing energy, the stopping thickness equaivalent to 1 mg/cm^2 of aluminum is always smaller than 1 mg/cm^2. This is important in experiments in which moderators which are equivalent in stopping to aluminum or air have to be used.

It can be seen from Figure 37 and Tables 27—30 that the relative electronic stopping powers for protons, deuterons and α-particles depend linearly on log Z of the stopping materials. Small deviations from linearity, showing fluctuations for neighboring elements, are mentioned by the authors of /155, 157, 263, 452/. These fluctuations are apparently connected with the occupation of the electronic shells and with the phases in transition elements (nickel-copper, tantalum-thorium). Direct proof of the dependence of the atomic stopping powers on the phases of the materials was obtained by Sofftky /469/. He showed that the atomic stopping power of graphite for 1.1 Mev protons is 6% higher than that of diamond.

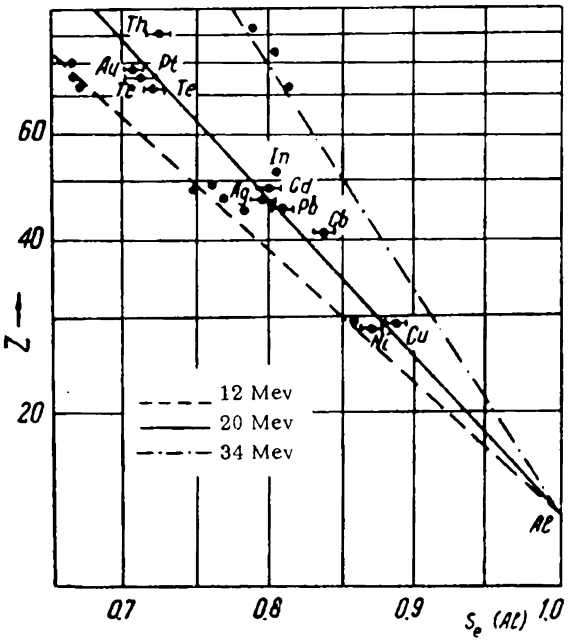

FIGURE 37. Relative electronic stopping power versus Z /452/, for three proton energies: 12 Mev /477/, 20 Mev /452/ and 340 Mev /158/

The universal stopping-power curve. It was noted in § 4, that Lindhard and Scharff /360/ proposed to determine the energy losses by the semi-empirical function $L(x)$, which is common for all elements. This function gives the stopping power per electron in relative units. The method is convenient for comparing the mean energy losses for various particles and velocities, even in the energy range where the binding corrections of the electrons are important (these corrections, as is known, cannot be accurately calculated for the L-, M-, and other shells). Madsen /382/ showed that the ionization losses of protons with energies of 0.4—2 Mev in silver, copper and gold are well represented by a curve, whose analytic expression is given by (4.35). This expression was proposed by Lindhard and is based on an extensive analysis of experimental data on stopping powers, obtained up to 1953.

Burkig and McKenzie /155/, using more recent experimental data on the electronic stopping powers /155, 159, 339, 452/, plotted the graph of $L(x)$ which differs considerably from the original universal curve obtained by Lindhard, given in Figure 38 (the crosses represent the experimental data used by Lindhard in /360/). Thus, $L(x)$ can be used to calculate the electronic stopping power for large ($x > 10$). For small x (< 10), the linear approximation is no longer sufficient. It was also shown in /492/ that Lindhard's curve cannot be used for calculating the stopping power in materials with $Z < 20$.

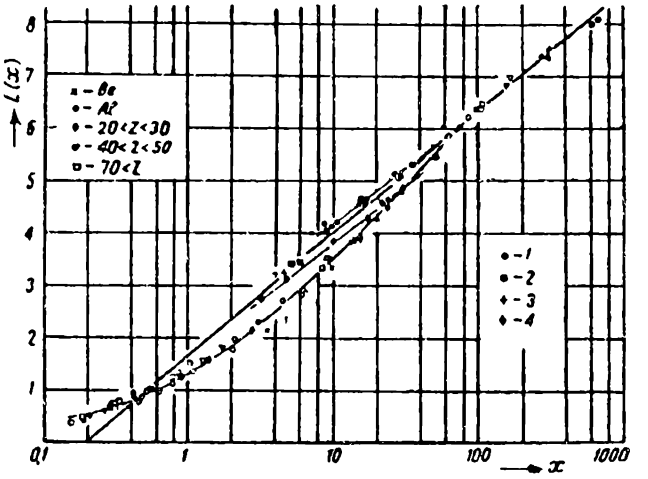

FIGURE 38. The graph of Lindhard and Scharff:

1—Sonnet /452/; 2—Teasdale /477/; 3—Kelly /339/; 4—Brolley and Ribe /159/.

It has been attempted /174/ to use the Lindhard-Scharff theory for the calculation of the stopping powers of complex compounds, in which the valency bonds have to be taken into account.

Stopping powers of complex compounds. According to Bragg's rule, the molecular stopping power of complex compounds can be calculated as the sum of the stopping powers of its constituent elements

$$\varepsilon_{\text{mol}}(X_n Y_m) = n\varepsilon_a(X) + m\varepsilon_a(Y). \qquad (5.9)$$

Small deviations from this rule may be expected, owing to the variation of the wave functions of the external electrons in the formation of the compound, which should lead to an increase in the mean excitation energy.

The experimental data generally confirm Bragg's rule, as shown by /296/ for the stopping power of chemical compounds for α-particles from natural radioactive sources (4 – 9 Mev). Garin and Faragg /268/ obtained confirmation from the study of the stopping of α-particles in silicon, zirconium, gold and in their compounds, and so did Ellis et al. /238/, who measured the stopping power of polyethylene in the form of a film or gas for the α-particles of Po^{210} ($T_\alpha = 5.3$ Mev).

Thompson /476/, studying the stopping of fast protons ($T_p = 200 - 340$ Mev) in compounds of carbon, nitrogen, oxygen and chlorine, found that the summation rule is fulfilled to within $\sim 1\%$. On the other hand, it was shown in /434/ that for proton energies lower than 150 kev, the molecular stopping powers of gaseous compounds of hydrogen, carbon, nitrogen and oxygen

are lower than the sums of the atomic stopping powers. Jorgensen, studying the stopping powers of solid compounds of the polyethylene (CH_2) or polystyrene $(C_8H_8)_n$ type, observed deviations from the rule for $T_p \sim 100$ kev.

TABLE 31

Experimental values /434/ of the molecular stopping powers of some compounds (in units of 10^{-15} ev·cm^2/molecule)

T_p, kev	C_2H_2	C_2H_4	C_2H_6	NH_3	NO	N_2O
30	43.4	—	116.0	29.7	—	—
40	47.4	54.4	126.0	32.0	32.6	47.0
50	49.5	57.4	133.0	33.6	34.5	48.6
60	49.8	58.7	135.7	34.6	35.7	49.9
70	49.2	58.8	135.5	34.7	36.4	50.5
80	48.0	58.0	134.4	34.4	36.6	50.9
90	46.7	56.7	133.5	33.9	36.6	51.0
100	45.0	55.5	134.7	33.5	36.4	50.7
150	38.5	48.8	116.5	30.1	33.2	47.0
200	32.9	41.4	102.0	25.6	29.7	42.0
250	29.0	36.1	89.2	22.3	26.7	37.6
300	25.9	32.0	79.8	19.9	24.1	34.0
350	23.5	28.8	72.2	17.9	22.0	31.0
400	21.4	26.2	66.3	16.4	20.3	28.6
450	19.7	24.1	61.4	15.1	18.9	26.6
500	18.4	22.4	57.3	14.0	17.6	25.0
550	17.2	20.9	53.9	13.1	16.6	23.5
600	16.2	19.6	51.0	12.3	15.7	22.2

Thus, at high energies of the charged particles the stopping powers of complex compounds can be determined from the stopping powers of their components (see, for example, Table 35). For low energies, it is preferable to use the experimental values for the molecular stopping powers.

TABLE 32

Experimental values* /157/ of the molecular stopping powers of some compounds (in units of 10^{-15} ev·cm^2/molecule)

T_p, kev	Lithium fluoride, LiF	Calcium difluoride, CaF_2
50	23.0	—
75	25.7	66.8
100	26.4	69.4
125	26.0	69.0
150	24.2	66.0
175	22.4	61.4
200	21.0	57.2
250	19.2	50.2
300	17.9	46.2
350	16.7	43.6
400	15.6	41.6
450	14.4	39.6
500	13.5	38.0
550	12.7	36.7
600	12.2	35.6

Tables 31—35 give the corresponding experimental data for low-energy protons. Useful semi-empirical expressions /281/ are given describing

* Calculated by Bragg's rule from the experimental /491/ and calculated /447, 288/ data on the stopping powers of carbon and hydrogen.

the stopping power of plastic scintillation crystals ($CH_{n\,105}$) for fast charged particles with energies of 1—150 Mev:

$$\left.\begin{aligned} \frac{dE}{dx} &= 17.91\,x - 0.448, \quad (p) \\ \frac{dE}{dx} &= 24.41\,x - 0.448, \quad (d) \\ \frac{dE}{dx} &= 29.30\,x - 0.448, \quad (t) \\ \frac{dE}{dx} &= 71.64\,x - 0.448, \quad (\alpha) \end{aligned}\right\} \qquad (5.10)$$

where x is the thickness of the material, g/cm^2; the type of the charged particles is indicated in brackets.

TABLE 33

Mass stopping power of mica (muscovite) for protons, according to the experimental data of /132, 340, 382/

T_p, kev	ε_m, Mev·cm^2/g	T_p, kev	ε_m, Mev·cm^2/g	T_p, kev	ε_m, Mev·cm^2/g
350	312	800	189	1250	143
400	286	850	182	1300	139
450	266	900	176	1350	136
500	250	950	171	1400	133
550	236	1000	165	1500	127
600	224	1050	160	1600	122
650	214	1100	154	1700	117
700	204	1150	150	1800	112
750	196	1200	146	1900	108
—	—	—	—	2000	102

TABLE 34

Experimental values /368/ of the mass stopping powers (Mev·cm /g) of some plastics for protons and α-particles

T_p, kev	Polystyrene CH	Polyethylene C_nH_{3n}	Plaiolit S-5A	T_α, kev	Polystyrene CH	Polyethylene C_nH_{2n}	Plaiolit S-5A
25	0.806	—	—	35	—	0.98	—
30	0.864	—	—	40	0.96	1.07	1.05
32	—	0.984	—	50	1.10	1.22	1.17
40	0.931	1.040	—	60	1.21	1.33	1.26
50	0.973	1.083	—	70	1.30	1.43	1.34
54	—	—	0.984	80	1.39	1.52	1.41
60	0.994	1.108	1.006	90	1.46	1.60	1.48
70	1.002	1.119	1.024	100	1.53	1.67	1.54
80	0.998	1.119	1.028	120	1.63	1.81	1.66
90	0.992	1.105	1.023	140	1.74	1.92	1.77
100	0.978	1.083	1.010	160	1.83	2.03	1.87
120	0.926	1.034	0.968	180	1.92	2.12	1.96
140	0.879	0.990	0.915	200	2.00	2.22	2.05
160	0.832	0.946	0.866	225	2.11	2.33	2.15
180	0.780	0.900	0.823	250	2.20	2.43	2.25
200	0.738	0.856	0.786	275	2.29	2.52	2.34
225	0.689	0.804	0.743	300	2.36	2.61	2.43
250	0.644	0.755	0.704	320	2.43	2.68	2.50
275	0.604	0.711	0.669	340	2.49	—	—
300	0.578	0.676	0.635	—	—	—	—
325	0.551	0.648	0.604	—	—	—	—
335	0.540	0.640	0.592	—	—	—	—

TABLE 35

Mass stopping powers of some organic compounds (kev·cm^2/g) for protons*

T_p, Mev	Polyethylene C_nH_{2n}	Anthracene $C_{14}H_{10}$	Stilbene
1	295	256	279
2	178	157	168
3	132	117	123
4	104	92.5	98
5	87	77.3	82
6	75.3	67.0	71
7	65.7	58.6	63
8	58.9	52.4	56
9	93.9	48.1	51
10	49.5	44.1	46.6
11	45.7	40.8	43
12	42.5	37.9	40
13	39.8	35.5	37.4
14	37.4	33.3	35.2
15	35.4	31.6	33.2
16	33.5	29.9	—
17	31.8	28.5	—
18	30.4	27.2	—
19	29.1	26.0	—
20	27.9	25.0	—
25	23.1	20.7	—
30	19.9	17.9	—

* See footnote to Table 32.

Experimental data on the distribution of the energy losses of heavy charged particles. The mean energy losses of heavy particles are often equal to the most probable losses, and they are distributed according to a gaussian curve with a half-width σ_E, determined by (4.43) or (4.45).

TABLE 36

Experimental data on the distribution of the energy losses of low-energy protons /382/

Stopping			
in nickel		in copper	
T_p, kev	$\frac{d\sigma_E^2}{dx}$, kev^2/mg/cm^2	T_p, kev	$\frac{d\sigma_E^2}{dx}$, kev^2/mg/cm^2
527	89	446	34
704	78	749	63
739	68	755	57
741	62	945	65
757	54	949	72
941	94	1004	76
1046	116	1006	96

Thus, for example, Madsen /382, 383/ and Chilton et al. /212/ have shown that the experimentally obtained parameter σ_E for low energy protons ($T_p < 2$ Mev) passing through sufficiently thick layers satisfies Bohr's simple relation (4.44)

Table 36 gives some results of Chilton's measurements. From these an estimate can be made of the order of magnitude of the distribution of energy losses for protons of relatively low energies in "thick" foils of nickel and copper.

It was shown in /234/ that the energy distribution of α-particles passing through mica and aluminum is in agreement with the formulas of Livingstone and Bethe (4.43)—(4.45).

The experimental distribution of the energy losses of heavy particles in "thin" layers of a stopping material is well described by Landau's formula (4.47). Eisberg et al. /312/, investigating the statistical fluctuations of the ionization energy losses of fast protons (31—37 Mev), have shown that as the thickness of the target is reduced, a gradual transition from a gaussian (symmetric) to the Landau energy loss distribution is observed.

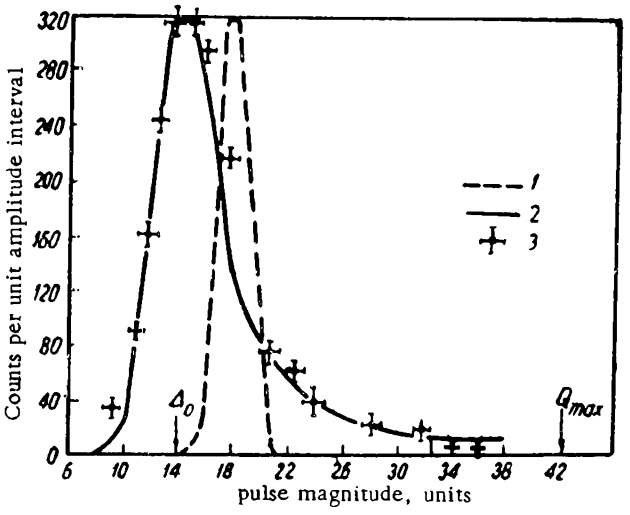

FIGURE 39. Experimental distribution of the energy losses of protons with an initial energy of 37 Mev after passing 10 cm in argon at 0.2 atm pressure in a proportional counter /261/:

1—Poisson distribution of the energy losses; 2—distribution of the energy losses according to Landau's theory; 3—experimental points.

The experimental distribution of pulse magnitudes in a proportional counter filled with argon at 0.2 atm for 37 Mev protons is shown in Figure 39. The experimental data are in good agreement with the theory developed by Landau.

§ 6. Experimental data on the relation between range and energy for fast protons and for α-particles

The basic mechanism of energy losses of fast protons and α-particles in a wide energy range is by inelastic collisions with electrons in which the particles lose small amounts of energy and do not suffer appreciable deviations from their direction of motion. This provides a well defined correspondence between the initial energy of the particles and their mean range in the material.

The importance of range-energy relations reaches far beyond the examination of the applicability of the classical and quantum mechanical stopping theories (§ 4). These relations are used in nuclear and in elementary particle physics for the determination of particle energies, and together with measurements of specific energy losses or other independent parameters — for the determination of the mass and charge of particles (§ 10).

The first attempt to establish the range-energy relation was made by Geiger, who already in 1910 investigated this relation for α-particles in air. Extensive theoretical and experimental material on the ranges of protons and α-particles in various elements has since been accumulated, and more accurate relations were obtained.

Theoretical relations between range and energy. The mean length of the path, along which the energy of a particle with mass M and charge ze decreases from T_1 to T_2, can be calculated by the Bethe-Bloch formula as follows:

$$\Delta R = -\int_{T_1}^{T_2} \frac{dE}{\left(\frac{dE}{dx}\right)} = \frac{M}{z^2} \frac{m}{4\pi e^4 n} F(v), \tag{6.1}$$

where $F(v)$ is a function depending on the velocity of the particle at the beginning and end of the path.

Thus, the mean range of a particle in a given medium is proportional to the product of $\frac{M}{z^2}$ and some function of the initial velocity of the particle. Owing to the failure of the Bethe-Bloch formula at low energies which is a result of the influence of atomic collisions and charge exchange, the integration in (6.1) cannot be performed up to $T_2 = 0$. In order to calculate the mean range of particles with energy T, the following relation is used:

$$R(T) = R(T_0) + \int_{T_0}^{T} dT \Big/ \left(-\frac{1}{\rho}\frac{dE}{dx}\right), \tag{6.2}$$

where $R(T_0)$ is the experimental value for the range of a particle with energy T_0, for which the influence of charge-exchange collisions (§ 7) is negligibly small. The lower limit for protons can be taken at $T_0 \sim 1.5$ Mev, and for α-particles at $T_0 \sim 5$ Mev.

Using the calculated values of $\frac{dE}{dx}$ (see Figures 18 — 23) and the experimental values of the mean range of protons with $T_0 = 2$ Mev, Sternheimer /447/ calculated according to (6.2) the relations between the proton energies and their mean range in beryllium, carbon, aluminum, air, copper and lead. The values of $R(T_0) = R$ (2 Mev) were determined from experimental data /156, 359/.

The results of the corresponding calculations by Sternheimer are represented by the solid curves in Figures 40 — 48*.

The range-energy relations of protons in gold and silver (Figures 40 — 41) were taken from the data of /156/. The broken curves in Figures 40 — 43

* Later, Sternheimer (Phys. Rev., 124, 205, 1961) observed that he used too large values of $I_{(Cu)}$ and $I_{(Pb)}$ in his calculations. The proton ranges in copper and lead given in Figures 46 — 48 are therefore somewhat overestimated (by ~2% for copper and by ~4% for lead at $T_p = 200$ Mev).

represent Smith's /449/ data, who used $I_{(Al)} = 150$ ev and did not take into a account the density and electron binding effects in aluminum.

In Table 37 a comparison is made between the experimental and calculated values of ranges and energy losses of protons in aluminum. The

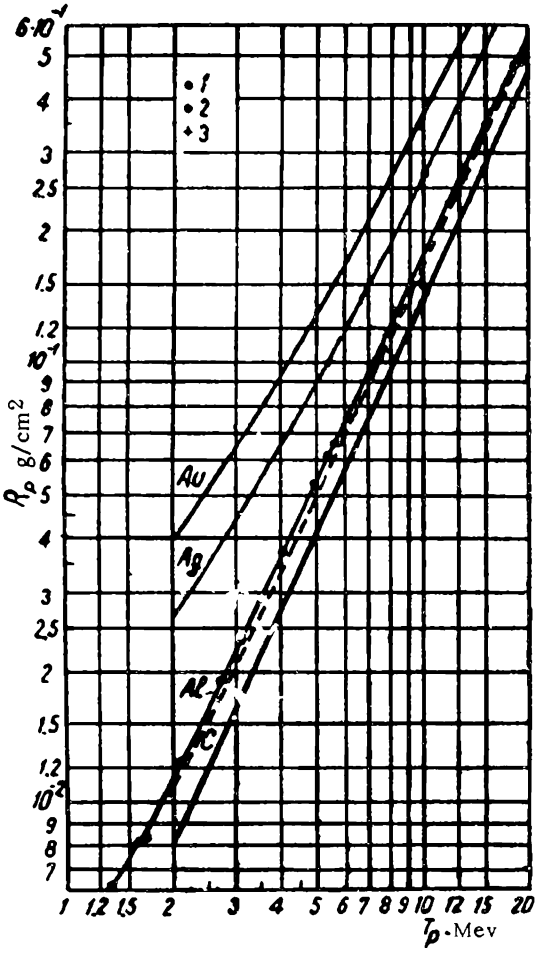

FIGURE 40. Mean range of protons in carbon, aluminum, silver and gold /156, 447/; T_p = = 1—20 Mev. The experimental values of the mean ranges are represented by the points: 1—/291/; 2—/156/; 3—/456/

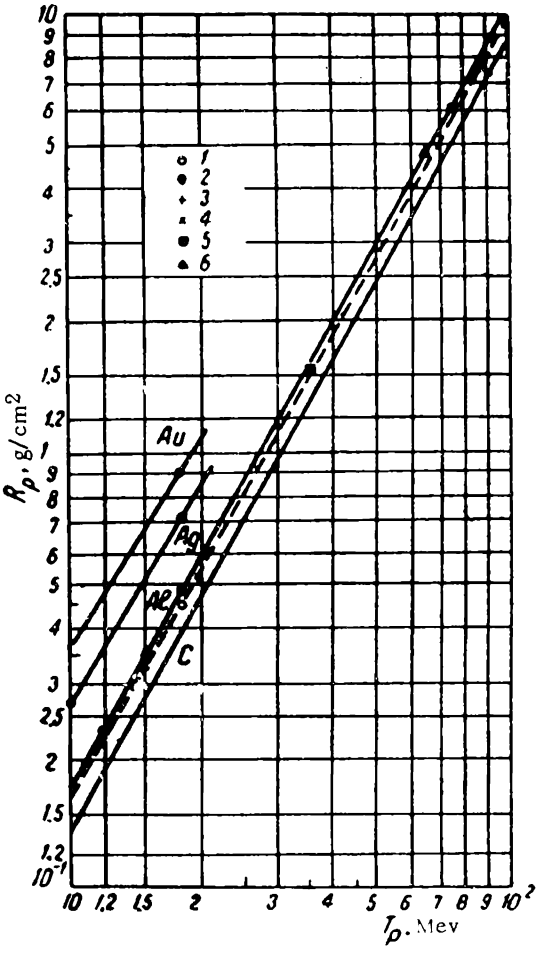

FIGURE 41. Mean range of protons in aluminum, silver and gold /156, 447/; $T_p = 10—10^2$ Mev: 1--/291/; 2—/156/; 3—/28/; 4—/246/; 5—/219/; 6—/161/

calculations were performed by Bichsel and Uehling /171/. $I_{Al} = 163$ ev was taken in the calculations. The experimental values of R(Al) were obtained by Bichsel /156/.

The calculated values of the proton ranges for $T > 10^9$ ev are more of a mathematical rather than of a practical importance. In fact, in passing a thickness R, corresponding to R_p (10^9 ev), the proton beam is very strongly attenuated (§ 3) due to nuclear interactions. R_p (10^9 ev) corresponds to approximately four mean free paths for nuclear interactions. However, the calculated data for the proton ranges with $T_p = 1—100$ Gev can be used for the calculation of meson ranges (see below).

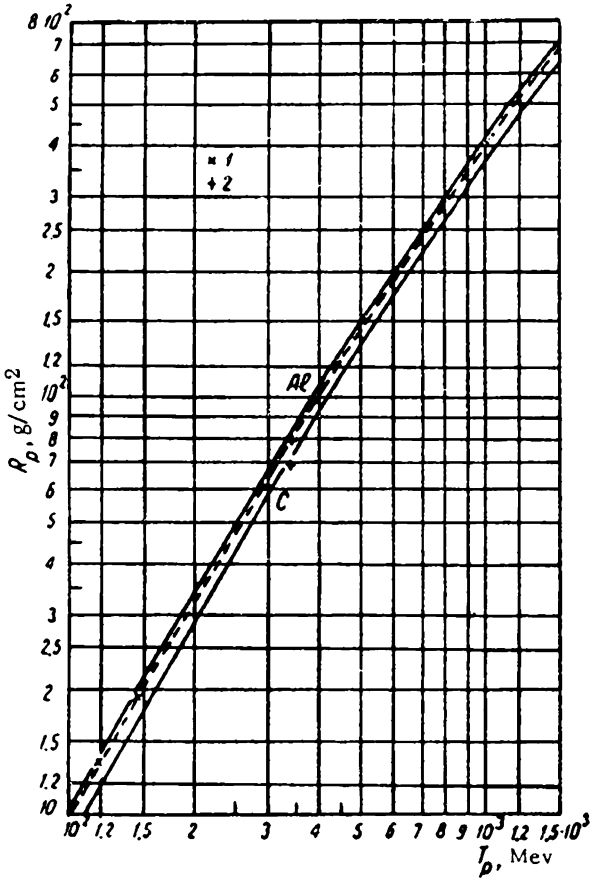

FIGURE 42. Mean range of protons in carbon and aluminum /447/; $T_p = 10^2$ Mev—$1.5 \cdot 10^3$ Mev;
1—/246/; 2—/384/

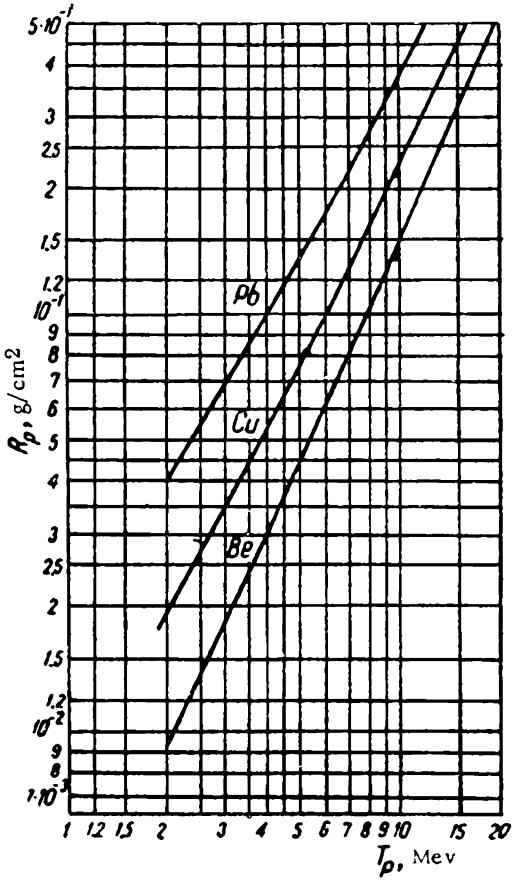

FIGURE 43. Mean range of protons in beryllium, copper and lead /447/; $T_p = 1$—20 Mev. Experimental data from /156/.

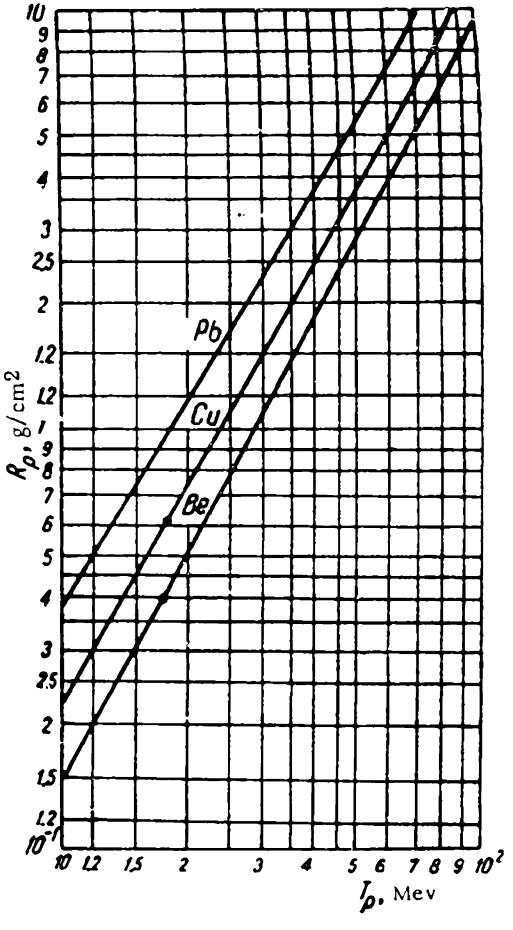

FIGURE 44. Mean range of protons in beryllium, copper and lead /447/; $T_p = 10$—10^2 Mev. Experimental data from /156/

The solid curves in Figures 49—50 represent the calculated results /154/, of the proton ranges in Ilford G—5 phtoemulsion ($\rho = 3.185$ g/cm^3, $n = NZ = 1.04 \cdot 10^{24}$ cm^{-3}). In the calculation $I_{em} = 331$ ev was taken, and the corrections C and δ in (4.42) were obtained from the calculations of Walske and Sternheimer (§ 4)*. In Figures 49—50 the abscissas are the

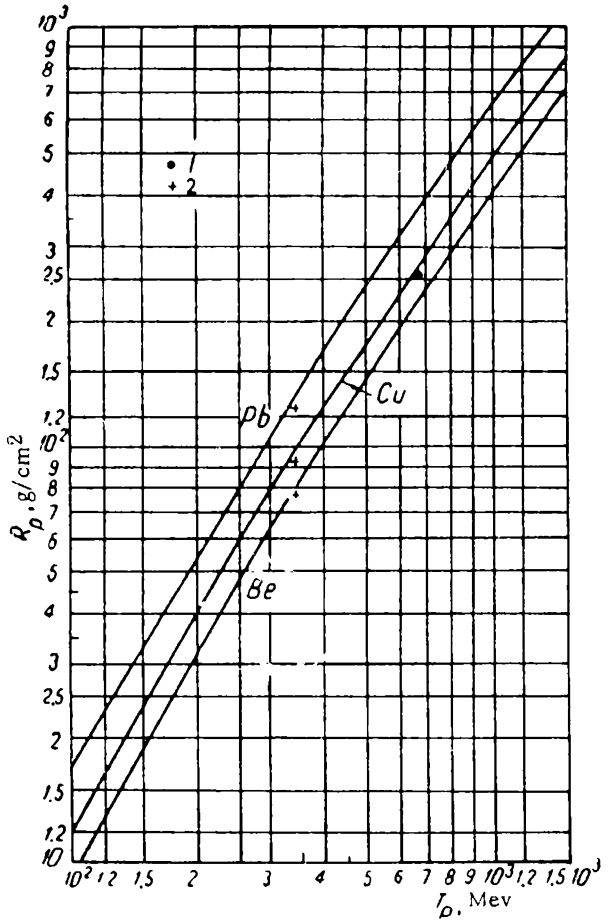

FIGURE 45. Mean range of protons in beryllium, copper and lead /447/: $T_p = 10^2$ Mev—$1.5 \cdot 10^3$ Mev. Experimental data taken from:

1—/49/; 2—/384/

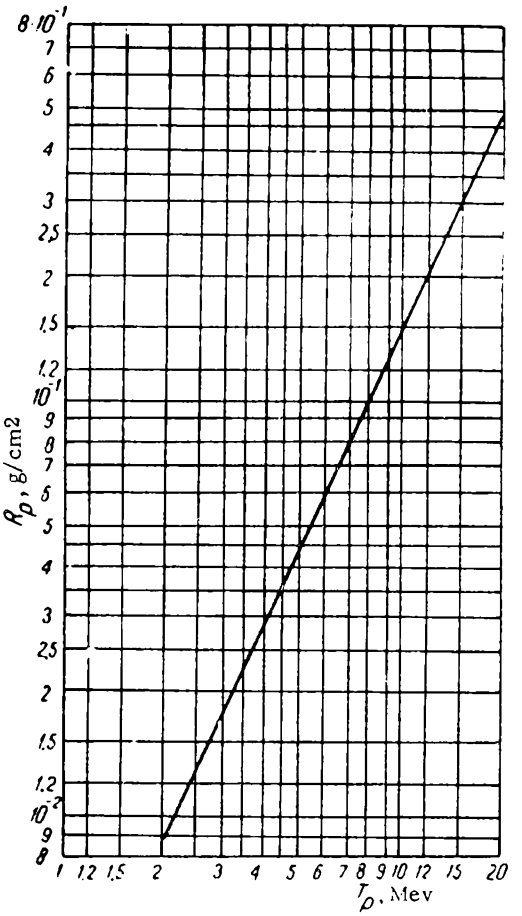

FIGURE 46. Mean range of protons in air /447/: $T_p = 1$—20 Mev

reduced values of the kinetic energy of the charged particles $\tau = \frac{T}{M_p}$ (M_p = = 938 Mev is the rest mass of the proton), and the ordinates are the ranges of charged particles with a charge z and mass M:

$$\lambda = \frac{z^2 R}{M} - 1.2 \cdot 10^{-5} z^2, \qquad (6.3)$$

where M is the mass of the particle in units of the proton mass;

R is the range of a particle with energy T.

The second term in (6.3) allows for differences in charge-exchange conditions at the end of the range (see below).

To obtain the theoretical relations between range and energy of protons in other materials with a given I, not shown in Figures 40—48, Sternheimer

* The theoretical values of the stopping power of the emulsion and the range-energy relations were also calculated in /490, 178/.

proposed /455/ the expression

$$R(T_p, I) = R\left(2\ \text{Mev}, I\right) + \frac{A}{2Z}\Phi_{Al}(T_p)\left(1 + G_{1\chi} + G_{2\chi}^2 + G_{3\chi}^3\right); \qquad (6.4)$$

where $R(2\ \text{Mev}, I)$ is the experimental value of the range of a proton with 2 Mev energy in a material with mean excitation potential I;

Z and A are the atomic number and atomic weight of the material;

$$\Phi(T_p) = \frac{2Z}{A}\left[R(T_p) - R(2\,\text{Mev})\right];$$

$$\chi = \log_{10}\frac{I}{I_{Al}} = \log_{10}\left(\frac{I(\text{ev})}{166}\right).$$

Expression (4.44) and the numerical values of the coefficients G, depending only on T_p, were obtained in this formula by interpolation of the theoretical

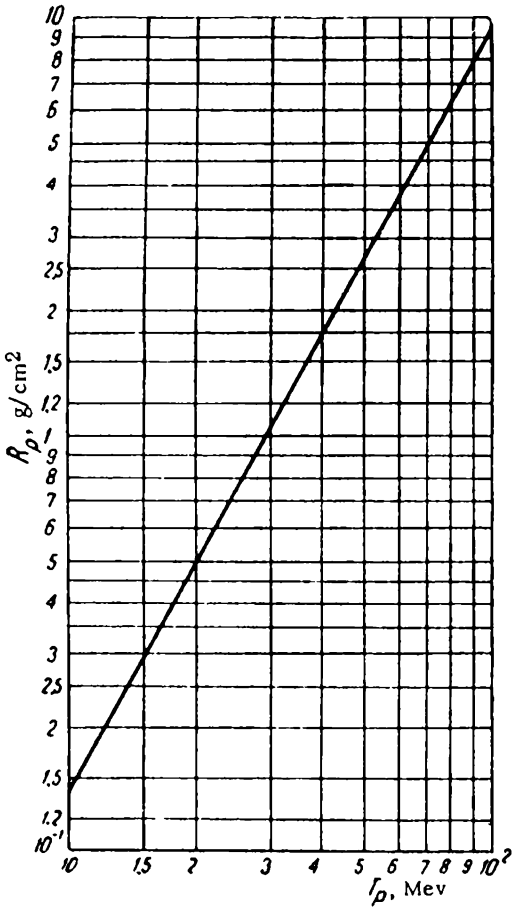

FIGURE 47. Mean range of protons in air /447/; $T_p = 10 - 10^2$ Mev

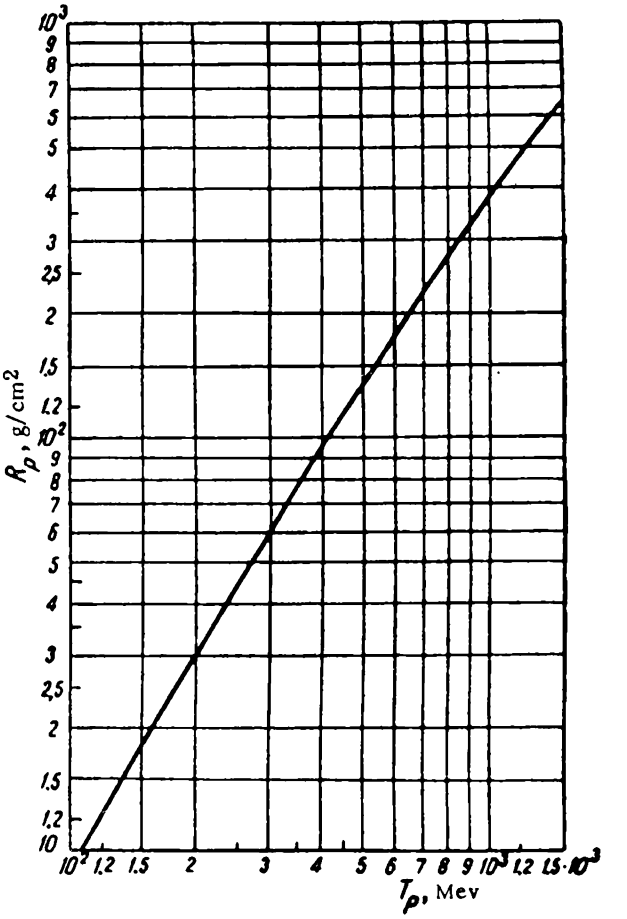

FIGURE 48. Mean range of protons in air /447/; $T_p = 10^2$ Mev $- 1.5 \cdot 10^3$ Mev.

raltions between the range and energy for beryllium, aluminum, copper and lead (see Table 37 and Figures 40—45). The numerical values of the

coefficients necessary for calculations according to (6.4) are contained in Table 38.

TABLE 37

Theoretical and experimental mean energy losses and ranges of protons in aluminum /171/

T_p, Mev	$-\frac{1}{\rho}\left(\frac{dE}{dx}\right)_{\text{theor}}$	$-\frac{1}{\rho}\left(\frac{dE}{dx}\right)_{\text{exp}}$*	R_{theor}	R_{exp}
	Mev·cm²/g		mg/cm²	
0.1	371	416	—	—
0.15	360	386	—	—
0.20	343	334	—	—
0.25	327	314	—	—
0.30	310	293	—	—
0.35	293	279	—	—
0.40	279	268	—	—
0.50	252	250	—	—
0.60	230	233	—	—
0.70	212	217	—	—
0.80	197	202	—	—
0.90	185	190	—	—
1.00	173	177	4.15	3.87
1.2	155	154	5.38	5.16
1.4	141	135	6.74	6.59
1.6	129	123	8.23	8.14
1.8	119	117	9.85	9.82
2.0	111	112	11.60	11.59
3.0	83.2	—	22.15	22.18
4 0	67.6	—	35.56	35.55
5.0	57.3	—	51.70	51.64
6.0	50.0	—	70.42	70.31
7.0	44.5	—	91.64	—
8.0	40.2	—	115.3	—
9.0	36.8	—	141.3	—
10.0	33.9	—	169.6	—
12.0	29.5	—	233.1	233.2
14.0	26.1	—	305.3	—
16.0	23.5	—	386.0	—
18.0	21.5	—	475.1	476.0
20.0	19.8	—	572.3	—

* See /491/ and Figure 32.

We give an example of the use of the interpolation formula /455/.

Let us determine the proton ranges with 50 and 100 Mev energy in silver. The following experimental values $I_{(Ag)} = 586$ ev /155, 156/ and $R(2\text{ Mev}) = 0.0263$ g/cm² /156/ are used. For 50 Mev protons we obtain from Table 38 $G_1 = 0.397$, $G_2 = 0.157$, $G_3 = 0.093$ and, consequently, $G = 1.2799$. For $\Phi_{Al} = 2.811$ g/cm² and $\frac{2Z}{A} = 0.8713$, the second term on the right hand side of (6.4/ is equal to 4.125 g/cm². Adding R(2 Mev), we obtain R_{Ag}(50 Mev)= = 4.155 g/cm². Similarly for $T_p = 100$ Mev we have $G = 1.2443$ and $R =$ = 13.79 g/cm².

Connections between the ranges of protons and other heavy charged particles. The theoretical relations between range and energy for protons can be used for other heavy particles. According to (6.1), the range R_{zM} for particles with mass M and charge ze is expressed in terms of the proton range in the same medium as follows:

$$R_{zM}(T) = \frac{1}{z^2}\frac{M}{M_p} R_p\left(\frac{M_p}{M} T\right), \qquad (6.5)$$

where $R_p\left(\frac{M_p}{M}T\right)$ is the range of a proton with the reduced energy $\frac{M_p}{M}T$.

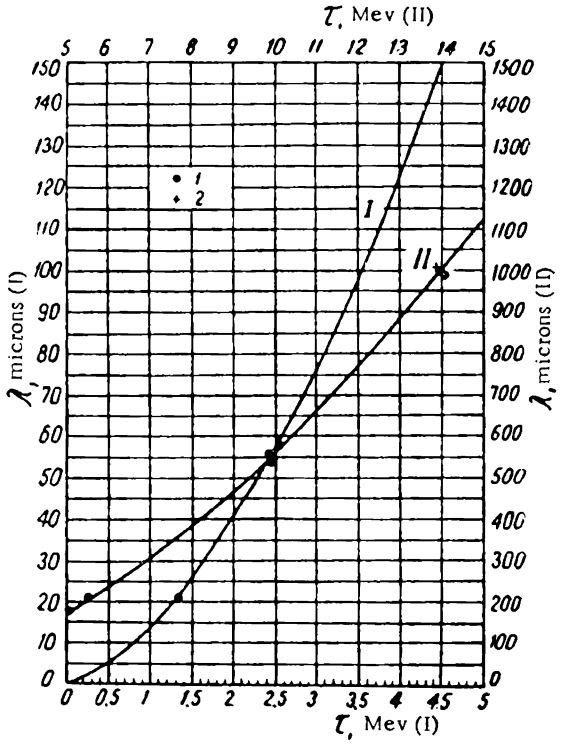

FIGURE 49. Reduced ranges of charged particles in Ilford G-5 photoemulsion with $\rho = 3.185$ g/cm^3. Experimental points from /154, 246, 219, 297/:
1—/154/; 2—/287/

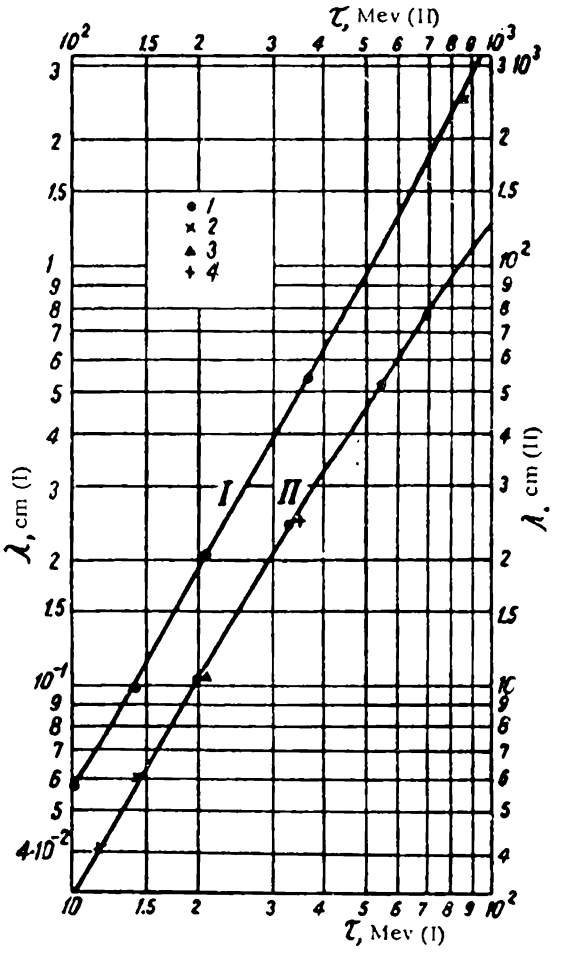

FIGURE 50. Reduced ranges of charged particles in photoemulsion /154, 287/:
1—/154/; 2—/246/; 3—/219/; 4—/297/

This relation is correct, if the particles have the same charge-exchange conditions at the end of their path. For example, the relations between the mean ranges of the hydrogen and helium isotopes are

$$R_d(T) = 1.999\ R_p\left(\frac{T}{1.999}\right) \cong 2R_p\left(\frac{T}{2}\right), \tag{6.6}$$

$$R_t(T) = 2.993\ R_t\left(\frac{T}{2.993}\right) \cong 3R_p\left(\frac{T}{3}\right), \tag{6.7}$$

$$R_{He_3}(T) = 0.753\ R_{He_4}\left(\frac{T}{0.734}\right) \cong {}^3/_4\ R_{He_4}\left(\frac{4}{3}T\right). \tag{6.8}$$

Similarly, the meson ranges are expressed in terms of the proton ranges by

$$R_\mu(T) = 0.114\ R_p(8.8\ T), \tag{6.9}$$

$$R_\pi(T) = 0.149\ R_p(6.7\ T), \tag{6.10}$$

and the relation between the ranges of π-mesons and μ-mesons by

$$R_\pi(T) = 1.31\ R_\mu\left(\frac{T}{1.31}\right). \qquad (6.11)$$

The relation between the ranges of particles with different charges can be obtained by taking into account the difference in charge-exchange for the

TABLE 38

Numerical values of the functions G_1, G_2 and Φ_{Al} in (6.4)

T_p, Mev	G_1	G_2	G_3	Φ_{Al}, g/cm^2	T_p, Mev	G_1	G_2	G_3	Φ_{Al}, g/cm^2
3	0.634	0.450	0.495	0.01016	375	0.295	0.085	0.055	91.16
4	0.595	0.379	0.468	0.02313	400	0.293	0.083	0.054	107.09
5	0.570	0.336	0.436	0.03871	450	0.288	0.081	0.053	121.80
6	0.551	0.307	0.404	0.05681	500	0.285	0.080	0.051	143.54
7	0.537	0.285	0.378	0.07734	550	0.282	0.079	0.049	166.19
8	0.525	0.269	0.353	0.1102	600	0.279	0.078	0.047	189.65
9	0.515	0.257	0.330	0.1254	700	0.273	0.077	0.045	238.6
10	0.507	0.247	0.309	0.1528	800	0.268	0.075	0.044	289.8
12	0.493	0.229	0.278	0.2142	900	0.264	0.074	0.042	342.8
14	0.481	0.218	0.250	0.2841	1000	0.259	0.073	0.041	397.2
16	0.472	0.211	0.225	0.3622	1250	0.251	0.071	0.040	537.6
18	0.464	0.204	0.205	0.4484	1500	0.243	0.068	0.039	682.2
20	0.457	0.198	0.189	0.5424	1750	0.236	0.066	0.038	829.4
22.5	0.449	0.193	0.172	0.6708	2000	0.231	0.064	0.037	977.9
25	0.442	0.188	0.158	0.8108	2250	0.226	0.063	0.035	1127.1
27.5	0.436	0.183	0.146	0.9625	2500	0.222	0.062	0.033	1276.6
30	0.430	0.180	0.136	1.1253	2750	0.218	0.061	0.030	1426.1
35	0.420	0.173	0.120	1.4839	3000	0.215	0.060	0.029	1575.5
40	0.412	0.166	0.109	1.8855	3500	0.209	0.058	0.024	1873.1
45	0.404	0.161	0.100	2.328	4000	0.205	0.057	0.020	2169
50	0.397	0.157	0.093	2.811	4500	0.200	0.056	0.017	2463
55	0.391	0.152	0.088	3.333	5000	0.197	0.056	0.013	2754
60	0.385	0.148	0.084	3.894	6000	0.190	0.055	0.007	3331
65	0.380	0.144	0.081	4.491	7000	0.185	0.054	0.002	3900
70	0.376	0.141	0.078	5.124	8000	0.181	0.054	−0.002	4463
75	0.372	0.138	0.076	5.793	9000	0.177	0.053	−0.007	5019
80	0.368	0.136	0.074	6.496	10000	0.174	0.053	−0.011	5569
90	0.361	0.131	0.071	8.003	12500	0.168	0.054	−0.019	6924
100	0.356	0.127	0.068	9.639	15000	0.163	0.054	−0.026	8255
110	0.350	0.123	0.066	11.400	17500	0.158	0.054	−0.032	9564
120	0.345	0.120	0.065	13.280	20000	0.155	0.055	−0.037	10 857
130	0.341	0.117	0.064	15.276	22500	0.152	0.056	−0.042	12 135
140	0.338	0.114	0.063	17.381	25000	0.149	0.056	−0.046	13 400
1500	0.334	0.112	0.061	19.593	27500	0.147	0.057	−0.050	14 655
160	0.331	0.110	0.060	21.91	30000	0.145	0.057	−0.054	15 900
180	0.326	0.106	0.058	26.83	40000	0.139	0.060	−0.065	20 797
200	0.321	0.102	0.057	32.13	50000	0.134	0.062	−0.074	25 594
225	0.316	0.098	0.057	39.24	60000	0.131	0.064	−0.082	30 316
250	0.311	0.095	0.057	46.85	70000	0.128	0.065	−0.088	34 978
275	0.307	0.092	0.057	54.92	80000	0.126	0.066	−0.093	39 589
300	0.303	0.090	0.057	63.41	90000	0.124	0.067	−0.097	44 158
325	0.300	0.088	0.056	72.30	100000	0.122	0.069	−0.101	48 691
350	0.297	0.086	0.055	81.56					

two kinds of particles. This cannot always be done. It has been established, for example, that the effective charge of α-particles begins to deviate from +2 at velocities higher than the velocity at which the proton charge deviates from +1. Thus, one should expect shorter ranges for protons and deuterons than for α-particles of an equivalent velocity. The reduction in the proton range in air, according to Blackett /180/, is 0.2 cm for $T_p > 500$ kev,

$$R_p(v) = \left[(M/z^2)_H \Big/ \left(\frac{Z^2}{M}\right)_{He}\right] R_\alpha(v) - 0.2\ \text{cm} = 1.007\ R_\alpha - 0.20\,\text{cm}. \qquad (6.12)$$

In the general case of an arbitrary stopping medium we have

$$R_p(T) = 1.007\ R_e(3.972\ T) - C_{pe}, \qquad (6.12a)$$

where for air C_{pe} is 0.2 cm ($T > 0.5$ Mev), 0.13 cm for $T = 0.1$ Mev and 0.02 cm for $T = 6.7$ kev /213/.

According to (6.3), for an emulsion $C_{pe} = 4.8 \cdot 10^{-5}$ cm other authors /178/ give $C_{pe} = 4 \cdot 10^{-5}$ cm ($T_e = 3 - 11$ Mev).

Statistical scatter of the ranges of heavy charged particles. As a result of statistical fluctuations of the ionization energy losses (see § 4), the ranges of charged particles with the same initial energy are scattered about the mean range R, determined by the Bethe-Bloch formula.

TABLE 39

Theoretical values /448/ of the relative scatter of protons, %

T_p, Mev	Beryllium Be	Carbon C	Aluminum Al	Copper Cu	Lead Pb	Air
2	1.704	1.867	1.968	2.293	2.659	1.981
4	1.550	1.631	1.814	2.030	2.331	1.679
6	1.469	1.526	1.720	1.875	2.187	1.564
8	1.419	1.466	1.649	1.779	2.079	1.498
10	1.382	1.424	1.597	1.749	1.994	1.452
15	1.322	1.357	1.507	1.667	1.865	1.376
20	1.286	1.315	1.450	1.609	1.828	1.335
25	1.259	1.285	1.408	1.562	1.783	1.304
30	1.238	1.263	1.377	1.526	1.742	1.280
40	1.206	1.230	1.330	1.468	1.674	1.244
50	1.183	1.203	1.297	1.425	1.619	1.218
60	1.165	1.183	1.271	1.390	1.571	1.197
70	1.149	1.166	1.249	1.363	1.536	1.180
80	1.135	1.152	1.231	1.339	1.505	1.165
100	1.112	1.128	1.201	1.300	1.464	1.141
120	1.094	1.109	1.178	1.271	1.431	1.121
140	1.078	1.093	1.157	1.245	1.401	1.104
160	1.065	1.078	1.140	1.225	1.376	1.087
200	1.041	1.054	1.112	1.190	1.333	1.060
250	1.017	1.029	1.084	1.155	1.289	1.036
300	0.997	1.009	1.060	1.127	1.254	1.016
350	0.980	0.991	1.040	1.104	1.225	0.999
400	0.966	0.976	1.023	1.085	1.200	0.984
500	0.942	0.952	0.996	1.052	1.160	0.959
600	0.924	0.932	0.974	1.028	1.127	0 939
800	0.897	0.904	0.943	0.991	1.081	0.909
1000	0.879	0.886	0.921	0.966	1.049	0.889
1500	0.856	0.862	0.891	0.928	1.002	0.860
2000	0.850	0.855	0.882	0.915	0.981	0.850
2500	0.853	0.857	0.882	0.913	0.973	0.849
3000	0.860	0.864	0.888	0.917	0.972	0.853
4000	0.881	0.884	0.907	0.933	0.982	0.869
5000	0.907	0.910	0.931	0.957	1.000	0.889
7000	0.964	0.965	0.985	1.010	1.047	0.935
10000	1.048	1.049	1.067	1.092	1.122	1.005
15000	1.178	1.179	1.195	1.220	1.244	1.115
20000	1.295	1.295	1.311	1.336	1.357	1.214
25000	1.401	1.401	1.416	1.442	1.460	1.304
30000	1.499	1.498	1.512	1.540	1.555	1.384
40000	1.674	1.674	1.686	1.716	1.727	1.508
60000	1.969	1.968	1.979	2.013	2.018	1.772
80000	2.214	2.212	2.223	2.260	2.262	1.983
100000	2.426	2.425	2.435	4.475	2.475	1.168

The range scatter is described by the square of the range fluctuation

$$\sigma_R^2 = \langle (x - R)^2 \rangle_{\text{mean}},$$

where R is the mean range determined by formula (6.1).

If we assume that the range scatter is represented by a gaussian distribution, then the value of σ_R^2 can be determined by

$$\sigma_R^2 = \int_0^R P\left(\frac{dE}{dx}\right)^{-3} dx = \int_0^E P\left(\frac{dE}{dx}\right)^{-3} dT.$$

TABLE 40

Theoretical values /448/ of the relative scatter of the ranges of μ-mesons, %

T_p, Mev	Beryllium Be	Carbon C	Aluminum Al	Copper Cu	Lead Pb	Air
0.225	5.081	5.566	5.866	6.835	7.927	5.904
0.450	4.621	4.862	5.408	6.052	6.948	5.005
0.676	4.379	4.550	5.127	5.588	6.520	4.662
0.901	4.229	4.371	4.917	5.302	6.198	4.467
1.126	4.120	4.244	4.761	5.213	5.944	4.328
1.689	3.941	4.044	4.491	4.968	5.558	4.101
2.252	3.834	3.921	4.322	4.798	5.448	3.981
2.815	3.753	3.831	4.197	4.657	5.315	3.888
3.378	3.690	3.764	4.104	4.548	5.193	3.815
4.50	3.596	3.666	3.966	4.375	4.991	3.709
5.63	3.527	3.587	3.867	4.247	4.826	3.630
6.76	3.472	3.527	3.788	4.144	4.693	3.569
7.88	3.425	3.477	3.724	4.063	4.580	3.519
9.01	3.384	3.435	3.670	3.992	4.487	3.474
11.26	3.316	3.364	3.580	3.876	4.365	3.401
13.51	3.260	3.306	3.511	3.788	4.265	3.341
15.76	3.214	3.258	3.450	3.713	4.178	3.290
18.02	3.174	3.214	3.399	3.652	4.102	3.240
22.52	3.104	3.142	3.315	3.548	3.972	3.160
28.15	3.031	3.069	3.231	3.442	3.844	3.090
33.78	2.973	3.006	3.161	3.360	3.737	3.029
39.4	2.922	2.955	3.101	3.291	3.653	2.977
45.0	2.878	2.910	3.050	3.234	3.577	2.932
56.3	2.809	2.837	2.970	3.136	3.456	2.858
67.6	2.754	2.780	2.904	3.064	3.360	2.798
90.1	2.673	2.695	2.809	2.953	3.221	2.709
112.6	2.621	2.641	2.744	2.879	3.124	2.648
168.9	2.536	2.553	2.641	2.749	2.969	2.549
225.2	2.511	2.526	2.607	2.703	2.900	2.512
281.5	2.515	2.526	2.602	2.692	2.871	2.504
337.8	2.530	2.542	2.614	2.699	2.864	2.511
450	2.586	2.596	2.661	2.740	2.884	2.548
563	2.655	2.663	2.725	2.800	2.930	2.600
788	2.803	2.808	2.867	2.938	3.048	2.719
1126	3.022	3.025	3.079	3.150	3.239	2.899
1689	3.350	3.354	3.400	3.471	3.542	3.171
2252	3.633	3.635	3.679	3.753	3.812	3.408
2815	3.882	3.881	3.923	4.000	4.051	3.614
3378	4.101	4.100	4.140	4.218	4.264	3.795
4504	4.475	4.475	4.510	4.592	4.628	4.103
6756	5.044	5.041	5.072	5.163	5.183	4.565
9008	5.461	5.457	5.487	5.584	5.597	4.904
11260	5.786	5.783	5.813	5.913	5.921	5.174

Taking into account (4.45) and the relativistic corrections we have

$$\sigma_R^2 = 4\pi z^2 e^4 n \int_0^T \frac{\left(1-\frac{\beta^2}{2}\right)}{(1-\beta^2)\left(1+\frac{2m}{M}\gamma\right)}\left(\frac{dE}{dx}\right)^{-3} K dT, \qquad (6.13)$$

where $\gamma = (1-\beta^2)^{-\frac{1}{2}}$ is the relativistic transformation factor;

$$\beta = \frac{v}{c};$$

M is the mass of the heavy particle; the rest of the notation is the same as previously.

Tables 39 and 40 give the values of the relative scatter of the ranges of protons and μ-mesons in percent, i.e., the values of $S_R = 100\frac{\sigma_R}{R}$. In the calculations of /448/, (6.13) and the calculated values of dE/dx were used (Figures 18 – 22).

The calculations for protons and μ-mesons were performed separately, since for $\frac{T}{Mc^2} \geqslant 5$ range straggling begins to depend on $\frac{M}{m}$. In the energy range where this dependence does not exist, the values of S_R for other heavy particles can be obtained from Table 39, by

$$S_M(\beta) = S_p(\beta)\left(\frac{M_p}{M}\right)^{1/2}, \tag{6.14}$$

i.e., the relative scatter S of the ranges, or the straggling parameter α for protons is twice as large as the corresponding value for α-particles of the same velocity.

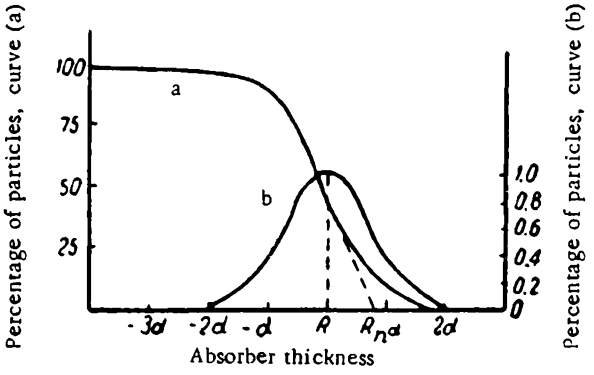

FIGURE 51. Integral (a) and differential (b) transmission curves of charged particles:

R – mean range; R_n – the range, extrapolated from the transmission curve; α – the parameter of the range scatter.

It also follows from Table 39 that the relative scatter of the ranges is almost independent of the Z of the stopping material. The quantity S, like $\frac{dE}{dx}$, has a minimum for $\frac{T}{Mc^2} \sim 2.5 - 3$.

If we take into account only the range scatter determined by the statistical nature of the energy transfer to the electrons in individual collisions, then the distribution of the ranges, resulting from this scatter, should be represented by a gaussian distribution

$$P(x)\,dx = \frac{1}{\alpha\sqrt{\pi}} e^{-\frac{(x-R)^2}{\alpha^2}}\,dx, \tag{6.15}$$

where

$$\alpha^2 = 2\sigma_R^2.$$

In a more rigorous approach to the problem, it is also necessary to take into account the small deviations from the gaussian distribution which are caused by nuclear collisions and multiple scattering.

Experimental methods for the determination of ranges and of range straggling. Usually (see, for example /93, 161, 272, 451/) the mean range is determined from the transmission curve of particles with the same initial energy through a foil of the material being investigated. For a given particle energy T, the absorber thickness is gradually increased and the number of particles passing through the absorber is measured as a function of the thickness. For heavy particles with a charge $z \approx 1$ (protons, α-particles), a typical transmission curve is shown in Figure 51a. From the integral transmission curve the mean range R and the extrapolated range R_n are calculated. The mean range R is defined as a thickness of the material which absorbs half the protons, or better, as the thickness corresponding to the maximum of the differentiated transmission curve (Figure 51b). The extrapolated range R_n is obtained from the integral curve by extrapolation from the point of the curve corresponding to the mean range R.

When the experimental geometry is ideal (very thin slits forming the beam, small energy scatter in the initial beam) the following relation exists between R and R_n, in agreement with (6.15),

$$R_n = R + \frac{\sqrt{\pi}}{2}\alpha = R + S. \tag{6.16}$$

The quantities S and σ_R are related by

$$S = \frac{\sqrt{\pi}}{2}\alpha = \sqrt{\frac{\pi}{2}}\sigma_R \tag{6.17}$$

(α is the straggling parameter; σ_R is the mean square range fluctuation).

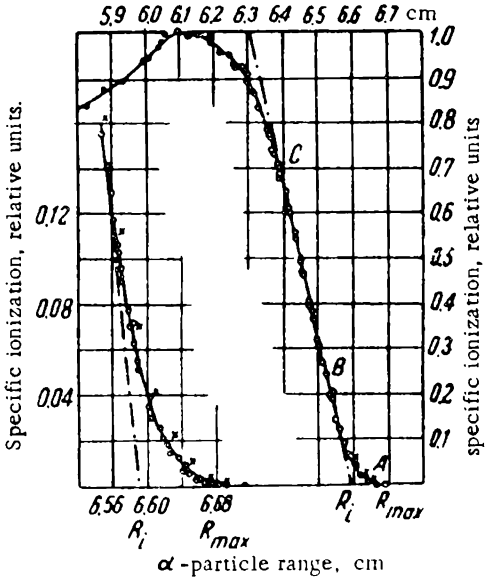

FIGURE 52. Bragg's curve near the end of the α-particle range:

R_i — the extrapolated range from the ionization;
R_{max} — the maximum range.

For the α-particles of Po^{210} ($T_\alpha = 5.3$ Mev), the mean range in air is $R = 3.842$ cm, and the extrapolated range $R_n = 3.879$ cm, i.e., 1.4% larger.

For α-particles with a mean range in air of ~10 cm, S is approximately 0.13 cm.

In practice, as will be seen below, owing to the crude experimental geometry, i.e., the energy scatter in the primary beam and the influence of the highly-multiple scattering, the experimentally obtained straggling parameter α is larger than the theoretical one.

There is another possible method to determine R from the passage of the particles. In the experiments of Bichsel /156/ the thickness of the absorber was fixed and the energy of a well-collimated proton beam was continuously varied. The energy T, at which half of the incident protons have passed a given absorber thickness R, was taken as the energy corresponding to the mean range.

In certain cases (for example, for gaseous absorbers) it is possible to measure the ionization produced by the particles along various sections of their path /285, 322/.

From curves, relating the ionization and the range (Bragg's curves) the range R_i extrapolated from the ionization was determined (Figure 52). The following relation was derived between the mean range of α-particles and the range extrapolated from the ionization in air:

$$R = R_i - 0.47\alpha + 0.006 \text{ cm air.} \tag{6.18}$$

R_i for the α-particles of Po^{210} is 3.87 cm, i.e., 0.7% larger than the mean range R, which is 3.842 cm of air. For the α-particles of RaC' (Po^{214}) with $T_\alpha = 7.68$ Mev, the range extrapolated from the ionization is 6.95 cm of air.

In order to measure the ranges of high-energy (≈ hundreds megaelectronvolts) protons the ionization obtained in two identical chambers between which the investigated substance is placed, is measured /49, 384/.

The ratio of the ionization currents in the two chambers as a function of the absorber thickness leads to Bragg's curve. Mather and Segrè /384/ showed that the mean range of protons corresponds to the ordinate on the Bragg curve $\frac{I_2}{I_1} = 0.8\left(\frac{I_2}{I_1}\right)_{max}$, where I_1 and I_2 are the ionization currents in the first and second chambers.

The mean range determined from the experimental transmission curve or from Bragg's curve cannot be directly compared with the theoretical mean range. Whereas the mean range, which is calculated from the ionization energy losses, is the total mean length R of the path traversed by the particle in the medium, in the experiments of the type indicated above one actually measures the mean effective range, which is the distance t along a straight line drawn between the positions of the particle before and after the absorber. Due to highly multiple scattering (§ 4)*, the total mean path length of a particle in a substance will be larger than the mean effective range

$$R = t + \frac{1}{2}\sum \theta_i^2 \Delta t_i = t + \frac{1}{2}\int \langle \theta^2 \rangle_{mean}\, dt; \tag{6.18a}$$

* At very high particle energies one should also take into account the difference between the true and effective ranges which is increased due to the formation of mesons (§ 3), and to fluctuations in the formation of δ-particles.

where θ_i is the angle between the direction of the incident beam and the direction of motion of the particles after the i-th collision;

θ^2 is the square of the multiple scattering angle.

The theory of the problem was worked out by Pomeranchuk /88/ and by Bichsel and Uehling /171, 172/. According to Pomeranchuk for high-energy particles the value of $\Delta R = (R - t)$ can be calculated approximately by

$$\Delta R \cong t \left(\frac{Z}{137}\right) \frac{E_s^2 E^2}{\pi m (E - M)^2} \frac{L_r}{L_i(E_1)} \ln \frac{(E + M)}{4EM}, \qquad (6.19)$$

where Z is the atomic number of the absorber;

E is the total energy of the incident particle;

$$E_s = m (4\pi 137)^{1/2} = 21 \text{ Mev};$$

M is the rest mass of the incident particle;

L_r is the radiational logarithm;

L_i is the ionization logarithm.

Values of $\frac{\Delta R}{t}$, calculated by (6.19) for some stopping materials are given in Figure 53.

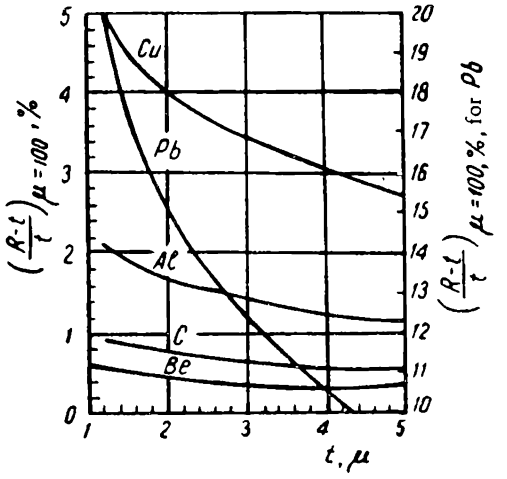

FIGURE 53. Correction curves for multiple scattering to the experimental range for particles with rest mass $m = 100\mu$ as a function of the total energy of the particles; E in units of $\mu = 0.5$ Mev /88, 49/

Mather and Segrè /384/, substituting in (6.18) Williams' approximate expression /505/ for $\langle \theta^2 \rangle_{mean}$ and assuming $R \approx T^{1.75}$, found

$$\frac{\Delta R}{R} \approx \frac{Z}{6400}. \qquad (6.20)$$

However, Bichsel indicated that the problem can be solved only within the framework of a more rigorous theory of multiple scattering. From Moliere's theory, he obtained an expression for the parameter which describes the range scatter for multiple scattering

$$\Delta R_0 = \frac{1}{2} \int_{E_1}^{E} \frac{\theta_1^2 B dE}{-\frac{dE}{dx}}, \qquad (6.21)$$

where θ_1 and B are quantities used in Moliere's theory (see § 2).

There is also a range scatter connected with the statistical fluctuation of the energy losses which is well represented by the gaussian curve (6.15).

Thus, the experimentally observed distribution is a superposition of two distributions, described by the parameters ΔR_0 and σ_R.

For experiments in which the range is determined from the transmission curves for a fixed absorber thickness and variable energy of the incident beam /156/, it is necessary to introduce corrections for multiple scattering. These corrections can be obtained from Figure 54, which gives the fraction of protons passing through the absorber, for which the mean difference between the true and the effective path length exceeds ΔR. The quantity $\xi = \frac{\sigma_R}{\Delta R_0}$ indicates the relative importance of the normal range straggling with respect to the straggling in multiple scattering.

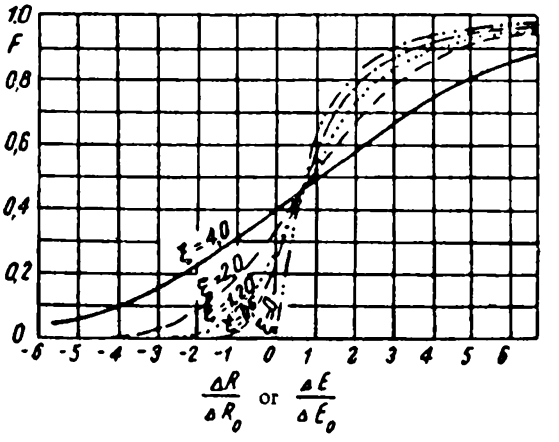

FIGURE 54. Curve of protons transmission for various ξ showing the ratio of the scatter parameter of energy losses to the parameter of multiple scattering /171/

The case $\xi = 0$ corresponds to multiple scattering, $\xi = \infty$ to the normal straggling. The curve in Figure 54, represented by the parameters $\xi = 0.69$; 1.2; 2.0 and 4.0, approximately describes the passage of protons with energy $T_p \approx 10$ Mev through layers of gold, silver, copper and aluminum.

The distribution function of the actual ranges can be obtained by differentiating one of the curves of Figure 54. For $\xi = 1$, the distribution of the ranges taking into account multiple scattering is given by the solid curve of Figure 55. In this figure $y = \frac{\Delta R}{\sigma_R} = \frac{t-R}{\sigma_R}$ is plotted on the abscissa axis, and $\frac{dN}{dy} = C(y)$ on the ordinate. Similar curves are necessary for corrections to the range t, measured in experiments with variable absorber thicknesses and fixed energies of the incident beam. This figure gives a gaussian curve (the broken curve) for comparison, giving the distribution about the mean range without allowing for multiple scattering.

As can be seen, the allowance for multiple scattering reduces the discrepancy between the theoretical and the observed values of the ranges.

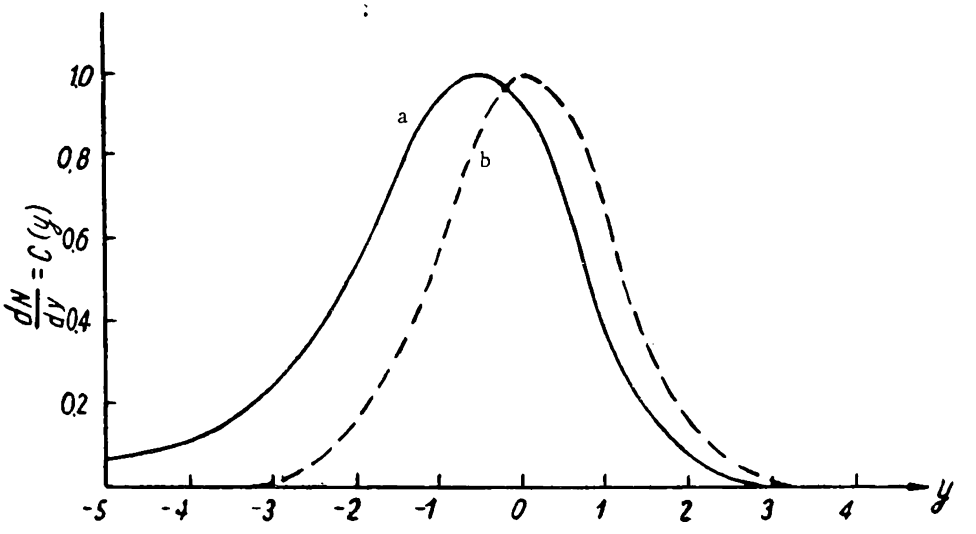

FIGURE 55. Distribution of range scatter:

a—with allowance for multiple scattering; b—without allowance for multiple scattering /171/

Experimental data on the ranges of α-particles and protons in air are very important, since air is often used as a standard stopping medium (see § 4).

For slow α-particles and protons ($v < 1.5 \cdot 10^9$ cm/sec, which corresponds to $T_\alpha \sim 5$ Mev, $T_p \sim 1.5$ Mev) only experimental information on the ranges is available due to the inadequacy of the theory.

The experimental data on the range-energy relation for α-particles in air, obtained until 1937 with natural radioactive materials, were analyzed by Livingston and Bethe /359/. In 1937 the extrapolated ranges R_n of protons in air with energies from 0.1 to 2 Mev were measured /413/. In 1938 the experimental investigations of Holloway and Livingston /285/ were published, in which results on the ionization produced by α-particles ($T_\alpha < 5.3$ Mev) in air, as a function of the residual range were reported. Assuming that the total ionization produced in air is proportional to the energy of the α-particle (which corresponds to the assumption that the energy w_i for the formation of an ion pair is independent of the energy of the incident particle, see § 8) the authors derived from their own data the range-energy relation for α-particles with energies below 5.3 Mev. In 1958—1960 in a series of works by Jesse et al. /316—318/ it was shown that the total number of ion pairs, produced in argon by α-particles with energies from 6.3 to 8.8 Mev is proportional to the energy of the particles to within 0.5%. At the same time such a proportionality was not observed for air, $w_{i(\text{air})}$ increased with decreasing energy. The number of ion pairs, produced by α-particles in argon and in air, was measured as a function of the residual range of the α-particles in air. Since the product of this ratio by the ionization in air was independent of the energy of the α-particles, it became possible to reconsider the range-energy relation according to Holloway and Livingston. In order to correlate the formulas, the values of the energy, determined from

the degree of ionization, have to be multiplied by $\frac{J_{(A)}}{J_{(air)}}$. The need to reconsider the relation arises also from a comparison of the ranges of proton and α-particles in air from nuclear reactions with the ranges from the corrected Bethe /153/ and Jesse /317/ range-energy curve for α-particles in air. This corrected relation between the range of α-particles in air and their energy is shown by the curves of Figure 56. The maximum error in the energy of the α-particles as determined from Figure 56 was 25 kev /153/. Thus, the experimentally determined range of α-particles from the reaction $Li^6(n,t)He^4$ is 1.04 ± 0.02 cm of air. This range, according to the corrected curve

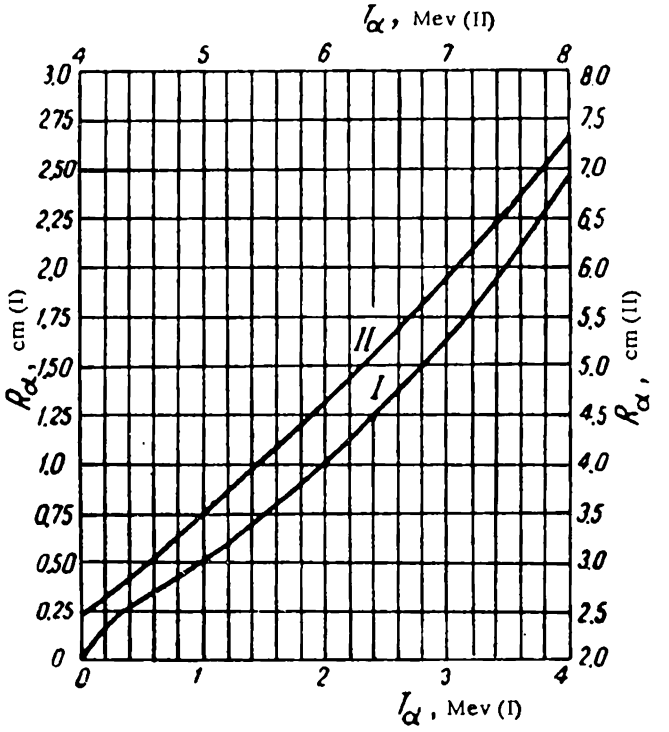

FIGURE 56. Range of α-particles in air versus their experimental energy according to /153/.

(Figure 56), corresponds to an α-particle energy T_α of 2.06 Mev. Measurements of the energy of α-particles from the reaction $Li^6(n,t)He^4$ by an independent method give $T_\alpha = 2.057 \pm 0.010$ cm. The range 1.04 cm according to the uncorrected curve of Holloway and Livingston /285/ corresponds to a lower value of $T_\alpha = 1.96$ Mev.

The curve relating the proton range in air to the energy is given in Figure 57. It is obtained from the experimental range-energy curve for α-particles (Figure 56) by applying (6.12); the maximum error in the determination of the proton energy according to these curves is about 20 kev /153/.

In one of the experiments, the protons obtained in the reaction $N^{14}(n,p)C^{14}$ had 1 cm of air. According to the uncorrelated curve of Holloway and Livingston /285/, such a range corresponds to a proton energy of 0.56 Mev, whereas from Figure 57 the proton energy is 0.58 Mev. The energy of the protons from the reaction $N^{14}(n,p)C^{14}$ determined by a different method is 0.581 Mev.

Although the curves of the ranges of low-energy α-particles and protons in air, given in Figures 56 and 57, are sufficiently accurate for many practical applications, it is mentioned in /322, 217/ that $w_e(A)$ also depends on the energy of the α-particles, and consequently, the reexamination of the experimental data of Holloway-Livingston, as done by Jesse et al. /317/ and Bethe /153/, is not quite correct (for more details see § 8).

At higher proton and α-particle energies, it is recommended to use the data of Tables 41—45, as well as the calculated data of Sternheimer (Figures 40—48). The ranges of α-particles are determined from the curves in Figures 46—48 and from (6.12). Figure 58 gives the dependence of the proton energy on their range in stilbene $C_{14}H_{12}$ which is of interest for investigations in neutron spectrometry.

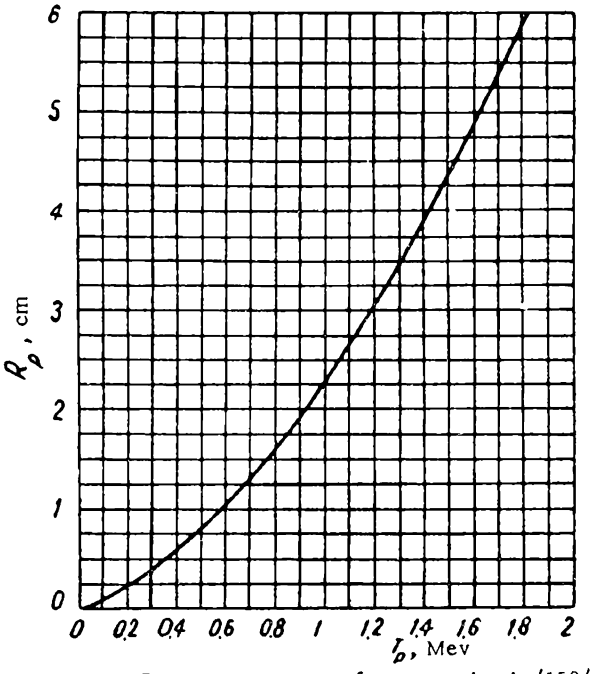

FIGURE 57. Range versus energy for protons in air /153/

Experimental range-energy relation for low-energy α-particles and protons in other gases. Tables 41 and 42 give data on the proton ranges with energies of 40 kev — 10 Mev and on α-particle ranges with energies of 3—40 Mev in various gases. These values were obtained by Whaling /491/ from averaged experimental results on stopping (Figures 31—35) by calculating the integrals in relations of type (6.2). The integration constants $R_p(T_0)$ in the calculation of the proton ranges in O_2, A, CH_4, CO_2, H_2, CH_4, N_2 and air are the experimental values of the range according to Cook et al. /213/. For neon, krypton, xenon and water vapor the integration constants R_p(100 kev) were determined by the values of ε_a(50 kev).

The integration constants $R_\alpha(T_0)$, used in the calculation of the α-particle ranges, were determined from the measurements of Mano /381/, Rosenblum /433/, Philipp /415/, Blackett /180/ and Briggs /147/, taking into account the calculated corrections by Bogaardt and Kondijs /160/.

The ranges of high-energy protons in hydrogen and deuterium can be determined from the calculated curves of Rich and Madey /432/; see Figures 24—26. If neither experimental nor calculated range data exist it is

recommended to use the interpolation of Sternheimer's calculated data, described above. The values of I required for the calculations can be taken from Table 19, and the values of R(2 Mev) from Tables 41 and 42.

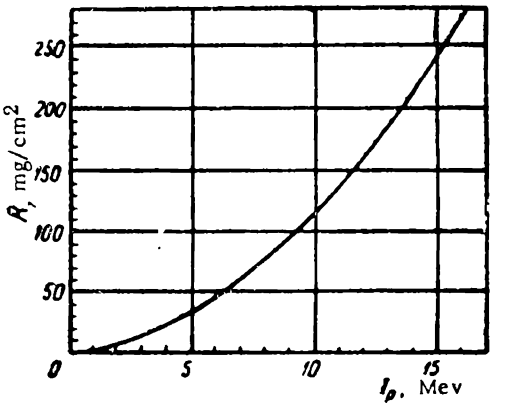

FIGURE 58. Range versus energy for protons in stilbene ($\rho = 1.09$ g/cm^3)

Experimental ranges of protons in metals. Tables 43 and 44 give the most reliable experimental absolute values of the mean ranges of protons in aluminum ($T_p > 1$ Mev) and in other metals. The data of Bichsel /156, 171/ and Hubbard and McKenzie /291/ are corrected for multiple scattering (see above). The absolute experimental values of the mean range of protons are in good agreement with the calculated values obtained by Sternheimer (see Figures 40—48), and exceed by 1—1.5% the calculated values of Smith for aluminum (see Figures 40—42).

Table 41 also gives the proton ranges ($T_p = 0.04 - 10$ Mev) in beryllium, aluminum, copper and gold, obtained by Whaling /497/ by expression (6.2) and the experimental values of ε_a (Figures 31—35). Whaling's data for copper and gold differ somewhat from the calculated data of Sternheimer and from the experimental absolute data (Table 44). However, in many practical cases this difference is insignificant.

In order to obtain data on the proton ranges in other metals it is recommended to interpolate the calculated data of Sternheimer (see above).

The α-particle ranges with energies of 3—40 Mev in lithium, aluminum, nickel, copper, silver, gold and lead are given in Table 42. These values were obtained by Whaling /491/ from expression (6.2), and the experimental values of $R_\alpha(T_0)$ and ε_a (Figures 31—35) were applied in the calculations.

Table 45 also lists further experimental data on the α-particle ranges in various materials.

Experimental ranges of charged particles in photoemulsions. The most reliable mean ranges for various particles with an initial charge of 1 and 2 in a dry emulsion are given in Table 46. In Figures 49—50* these values are denoted by points. The particle ranges were calculated by relation (6.3), proposed by Barkas /164/.

The experimental ranges of protons, mesons and α-particles are generally in satisfactory agreement with the calculated values in a wide range of particle energies. It should be noted that the experiments were carried

* Experimental data on the ranges of charged particles in emulsions, obtained in earlier works (for example, 196 255, 260, 370, 437), were not taken into account here.

TABLE 41

Mean proton ranges. Calculated /491/ from the mean experimental data on energy losses (Figures 31-35).
Ranges in gases at 15° and at 760 mm Hg

T_p, Mev	Hydrogen H_2	Helium He	Beryllium Be	Nitrogen N_2	Oxygen O_2	Neon Ne	Aluminum Al	Argon A, cm	Copper Cu,	Krypton Kr	Xenon Xe	Gold Au,	H_2O (vapor)	CH_4	CO_2	Air
	cm		mg/cm^2	cm			mg/cm^2		mg/cm^2	cm		mg/cm^2	cm			
0.040	0.174	0.346	—	0.0459	0.0561	—	—	0.0535	—	—	—	—	—	0.0424	0.0361	0.0600
0.045	0.190	0.375	—	0.0575	0.0623	—	—	0.0597	—	—	—	—	—	0.0474	0.0406	0.0658
0.050	0.205	0.404	—	0.0632	0.0684	—	—	0.0656	—	—	—	—	—	0.0523	0.0449	0.0715
0.055	0.220	0.433	—	0.0687	0.0744	—	—	0.0715	—	—	—	—	—	0.0571	0.0491	0.0772
0.060	0.236	0.461	—	0.0742	0.0802	—	—	0.0772	—	—	—	—	—	0.0619	0.0532	0.0828
0.065	0.251	0.488	—	0.0796	0.0861	—	—	0.0830	—	—	—	—	—	0.0667	0.0572	0.0883
0.070	0.266	0.515	—	0.0849	0.0918	—	—	0.0888	—	—	—	—	—	0.0715	0.0612	0.0938
0.075	0.282	0.541	—	0.0902	0.0976	—	—	0.0946	—	—	—	—	—	0.0763	0.0651	0.0994
0.080	0.297	0.568	—	0.0955	0.103	—	—	0.100	—	—	—	—	—	0.0811	0.0691	0.105
0.085	0.313	0.594	—	0.101	0.109	—	—	0.106	—	—	—	—	—	0.0859	0.0730	0.110
0.090	0.329	0.621	—	0.106	0.115	—	—	0.112	—	—	—	—	—	0.0908	0.0769	0.116
0.095	0.346	0.648	—	0.112	0.120	—	—	0.118	—	—	—	—	—	0.0957	0.0808	0.121
0.100	0.362	0.674	0.16	0.117	0.126	0.372	0.26	0.124	0.552	0.119	0.087	1.32	0.163	0.101	0.0847	0.127
0.15	0.551	0.963	0.24	0.175	0.185	0.504	0.38	0.188	0.770	0.172	0.128	1.76	0.239	0.154	0.125	0.186
0.20	0.780	1.29	0.32	0.240	0.249	0.639	0.51	0.263	0.992	0.233	0.173	2.19	0.323	0.218	0.169	0.253
0.25	1.05	1.67	0.42	0.314	0.320	0.784	0.65	0.348	1.22	0.300	0.242	2.61	0.417	0.292	0.218	0.328
0.30	1.37	2.09	0.52	0.398	0.398	0.939	0.80	0.444	1.46	0.374	0.275	3.05	0.521	0.376	0.272	0.410
0.35	1.73	2.56	0.63	0.491	0.484	1.10	0.96	0.549	1.72	0.454	0.332	3.52	0.637	0.470	0.332	0.500
0.40	2.13	3.07	0.76	0.593	0.576	1.28	1.13	0.663	1.99	0.540	0.393	4.02	0.764	0.574	0.398	0.508
0.45	2.57	3.62	0.89	0.703	0.676	1.47	1.31	0.786	2.26	0.632	0.458	4.55	0.902	0.687	0.408	0.702
0.50	3.05	4.21	1.03	0.821	0.783	1.67	1.50	0.916	2.55	0.727	0.527	5.10	1.05	0.809	0.544	0.814
0.55	3.57	4.85	1.19	0.947	0.897	1.88	1.70	1.05	2.86	0.828	0.600	5.68	1.21	0.940	0.624	0.923
0.60	4.12	5.53	1.35	1.08	1.02	2.10	1.91	1.20	3.17	0.933	0.676	6.29	1.38	1.08	0.709	1.06
0.65	4.72	6.25	1.52	1.22	1.14	2.34	2.13	1.35	3.50	1.04	0.756	6.92	1.56	1.23	0.799	1.19
0.70	5.35	7.01	1.69	1.37	1.27	2.58	2.35	1.51	3.84	1.15	0.840	7.57	1.75	1.38	0.803	1.33
0.75	6.02	7.81	1.88	1.52	1.41	2.84	2.58	1.67	4.20	1.27	0.927	8.24	1.95	1.55	0.992	1.48
0.80	6.72	8.65	2.07	1.69	1.56	3.11	2.83	1.84	4.56	1.39	1.02	8.94	2.15	1.73	1.09	1.63
0.85	7.46	9.54	2.28	1.86	1.71	3.39	3.08	2.02	4.93	1.51	1.11	9.65	2.37	1.91	1.20	1.79
0.90	8.24	10.5	2.58	2.03	1.86	3.68	3.34	2.20	5.32	1.64	1.20	10.4	2.60	2.10	1.31	1.96
0.95	9.06	11.5	2.70	2.22	2.02	3.98	3.61	2.39	5.71	1.77	1.30	11.1	2.83	2.30	1.43	2.13
1.00	9.91	12.5	2.92	2.41	2.18	4.29	3.89	2.58	6.12	1.91	1.41	11.9	3.08	2.51	1.55	2.31
1.5	20.2	24.6	5.56	4.63	4.07	7.93	7.14	4.86	10.7	3.44	2.57	20.4	5.95	5.02	2.97	4.43
2.0	33.8	40.4	8.91	7.42	6.55	12.5	11.2	7.66	16.3	5.27	3.99	30.3	9.60	8.24	4.76	7.13
2.5	50.6	60.0	13.0	10.7	9.52	17.9	16.1	10.9	22.7	7.40	5.64	41.9	14.0	12.2	6.83	10.4
3.0	70.3	82.8	17.7	14.6	13.0	24.0	21.7	14.7	30.0	9.79	7.47	54.7	19.2	16.7	9.31	14.2
3.5	92.8	109	23.0	19.0	16.9	30.9	27.9	18.9	38.2	12.4	9.51	68.9	25.0	22.0	12.1	18.5
4.0	118	138	29.0	23.9	21.3	38.5	34.9	23.6	47.2	15.3	11.7	84.1	31.5	27.9	15.3	23.3
4.5	146	171	35.4	29.3	26.1	47.0	42.7	28.8	57.0	18.5	14.1	100	38.8	34.5	18.7	28.5
5.0	177	206	42.9	35.2	31.4	56.0	51.1	34.3	67.6	21.9	16.6	118	46.7	41.6	22.5	34.3
5.5	210	245	50.8	41.6	37.1	65.9	60.2	40.2	78.9	25.5	19.3	136	55.3	49.4	26.6	40.5
6.0	246	287	59.1	48.5	43.2	76.4	70.0	46.7	91.0	29.3	22.2	156	64.5	58.8	31.0	47.2
6.5	285	331	67.8	55.8	49.7	87.7	80.4	53.5	104	33.4	25.3	176	74.4	66.7	35.7	54.3
7.0	326	379	76.9	63.6	56.7	99.6	91.5	60.7	118	37.8	28.5	198	85.0	76.3	40.8	61.9
7.5	370	430	86.5	71.9	64.0	112	103	68.3	132	42.3	31.8	220	96.2	86.5	46.1	70.0
8.0	417	483	96.5	80.7	72.0	125	115	76.4	147	47.1	35.4	243	108	97.2	51.7	78.5
8.5	466	539	107	89.9	80.2	139	128	84.8	163	52.2	39.1	267	120	108	57.6	87.4
9.0	518	598	118	99.6	88.8	154	142	93.7	180	57.4	42.9	292	133	120	63.9	96.7
9.5	572	660	129	110	97.8	169	156	103	197	62.9	46.9	319	147	133	70.4	106
10.0	628	724	140	120	107	185	171	113	215	68.7	51.1	345	161	146	77.2	117

TABLE 42

Mean ranges of α-particles. Calculated /491/ from the mean experimental data on energy losses (Figures 31—35). The integration constants in (6.4), the experimental ranges, are indicated in the lower part of the table

E_α, Mev	Hydrogen H_2	Helium He	Lithium, Li	Nitrogen N_2	Oxygen O_2	Neon Ne	Aluminum Al,	Argon A, cm	Nickel Ni,	Copper Cu,	Krypton Kr, cm	Silver Ag,	Xenon Xe, cm	Gold Au	Lead Pb	H_2O	CH_4	CO_2	Air
	cm		mg/cm²	cm			mg/cm²		mg/cm²	mg/cm²		mg/cm²		mg/cm²		cm			
3.0	7.00	8.64	2.00	1.60	1.45	2.97	3.81	1.70	5.80	5.10	1.43	6.72	0.99	8.98	9.90	2.29	1.77	1.15	1.66
3.5	8.80	10.8	2.48	2.01	1.81	3.67	4.50	2.14	6.69	6.01	1.74	7.99	1.20	10.7	11.7	2.90	2.25	1.41	2.06
4.0	10.8	13.0	3.01	2.47	2.21	4.41	5.18	2.61	7.61	7.01	2.09	9.22	1.45	12.6	13.5	2.47	2.76	1.70	2.50
4.5	13.0	16.0	3.61	3.00	2.63	5.24	5.88	3.12	8.70	8.09	2.42	10.6	1.73	14.6	15.5	4.15	3.33	2.02	2.97
5.0	15.5	19.0	4.25	3.55	3.09	6.15	6.63	3.69	9.80	9.20	2.81	12.0	2.01	16.7	17.5	4.85	3.94	2.35	3.49
5.5	18.2	22.1	4.91	4.12	3.60	7.09	7.48	4.30	11.0	10.4	3.20	13.5	2.30	18.9	19.5	5.59	4.58	2.74	4.02
6.0	21.0	25.5	5.62	4.72	4.10	8.07	8.41	4.90	12.2	11.6	3.62	15.1	2.63	21.1	21.6	6.40	5.25	3.13	4.62
6.5	24.4	29.0	6.40	5.35	4.68	9.13	9.40	5.57	13.5	12.7	4.05	16.7	2.95	23.5	24.0	7.27	6.00	3.57	5.26
7.0	27.7	32.8	7.22	6.03	5.30	10.2	10.3	6.23	14.8	14.4	4.50	18.5	3.30	26.0	26.2	8.13	6.78	4.00	5.93
7.5	31.2	36.9	8.10	6.75	5.90	11.3	11.3	6.97	16.2	15.7	4.96	20.4	3.65	28.5	28.6	9.05	7.60	4.45	6.62
8.0	35.0	41.3	9.02	7.42	6.60	12.6	12.5	7.70	17.6	17.3	5.47	22.3	4.01	31.1	31.1	10.0	8.41	4.90	7 35
8.5	38.8	45.7	10.0	8.30	7.35	13.8	13.6	8.46	19.2	18.8	5.97	24.3	4.41	33.8	33.7	11.1	9.37	5.42	8.10
9.0	43.0	50.5	11.0	9.10	8.04	15.1	14.9	9.33	20.6	20.4	6.49	26.3	4.82	36.8	36.1	12.2	10.3	5.92	8.99
9.5	47.5	55.5	12.0	9.90	8.80	16.4	16.1	10.1	22.2	22.0	7.02	28.4	5.25	39.7	39.0	13.3	11.3	6.48	9.74
10	52.0	60.6	13.1	10.8	9.70	17.8	17.4	11.0	24.0	23.6	7.58	30.6	5.69	42.7	41.8	14.4	12.4	7.01	10.6
11	61.0	71.0	15.4	12.7	11.4	20.7	20.0	12.7	27.4	27.3	8.76	35.0	6.59	49.0	47.6	16.7	14.5	8.21	12.4
12	71.9	83.0	17.9	14.7	13.2	23.9	22.9	14.6	31.0	31.0	9.98	39.9	7.50	55.4	53.9	19.5	17.0	9.48	14.3
13	82.0	96.4	20.5	16.7	15.1	27.1	26.0	16.7	35.0	35.0	11.3	44.9	8.50	62.1	60.0	22.1	19.6	10.8	16.5
14	94.0	110	23.2	18.9	17.2	30.7	29.4	18.9	39.0	39.3	12.6	50.0	9.60	69.7	66.9	25.1	22.4	12.2	18.6
15	105	125	26.2	21.3	19.3	34.3	32.9	21.2	43.2	43.8	14.0	55.1	10.7	76.4	74.0	28.4	25.1	13.6	20.9
16	118	139	29.5	23.8	21.5	38.3	36.4	23.6	47.9	48.4	15.5	60.9	11.7	84.4	81.7	32.0	28.4	15.4	23.5
17	131	156	33.0	26.5	23.7	42.5	40.1	26.2	52.5	52.9	17.1	66.8	12.9	92.3	89.5	25.2	31.6	17.0	26.0
18	146	172	36.5	29.2	26.4	46.9	44.1	28.7	57.2	57.9	18.7	72.3	14.1	101	97.2	39.0	34.9	18.7	28.7
19	163	190	40.1	32.2	28.8	51.3	48.2	31.8	62.1	63.1	20.4	79.4	15.4	110	106	43.0	38.2	20.5	31.7
20	179	209	44.0	35.2	31.5	56.0	52.5	34.4	67.9	68.4	22.0	85.2	16.7	118	114	47.1	42.0	22.5	34.5
25	268	310	65.7	52.3	46.9	82.0	76.8	50.1	97.0	98.0	31.5	121	23.7	167	160	69.9	62.7	33.1	51.0
30	374	433	90.5	72.2	64.2	113	105	68.2	131	132	42.7	162	31.8	222	215	96.0	86.7	46.0	70.0
35	492	570	119	94.8	84.2	147	137	89.8	169	172	55.0	209	41.0	280	275	127	115	61.0	92.0
40	630	720	150	120	108	186	173	114	212	216	70.0	259	51.2	349	342	162	146	79.0	116
5.298	17.21*1	21.3*1	—	3.87*1	3.63*1	6.74*1	—	4.15*1	—	—	3.03*1	—	2.17*1	—	—	—	4.33*5	2.58*1	3 77*1
6.054	21.70*1	26.26*1	—	4.76*1	4.48*1	8.20*1	—	5.02*1	—	—	—	—	—	—	—	—	—	—	4 74*1
7.680	32.55*1	38.65*1	8.5*3	6.96*1	6.54*1	11.78*1	11.8*3	7.25*1	15.8*3	16.3*3	5.17*2	21.1*3	3.81*2	29.4*3	29.6*2	9.43*4	8.00*5	—	6 91*1
8.776	40.85*1	48.5*1	—	8.66*1	8.09*1	14.49*1	—	8.97*1	—	—	—	—	—	—	—	—	—	—	8 57*1

Remark. *1 From /160/; *2 Bates /162/; *3 Rosenblum /433/; *4 Philipp /415/; *5 Briggs /147/.

out not only with the Ilford G—2 emulsion, but also with other emulsions (Ilford G—2, Co, E 1, Kodak NTB and so on)*. These emulsions differ from each other only slightly in their composition and density. In addition, it should also be considered that the humidity of the emulsions and their processing were not identical in the various experiments. The discrepancies (~1—2%) between the experimental data obtained by different authors are therefore to be expected. The calculated curves in Figures 49 and 50 were drawn for the dry emulsion G—5 with $\rho = 3.185$ g/cm^3.

The straggling values of the proton ranges in emulsions are given in Table 47 /18/.

For singly-charged particles with a mass different from the proton mass, the straggling values are determined by multiplication of the straggling for protons of the same velocity by the square root of the ratio of the proton mass to the particle mass, see (6.14).

The experimental values of the mean ionization potentials. The mean ionization potentials are determined by measuring the absolute and relative values of $\frac{dE}{dx}$ and R for heavy charged particles**. For relative measurements it is assumed that I for the standard material is sufficiently accurately determined.

TABLE 43

Absolute experimental mean ranges of protons in aluminum

T_p, Mev	R_p, mg/cm^2	The measured accuracy as determined by the authors, %	Reference	T_p, Mev	R_p, mg/cm^2	The measured accuracy as determined by the authors, %	Reference
1.130	4.66	0.1	/156/	6.150	73.01	0.1	/156/
1.352	6.19	0.1	/156/	10.00	141.2	0.1	/156/
1.519	8.10	0.1	/156/	11.820	226.33	0.1	/156/
1.623	8.27	0.1	/156/	14.971	342.63	0.1	/156/
1.911	10.68	0.1	/156/	17.837	466.92	0.1	/156/
2.114	12.64	0.1	/156/	18.00	477.0	0.1	/291/
2.677	18.31	0.1	/156/	34.96	1541		/290/
3.062	22.85	0.1	/156/	66.1	4774	0.2	/161/
4.023	35.74	0.1	/156/	75.84	6063		/220/
5.038	52.31	0.1	/156/	87.4	7820	0.37	/246/
5.504	60.51	0.1	/156/	117.9	13230	0.22	/246/
				146.5	19310	0.17	/246/
				339	79020	0.7	/384, 385/

The available experimental data on I, with the exception of early publications by Mano /381/, are given in Table 19 (§ 4). The considerable differences between the data obtained by various authors are shown. One of the reasons for these discrepancies is the inaccuracy of the experiments for $\frac{dE}{dx}$ and the lack of corrections for the electron binding and density effects, as well as for multiple scattering.

The accuracy requirements of such experiments are very stringent, since from the experimental data log I, and not I itself, is actually

* Information on the properties of nuclear emulsions manufactured in the USSR and abroad, and the methods of their elaboration, can be found in /18/ and in /95/.

** Due to the straggling and the large scattering, electrons cannot be used in experiments whose purpose is the determination of I.

determined. In fact, from (4.20), it follows that

$$\frac{\delta I}{I} = \frac{\delta\left(\frac{dE}{dx}\right)}{\left(\frac{dE}{dx}\right)} \ln \frac{2mv^2}{I}.$$

The logarithmic factor in this expression is between 5 and 10, and therefor an error of approximately 1% in the ionization losses leads to an

TABLE 44

Absolute experimental mean ranges of protons in metals

Material	Proton energy T_p, Mev	Proton range R_p, mg/cm^2	Reference
Beryllium, Be	9.578	137.90	/156/
	17.340	399.99	/156/
	340	76 730	/385/
Carbon, C	340	70 030	/384, 385/
Copper, Cu	9.938	218.60	/156/
	17.893	594.62	/156/
	340	91 800	/385/
	658	257 600	/ 49/
Silver, Ag	10.022	268.12	/156/
	17.923	704.81	/156/
Gold, Au	9.698	341.80	/156/
	17.549	882.60	/156/
Lead, Pb	340	123.6	/384, 385/

error of 5—10% in the calculation of I. On the other hand, the use of inaccurate values of I in calculations of $\frac{dE}{dx}$ by the Bethe-Bloch formula does not seriously affect the accuracy of the results (see § 4).

TABLE 45

Experimental data on the α-particle range

Material	T_α, Mev	R_α, mg/cm^2	Reference
Carbon, C	5.3	4.43	/175/
Silicon, Si	4.5	5.2 ± 0.1	/268/
Zirconium, Zr	4.5	11 ± 0.35	/268/
Gold, Au	4.5	17 ± 0.6	/268/
Uranium, U	4.5	19.2 ± 0.4	/268/

For the same reason, small errors in the determination of the mean range of particles are associated with large errors in the determination of I. The magnitude of these errors can be obtained by turning to the data

of Table 48, which gives numerical values of the quantity

$$q = (dR/R) \Big/ \left(\frac{dI}{I}\right)$$

for beryllium, carbon, aluminum, copper and lead /448/. For a proton energy of 100 Mev, an error in the determination of the mean range in aluminum (~1%) is associated with an error in the calculation of I $(1/q)$ times as large, i.e., with an error of ~6%.

TABLE 46

Experimental data on the range of charged particles in photoemulsions

Type of particles	τ, Mev	λ, cm	Reference
α	1.295	$(20.7 \pm 0.2)\ 10^{-4}$	
p	2.421	$(53.9 \pm 0.6)\ 10^{-4}$	
t	2.450	$(55.67 \pm 0.34)\ 10^{-4}$	
d, t, He^3 α	5.00	$(175.1 \pm 2.0)\ 10^{-4}$	
d	5.477	$(204.6 \pm 0.64)\ 10^{-4}$	
α	5.477	$(205.5 \pm 1.1)\ 10^{-4}$	
He^3	10.00	$(562.7 \pm 2.6)\ 10^{-4}$	
p	13.96	$(988.3 \pm 7.4)\ 10^{-4}$	
p	21.21	$(2056 \pm 5)\ 10^{-4}$	
μ^+	36.55	$(5345 \pm 22)\ 10^{-4}$	/145, 154/
π^+	200	10.31 ± 0.07	/145, 154/
π^+	340	24.74 ± 0.10	/145, 154/
π^+	540	51.15 ± 0.45	/145, 154/
π^+	700	74.97 ± 0.36	/145, 154/
p	87.4	2.518 ± 0.021	/246/
p	117.9	4.142 ± 0.017	/246/
p	146.5	6.013 ± 0.02	/246/
p	208	10.83	/219/
p	342.5	24.4	/297/

According to /156/, the constant I in Bloch's relation (4.32) is ~12.6 for $Z = 13-79$ and ~15.3 for beryllium*. These values are also confirmed by other authors when investigating the stopping and the proton ranges in the region from 40 to 70 Mev (see Table 19). The value $I_0 = 11.5$, taken in

TABLE 47

Range scatter of protons in emulsion /18/

T, Mev	$\frac{\Delta R}{R}$, %	T, Mev	$\frac{\Delta R}{R}$, %
1	2.11	100	1.21
2	1.94	200	1.13
5	1.66	500	1.02
10	1.53	1000	0.952
20	1.42	2000	0.904
50	1.29	5000	0.963
—	—	10 000	1.1

early works, is underestimated and does not correspond to the experimental data of the more accurate investigations (§ 5 and 6).

* The abnormally large value of I for beryllium is according to /12/ due to the density effect in conductors.

For high proton energies (300—650 Mev) the measured results give smaller values of I_0 (Table 19). For example, according to Bakker and Segré /158/, for heavy ($Z>74$) elements $I_0 = 8.8$.

The reason for the discrepancies in the determination of I_0 between low (tens of megaelectronvolts) and high (hundreds of megaelectronvolts) proton energies remains unclear. Exact corrections for multiple scattering, as suggested by Bichsel /172/, apparently eliminate the discrepancy only partly. In this connection, one should also mention the work of Brandt /174/ who indicates the need to take into account the valency binding and the polarization effect.

TABLE 48

Values of $q = \frac{\left(\frac{dR}{R}\right)}{\left(\frac{dI}{I}\right)}$ for beryllium, carbon, aluminum, copper and lead /448/

T_p, Mev	Stopping material				
	Beryllium Be	Carbon C	Aluminum Al	Copper Cu	Lead Pb
10	0.232	0.214	0.217	0.258	0.337
20	0.200	0.192	0.205	0.236	0.300
50	0.159	0.159	0.181	0.201	0.244
100	0.143	0.143	0.163	0.178	0.214
200	0.131	0.131	0.147	0.159	0.191
500	0.119	0.118	0.131	0.140	0.171
1000	0.106	0.106	0.119	0.128	0.155
2000	0.094	0.094	0.106	0.115	0.142
5000	0.074	0.076	0.090	0.097	0.113
10 000	0.058	0.062	0.084	0.084	0.088

Empirical analytic relations between the range and energy of protons and α-particles. Beginning with Geiger, who established in 1910 a simple empirical relation between the energy and range of α-particles in air, the possibility of using simple analytic relations has been repeatedly discussed in the literature. However, there is still no universal relation suitable for all kinds of particles at all energies. Each relation has a limited range of application and accuracy. In all cases, when more accurate results are required, Tables 40—46, 49, etc. should be consulted. If, however, it is necessary to estimate the orders of magnitude, it is possible to use the semi-empirical relations given below.

Geiger's relation in its initial form:

$$R_\alpha = K v_\alpha^3 = a T_\alpha^{3/2} \quad (R_\alpha = 3-7 \text{ cm of air}), \qquad (6.22)$$

where $a \approx 0.3$, T_α is expressed in Mev.

In 1933 Briggs pointed out that for α-particles with $R_\alpha > 5$ cm of air it is better to use the relation

$$R_\alpha = K v_\alpha^{3.26}.$$

Thus, for high velocities, R_α increases faster than the cube of the velocity, and for low velocities slower.

A rough empirical formula, relating the mean range of α-particles in a medium of atomic number A, with the mean range of these particles in air under normal conditions, is the following:

$$R_A = 3.2 \cdot 10^{-4} \frac{\sqrt{A}}{\rho} R_{air}, \tag{6.23}$$

where ρ is the density of the medium, g/cm^3.

TABLE 49

Early experimental data on the range-energy of protons and α-particles in Ilford G-2 emulsion

T_p, Mev	R, microns	Reference	$T\alpha$, Mev	R, microns	Reference
0.58	6.1 ± 0.15	/255/	0.95	3.5 ± 0.2	/255/
0.91	12.1 ± 0.06	/250/	1.52	5.0 ± 0.2	/255/
1.20	19.3	/370/	2.04	6.7 ± 0.2	/255/
2.59	59.6	/370/	2.15	7.2 ± 0.2	/255/
3.20	82.7	/370/	2.18	6.95 ±0.05	/370/
3.25	83.6	/370/	3.20	11.4 ± 0.2	/255/
4.51	159.5	/370/	3.85	14.2 ± 0.1	/255/
4.99	171.0	/370/	4.18	16.0 ± 0.2	Green, Livsy
6.24	256.0	/370/	4.64	18.2 ± 0.1	/370/
7.09	321.0	/370/	4.71	19.0 ± 0.2	/255/
7.8	389 ± 2.7	/196/	4.76	19.0 ± 0.2	Green, Livsy
16.4	1358 ± 8.1	/196/	5.30	22.5 ± 0.06	/370/
17.6	1465 ± 4.5	/196/	5.30	22.5 ± 0.2	Green, Livsy
17.6	1497 ± 6.0	/196/	5.38	22.9 ± 0.2	/255/
22.3	2244 ± 8.0	/196/	6.19	27.5 ± 0.3	Green, Livsy
25.6	2849 ± 7.1	/196/	6.28	28.7 ± 0.2	"
28.2	3369 ± 10.0	/196/	8.78	47.5 ± 0.05	"
33.5	4597 ± 13.8	/196/	11.32	70.8 ± 0.02	/370/
33.5	4762 ± 24.0	/196/	—	—	
33.5	4996 ± 10.0	/196/	—	—	
39.5	6123 ± 18.0	/196/	—	—	

In order to calculate the mean ranges of α-particles in semi-conducting materials, the following expressions can be used /266/:

$$\left.\begin{aligned} R_{Si\,(\mu)} &= 2.13\ T_{\alpha(Mev)}^{1.45} + 2.20 \\ R_{Ge\,(\mu)} &= 1.95\ T_{\alpha(Mev)}^{1.34} + 1.72 \\ R_{InSb\,(\mu)} &= 2.08\ T_{\alpha(Mev)}^{1.30} + 1.65 \end{aligned}\right\}. \tag{6.24}$$

Wilson and Brobeek /503/ proposed the following expression for the calculation of the range of fast protons (10—200 Mev) in air

$$R_{p(meters)} = \left[\frac{T_p\,(Mev)}{9.3}\right]^{1.8}. \tag{6.25}$$

For protons with energies of 50—250 kev, according to Cook /213/, the range can be calculated by

$$R = C\,[E + E_1]^{3/2}, \tag{6.26}$$

where C and E_1 are empirical constants.

Varshni /486/ used for the calculation of the proton ranges with energies of 1 — 100 Mev the expression:

$$R_p = a\ (T_p + C)^n$$

or

$$\log_{10} R_p = n \log_{10} (T_p + C) + B. \qquad (6.27)$$

The constants in (6.27) were obtained by comparison with the experimental data.

At present the most accurate analytic expressions are those of Bichsel /173/ for the range of protons in aluminum

$$\left.\begin{aligned} R_p &= 3.837\ T_p^{1.5874}\ (1 < T_p < 2.7\ \text{Mev}) \\ R_p &= 2.837\ T_p^2/(0.68 + \log_{10} T_p)\ (2.7 < T_p < 20\ \text{Mev}) \end{aligned}\right\}. \qquad (6.28)$$

Calculations by (6.28) are in agreement with the absolute experimental ranges (Table 43) to within $\sim 0.2\%$ for $T > 3$ Mev and to within $\sim 0.4\%$ for $T < 3$ Mev.

The range of protons with 8 — 40 Mev in a photoemulsion is satisfactorily given by /196/

$$T_p\,(\text{Mev}) \approx 0.251\ R_{(\mu)}^{0.581}, \qquad (6.29)$$

where $R_{(\mu)}$ is the proton range in microns.

§ 7. Inelastic collisions of heavy charged particles with atoms. The stopping process and the ranges of heavy ions in matter

The stopping of heavy ions in matter is in many respects different from the stopping of fast protons and alpha-particles (§ 5). Whereas the light charged particles mostly keep their nuclear charge, the heavy ions tend to lose their effective charge which may be different from the nuclear charge at the beginning of their path owing to the exchange of electrons with the atoms of the medium during the retardation. The importance of the "impact" collisions with the atomic electrons of the stopping medium then decreases and the corresponding ionization energy losses decrease accordingly (§ 4). At the same time, the elastic (§ 2) and inelastic atomic collisions, which in contrast to the ionizing collisions are connected with complex energy and momentum exchanges between the overlapping electron shells of the colliding atoms, become increasingly important. A result of the mutual penetration of the shells of these atoms is the conversion of a certain fraction of the kinetic energy of the particles into excitation energy, which, as a rule, is exhibited in autoionization processes /115, 442/. The charge of one or both atoms then changes.

According to the classification used, for example, in /107/, three types of inelastic collisions associated with a change in the charge of the colliding particles can be distinguished:

1) Pure ionization, i.e., collisions in which the incident (primary) particle ionizing an atom of the medium keeps its charge

$$A^{K+} + B \rightarrow A^{K+} + B^{n+} + ne; \qquad (7.1)$$

2) charge exchange, i.e., collisions with exchange of electrons between the particles

$$A^{n+} + B \to A^{m+} + B^{K+}, \tag{7.2}$$

$$m + K = n;$$

3) ionization with capture:

$$A^{n+} + B \to A^{m+} + B^{K+} + (m + K - n)\ e. \tag{7.3}$$

As before, we are interested only in the state of the primary particles after the collision. Therefore, in the following we shall not confine ourselves to processes (7.2) and (7.3).

The cross section of an inelastic process, in which the primary particle with initial charge i acquires a charge f, is denoted by σ_{if}, the total cross section for electron capture by the particle (as is sometimes done) — by σ^c, and the total losses cross section — by σ^l.

Charge exchanges in atomic collisions are essentially many-body processes. As a result, an exact theoretical treatment is impossible. Nevertheless, the accumulated data on atomic collisions established some general features and verified the theoretical estimates and calculations.

Experimental and theoretical investigations of the total ionization cross section. The total ionization cross section characterizes the liberation probability of an electron in ionizing collisions, referred to one atom and one freed electron. It is equal to the sum of the ionization and the charge-exchange cross sections multiplied by the number of freed electrons. In pure ionization the incident particle preserves its charge. These processes and in particular, single-electron ionization, are decisive at high velocities $\left(v > \frac{cz_{\text{eff}}}{137}\right)$ of the incident particles, at which the charge-exchange cross section is negligibly small. As the velocity decreases, a noticeable contribution to the total ionization cross section is made, as was already stated above, by charge-exchange processes. Therefore, it is of the greatest interest to measure the total ionization cross sections for particles with energies $\sim 10^4 - 10^6$ ev. These measurements are performed, as a rule, by the condenser method: the charge accumulated on the plates of a condenser, placed in a chamber with the gas being investigated, is recorded.

The basic results of the investigation of the total ionization cross sections of gases for ions with energies of 10-200 kev are summarized in the following /107/*.

1) The total ionization cross section σ_- is a function of the relative velocity of the colliding particles and of their charge numbers. With increase in the velocity the cross section increases rapidly at first, reaches a maximum, and then decreases (at high velocities it decreases as v^{-2}, see § 4).

According to /311/, for $T > 0.15$ Mev the measured total ionization cross section of hydrogen by protons is satisfactorily given by

$$\sigma = (3.45 \pm 0.20)\ T^{(-0.824 \pm 0.010)} \cdot 10^{-17}\ \text{cm}^2/\text{molecule}.$$

* Works carried out until 1950 are discussed in Massey and Burhop /72/.

This result is in agreement with Bates' calculations /163/ in the Born approximation.

For hydrogen ions in hydrogen and argon, the maximum cross section occurs for $v \sim 1.5 \quad u_0 = 3.3 \cdot 10^8$ cm/sec (Figures 59 and 60).

2) For a given ion velocity the absolute value of the total ionization cross section increases with the charge numbers of the atoms of the stopping medium (Z).

3) The total ionization cross section depends on the molecular structure and on the character of the levels of the colliding particles.

From the curves of Figure 61, the normalized /107/ experimental data on the total ionization cross sections can be compared with the theoretical data obtained by Firsov /115/ on the basis of an estimate of the mean excitation energy of the electrons in atomic collisions. According to Firsov,

$$\sigma_- = \sigma_Z \left[\left(\frac{v}{v_Z} \right)^{1/3} - 1 \right]^2, \qquad (7.4)$$

where v_Z and σ_Z are characteristic quantities of each pair of colliding particles:

$$v_Z = 23.3 \frac{I_{1a}}{(z+Z)^{1/2}} \cdot 10^8 \text{cm/sec};$$

$$\sigma_Z = \frac{32,7}{(z+Z)^{1/2}} \cdot 10^{-16} \text{cm}^2;$$

I_{1a} is the first ionization potential of the atoms of the medium, ev.

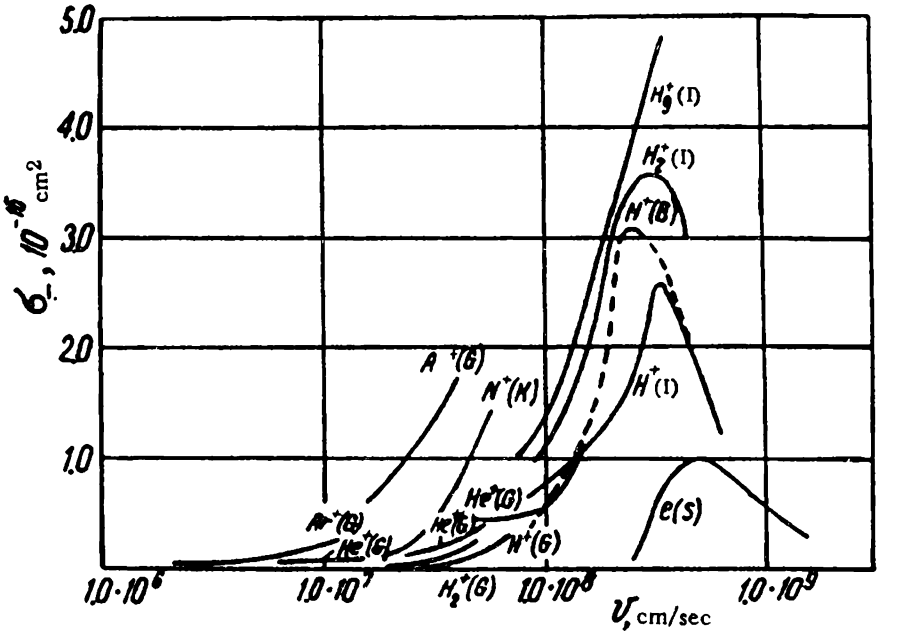

FIGURE 59. Total ionization cross section of hydrogen as a function of the ion velocity /107/. The symbols outside the parentheses indicate the ionizing particles; the letters in parentheses stand for the investigators: G for Gilbody and Hasted /270/; I for Afrosimov, Il'in, Fedorenko /7/; K for Telp, Khizeng, Kistemaker; B for Bates and Griffing, theoretical curve; S for Tate and Smith (ionization by electrons)

In the velocity range 10 - 10 cm/sec, Firsov's theory is in agreement with the experimental data given above on the dependence of the total cross section on the velocity and charge of the colliding particles, and for heavy colliding particles it gives correct values of the absolute cross sections.

Scattering of heavy ions associated with a change of charge. It was stated in § 2 that the differential cross sections for elastic scattering of ions on atoms differ greatly from the theoretical values (calculations of Everhard and Firsov) for large scattering angles ($\theta > 20^0$)*. It was also pointed out that one of the reasons for this is the contribution of inelastic processes, in particular, the stripping of electrons from the incident ions.

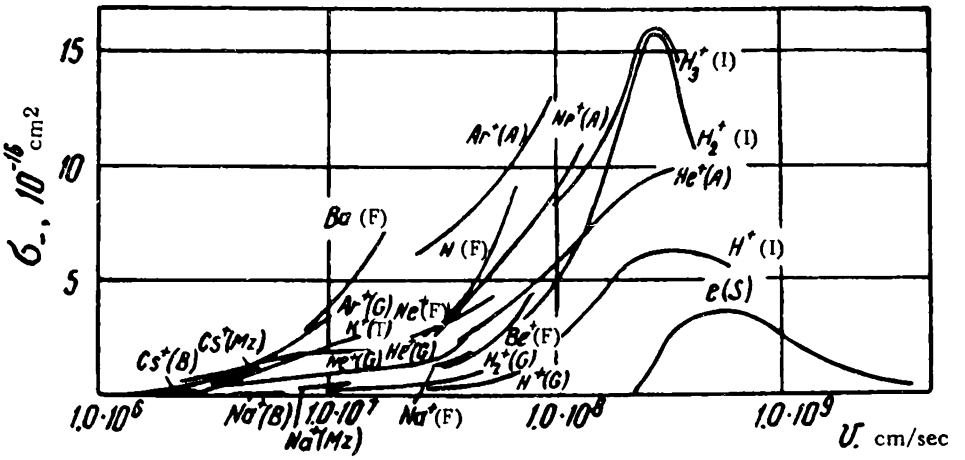

FIGURE 60. Total ionization cross section of argon by various ions and electrons as a function of velocity /107/; G — Gilbody and Hasted /270/; I — Afrosimov et al. /7/; A—Fedorenko et al. /109/; F—Fedorenko; Mz—Mauzon; B—Bek and Mauzon; T —Frishe; S—Smith (ionization by electrons)

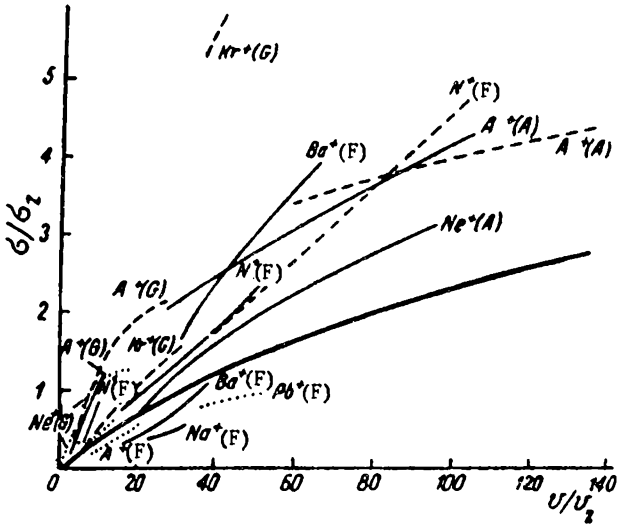

FIGURE 61. Universal dependence of the total ionization cross section on the velocity according to Firsov /112, 115/ and experimental values:
G—Gilbody /270/; F—Fedorenko /108/; A—Fedorenko et al. /110/. The experimental values for the ionization of argon are represented by the thin solid curves, of krypton — by the broken lines, of neon — by the dotted lines. The thick solid line represents calculations by Firsov

* For small scattering angles, when inelastic energy losses are relatively small, the kinematics of inelastic scattering are identical in practice to the kinematics of elastic collisions /114/.

The scattering of slow heavy ions (mainly He^+, A^+, N^+ ions) associated with a change of charge was investigated by Kaminker, Fedorenko /56/, and by Everhardt et al. /220, 247/. The results of these works are generally in agreement and complementary.

As an example Figure 62 shows the angular distribution of argon ions scattered on argon which acquired the charges 0, 1, 2, 3, 4, 5 after the scattering (neutral particles were formed upon the capture of an electron, and particles with charges 2, 3, 4, 5 as a result of stripping).

As the energy of the primary particles increases, the maxima of the angular distribution curves become narrower and are displaced toward smaller angles.

The scattering of negative ions with energies 5 to 30 kev, associated with electron capture, was studied by Dukel'skii and Fedorenko /41/.

The phenomenological theory of ion scattering on atoms based upon considerations of their charge was developed by Russek /442/. He considered the interpenetration of the electronic shells of the colliding atoms and related the probability for the formation of various charge states to the impact parameter ρ (see § 2).

General remarks on the calculations of the cross sections for charge-exchange processes. In charge exchange, the incident particle captures or loses one or several electrons. This process is connected with a variation in the internal energy of the colliding particles and with an energy defect $(\Delta E)^*$, except for resonance charge exchange, in which the charge exchange occurs between atoms of the same species. Thus, other conditions being equal, resonance charge exchange has the highest probability (see below).

The essentials of the process are best explained in the example of the charge exchange of helium ions, which also provided the first experimental proof of the existence of charge exchanges by the detection of charge inhomogeneity of a beam of retarded alpha-particles /305/. As was shown by Rutherford, the charge inhomogeneity of the beam occurring during their motion in the medium is due to a certain probability that the retarded alpha-particles capture and lose electrons. The corresponding probabilities are characterized by the electron capture σ^c and electron loss σ^l cross sections.

According to general considerations, for alpha-particle velocities v exceeding their proper K-shell electron velocity u_K

$$(u_K = \frac{2\pi e^2 z}{h} = 4.4 \cdot 10^8 \text{ cm/sec}),$$

the cross section for electron loss is much larger than the capture cross section. In other words, in this case most of the time or over most of the path length in the substance an alpha-particle possesses no electrons. When $v \sim u_K$, the cross sections for capture and loss of electrons become comparable, and, consequently, an alpha particle is for a considerable part of the time a singly-charged ion or a neutral atom. The capture and loss cross sections also depend on the properties of the stopping medium.

The loss cross section of electrons in light materials $(Z \leqslant 4)$ can be calculated according to Bohr /12/, by the following approximate formula:

$$\sigma_n^l \cong 4\pi \left(\frac{a_0}{z}\right)^2 (Z + z)^2 \left(\frac{n_0}{v}\right)^2, \qquad (7.5)$$

* Energy defect, or, as it is often called, resonance defect, is the difference in the energy levels between which the passage of electrons occurs

where ze and v are the charge and velocity of the incident particles;
Z is the atomic number of the stopping medium;
a_0 and u_0 are the radius of the hydrogen orbit and the electron velocity in it.

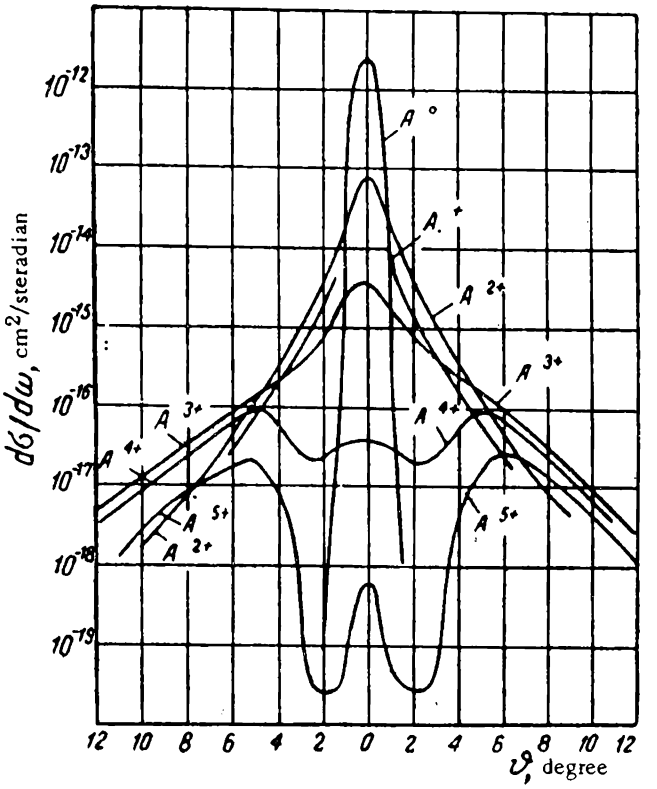

FIGURE 62. Angular distribution of argon ions which acquired charges of 0, 1, 2, 3, 4, 5 /56/ after scattering in argon. The initial energy of the argon ions is T = 75 kev

Formula (7.5) was obtained by a method used for pure ionization cross sections. It is assumed that the nucleus and the electron of the atom of the medium act independently on the incident ion. The formula is valid when the dimensions of the electronic orbits of the stopping atoms are of the same order of magnitude as the dimensions of the orbits from which the electron loss occurs.

The dependence of σ^l on the velocity in heavy substances is weaker, i. e., the nuclei of the stopping medium are screened by the electrons (§ 2). For materials with intermediate Z values ($\approx 4-8$) we have according to Bohr /12/

$$\sigma^l = \pi a_0^2 Z^{2/3} z^{-1} \left(\frac{u_0}{v}\right). \qquad (7.6)$$

Finally, the cross section for single-electron loss in heavy materials is, according to Bohr, equal to $\sim \pi a_0^2$, i. e., is almost independent of Z and v.

It is much more difficult to calculate the electron capture cross section. Approximate expressions for σ^c were obtained by the authors of /12, 79, 146/. They all found a strong dependence of σ^c on the velocity of the particle. Thus, according to Bohr /12/, light charged particles (protons,

alpha particles) capture in sufficiently heavy materials electrons whose orbital velocities are comparable with the velocity of the particle. Bohr estimated the velocities of the electrons on the basis of the statistical model of the atom using the above-given criterion, and obtained the following approximate expression for the electron capture cross section:

$$\sigma^c \sim 4\pi a_0^2 z^5 Z^{1/3} \left(\frac{u_0}{v}\right)^6 \qquad (7.6a)$$

$$(v \gg u_0).$$

If the electron velocities in the stopping medium are small as compared with the velocity of the incident particle a different criterion is necessary. According to Brinkman and Kramers /169/, the expression

$$\sigma^c \cong \frac{2^{16}}{5} \pi a_0^2 z^5 Z^5 \left(\frac{u_0}{v}\right)^{12}, \qquad (7.7)$$

obtained in the Born approximation, is valid only if the velocity of the particle is above zu_0 and Zu_0.

The expressions given above for the cross sections of charge exchanges are only suitable for rough estimates.

Unfortunately, no rigorous theory of charge exchanges is as yet available. An exception, perhaps, are the simplest cases of charge exchange collisions of light atoms in hydrogen and helium. Thus, Bates et al. /162/ and Kahn /340/ used the method of impact parameters for the calculation of cross sections of resonance charge exchange of protons in hydrogen. The same method was used by Jackson /445/ for the calculation of the cross sections of resonance charge exchange of helium. Their calculations are in qualitative agreement with the experimental data (see below).

In the works of Bates and Dalgarno /163/ and Jackson and Schiff /321, 445/, an improvement in the calculations of Brinkman and Kramers led to different results from those obtained by formula (7.7). Gerasimenko and Rozentsveig /37/ calculated the capture cross sections of two electrons by protons and helium ions in helium. The calculations were performed in the Born approximation. The cross section for electron capture by protons, obtained by new calculations, are in better agreement with the experimental cross sections (for $v > u_0$).

For qualitative estimates of the dependence of the charge-exchange cross sections on the velocity for the low velocities range ($v < u_0$) the so-called adiabatic hypothesis of Massey /71/ may be used /108, 120, 270/. It is based on a comparison of the characteristic atomic transition times with the collision times. According to this hypothesis, for

$$2\pi a |\Delta E| / \hbar v \gg 1$$

the effective cross sections for inelastic collisions are small, but increase with velocity by an exponential factor which is determined by the parameter $2\pi a\left(\frac{\Delta E}{\hbar v}\right)$, so that the maximum cross section is expected at a velocity v_{max}, satisfying the condition:

$$\frac{2\pi a |\Delta E|}{\hbar v_{max}} \cong 1 \qquad (7.8)$$

where a is a distance characteristic of the range of the forces involved in the process;

ΔE is the variation in the internal energy of the particles obtained in the process.

For $v > v_{max}$, the cross section should decrease monotonically. The experimental dependence $\sigma(v)$ agrees in many cases with the conclusions from Massey's adiabatic hypothesis (see below). However, the physical meaning of the parameter a, chosen in order to match the experiment with the theory, is unclear.

The work of Bell /170/ should also be mentioned. He shows that the cross sections for charge-exchange collisions of fast fission fragments can be calculated in the classical approximation.

Experimental data on the capture and loss of electrons by ions and hydrogen atoms. A detailed review and systematic experimental data on the variation in the charge of atoms and hydrogen ions in collisions with atoms of various materials can be found in Allison /132, 133/. Fogel''s paper /120/ deals with the formation of negative hydrogen ions.

Only a small part of the data related to this problem will be presented here as summarized in /133/ from results obtained in various laboratories.

A beam of hydrogen particles in matter is generally assumed to be a three-component system (a mixture of H^0, H^- and H^+). The charge distribution of the particles in this system can be determined if the dependence of the cross sections on the energy for the six possible types of collisions σ_{01}, $\sigma_{0\bar{1}}$, $\sigma_{1\bar{1}}$, σ_{10}, $\sigma_{\bar{1}0}$, $\sigma_{\bar{1}1}$ is known. The first index denotes the charge of the particle before collision, the second that after collision. Thus, $\sigma_{0\,\bar{1}}$ is the cross section of the process in which a neutral atom is transformed into a negative ion (cross section for electron capture by an atom); $\sigma_{1\,\bar{1}}$ is the cross section for capture of two electrons by a proton, and so on.

At energies $T > 50$ kev, processes with the participation of H^- are of no importance (Table 50). In this case, the beam of hydrogen particles is a two-component system, in which the charge distribution is determined by the cross sections σ_{01} and σ_{10}.

The energy dependence of the capture and stripping cross sections for H^-, H^0 and H^+ particles passing through hydrogen, is given in Figure 63 on a logarithmic scale. There is a similar energy dependence of the charge-exchange cross sections for these particles in other materials. Values of experimental charge-exchange cross sections in other gases are given in Table 50. The charge-exchange cross sections in oxygen and nitrogen have similar magnitudes, so that the data for nitrogen can be used for air. In plotting the curves of Figure 63 and in compiling Table 50 the data of /293, 343, 117, 108, 184, 471, 227/ were used.

It is interesting to note that in accordance with Bohr's criterion, the total cross sections for the capture and loss of an electron by a proton in air and other gases for $\frac{v}{u_0} \approx 1$ are equal ($T \approx 25$ kev). An exception is hydrogen, where equality is obtained for $\frac{v}{u_0} \approx 1.4$.

In a stopping medium of sufficient thickness many charge-exchange collisions take place so that eventually an equilibrium ratio between the number of particles of different charges is established. The corresponding equilibrium fractions of the charge components $F_{i\infty}$ for a hydrogen beam ($i = 1, 0, -1$), after passing thick layers of various materials, are given

TABLE 50

Cross sections for charge exchange collisions (in units of 10^{-17} cm^2/atom) for ions and atoms of hydrogen

T, kev	Helium, He							Nitrogen, N						Neon, Ne							Argon, A						
	$\sigma_{\bar{1}0}$ /293/	$\sigma_{\bar{1}0}$ /471/	$\sigma_{\bar{1}1}$	$\sigma_{0\bar{1}}$	σ_{01}	$\sigma_{1\bar{1}}$	σ_{10}	$\sigma_{\bar{1}0}$	$\sigma_{\bar{1}1}$	$\sigma_{0\bar{1}}$	σ_{01}	$\sigma_{1\bar{1}}$	σ_{10}	$\sigma_{\bar{1}0}$	$\sigma_{\bar{1}0}$	$\sigma_{\bar{1}1}$	$\sigma_{0\bar{1}}$	σ_{01}	$\sigma_{1\bar{1}}$	σ_{10}	$\sigma_{\bar{1}0}$ /293/	$\sigma_{\bar{1}0}$ /471/	$\sigma_{\bar{1}1}$	$\sigma_{0\bar{1}}$	σ_{01}	$\sigma_{1\bar{1}}$	σ_{10}
0.2	26	—	—	—	—	—	0.24	—	—	—	—	—	—	22	—	—	—	—	—	~ 0.5	52	—	—	—	—	—	20
0.4	30	—	—	—	—	—	0.22	—	—	—	—	—	—	24	—	—	—	—	—	~ 0.6	54	—	—	—	—	—	38
0.6	34	—	—	—	—	—	0.25	—	—	—	—	—	—	25	—	—	—	—	—	1.2	58	—	—	—	—	—	62
0.8	36	—	—	—	—	—	0.30	—	—	—	—	—	—	25	—	—	—	—	—	2.0	65	—	—	—	—	—	95
1	37	—	—	—	—	—	0.50	—	—	—	—	—	—	25	—	—	—	—	—	3.0	68	—	—	—	—	—	120
2	40	—	—	—	—	—	1.00	—	—	—	—	—	—	35	—	—	—	—	—	8.5	75	—	—	—	—	—	140
3	45	—	—	—	—	—	1.50	—	—	—	—	—	—	39	—	—	—	—	—	13.5	85	—	—	—	—	—	145
4	50	57.0	—	—	11.5	—	1.95	88.0	—	0.52	10.0	—	59.0	41	34	—	0.44	6.7	—	17.5	100	80	—	3.7	13.0	—	155
5	55	56.0	4.50	—	13.3	—	2.60	90.0	5.40	0.80	11.5	—	58.0	45	35	3.0	0.65	8.0	—	20.5	125	88	3.75	3.5	15.5	—	130
7	65	55.5	4.50	—	15.0	—	5.60	88.0	5.45	1.20	14.5	—	55.0	49	39	3.5	1.30	10.5	—	27.0	166	105	4.50	3.0	18.0	—	117
9	72	51.0	4.50	0.32	15.0	0.13	8.00	81.0	5.47	1.50	16.5	0.34	58.0	52	40	4.2	1.50	11.5	0.19	29.0	177	120	5.90	2.5	20.5	0.39	105
11	75	50.5	4.40	0.56	15.0	0.13	10.5	78.0	5.50	1.60	16.5	0.32	50.0	54	41	4.8	1.50	12.0	0.18	29.5	184	135	7.20	2.2	24.0	0.38	90.0
13	70	49.5	4.30	0.60	15.0	0.14	14.0	74.0	5.55	1.60	18.2	0.31	48.3	57	42	5.0	1.40	15.0	0.17	29.0	190	150	7.80	1.9	26.0	0.37	83.0
15	68	48.5	4.20	0.62	14.0	0.14	17.5	70.0	5.62	1.45	19.0	0.29	43.0	58	44	5.1	1.30	16.5	0.12	28.0	195	160	8.75	1.4	29.0	0.36	80.0
20	58	44.5	3.50	0.68	13.5	0.12	19.2	68.0	6.00	1.10	20.5	0.27	39.5	60	48	5.2	1.00	17.7	0.10	23.5	205	175	11.7	1.1	33.0	0.33	71.0
25	50	41.0	3.20	0.67	13.0	0.12	19.5	68.0	6.87	0.92	21.5	0.20	34.5	62	49	5.3	0.85	18.5	0.08	20.0	215	180	13.2	1.1	31.0	0.31	64.0
30	48	—	3.00	0.60	13.0	0.10	19.0	66.0	7.50	0.75	22.5	0.13	28.5	62	49	5.4	0.60	18.7	0.05	19.0	224	180	15.0	1.0	40.0	0.33	59.0
35	—	—	2.70	—	12.6	—	17.5	—	8.25	—	23.0	—	25 5	62	—	5.52	—	19.0	—	16.5	226	—	16.2	—	43.0	—	50.0
40	—	—	2.50	—	12.4	—	16.0	—	8.75	—	23.5	—	22 5	63	—	5.73	—	19.5	—	14.0	230	—	17.4	—	45.0	—	44.0
45	—	—	—	—	12.4	—	14.5	—	—	—	24.0	—	19 5	—	—	—	—	19.7	—	12.0	—	—	—	—	46.0	—	38.0
50	—	—	—	—	12.3	—	11.8	—	—	—	24.5	—	17 7	—	—	—	—	20.0	—	11.5	—	—	—	—	47.5	—	33.0
60	—	—	—	—	12.0	—	9.70	—	—	—	24.0	—	15 0	—	—	—	—	20.0	—	9.80	—	—	—	—	47.5	—	22.0
70	—	—	—	—	10.8	—	6.30	—	—	—	24.0	—	11 0	—	—	—	—	20.0	—	8.50	—	—	—	—	48.0	—	20.0
80	—	—	—	—	10.0	—	4.90	—	—	—	24.0	—	7 6	—	—	—	—	20.0	—	7.50	—	—	—	—	48.0	—	16.5
90	—	—	—	—	9.20	—	3.80	—	—	—	24.0	—	6 3	—	—	—	—	19.7	—	6.20	—	—	—	—	48.0	—	12.0
100	—	—	—	—	8.80	—	3.00	—	—	—	24.0	—	5 0	—	—	—	—	19.5	—	5.75	—	—	—	—	45.0	—	9.80
150	—	—	—	—	6.95	—	0.930	—	—	—	21.0	—	2 2	—	—	—	—	18.7	—	2.80	—	—	—	—	40.0	—	3.80
200	—	—	—	—	5.65	—	0.360	—	—	—	19.3	—	0.75	—	—	—	—	18.0	—	1.40	—	—	—	—	37.0	—	1.08
250	—	—	—	—	4.90	—	0.160	—	—	—	17.7	—	0.34	—	—	—	—	—	—	—	—	—	—	—	30.0	—	0.380
300	—	—	—	—	4.00	—	0.070	—	—	—	15.0	—	0.16	—	—	—	—	—	—	—	—	—	—	—	28.7	—	0.150
350	—	—	—	—	3.35	—	0.038	—	—	—	14.0	—	0.080	—	—	—	—	—	—	—	—	—	—	—	26.5	—	0.074
400	—	—	—	—	3.10	—	0.020	—	—	—	13.3	—	0.050	—	—	—	—	—	—	—	—	—	—	—	22.5	—	0.050
450	—	—	—	—	2.90	—	0.011	—	—	—	11.5	—	0.032	—	—	—	—	—	—	—	—	—	—	—	22.0	—	0.038
500	—	—	—	—	2.45	—	0.0068	—	—	—	10.0	—	0.020	—	—	—	—	—	—	—	—	—	—	—	20.0	—	0.029
600	—	—	—	—	2.20	—	0.0030	—	—	—	9.60	—	0.011	—	—	—	—	—	—	—	—	—	—	—	19.5	—	0.019
700	—	—	—	—	1.95	—	0.0013	—	—	—	8.70	—	0.0067	—	—	—	—	—	—	—	—	—	—	—	19.0	—	0.015
800	—	—	—	—	1.65	—	0.0,85	—	—	—	8.00	—	0.0040	—	—	—	—	—	—	—	—	—	—	—	18.0	—	0.011
900	—	—	—	—	1.50	—	0.0,68	—	—	—	7.70	—	0.0030	—	—	—	—	—	—	—	—	—	—	—	17.0	—	0.0088
1000	—	—	—	—	1.41	—	0,52	—	—	—	7.00	—	0.0020	—	—	—	—	—	—	—	—	—	—	—	16.5	—	0.0076

in Tables 51 and 52 /133/. These data are important for the choice of a target material to provide a chosen charge composition of a beam passing through it, as well as for the calculation of the mean ($\bar{i}$) and the mean square ($\bar{i^2}$) ion charges in the beam. It is seen from Tables 51 and 52 that for light elements the equilibrium charge composition of the beam is weakly dependent on the medium in which the equilibrium is established.

The value of $F_{i\infty}$ can either be measured directly (see /120, 133/), or it can be calculated from the values of the charge-exchange cross sections. For a two-component charge system ($i = 0,1$), we have

$$F_{1\infty} = \frac{\sigma_{01}}{\sigma_{01} + \sigma_{10}}; \tag{7.9}$$

$$F_{0\infty} = \frac{\sigma_{10}}{\sigma_{01} + \sigma_{10}}.$$

The mean effective ion charge $\bar{i}$ and the mean square charge $\bar{i^2}$ can be calculated from the quantities F_i:

$$\bar{i} = \sum_i F_i i, \tag{7.10}$$

$$\bar{i^2} = \sum_i F_i i^2. \tag{7.11}$$

Experimental data on the capture and loss of electrons by ions and atoms of helium. Neglecting processes with negative He^- ions /43/, a beam of helium particles in a medium will be a three-component system (a mixture of He^0, He^+, He^{++}). The composition of the beam is in this case determined by the six cross sections.

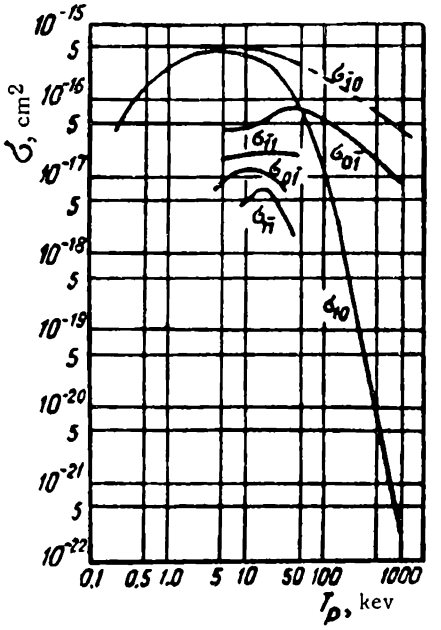

FIGURE 63. Cross sections for charge exchange by protons in hydrogen as a function of energy /133/

Allison's review /133/ gives experimental data on the charge-exchange collision cross sections of ions and helium atoms with molecules of hydrogen, nitrogen, oxygen, helium, neon, argon and xenon ($T = 0.2 - 200$ kev) and with molecules of hydrogen, helium and air $T = 0.2 - 450$ kev).

Figure 64 shows experimental curves of the capture and loss cross sections of electrons by ions and helium atoms $T = 0.2 - 1.5$ Mev) in hydrogen, helium, nitrogen, argon and krypton as a function of energy /87/. The experimental data /87/ (Figure 64) are in good agreement with the results of /133, 184/, obtained at lower particle energies.

The broken curve in Figures 64a, b represents the calculated cross section σ_{21} (in hydrogen) and of σ_{10} (in helium) in the Born approximation /445/. The experimental dependence of the capture cross section of an electron σ_{21} in nitrogen, argon and krypton on the particle velocity is satisfactorily represented by (7.6).

Tables 53 and 54 contain experimental data on the equilibrium fractions $F_{l\infty}$ $(l = 0, 1, 2)$ of the charge components of helium.

Experimental data on the capture cross sections of electrons by heavy ions and atoms. In the works of Fogel' et al. /120/ a study was made on inelastic collisions of atoms and ions ($T = 5 - 60$ kev, $v < 3 \cdot 10^8$ cm/sec) in which the incident particle, upon capturing an electron, became a negative ion:

$$A^+ + B \to A^- + B^{2+}, \tag{7.12}$$

$$A + B \to A^- + B^+. \tag{7.13}$$

Experimental curves of the cross section $\sigma_{\bar{1}1}$ for the pairs $H^+ - H_2$, $H^+ - He$ and $Li^+ - H_2$ are given in Figure 65a. These curves are characteristic for two-electron charge exchange, in which particles in excited states cannot participate. When the particles participating in inelastic collisions of atoms and ions in (7.12) and (7.13) also acquire excited states, the curve $\sigma(v)$ has a complex structure (presence of two maxima, asymmetry); see for example, Figure 65b.

TABLE 51

Equilibrium charge fractions in a beam of hydrogen after passing gaseous targets

T, kev	Hydrogen, H			Helium, He			Nitrogen, N			Argon, A		
	$F_{\bar{1}\infty}$	$F_{0\infty}$	$F_{1\infty}$	$F_{\bar{1}\infty}$	$F_{0\infty}$	$F_{1\infty}$	$F_{\bar{1}\infty}$	$F_{0\infty}$	$F_{1\infty}$	$F_{\bar{1}\infty}$	$F_{0\infty}$	$F_{1\infty}$
3	0.008	0.897	0.095	—	—	—	—	—	—	—	—	—
4	0.010	0.895	0.095	—	0.125	0.875	0.004	0.871	0.125	0.40	0.910	0.050
5	0.014	0.891	0.095	—	0.185	0.815	0.006	0.854	0.140	0.036	0.889	0.075
7	0.019	0.886	0.095	—	0.280	0.720	0.011	0.815	0.175	0.022	0.878	0.100
9	0.020	0.885	0.095	—	9.400	0.600	0.012	0.778	0.210	0.015	0.810	0.175
11	0.020	0.880	0.100	0.003	0.450	0.547	0.014	0.756	0.230	0.011	0.789	0.200
13	0.020	0.875	0.105	0.007	0.530	0.463	0.013	0.712	0.275	0.008	0.752	0.240
15	0.020	0.855	0.125	0.008	0.550	0.442	0.012	0.688	0.300	0.007	0.718	0.275
20	0.018	0.797	0.185	0.009	0.600	0.391	0.010	0.640	0.350	0.004	0.666	0.330
25	0.016	0.764	0.220	0.009	0.600	0.391	0.008	0.587	0.405	0.004	0.601	0.395
30	0.014	0.706	0.280	0.010	0.599	0.391	0.006	0.544	0.450	0.003	0.567	0.430
35	—	0.680	0.320	—	0.575	0.425	—	0.500	0.500	—	0.525	0.475
40	—	0.620	0.380	—	0.535	0.465	—	0.480	0.520	—	0.490	0.510
45	—	0.580	0.420	—	0.515	0.485	—	0.430	0.560	—	0.445	0.555
50	—	0.525	0.475	—	0.490	0.510	—	0.410	0.590	—	0.405	0.595
60	—	0.447	0.553	—	0.447	0.553	—	0.384	0.616	—	0.316	0.684
70	—	0.361	0.639	—	0.369	0.631	—	0.314	0.686	—	0.294	0.706
80	—	0.276	0.724	—	0.329	0.671	—	0.240	0.760	—	0.256	0.744
90	—	0.237	0.763	—	0.292	0.708	—	0.208	0.792	—	0.200	0.800
100	—	0.183	0.817	—	0.254	0.746	—	0.172	0.828	—	0.179	0.821
150	—	0.063	0.937	—	0.118	0.882	—	0.095	0.905	—	0.087	0.913
200	—	0.024	0.976	—	0.060	0.940	—	0.038	0.962	—	0.028	0.972
250	—	0.075	0.993	—	0.032	0.968	—	0.019	0.981	—	0.012	0.988
300	—	0.0041	0.996	—	0.017	0.983	—	0.010	0.990	—	0.0054	0.996
350	—	0.0024	0.998	—	0.011	0.989	—	0.0057	0.994	—	0.0027	0.997
400	—	0.0012	0.999	—	0.0064	0.994	—	0.0037	0.996	—	0.0022	0.998
450	—	0.0_357	—	—	0.0038	0.996	—	0.0028	0.997	—	0.0017	0.998
500	—	0.0_339	—	—	0.0028	0.997	—	7.0020	0.998	—	0.0014	0.999
600	—	0.0_316	—	—	0.0014	0.999	—	0.0012	0.999	—	0.0_397	—
700	—	0.0_496	—	—	0.0_392	—	—	0.0_377	—	—	0.0_379	—
800	—	0.0_454	—	—	0.0_352	—	—	0.0_350	—	—	0.0_361	—
900	—	0.0_440	—	—	0.0_345	—	—	0.0_339	—	—	0.0_352	—
1000	—	0.0_427	—	—	0.0_336	—	—	0.0_328	—	—	0.0_346	—

Fogel' concludes that processes of type (7.12) and (7.13) are described satisfactorily, at low incident particle velocities, by the adiabatic hypothesis of Massey (see above). The positions of the maxima on curves similar to those in Figures 65 *a* and 65 *c* are determined by condition (7.8), the quantity a being approximately equal to 1.5 Å for processes of type (7.13). The dependence of a, (7.8), on the colliding particles is very weak.

In the studies of Hasted et al. /293/ on electron capture by slow singly-charged ions it was shown that the cross sections $\sigma_{10}(v)$ have a maximum whose position is determined by (7.8), if we take $a \approx 8$ Å. The value of a is also only weakly dependent on the colliding particles.

The capture cross section of several electrons by multiply-charged ions with $v < 10^8$ cm/sec was also studied in /108, 122/. The dependence of the cross sections on the absolute value and sign of the resonance defect ΔE was observed. For the same particle velocity and absolute value of ΔE, the cross section for endothermic processes ($\Delta E < 0$) is considerably larger than for exothermic processes ($\Delta E > 0$) /122/.

In the works of Nikolaev, Dmitriev, Fateeva and Teplova /80, 83/ the capture cross sections of one and two electrons by fast multiply-charged ions ($z = 2 - 18$, $v = 2.6 - 12 \cdot 10^8$ cm/sec) in helium, nitrogen, argon and krypton were studied. The following features were established.

1) The dependence of the cross sections $\sigma_{i,\,i-1}$ on the velocity is mostly the same as the dependence of σ_{10} for protons (see /184/ and Table 50); a difference occurs in the absolute values of the cross sections and in the rate of decrease of the cross section;

2) when the ion velocity increases, the cross section for capture of two or more electrons decreases faster than the cross section for capture of s single electron

$$\frac{\sigma_{i,\,i-2}(v)}{\sigma_{i,\,i-1}(v)} < 1;$$

3) the quantities $\sigma_{i,\,i-1}$ and $\sigma_{i,\,i-2}$ for a given medium vary non-monotonically with z (the nuclear charge of the incident particle); the probability of electron capture depends only on the charge of the forming ion and depends weakly on the number of captured electrons;

4) Bohr's criterion (the capture of an electron is most probable if the orbital velocity of the captured electron is approximately equal to the velocity of the ion) and the theoretical calculations of the capture cross section of two electrons by helium ions are confirmed /37/;

5) in contrast to electron capture by ions with $v \leqslant 10^8$ cm/sec, in which a correlation between the capture cross section and the resonance defect is observed /120, 122/, for velocities $v > 3 \cdot 10^8$ cm/sec this correlation is not observed.

The experimental dependence of electron capture on the velocity of the total cross sections when protons (H^+), alpha-particles (He^{2+}), and lithium nuclei (Li^{3+}) pass through hydrogen, is given in Figure 66. It follows from this figure that at high velocities the capture cross sections are proportional to the squares of the nuclear charges (9:4:1), see formula (7.6). When the particle velocities decrease, the differences in the cross sections are less well defined.

TABLE 52

Equilibrium charge fractions in a hydrogen beam after passing through solid targets

T, kev	Beryllium, Be			Aluminum, Al			Calcium, Ca			Silver, Ag			Gold, Au		
	$F_{\bar{1}\infty}$	$F_{0\infty}$	$F_{1\infty}$	$F_{\bar{1}\infty}$	$F_{0\infty}$	$F_{1\infty}$	$F_{\bar{1}\infty}$	$F_{0\infty}$	$F_{1\infty}$	$F_{\bar{1}\infty}$	$F_{0\infty}$	$F_{1\infty}$	$F_{\bar{1}\infty}$	$F_{0\infty}$	$F_{1\infty}$
4	—	—	—	0.062	0.856	0.082	—	—	—	—	—	—	0.042	0.856	0.102
7	0.035	0.828	0.137	0.048	0.840	0.112	0.024	0.801	0.175	0.029	0.771	0.200	0.038	0.830	0.132
10	0.031	0.793	0.176	0.040	0.818	0.142	0.013	0.683	0.304	0.023	0.730	0.247	0.035	0.800	0.165
20	0.019	0.671	0.310	0.024	0.725	0.251	0.005	0.462	0.533	0.117	0.682	0.301	0.028	0.705	0.267
25	0.014	0.611	0.375	0.017	0.643	0.340	0.003	0.41	0.59	0.014	0.67	0.350	0.023	0.637	0.340
—	—	—	—	—	—	—	0.001	0.262	0.737	0.004	0.398	0.598	0.004	0.401	0.595
50	0.003	0.341	0.656	0.0037	0.356	0.640	—	0.17	0.83	0.001	0.27	0.730	0.002	0.27	0.73
75	0.015	0.195	0.790	0.0015	0.20	0.80	—	0.117	0.883	0.0_27	0.184	0.815	0.019	0.195	0.804
100	—	0.134	0.866	0.0_36	0.120	0.879	—	0.08	0.92	—	0.13	0.87	—	0.16	0.840
125	—	0.08	0.92	—	0.08	0.92	—	0.05	0.950	0.0_32	0.088	0.912	0.015	0.134	0.876
150	—	0.048	0.95	0.0_34	0.045	0.955	—	0.03	0.97	—	0.07	0.93	—	0.10	0.90
175	—	0.03	0.97	—	0.03	0.97	—	0.01	0.99	—	0.05	0.95	—	0.08	0.92
200	—	0.01	0.99	—	0.02	0.98	—	—	—	—	—	—	—	—	—

TABLE 53

Equilibrium distribution of the charges of helium ions in various media /87/

Energy, kev	Hydrogen, H			Helium, He			Nitrogen, N			Argon, A			Krypton, Kr		
	$F_{0\infty}$	$F_{1\infty}$	$F_{2\infty}$	$F_{0\infty}$	$F_{1\infty}$	$F_{2\infty}$	$F_{0\infty}$	$F_{1\infty}$	$F_{2\infty}$	$F_{0\infty}$	$F_{1\infty}$	$F_{2\infty}$	$F_{0\infty}$	$F_{1\infty}$	$F_{2\infty}$
200	0.43	0.556	0.014	0.495	0.485	0.02	0.335	0.628	0.037	0.36	0.615	0.025	0.5	0.49	0.01
300	0.24	0.696	0.064	0.307	0.637	0.056	0.23	0.66	0.11	0.19	0.72	0.09	0.258	0.697	0.045
400	0.128	0.712	0.16	0.204	0.666	0.13	0.13	0.685	0.185	0.102	0.7	0.198	0.170	0.725	0.105
500	0.07	0.67	0.26	0.125	0.67	0.205	0.086	0.63	0.284	0.056	0.604	0.34	0.09	0.68	0.23
600	0.045	0.57	0.385	0.08	0.63	0.29	0.05	0.55	0.4	0.03	0.48	0.49	0.05	0.55	0.4
700	(0.02)	0.43	0.55	0.06	0.58	0.36	0.03	0.47	0.5	0.017	0.383	0.6	0.025	0.46	0.515
800	(0.010)	0.35	0.64	0.045	0.525	0.43	0.02	0.41	0.57	0.009	0.281	0.71	0.015	0.35	0.635
900	(0.006)	0.264	0.73	(0.03)	0.47	0.5	0.012	0.35	0.64	0.006	0.224	0.77	0.01	0.266	0.724
1000	(0.004)	(0.22)	0.776	(0.02)	0.42	0.56	0.008	0.3	0.700	0.003	0.178	0.819	(0.006)	0.214	0.78
1100	(0.0025)	(0.17)	0.828	(0.013)	0.37	0.617	(0.006)	0.224	0.77	(0.0023)	0.146	0.852	(0.0045)	0.18	0.815
1200	(0.0015)	(0.125)	0.874	(0.01)	0.31	0.68	(0.0037)	0.19	0.806	(0.002)	0.119	0.879	(0.003)	0.162	0.835
1300	(0.0012)	(0.105)	0.894	(0.007)	0.26	0.733	(0.003)	0.165	0.832	(0.0015)	0.099	0.9	(0.002)	0.15	0.848
1400	(0.001)	(0.09)	0.909	(0.005)	0.215	0.78	(0.002)	0.145	0.853	(0.0012)	0.084	0.915	(0.0016)	0.135	0.863
1500	—	(0.07)	0.93	(0.0035)	0.187	0.81	—	0.123	0.877	(0.001)	0.073	0.926	(0.0014)	0.122	0.877

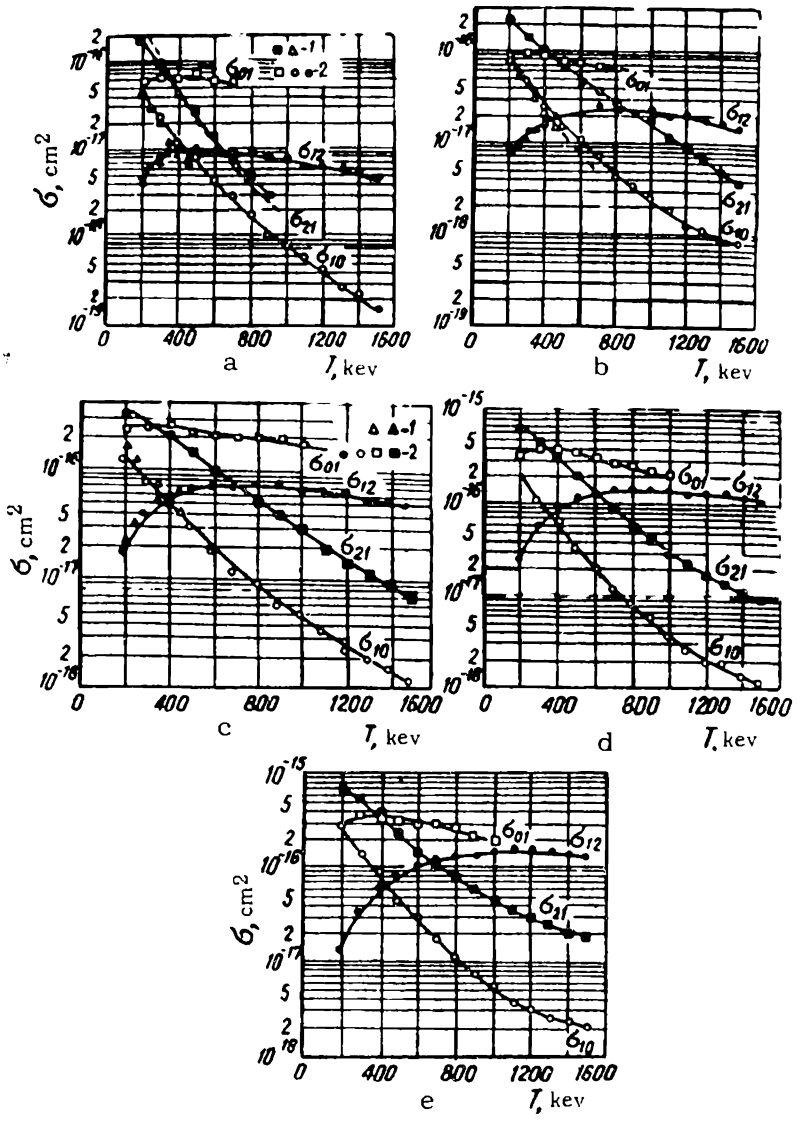

FIGURE 64. Cross sections for loss and capture of electrons by helium ions

a — in hydrogen: 1 — experimental values of σ_{10} and σ_{12} from /133/; 2 — from /87/, the broken curve represents the theoretical dependence of σ_{21}, according to /37/; b — in helium, same notation; c — in nitrogen: 1 — data from /133/ for σ_{10} and σ_{12} in air; 2 — data from /87/; d — in argon /87/; e — in krypton /87/

Equilibrium distribution of the charges of heavy ions in various media. Both theoretical /12, 44, 79, 146, 165, 182, 264, 402/, and experimental /42, 57, 78, 81, 101, 110, 147, 287, 402, 431, 436, 512/ works are devoted to the study of the equilibrium charge distribution and mean charge of a beam of ions of light elements ($z \geqslant 3$) passing through various materials.

In accordance with Bohr's criterion /146/, an ion retains at each point of its path those electrons whose velocities are equal or higher than the ion velocity v. When this condition is satisfied, the mean effective ion charge $\langle z_{\text{eff}} \rangle_{\text{mean}} = \bar{i}$ is

$$i = z^{1/3}\frac{v}{u_0} \qquad (7.12a)$$

$$(u_0 < v < z^{2/3}u_0).$$

Knipp and Teller /338/, and Brunning, Knipp and Teller /165/ modified Bohr's criterion based on more accurate calculations of the orbital velocities of the electrons (again in the framework of the Thomas-Fermi model) and on experimental data available in 1940 on the charge distribution of alpha particles and heavy ions in air and hydrogen.

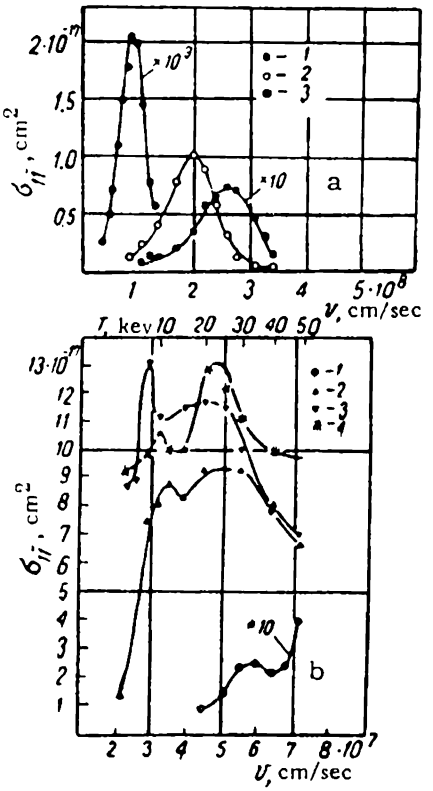

FIGURE 65. Dependence of the cross sections on the velocity

a — for capture of two electrons by lithium ions in hydrogen (1), by protons in hydrogen (2), and by helium in helium (3); b — two-electron exchange by ions of neon (1), argon (2), krypton (3), and xenon (4), according to Fogel' /120/.

According to /165/, an ion retains electrons with velocities $u > \gamma v$, where γ is determined from experimental data. If we consider the least firmly bound electrons in the ion, then the value of $\gamma = \gamma_1$ increases from 1.3 for $z = 6$ to 1.8 for $z = 55$. However, if we assume that the farthest electrons are the most important in the charge exchange, then the value of $\gamma = \gamma_2$ decreases from 0.6 for $z = 6$ to 0.35 for $z = 55$.

It can be expected (and this is confirmed experimentally, see below) that the characteristic velocity of electrons in an ion, determining the mean effective ion charge, has a value between $\gamma_1 v$ and $\gamma_2 v$.

Dmitriev /44/ calculated the mean charge and the charge distribution of certain ions in air, assuming that the probability for the loss of an electron is a function of the ratio of the ion velocity to orbital electron velocity. The effective interaction of fast ions with a medium was determined by a summation over the individual electrons of the atoms. Gluckstern /264/ determined the effective charge of the ion in a medium from data on the electron capture and loss cross sections by ions.

According to the estimates given above of the capture and loss cross sections of electrons (see also /79, 182/), it should be expected that for sufficiently high velocities the mean effective ion charge will be larger in light materials. Calculations /182, 402/ also show that the effective charge of an ion in a condensed medium (a solid or liquid substance) should be larger than in the corresponding vapors or gases. Consequently, the atomic stopping power of a medium in the condensed state should be higher.

Systematic measurements of the equilibrium charge distributions of ions of light elements ($z = 2$-18) in various gases and in a celluloid film were performed by Nikolaev, Dmitriev, Teplova and Fateeva /42, 78, 101/. Some results of their measurements are given in Figures 67, 68, and in Tables 55, 56, 57. The charge distributions of ions with $3 \leqslant z \leqslant 10$ in all the stopping media investigated are close to gaussian:

$$F_l = \frac{1}{\sigma\sqrt{2\pi}} \exp\left[-\frac{(l-\bar{l})^2}{2\sigma^2}\right],$$

where $\bar{i}$ is the mean equilibrium charge, determined by (7.10); $\sigma = [\sum F_i (i - \bar{i})^2]^{1/2}$ is the distribution width.

As z increases, the value of σ also increases and is ~0.55, 0.6, 0.7, 0.8 and 0.9 respectively, for helium, lithium, boron, nitrogen, and neon ions in gases. For a given ion velocity the values of σ in different gases vary by no more than 10%. The value of σ in celluloid for $v \leqslant 5 \cdot 10^8$ cm/sec is 10-20% higher than in gases, and at $v > \cdot 10^8$ cm/sec begins to decrease.

TABLE 54

Equilibrium charge composition of a beam of helium after passing through solid targets /132/

T, kev	Scattering and passage through beryllium, aluminum and silver foils			$F_{1\infty}$ determined from the yield from	
	$F_{0\infty}$	$F_{1\infty}$	$F_{2\infty}$	mica	gold
130	0.58	0.40	0.017	—	—
200	0.39	0.57	0.04	—	—
300	0.24	0.65	0.11	—	—
400	0.15	0.65	0.20	—	—
406	—	—	—	0.68	—
500	0.09	0.59	0.32	—	—
590	—	—	—	0.60	—
600	0.06	0.52	0.42	—	—
640	—	—	—	0.50	—
700	0.02	0.43	0.55	—	—
787	—	—	—	0.35	—
800	—	0.36	0.64	—	—
900	—	0.29	0.71	—	—
1000	—	0.24	0.76	—	—
1100	—	0.20	0.80	—	—
1260	—	—	—	0.16	—
1355	—	—	—	0.14	0.14
1521	—	—	—	—	0.12
1696	—	—	—	0.12	—
1935	—	—	—	0.061	0.065
2323	—	—	—	—	0.045
2408	—	—	—	0.038	0.038
2719	—	—	—	0.032	0.036
3406	—	—	—	—	0.024
4262	—	—	—	—	0.015
4440	—	—	—	0.015	—
4915	—	—	—	0.012	—
6028	—	—	—	0.0079	0.0088

As can be seen from Figure 67 and Tables 55, 56, and 57, the value of $\bar{i}$ for a given velocity varies monotonically with z. In the range of values i/z = 0.2-0.6, the degree of ionization i/z in gases is a function of the parameter $v\, z^{-\alpha}$, where α = 0.45, which is in qualitative agreement with the theory /165/. However, the degree of ionization i/z for a given ion velocity is not the same in a gas as in a solid (celluloid), but also varies appreciably with the kind of gas (Figure 68). This fact cannot be explained by existing theories /182, 264/.

For ions with $z > 10$ of the same velocity, an increase in the mean charge $\bar{i}$ and a monotonic decrease of i/z with increasing nuclear charge z is observed. Particularly large differences between the values of i are observed for gases and celluloid. The violation of the smooth dependence of $\bar{i}$ and F_i on z is connected, according to the authors of /78/, with the influence of the periodic structure of the electronic shells.

The equilibrium charge distribution of heavy ions ($z > 2$) in the range of lower velocities was also investigated in /135, 443, 470, 363, 284, 504/, and in the range of high velocities, corresponding to energies of 1 to 10 Mev/nucleon*, in /287, 403, 431, 435, 436/. The effective charges of fission fragments in various media were determined by Lassen /364/.

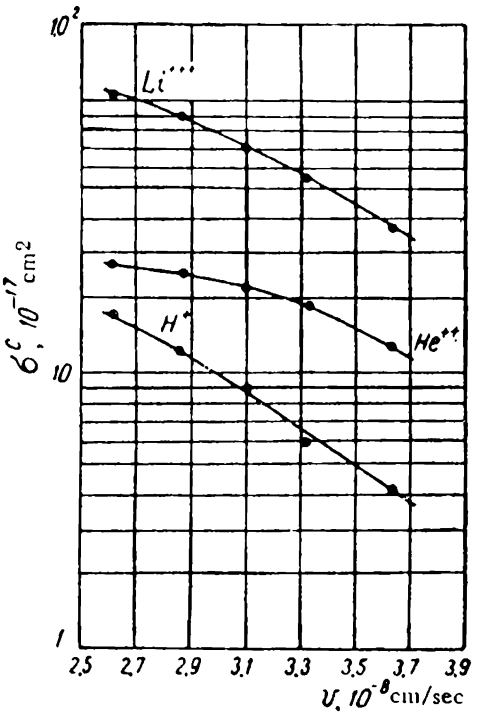

FIGURE 66. Total cross sections for electron capture by protons, alpha-particles, and lithium nuclei /134/

Experiments /364, 431, 436/ show that the charge state of heavy ions depends on the type of absorber, and that the mean and mean square ion charges in solid bodies are larger than in gases for the same particle velocities.

The effective mean and mean square charges of heavy ions can be determined in two ways:

1) by measuring the cross sections σ_{ij} for charge exchange collisions, or of the equilibrium charge distribution F_i; the effective charges are calculated in this case by the relations (7.10) and 7.11);

2) from the experimental values of the energy losses $\frac{dE}{dx}$ or from the range-energy curves for the ions in the material being investigated. The mean square effective ion charge $\overline{i^2}$ is determined from the ratio of the specific energy losses of an ion of a given velocity to the specific losses of a proton or of an alpha-particle of the same velocity and in the same material (the latter should be completely "stripped", i. e., devoid of electrons).

A second method was used to determine the effective charge of heavy ions in /287, 431, 436, 403/.

TABLE 55

Equilibrium charge distribution of helium ions /81/

Medium	$10^{-8}v$, cm/sec	$F_{0\infty}$	$F_{1\infty}$	$F_{2\infty}$	$\overline{i}$	σ
		%				
Helium, He	5.67	6.4	61.4	32.2	1.26	0.56
	7.92	0.3	27.7	72.0	1.72	0.45
	11.67	—	4.0	96.0	1.96	0.20
	16.86	—	0.6	99.4	1.99	0.11
Nitrogen, N_2	5.67	2.6	51.2	46.2	1.44	0.55
	7.92	0.05	17.3	82.7	1.83	0.38
	11.67	—	3.8	96.2	1.96	0.19
	16.86	—	0.75	99.25	1.99	0.095
Argon, A	5.67	1.3	42.9	55.8	1.54	0.52
	7.92	0.04	10.1	89.9	1.90	0.30
	11.67	0.01	4.4	95.6	1.96	0.21
	16.86	—	1.15	98.85	1.99	1.11
Krypton, Kr	3.89	14	78	8	0.93	0.46
	5.67	1.4	49.1	49.5	1.48	0.53
	7.92	0.06	16.2	83.7	1.84	0.37
	11.67	0.01	7.6	92.4	1.92	0.26
	16.86	—	1.6	98.4	1.98	0.13

* The measurements of Nikolaeva and others /78, 101/ refer to the energy range $\frac{T}{A}$ = 0.04—0.7 Mev/nucleon.

TABLE 56

Equilibrium charge distribution of lithium ions /81/

Medium	$10^{-6}\,v$, cm/sec	$F_{0\infty}$	$F_{1\infty}$	$F_{2\infty}$	$F_{3\infty}$	$\bar{i}$	σ
		%					
Helium, He	4.01	5	78	17	0 2	1.12	0.46
	5.69	1.4	47.9	47.8	2.9	1.52	0.58
	8.03	0.2	11.6	59.6	28.6	2.17	0.62
	11.64	—	0.5	18.0	81.5	2.81	0.41
Nitrogen, N_2	4.01	3	70	27	0.2	1.25	0.50
	5.69	0.5	32.1	61.3	6.1	1.73	0.57
	8.06	0.03	5.3	51.2	43.5	2.38	0.59
	11.64	—	0.5	19.0	80.5	2.80	0.42
Argon, A	4.01	2	70	28	0.4	1.27	0.49
	5.69	0.3	25.5	66.0	8.2	1.82	0.56
	8.06	0.03	3.1	44.5	52.4	2.50	0.56
	11.64	—	0.6	22.1	77.3	2.77	0.44
Krypton, Kr	4.01	3	81	16	0.1	1.14	0.42
	5.69	0.5	36.8	58.9	3.8	1.66	0.56
	8.03	0.1	7.2	58.0	34.7	2.28	0.57
	11.64	—	1.6	32.6	65.8	2.64	0.52

TABLE 57

Equilibrium charge distribution of boron ions /81/

Medium	$10^{-8}\,v$, cm/sec	$F_{0\infty}$	$F_{1\infty}$	$F_{2\infty}$	$F_{3\infty}$	$F_{4\infty}$	$F_{5\infty}$	$\bar{i}$	σ
		%							
Helium, He	2.75	12.6	62.9	23.7	0.8	—	—	1.13	0.61
	3.79	7.6	52.7	36.4	3.3	0.01	—	1.35	0.67
	7.00	0.1	5.3	38.1	52.2	4.3	0.03	2.55	0.67
	7.87	0.03	1.9	23.7	62.0	12.2	0.2	2.85	0.65
Nitrogen, N_2	2.75	10.2	59.8	28.8	1.2	—	—	1.23	0.60
	3.78	4.2	41.9	47.5	6.3	0.05	—	1.56	0.58
	7.87	—	0.6	15.5	65.0	18.4	0.5	3.03	0.62
Argon, A	2.75	10.8	59.4	28.6	1.2	—	—	1.20	0.60
	3.78	3.6	42.2	47.9	6.2	0.06	—	1.57	0.67
	7.00	—	1.0	32.9	66.2	9.7	0.2	2.85	0.60
	7.87	—	0.3	31.0	67.5	20.7	0.5	3.10	0.59
Krypton, Kr	2.75	16.2	63.1	20.3	0.4	—	—	1.05	0.58
	3.79	5.2	48.1	43.1	3.6	0.02	—	1.45	0.65
	7.00	—	1.3	24.5	66.7	7.4	0.1	2.80	0.58
	7.87	—	0.5	13.2	70.0	16.0	0.3	3.02	0.57
Celluloid film	2.72	8.1	48.6	36.6	6.6	0.07	—	1.42	0.74
	3.05	6.3	43.6	40.7	9.3	0.1	—	1.53	0.76
	3.77	2.5	28.1	48.7	20.1	0.6	—	1.88	0.77
	6.98	—	1.0	18.1	58.4	21.3	1.2	3.03	0.70
	7.63	—	0.4	10.8	53.3	32.5	3.0	3.27	0.70

It should be expected that the effective charges determined by the two methods would differ. When measuring the specific energy losses of heavy ions both losses by electronic collisions ($\sim \bar{i}^2$) and other types of energy losses in nuclear and inelastic atomic collisions are taken into account. Consequently, data on the specific energy losses may yield overestimated values of $\bar{i}^2$. Actually, the other types of energy losses are significant for very heavy ions (fission fragments) and for comparatively slow ions. A special investigation /403/ has shown that both methods give well corresponding values of $\bar{i}^2$, if the velocity of the particles is sufficiently high.

As an example of measurements of the effective charge of fast heavy ions by means of the range-energy curves, Figures 69 and 70 give the results of /403, 431, 436/. The abscissa in these curves is the ratio of the ion velocity to the characteristic velocity $\left(\frac{c}{137}\right) z^{2/3}$ of the electron in the Thomas-Fermi model. Figure 69 a shows that the effective charge of ions, which still retain a sufficiently large number of electrons $\left(\frac{\bar{l}}{z} < 0.8-0.9\right)$, is a monotonic function of the parameter $137\,\beta z^{-2/3}$; for large values of $\frac{\bar{l}}{z}$ or, rather, at particle velocities close to the velocity of their K-electrons, it is better to choose the parameter $137\,\beta z^{-1}$, i.e., the ratio of the ion velocity v to the velocity $\frac{cz}{137}$ of its K-electron.

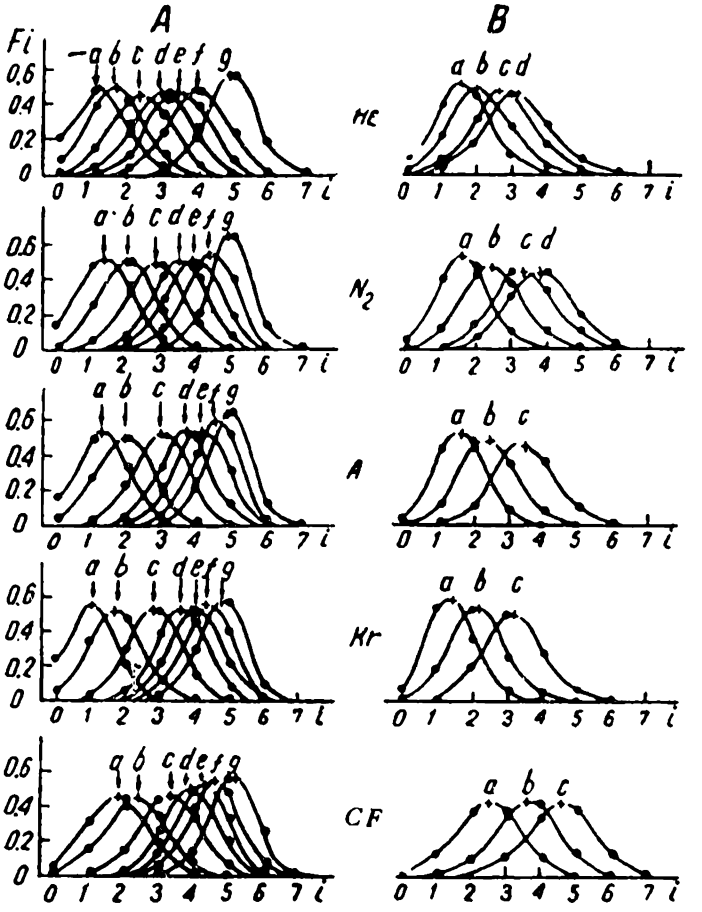

FIGURE 67. Equilibrium charge distribution of nitrogen (A) and neon (B) ions in gases and in celluloid film (CF) /81/. The velocities (in units of 10^8 cm/sec) for nitrogen ions are: 2.60 (a), 4.11 (b), 5.69 (c), 7.02 (d), 7.91 (e), 9.15 (f), 11.64 (g). For neon ions: 2.65 (a), 4.04 (b), 5.52 (c), 6.33 (d). For each distribution, the sign "+" on the abscissa is the value of i, and on the ordinate — the value of $(2\pi\sigma^2)^{-1/2}$

Thus, when the degrees of ionization are not very high, the experimental data on effective atomic charge can be featured within a wide velocity range by the parameter $137\,\beta z^{-a}$, where $|a| < 1$.

Figure 69 b gives the dependence of $\left(\frac{\bar{i}}{z}\right)^2$ on $\beta z^{-2/3}$ for fluorine ions in various gaseous and solid media. The experimental points are grouped about two curves, one of which corresponds to solid absorbers (aluminum, nickel), and the other to gaseous absorbers (oxygen, argon). For a given velocity, the effective charge of heavy ions in metals is larger than in gases. The same conclusion follows from the experiments of Nikolaev et al. (see above) as well as from Lassen's work /364/, showing that fission fragments have a smaller effective charge in gases than in a condensed medium.

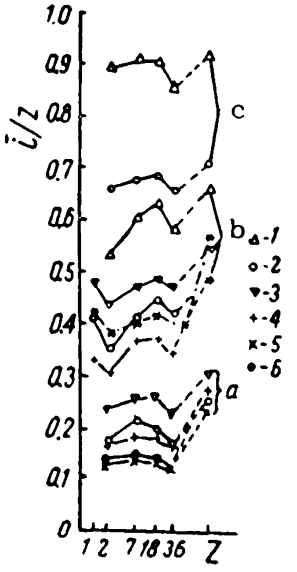

FIGURE 68. Degree of ionization i/z for ions in various media /81/:

a — $v = 3 \cdot 10^8$ cm/sec; b — $v = 6 \cdot 10^8$ cm/sec; c — $v = 11 \cdot 10^8$ cm/sec; 1 — lithium ions, 2 — nitrogen ions; 3 — boron ions; 5 — argon ions; 6 — phosphor ions

According to Bohr and Lindhardt /182/, this effect may be due to the dependence of the ratio of the capture to loss cross sections of an electron on the residual excitation of the ions. It contributes to the loss of electrons and prevents their capture in condensed media, where the deexcitation time of excited states is large.

The broken curve in Figure 69 b represents the dependence (7.12).

Fulmer and Cohen /258, 259/ studied the equilibrium charges of fission fragments in hydrogen and helium by magnetic analysis. As in the works of Lassen, an almost linear dependence of $\bar{i}$ on the velocity of the fragments in the range $v \simeq 2u_0 - 6\ u_0$ was observed, which corresponds to a variation of $\bar{i}$ from ~ 5 to 17 (Figure 70). Fulmer and Cohen also confirmed Lassen's conclusion that the effective charge of the fragments depends on the pressure of the gas in which they are moving.

Stopping (energy losses) of heavy ions in matter. The stopping of fast protons and alpha-particles is obtained along the entire path by inelastic collisions with the electrons of the stopping medium; elastic and inelastic nuclear collisions are of negligible importance (see § 2-5). In the stopping of fast heavy ions it is also possible to neglect the energy losses in inelastic nuclear collisions (§ 3). However, energy losses due to elastic nuclear and inelastic atomic collisions are important along a considerable part of the path of heavy ions (as we already noted above, charge exchange collisions are themselves a source of energy losses for the incident particles).

The energy losses in electronic collisions are determined by the mean square effective ion charge

$$\langle z^2 \rangle_{cp} \equiv \bar{i}^2.$$

The stopping power of a medium for ions due to inelastic collisions with electrons can be calculated by substituting $\bar{i}^2$ for z^2 in Bethe's formula (4.20), if

$$\bar{i}\left(\frac{2\pi e^2}{hv}\right) \ll 1$$

or in Bohr's formula (4.8), if

$$\bar{i}\left(\frac{2\pi e^2}{hv}\right) \gg 1.$$

For fission fragments the last condition is fulfilled, for example, along most of their path length.

The energy losses in elastic nuclear collisions are determined by (2.54)*. An example of calculated data for carbon and oxygen ions is given in Tables 5 and 6.

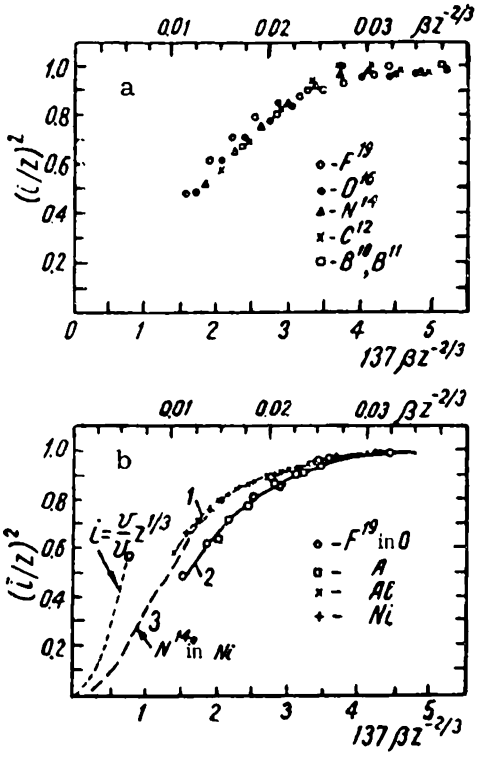

FIGURE 69. Experimental dependence of $(\bar{i}/z)^2$ on 137 $\beta z^{-2/3}$ for various heavy ions

a — in oxygen /436/; b — in aluminum and nickel (curve 1), in oxygen and argon (curve 2), according to /436/; the broken line 3 gives the dependence for nitrogen ions in nickel.

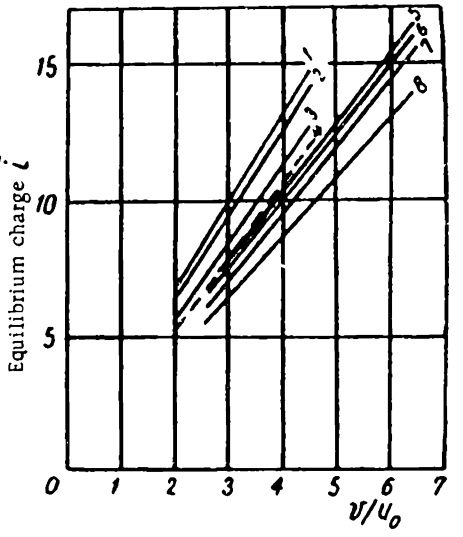

FIGURE 70. Equilibrium charge of light and heavy fission fragments in various gases as a function of the velocity of the fragments /258/

For heavy fragments: 1 — in argon, 2 — in air, 3 — in hydrogen; 4 — in helium. For light fragments: 5 — in argon, 6 — in air, 7 — in hydrogen, 8 — in helium.

If we disregard the logarithmic terms in the expressions for the energy losses in electronic (§ 4) and in nuclear (§ 2) collisions, the ratio of the energy losses by heavy ions in nuclear collisions to the losses in electronic collisions at a given ion velocity will be

$$\left(\frac{Zm}{\mu}\right)\left(\frac{z}{\bar{i}}\right)^2,$$

where m is the electron mass, and

μ is the reduced mass of the colliding atoms.

The ratio increases with decreasing particle velocity.

* Knipp and Teller /338/ give an expression for the energy losses in nuclear collisions which is different from (2.54) in the logarithmic term. In most cases the corrections of Knipp and Teller can be neglected.

The energy losses in inelastic atomic collisions, connected with pure ionization or charge exchange, cannot be calculated accurately. However, some estimates were obtained /29, 79, 115/.

TABLE 58

Atomic stopping power of gases for ions of lithium, nitrogen and neon (in units of 10^{-14} ev·cm^2/atom)

T, kev	Lithium ions /135/				Nitrogen ions /498/				Neon ions /498/			
	Hydrogen, H_2	Helium, He	Air	Argon, A	Hydrogen, H_2	Helium, He	Air	Argon, A	Hydrogen, H_2	Helium, He	Air	Argon, A
100	4.24	4.56	15.5	23.4	—	—	—	—	—	—	—	—
150	6.36	5.66	20.2	10.1	12.7	16.7	—	—	—	10.5	—	—
175	—	—	—	—	13.3	17.7	—	—	6.9	11.8	—	—
200	7.69	8.25	23.1	41.2	13.8	18.7	52.6	90	7.3	12.8	41	63
250	10.1	9.92	29.2	53.8	15.2	20.5	59.0	102	7.9	14.3	46	70
300	11.0	11.2	32.0	57.6	17.0	22.2	64.5	114	8.8	16.0	50.5	77
350	11.4	13.1	34.1	66.2	17.7	23.7	70.0	125	9.6	17.5	54.5	83
400	12.4	13.4	37.7	70.4	18.5	25.0	74.5	135	10.3	18.0	58	86
450	13.4	15.0	43.5	73.7	—	—	—	—	—	—	—	—

At present, a considerable number of experimental data are available on the energy losses of fast heavy particles in various media. However, these data are confined to narrow energy ranges and do not provide a complete picture.

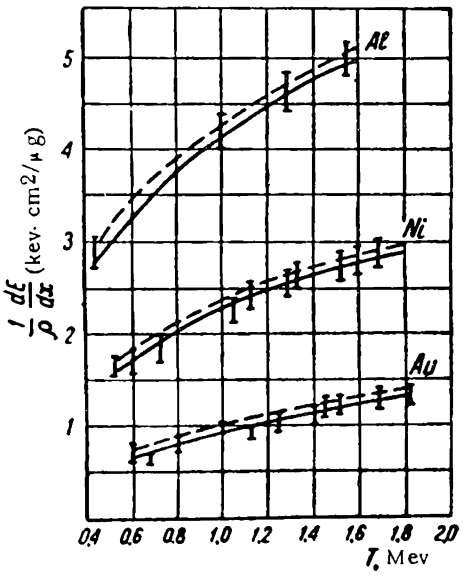

FIGURE 71. Stopping power of metals for nitrogen ions /422/. The solid curve represents the stopping due to inelastic collisions with electrons, the broken curve gives the stopping with allowance for nuclear collisions

The stopping power of various gases for slow ions of lithium, nitrogen and neon with energies up to 450 kev was studied in /135, 224, 498, 289/. The data are given in Table 58.

The stopping power of solid materials for ions of carbon and oxygen with energies of 0.36-3.6 Mev and for ions of nitrogen with energies of 0.46-1.8 Mev was measured by Porat and Ramavataram /416, 422/. Their results are given in Tables 5 and 6 and in Figure 71.

Lillie /363/ determined the stopping power of air for B^{11} and C^{13} ions with energies from 0.5 to 6 Mev. Reynolds et al. /435/ found that for nitrogen ions with energies 8-29 Mev, the energy losses in nickel are almost constant and equal to 3.7 Mev·cm^2/mg.

The dependence of $\frac{dE}{dx}$ on the energy for fast $\left(\frac{T}{A} \simeq 2 - 10\,\text{Mev/amu}\right)$ heavy ions in nickel, oxygen and nuclear emulsions was obtained by differentiation of the range-energy curves (see Figures 81-82) in /431/. These relations are presented by the curves of Figures 72 and 73. Similarly Northcliffe et al. /403, 465/ obtained data

on the dependence of the stopping power of aluminum, Mylar and polyethylene for boron, carbon, nitrogen, oxygen, fluorine, and neon ions with energies from 1 to 10 Mev/nucleon. For the same energy loss, the ratio of the absorber thicknesses (mg/cm^2) is equal to 0.783 $\left(\frac{\text{Mylar}}{\text{aluminum}}\right)$ and 0.692 $\left(\frac{\text{polyethylene}}{\text{aluminum}}\right)$.

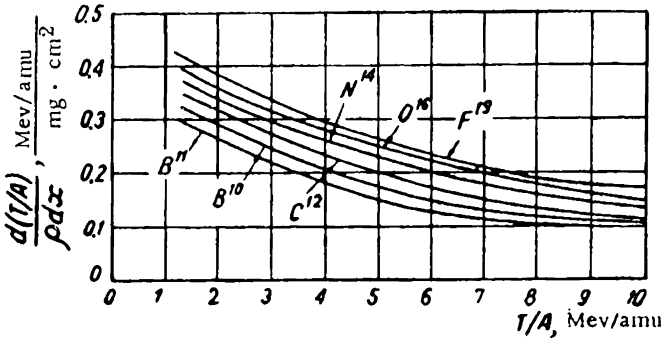

FIGURE 72. Stopping power of oxygen for heavy ions /431/

Teplova et al. /101/ studied the stopping of heavy ions in air, argon, and hydrogen in the velocity range from $1.5 \cdot 10^8$ to $12 \cdot 10^8$ cm/sec. The results are shown in Figure 74. It follows from Figure 74 that for $v < 5 \cdot 10^8$ cm/sec the specific energy loss (and its proportional ionization) varies for ions with $z = 4 - 10$ almost linearly with the velocity.

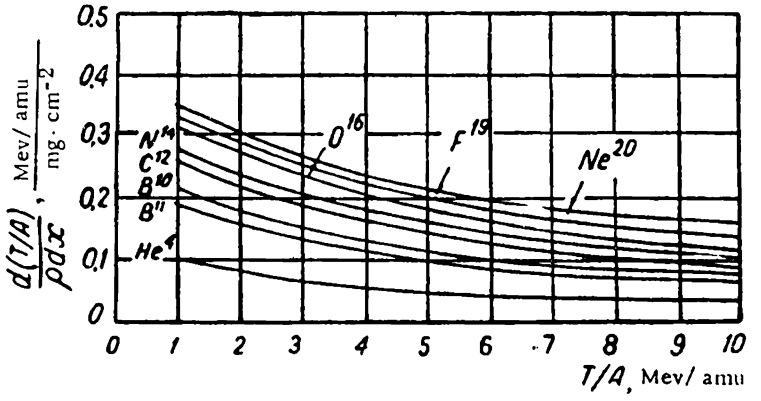

FIGURE 73. Stopping power of nickel for heavy ions /431/

Figure 75 gives experimental curves of the dependence of the specific ionization on the range (Brigg's curve) for heavy and light fission fragments in hydrogen and deuterium (for other gases similar curves are obtained). The existence of different Brigg's curves for particles of small charge and for fragments should be observed. In contrast to alpha-particles and protons whose specific ionization increases continuously with the range, the specific ionization along the path of a fragment decreases continuously. The form of the final sections of Brigg's curves is the same in both cases.

As the charge of the ions decreases, Brigg's curves are gradually changed, which can be seen from a comparison of Figures 75 and 84.

Ranges of fast heavy ions in matter. The dependence of the range on the energy of heavy ions in matter was experimentally studied in /73, 87, 90, 101, 154, 164, 218, 224, 287, 403, 431, 379, 435, 440/. Semi-empirical range-energy relations for heavy ions in emulsions were proposed by Livesey /362/, Papineau /417/, Lonchamp /361/, Barkas et al. /287/. As a rule, the method proposed by Knipp and Teller was used /165, 338/, which is based on the Thomas-Fermi model. In the work of Maksimov /76/, a universal range-energy relation for multiply-charged ions was obtained from experimental data on the assumption that the specific energy losses and range of the ions depend only on T/A of the incident particle and on the mean ionization potential of the medium.

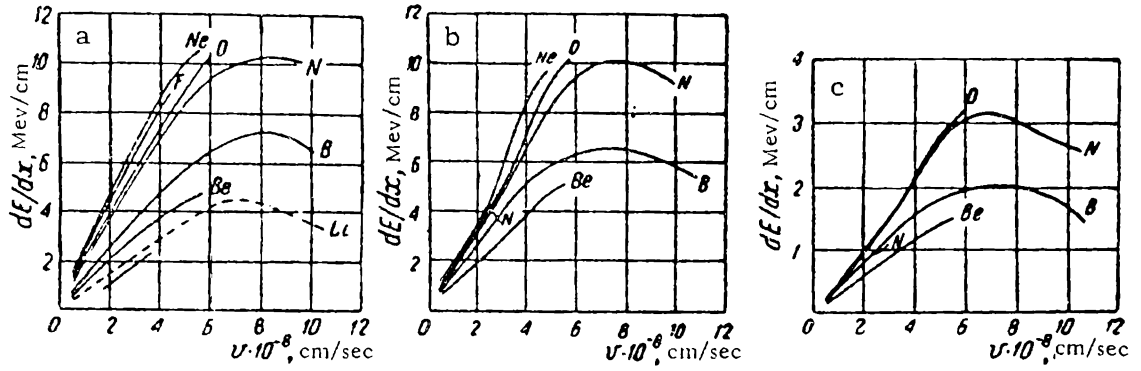

FIGURE 74. Specific energy losses of multiply-charged ions in air (a), argon (b), hydrogen (c), according to the measurements of /101/

Figure 76 gives semi-empirical range-energy curves for heavy ions in a nuclear photoemulsion ($\rho = 3.181$ g/cm^3). The points in this figure represent some experimental ranges; see also /73, 90, 218, 396 440, 164/.

The ranges in an emulsion of other heavy ions with charge z and mass M can be determined by the relation

$$R = \left(\frac{M}{z^2}\right)\lambda(\beta) + Mz^{2/3}\, C_z\left(\frac{\beta}{z}\right). \quad (7.13)$$

The values of $\lambda(\beta)$ should be taken from Table 46. The numerical values of C_z, an empirical function taking into account the residual range, which is mainly controlled by electron capture, are given in Figure 77.

Figure 78 gives experimental curves of the given ranges of heavy ions in air, argon and hydrogen as a function of the particle velocities.

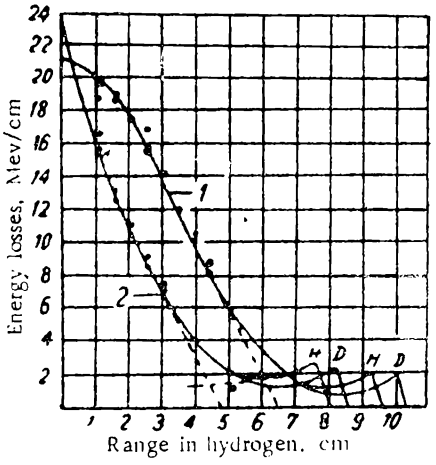

FIGURE 75. Ionization (specific energy losses) as a function of the range of light (curve 1) and heavy (curve 2) fission fragments in hydrogen and deuterium /369/

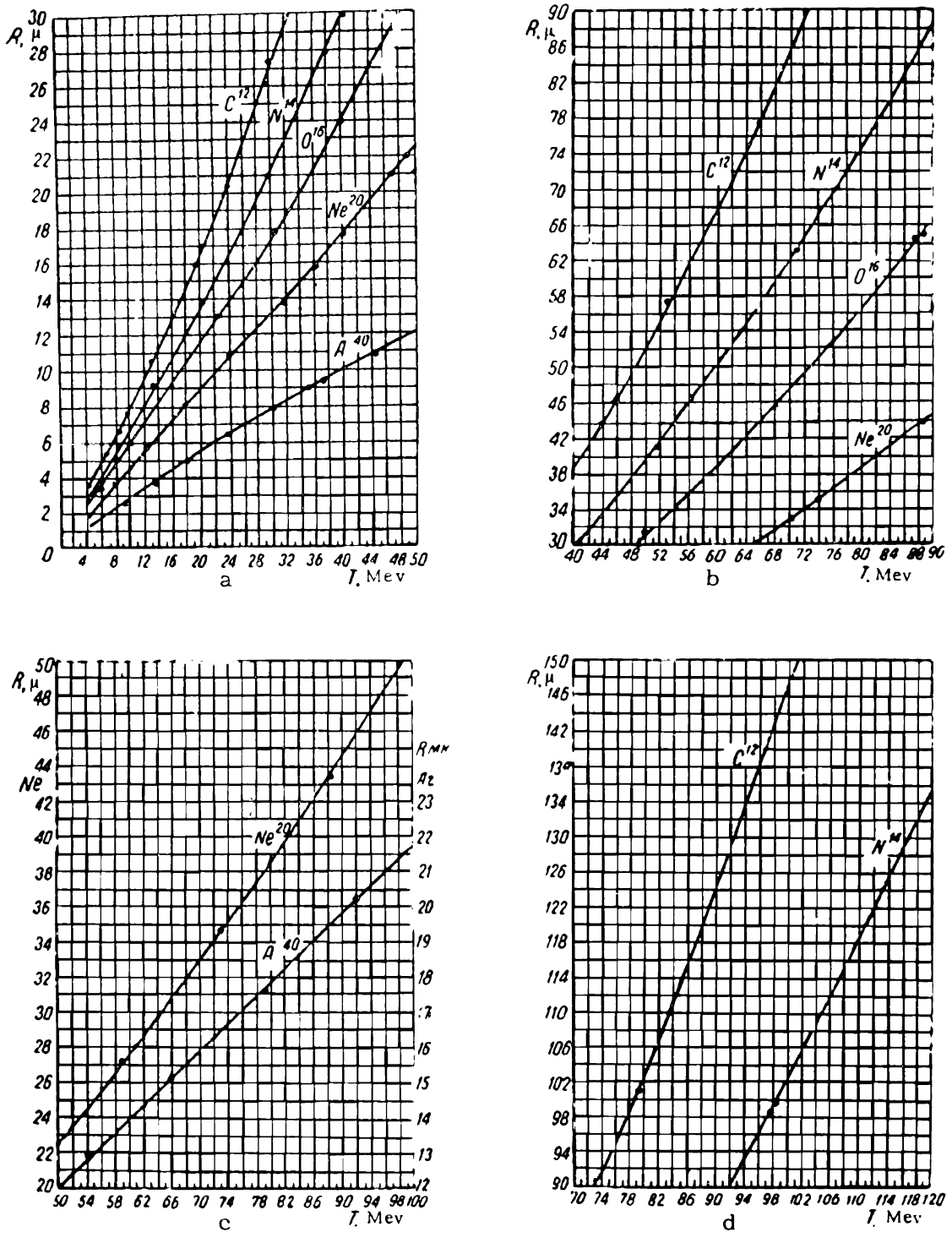

FIGURE 76. Range in a photoemulsion versus energy of heavy ions /287/

a — T = 0-50 Mev; b — T = 40-90 Mev; c — T = 50-100 Mev; d — T = 70-120 Mev

The solid curves were obtained by integration of the curves of the specific energy losses (Figure 78), and the points represent the results of direct measurements /101/.

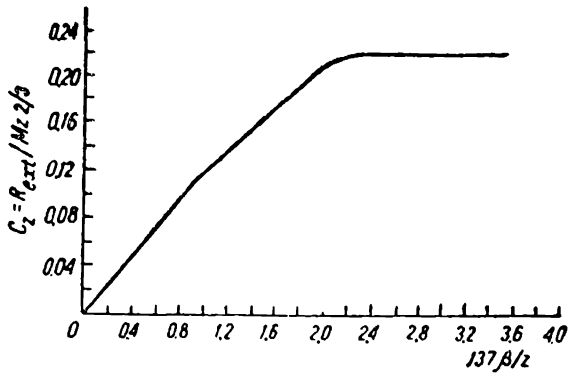

FIGURE 77. The function C_z versus the ion velocity /287/

Experimental range-energy curves for heavy ions in aluminum, Mylar and polyethylene, obtained in the works of Northcliffe et al. /403, 465/, are given in Figures 79 and 80.

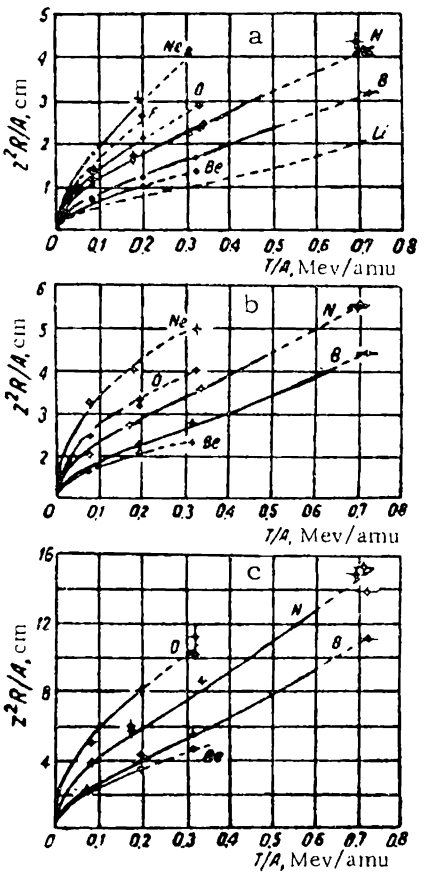

FIGURE 78. Range of heavy ions in air (a), argon (b) and hydrogen (c) versus energy

Experimental curves of the range of heavy ions in oxygen and nickel are given in Figures 81 and 82 /431/. The data given in Figures 79-82 (see below) are normalized to an initial energy of $\frac{T}{A} = 10$ Mev/nucleon for the fast ions. The experimental data for helium ions obtained in /403, 465/ are in satisfactory agreement with the data of independent measurements (Table 42).

Table 59 contains some experimental data on the ranges of heavy ions in various media /86, 435, 440, 514/.

Results of measurements of the mean range of Li^8 ions in hydrogen, deuterium and helium are given in Table 60. The difference in the ranges in hydrogen and deuterium is due to differences in the nuclear collisions during the stopping of the ions (§ 2).

Figure 83 shows on a logarithmic scale the dependence of the range on the energy of light ($A_{mean}=94.7$) and heavy ($A_{mean}=138.8$) fission fragments in various media. For this purpose the data of experimental works /142, 258, 346, 376/ were used.

The range-energy relation for the fragments is satisfactorily given by

$$R = k\,T^{\alpha},$$

where the constant α is approximately 2/3 (more accurate values of α are given with the experimental curves of Figure 83).

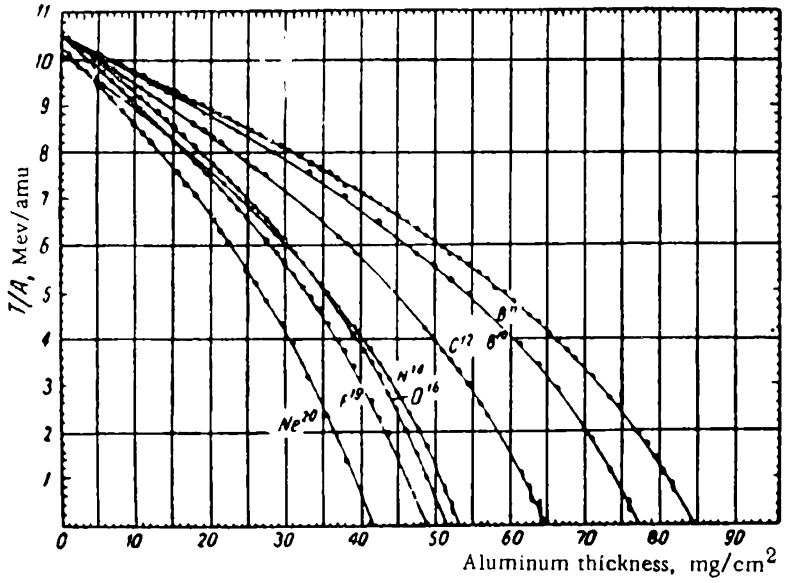

FIGURE 79. Range of heavy ions in aluminum /403/

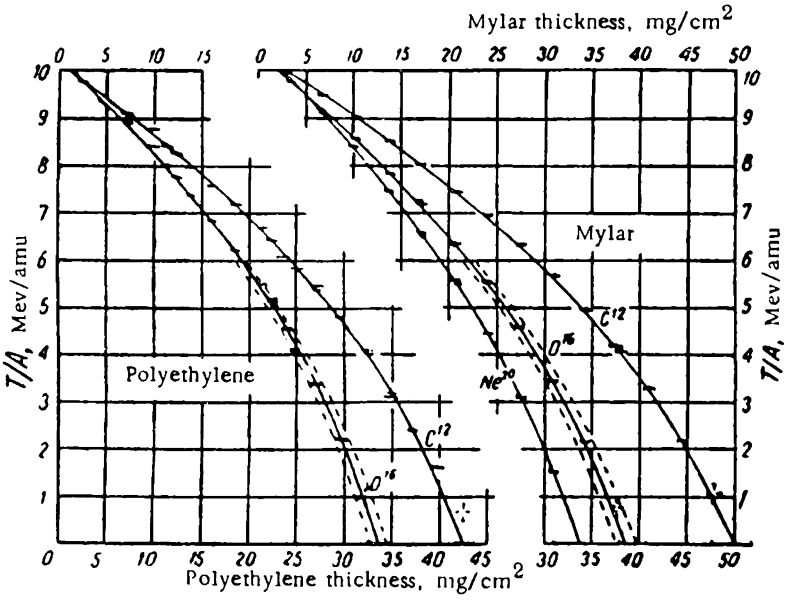

FIGURE 80. Range of heavy ions in Mylar and polyethylene /465/

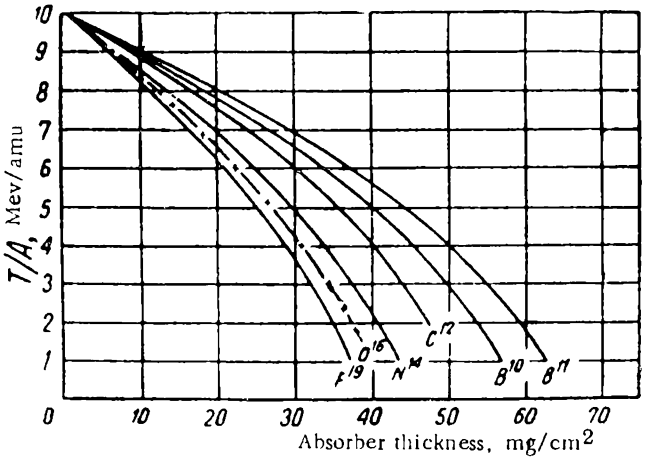

FIGURE 81. Energy versus range of heavy ions in oxygen /431/

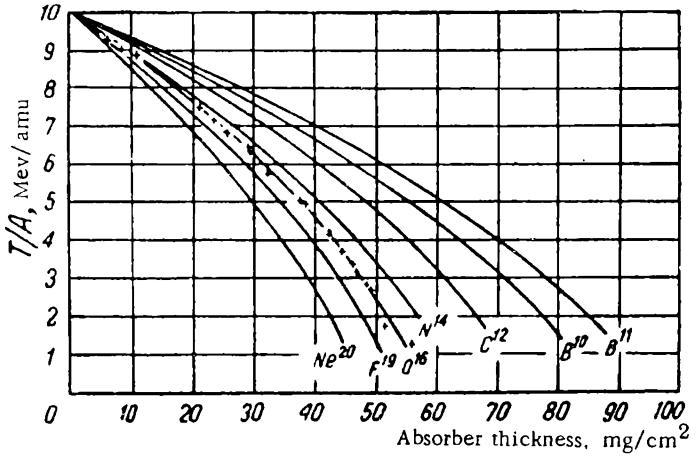

FIGURE 82. Energy versus range of heavy ions in nickel /431/

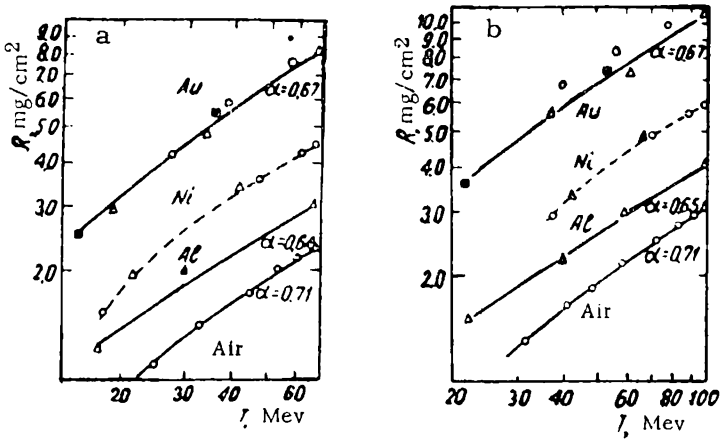

FIGURE 83. Experimental range-energy curves for heavy (a) and light (b) fission fragments /142/

TABLE 59

Experimental values of the mean range of heavy ions for various values of their energy

Ion ranges									
Nitrogen in nickel /435/		Carbon in cc per /86/		Carbon in gold /86/		Oxygen in copper /86/		Oxygen in gold /86/	
T, Mev	R, mg/cm^2	T, Mev	R, mg/cm^2	T, Mev	R, mg/cm^2	T, Mev	R, mg/cm^2	T, Mev	R, mg/cm^2
8	2.25	52.0	18.9	36.0	22.3	75.2	18.8	73.0	30.0
9.5	2.9	66.0	27.1	50.5	30.0	96.5	27.1	85.0	37.6
13	3.6	69.5	32.0	56.0	37.0	37.9	—	90.3	40.2
18	5.8	—	—	66.5	47.2	—	—	—	—
23	6.1	—	—	—	—	—	—	—	—
27.5	7.2	—	—	—	—	—	—	—	—

§ 8. Relation between energy losses and ionization

Ionization methods of detecting and determining radiation energies are based on the ionization effects of particles in the sensitive volume of the detector /3, 23, 39/. The relation between the energy lost by the particle and the ionization produced by it is very important.

The specific ionization $\frac{dJ}{dx}$ (the number of ion pairs per unit path length of the ionizing particle) in contrast to $\frac{dE}{dx}$ cannot be determined theoretically. Values of $\frac{dJ}{dx}$ are therefore obtained only from experiments, and it was established that a proportionality exists between $\frac{dJ}{dx}$ and $\frac{dE}{dx}$ in a wide range of incident particle energies.

Primary, secondary and total ionization are distinguished.

Primary ionization is determined by the number of ion pairs formed directly in collisions with atoms of the stopping medium. The emerging electrons, and in elastic nuclear collisions, the recoil atoms, may have energies sufficient to cause further ionization. The maximum energy given to an electron by a heavy particle is, according to (2.3), $4\frac{m}{M}T$ and the maximum velocity transferred is $2v$, where m, T and v are the mass, energy, and velocity of the incident particles.

Thus, a fraction of the electrons appearing upon primary ionization have energy sufficient to cause secondary ionization. The maximum energy transferred by a 5 Mev alpha-particle to an electron is $\sim$3 kev. Ionization electrons acquire an average energy of 200 ev; this is sufficient to produce secondary ionization, which constitutes a considerable fraction of the total ionization.

TABLE 60

Experimental mean ranges of Li^8 ions in hydrogen, deuterium and helium /224/

T, kev	Range at normal temperature and pressure, cm		
	Hydrogen, H_2	Deuterium, D_2	Helium, He
36	—	—	0.26±0.17
42	0.21±0.04	—	—
62	—	—	0.66±0.10
66	0.32±0.04	0.38±0.04	0.60±0.05
100	0.72±0.04	0.82±0.05	1.21±0.07
201	—	0.90±0.04	—
233	0.90±0.07	0.97±0.06	1.50±0.07
275	0.96±0.04	—	1.52±0.07
291	0.96±0.04	—	—
328	—	1.12±0.04	1.73±0.07
377	1.14±0.04	—	1.79±0.06
454	1.22±0.04	1.32±0.04	1.99±0.08

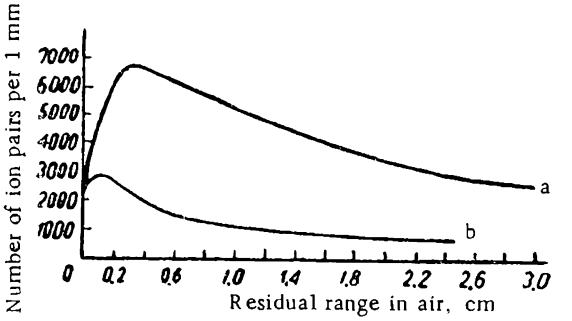

FIGURE 84. Specific ionization as a function of the residual range in air for alpha-particles (a) and protons (b)

The total ionization is the sum of the primary, secondary, tertiary and higher order ionizations. The total ionization is the quantity measured in proportional counters and ionization chambers.

In order to separate the primary ionization, either measurements in a cloud chamber are made /512/, or the dependence of the efficiency of the Geiger counters on the velocity and mass of the particles is studied /427/.

In the first case, the ion groups in the track are counted until the ions begin to scatter. In the second case, use is made of the fact that the efficiency of a Geiger counter is

$$\varepsilon = 1 - \exp(-j_p \rho l),$$

where j_p is the specific primary ionization, pairs·cm^2/g;
ρ is the gas density in the counter;
l is the particle range in the counter.

A very important experimental fact is the almost complete independence of the energy w, spent on the formation of one ion pair, of the initial energy of the ionizing particle. In fact, as will be seen later, the values of w for different particles in a wide velocity range differ by a factor of no more than 1.5-2 in various stopping media. The constancy of the energy

spent on the formation of one ion pair is significant in the use of gaseous and solid counters for spectrometric measurements and for the determination of the range-energy relation.

Specific ionization is the term applied to the total number of ion pairs formed by a particle per unit path length expressed in grams per cm^2 or in centimeters.

The dependence of the specific ionization on the residual range for fast particles of small charge is shown in Figure 84. The initial rise in the curves with the decreasing residual range is due to the increase in the specific energy losses; the fall off, following the maximum, is caused by charge exchange collisions and by the decrease in the effective charge of the particles (§ 7).

The most careful measurements of the specific ionization produced by alpha-particles in air were performed by Holloway and Livingston /285/ with a small ionization chamber*. It was shown that the maximum specific ionization is observed for a residual alpha-particle range equal to 0.40±0.02 cm of air, and for an average effective charge of 1.5 (see § 7). Direct measurements by Stetter and Jentschke /461/ have shown that the maximum specific ionization for alpha-particles in air corresponds to the formation of 6600 pairs/mm (cf. Figure 84).

The specific ionization of protons in air was studied by Jentschke /327/. He found that the maximum specific ionization is observed for a residual range of 0.1 cm and is then equal to 2750 pairs/mm.

For large residual ranges the specific ionization of alpha-particles is four times as large as the corresponding values for protons. At the maxima of the specific ionization curves this ratio is not satisfied partly because two electrons participate in charge exchange in alpha-particles, whereas in protons — only one. It follows from the theory (§ 4) that $\frac{dE}{dx}$ and consequently also $j = \frac{dJ}{dx}$ vary as β^{-2} up to $\beta \approx 0.97$, and then the ionization should increase as $\log \beta\gamma$, where $\gamma = (1 - \beta^2)^{-1/2}$ (if the density effect is not taken into consideration).

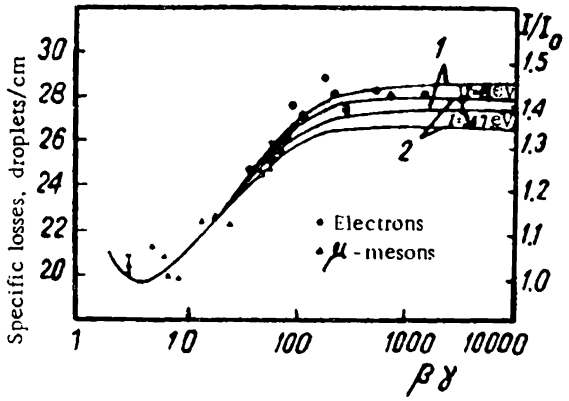

FIGURE 85. Specific energy losses of μ-mesons and electrons on ionization in helium

1—theoretical curve taking into account the density effect according to Sternheimer /446/; 2—the same, according to Budini and Taffara /211/.

* See also more recent measurements /322, 461/.

The relativistic increase in the energy loss and the corresponding increase in the ionization was studied by several authors; see, for example, /127, 332, 365, 198, 428/. Figure 85 gives the results of /332/ on the specific ionization produced by electrons and μ-mesons in a cloud chamber. These data are compared with the theoretical curves of Sternheimer /446/ and Budini /211/, taking into account the density effect.

Energy spent by an alpha-particle on the formation of one ion pair. In order to determine the energy w_α, spent by an alpha-particle on the formation of one ion pair, the ion or electron current, generated when alpha-particles are absorbed in the sensitive volume of ionization chambers, is measured.

Early results of the determination of w_α are considered in Gray /269/, whereas more recent work is dealt with in the review by Valentine and Curran /485/*. In early experiments air was used as the standard medium for relative measurements of w_α. Table 61 gives values of w_α for various gases, calculated on the basis of measurements by Schmieder /457/, Stetter /458/, Alder et al. /139/, which were the most reliable at the time. These authors used the alpha-particles of Po^{210} and air as the standard working medium of the ionization chambers. Schmieder determined the absolute values of w_α for various gases, assuming the energy of Po^{210} alpha-particles to be 5.27 Mev, and the number of ion pairs from one alpha-particle in air to be $1.5 \cdot 10^5$. For the convenience of comparison, Table 61 also gives values of $w_{\alpha(gas)}$, reduced to the same standard value $w_{\alpha(air)} = 34.7$ ev /139, 20/.

TABLE 61

Energy w_α(ev) produced by alpha-particles on the formation of one ion pair in various gases (calculated on the basis of experimental values of $w_{\alpha(gas)}/w_{\alpha(air)}$)

Gas	Gray /269/	Schmieder /457/	Stetter /458/	Alder et al. /139/
Air	35.1 (34.7)	34.8 (34.7)	35.7 (34.7)	34.7 ± 0.5
Hydrogen, H_2	36.0 (35.6)	—	36.8 (35.1)	—
Helium, He	31.0 (30.7)	—	—	—
Nitrogen, N_2	—	36.1 (36.2)	37.3 (36.2)	36.3 ± 0.4
Oxygen, O_2	—	32.4 (32.3)	—	—
Neon, Ne	—	27.2 (27.1)	29.9 (29.0)	—
Argon, A	—	24.37 (24.3)	28.5 (27.7)	—
Krypton, Kr	—	22.43 (22.3)	26.4 (25.6)	—
Xenon, Xe	—	21.4 (21.3)	23.6 (22.9)	—
Nitric oxide, NO	—	30.05 (29.9)	—	—
Nitrogen dioxide, NO_2	—	33.0 (32.9)	—	—
Nitrous oxide, N_2O	—	32.4 (32.3)	—	—
Carbon monoxide, CO	—	34.0 (33.9)	—	—
Carbon dioxide, CO_2	—	33.9 (33.8)	—	—
Methane, CH_4	—	29.4 (29.3)	—	—
Ethane, C_2H_4	—	27.0 (26.9)	—	—

Remark. The figures in parentheses are the values of $w_{\alpha(gas)}$, reduced to the same standard value of $w_{\alpha(air)} = 34.7$ ev /20/.

* Theoretical calculations of w_α for hydrogen and helium were performed by Erskine /240/. See also /411/.

TABLE 62

Experimental values of $\frac{w_\alpha(\text{gas})}{w_\alpha(\text{A})}$

Gas	w_α, ev	$\frac{w_\alpha(\text{gas})}{w_\alpha(\text{A})}$	w_α, ev	$\frac{w_\alpha(\text{gas})}{w_\alpha(\text{A})}$	w_α, ev	$\frac{w_\alpha(\text{gas})}{w_\alpha(\text{A})}$	w_α, ev ($T_\alpha = 5.3$ Mev)	$\frac{w_\alpha(\text{gas})}{w_\alpha(\text{A})}$	w_α, ev ($T_\alpha = 5.3$ Mev)	$\frac{w_\alpha(\text{gas})}{w_\alpha(\text{A})}$	w_α, ev ($T_\alpha = 5.3$ Mev)	$\frac{w_\alpha(\text{gas})}{w_\alpha(\text{A})}$	w_α, ev /167/
	/319, 328/		/189/		/484/		/190, 301/		/464/		/302/		
Argon, A	26.4	1.00	26.4	1.00	25.9	1.00	26.25	1.00	26.3	1.00	27.2	1.00	28.9
Helium, He	42.7	1.617	46.0	1.74	31.7	1.22	29.6	1.13	—	—	44.2	1.62	—
Neon, Ne	36.8	1.394	—	—	—	—	—	—	—	—	38.6	1.41	—
Krypton, Kr	24.1	0.913	—	—	—	—	—	—	—	—	25.7	0.945	—
Xenon, Xe	21.9	0.830	—	—	—	—	—	—	—	—	—	—	—
Hydrogen, H_2	36.3	1.375	37.0	1.40	37.0	1.43	35.96	1.36	—	—	—	—	—
Carbon dioxide, CO_2	34.5	1.307	34.3	1.30	—	—	34.3	1.31	34.2	1.30	—	—	—
Air	35.5	1.345	35.0	1.33	35.2	1.36	34.95	1.33	35.6	1.354	—	—	—
Oxygen, O_2	32.5	1.231	32.2	1.22	32.2	1.24	32.17	1.275	32.9	1.251	—	—	—
Nitrogen, N_2	36.6	1.386	36.3	1.37	36.0	1.39	36.5	1.39	36.4	1.384	38.8	1.43	37.9
Methane, CH_4	29.2	1.106	29.4	1.11	29.0	1.12	29.0	1.105	29.1	1.106	—	—	—
Acetylene, C_2H_2	27.5	1.042	—	—	—	—	—	—	—	—	—	—	—
Ethane, C_2H_6	26.6	1.008	28.0	1.06	—	—	—	—	—	—	—	—	—
Boron trifluoride, BF_3	—	—	36.0	1.36	—	—	35.3	1.36	—	—	—	—	—
Sulfur hexafluoride, SF_6	—	—	35.7	1.35	—	—	—	—	—	—	—	—	—
Sulfurous anhydride, SO_2	—	—	—	—	—	—	32.5	1.24	—	—	—	—	—
Carbon Tetrachloride, CCl_4	—	—	—	—	—	—	25.9	0.99	—	—	—	—	—
Ethyl alcohol, C_2H_5OH	—	—	—	—	—	—	32.6	1.24	—	—	—	—	—
Ammonia, NH_3	—	—	—	—	—	—	30.5	1.16	—	—	—	—	—

In /508/ it was assumed that the dependence $w_{\alpha(air)}$ on the energy of the alpha-particles is only an artifact and is connected with the difficulties of ion collection. In particular, the authors of /508/ indicated an effect which is independent of the recombination field and amounts to ~3.3% in air under atmospheric pressure.

In /201, 330/ it is shown that the conclusions made by Wingate et al. /508/ are mistaken; the validity of the extrapolation method of the saturation current in the chamber, normally used in the measurement of w, was again confirmed. This method gives for the alpha-particles of Po^{210}, $w_{\alpha(air)} = 34.99$ ev and a total number of ions of 151,160 /330/; see also Table 62.

The absolute measurements of Bay et al. /201/ with an ionization chamber, which contained the whole range of the alpha-particles, led to the following results: $w_{\alpha(air)} = 34.97 \pm 0.07$ ev, $w_{\alpha(N_2)} = 36.38 \pm 0.07$ ev; $w_{\alpha(CO_2)} = 34.04 \pm \pm 0.1$ ev.

The weighted mean of four independent absolute measurements of w_α(A) for $T_\alpha = 5.3$ Mev//319, 189, 464, 506/ is equal to $w_\alpha = 26.39$ ev and exceeds by 0.5% the weighted mean absolute value of w_e(A) for T=50-1000 kev (see § 16).

Energy spent by protons on the formation of one ion pair. There are considerably less data on w_p (the energy spent by protons on the formation of one ion pair) than data on w_α. The available results of measurements of w_p are given in Table 63.

TABLE 63

Experimental values of $\frac{w_p\,(\text{gas})}{w_\alpha\,(\text{A})}$

Gas	w_p, ev (T_p=10-250 kev)	w_p, ev (T_p=340 Mev)	$\frac{w_p\,(\text{gas})}{w_p\,(\text{A})}$	w_p, ev (T_p=7.56 Mev)	w_p, ev (T_p=2 Mev)
	/358/	/158/		/327/	/375/
Argon, A	26.5 ± 0.5	25.5	1.00	—	26.66 ± 0.26
Helium, He	—	29.9	1.17	—	—
Hydrogen, H_2	—	35.3	1.38	—	—
Nitrogen, N_2	36.6 ± 0.7	33.6	1.31	—	36.68 ± 0.34
Air	—	33.3	1.30	35.1	35.18 ± 0.42
Oxygen, O_2	—	31.5	1.23	—	—
Neon, Ne	—	28.6	1.12	—	—
Carbon dioxide, CO_2 . .	—	—	—	—	34.37 ± 0.33

Comparing the data of Tables 62 and 63, it can be seen that the absolute and relative values of w_p and w_α for the same particle energy are somewhat different.

Special measurements of the relative ionization produced by protons, deuterons and alpha-particles /475/ have shown that w_p(A) for proton energies 0.2-0.5 Mev is 8% larger than w_α (A) for the same alpha-particle energies.

Bakker and Segré /158/ measured the ratio $\frac{w_p}{w_p\,(\text{A})}$ in various gases, using two identical ionization chambers, filled with gas being investigated and with argon (the chamber with argon served for monitoring). The value

of w was determined by

$$w = -\frac{dE}{dN} = -\frac{\frac{dE}{dx}}{\frac{dN}{dx}}, \qquad (8.3)$$

where $\frac{dE}{dx}$ was calculated, and $\frac{dN}{dx}$ was determined experimentally from the ionization. In the calculations $w_p(A) = 25.5$ev was taken.

The values of $\frac{w_p(\text{gas})}{w_p(A)}$ turned out to be closer to the values for electrons than for alpha particles.

Energy spent by recoil atoms and fission fragments on the formation of one ion pair. At high velocities, the value of w for fragments and heavy recoil atoms differs only slightly from w_α, since at high velocities electron collisions are most important. As the velocity decreases, a considerable part of the energy of the heavy ions is transferred to the recoil atoms and the value of w begins to depend on the ionization efficiency of the secondary particles, i.e., the recoil atoms. Knipp and Ling /344/ considered this problem theoretically and introduced the concept of the ionization defect, which they defined as follows:

$$\Delta T = T - w'_\alpha J,$$

where T is the energy of the primary particle;
J is the number of ion pairs formed by it;
w'_α is the energy spent by an alpha-particle on the formation of one ion pair $\left(w'_\alpha = dT/dJ\right)$.

According to these authors, for fast A^+ ions in argon the ionization defect ΔT is equal to 0.78 Mev, for light fission fragments ($T = 98$ Mev) $\Delta T =$ = 2.5 Mev, and for heavy fission fragments ($T = 67$ Mev) $\Delta T = 4.2$ Mev. According to the theory, the ionization defect in light gases, for example in helium, should be smaller than in argon. Special investigations /481/ confirm these theoretical conclusions qualitatively, although experimental data /303/ exist which contradict this theory.

Some investigators measured the quantity $\frac{w_{\text{recoil}}}{w_\alpha}$. Thus, according to Vertenstein (1913), the recoil atoms formed upon the disintegration of ThC spend several times as much energy as their associated alpha-particles on the formation of one ion pair in air.

On the other hand, Gerthsen and Grimm /272/, studying the disintegration of ThC' in an ionization chamber filled with air, found that $\frac{w_{\text{recoil}}}{w_\alpha}$ is approximately equal to one. Madsen /380/ measured with proportional counters the ionization produced in argon by the recoil atoms and the alpha-particles from the disintegration of Po, ThC, and ThC'. He found that $\frac{w_{\text{recoil}}}{w_\alpha}$ are equal to 4.4, 3.8, and 3.4 respectively. The absolute value

$$w_{\text{recoil}} = \frac{dE}{dJ}$$

for recoil atoms with energies 100-170 kev was then found to be 67 ev, i.e., 2.5 times as high as $w_\alpha(A)$.

Stone and Cochran /459/ used a modification of Madsen's technique (proportional counters in coincidence circles) and obtained the results given in Table 65. Their data /459/ differ considerably from the results of Madsen /380/ and Jesse and Sadauskis /325/.

Ionization fluctuations. The resolving power of ionization chambers and counters used for spectrometry, as well as the accuracy of the energy

measurement of particles from the ionization produced by them, depends on the fluctuation in the number of ion pairs formed by particles of the same initial energy. This problem was investigated theoretically by Fano /248/ in 1947. According to his calculations, the mean square fluctuation in the number of ion pairs formed by charged particles of the same energy is

$$\delta_N^2 = \langle (N - N_0)^2 \rangle_{\text{mean}} = FN_0, \tag{8.4}$$

where N_0 is the mean number of ion pairs, and F is defined by the expression

$$F = \frac{(1-p)}{p^2}\frac{W_l^2}{w^2} + \frac{1}{w^2 p}\left[\sum_{\text{ion}} p_k^{(l)}\left(w_k^{(l)} - W_l\right)^2 + \sum_{\text{ext}} p_k^{(l)}\left(w_k^{(l)} - W_l\right)^2\right]. \tag{8.5}$$

here $p_k^{(i)}$ is the fraction of the collisions associated by energy losses $w_k^{(i)}$ and leading to ionization;

$p_k^{(l)}$ and $w_k^{(l)}$ are the corresponding values for inelastic collisions exciting the atoms;

W_l is the mean ionization energy loss for all the collisions;

w is the mean energy spent on the formation of one ion pair, so that

$$w = W_l + W_l\left(\frac{1-p}{p}\right).$$

TABLE 64

Values of $\frac{w_{\text{recoil}}}{w_\alpha}$ for the alpha-particles of ThC and ThC' and their associated recoil atoms /459/

Gas	w_α /189/	ThC		ThC'	
		w_{recoil}	$\frac{w_{\text{recoil}}}{w_\alpha}$	w_{recoil}	$\frac{w_{\text{recoil}}}{w_\alpha}$
Carbon dioxide, CO_2	34.3	102	2.98	99	2.88
Propylene, C_3H_6	25.9	99	3.68	92	3.55
Ethylene, C_2H_4	28.0	104	3.72	90	3.21
Helium, He (with impurities) .	30	60	2.00	55	1.83
Hydrogen, H_2	37.0	81	2.19	68	1.84
Methane, CH_4	29.4	111	3.78	96	3.26

The exact values of the quantities involved in (8.5) are unknown, and therefore the theory allows only an estimate of the upper limit of F as $F < 3/4$. This conclusion is confirmed by the results of Hanna, Pontecorvo and Kirkwood /309/, who measured the fluctuations in the pulses formed in a proportional counter with argon by low-energy electrons (0.25-17 kev). More definite conclusions on the magnitude of F and on the limit of the resolving power of ionization chambers filled with argon were obtained by Komar, Vorob'ev and Korolev /59/. They measured the half-width of the lines formed by the alpha-particles of Ra^{224} and Fr^{221}, and the mean square fluctuations δ_n of the radionoises. They found that δ_n (6 Mev) is equal to 5.8 kev, so that for $\delta_n \simeq 4.7$ kev the resolving power of an ionization chamber for alpha-particles with an energy of $\sim$6 Mev is 17 kev. These measurements also made it possible to determine the experimental value of F, equal to 0.22.

§ 9. Vavilov-Cerenkov radiation

The Vavilov-Cerenkov (V-C) effect manifests itself in the radiation of light when charged particles pass through a medium with a velocity v exceeding the phase propagation velocity of light waves in the medium, $u = \frac{c}{n}$ (c being the velocity of light in vacuum; n is the refractive index of the medium). This effect was observed and studied in the experiments of P. A. Cerenkov /124/ which are concerned with the investigation of the glow of pure liquids, caused by the gamma-rays of radium. Vavilov and Cerenkov correctly explained the physical nature of the effect, showing in special investigations /124, 125/ that the radiation is not due to the emission from excited atoms and molecules of the medium (luminescence). It is emitted by fast electrons appearing in the compton scattering of gamma rays. In fact, this specific radiation is practically instantaneous and possesses a sharply pronounced spatial asymmetry. It is emitted forward in a direction making an angle Θ with the direction of motion of the charged particle. The cosine of the angle between the direction of motion of the particle and the direction of propagation of the Cerenkov radiation is

$$\cos\Theta = \frac{u}{v} = \frac{1}{\beta n}, \tag{9.1}$$

where $\beta = \frac{v}{c}$.

This follows from the condition that the optical difference in the path of the waves emitted by the moving particle at various points of its trajectory is equal to zero, and from the natural assumption that waves emitted in other directions eliminate one another by interference.

It also follows from (9.1) that radiation is emitted only on the condition that $\beta n > 1$.

In a medium with a refractive index $n = 1.5$, the minimum velocity at which a particle radiates is $v_{min} = 0.667\,c$. This corresponds to a threshold energy of $\sim$200 kev for electrons, and $\sim$320 Mev for protons. As the refractive index decreases, the threshold velocity increases.

Cerenkov also showed /124/ that the radiation has a continuous spectrum and is so polarized that the electric vector lies in the plane passing through the ray and the direction of motion of the particles.

The V-C radiation, on the one hand, has a continuous spectrum of light energy and, on the other hand, a real medium has dispersion, i. e., the refractive index depends on the frequency, and therefore the cone of the Cerenkov radiation has some "thickness", depending on the stopping and dispersion properties of the medium (§ 4).

In some respects, the formation of Cerenkov radiation is similar to the formation of shock waves (Mach waves) in air by the motion of bodies with supersonic velocities.

Intensity and spectral composition of the V-C radiation. The classical theory of the V-C effect, explaining the basic features of this phenomenon, was given in the works of Frank and Tamm /106, 102/. Since the V-C radiation is due not to interaction of particles with individual atoms, but is a result of the interaction with the medium as a whole, Frank and Tamm considered the medium as continuous and characterized it by a macroscopic parameter — the dielectric constant $\varepsilon(\nu)$, or by the refractive index $n(\nu)$.

According to Frank and Tamm, the mean number of photons with frequencies from ν to $\nu + d\nu$, emitted per unit path length of a particle

with charge ze, is

$$N(\nu)\,d\nu = 4\pi^2 \frac{z^2e^2}{hc^2}\left[1 - \frac{1}{(n\beta)^2}\right]d\nu = \frac{2\pi z^2 \Delta\nu}{137c}\sin^2\theta = \frac{2\pi z^2}{137}\left(\frac{1}{\lambda_1} - \frac{1}{\lambda_2}\right)\sin^2\theta, \qquad (9.2)$$

i.e., the radiation has a continuous spectrum, with maximum energy concentrated at the highest frequencies. The radiation contains components of all frequencies, for which the refractive index n is higher than $\frac{1}{\beta}$. For example, X-ray quanta cannot be radiated since for them $n < 1$.

Assuming that the refractive index n is independent of the frequency in the range $\Delta\nu = 3 \cdot 10^{14}$ c.p.s. (the frequency range of the visible light), we have

$$dN \cong 450 \sin^2\theta \text{ quanta/cm} \qquad (9.3)$$

For lucite (n = 1.50) a particle with charge z = 1 and velocity $\beta \approx 1$ gives a radiation yield of 250 quanta/cm.

The energy losses on V-C radiation over a distance dx traversed by a particle is according to (9.2)

$$\left(\frac{dE}{dx}\right)_{V\text{-}C} = \frac{4\pi^2 z^2 e^2}{hc^2} \int_{(\beta n > 1)} \left(1 - \frac{1}{\beta^2 n^2}\right)\nu\, d\nu \qquad (9.4)$$

and is of the order of ~1 kev/cm, i.e., negligibly small compared with ionization and other forms of energy losses (§ 5).

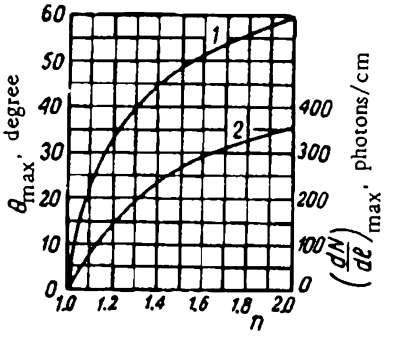

FIGURE 86. Maximum angle of Vavilov-Cerenkov (1) and the radiation yield (2) for singly-charged particles as a function of the refractive index of the medium. Calculated for the band 3500 - 5500 Å

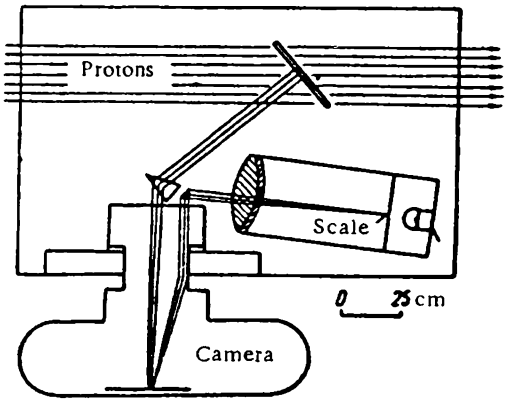

FIGURE 87. Schematic layout of equipment for measuring fast proton energies from the angle of the Cerenkov radiations /384/

Figure 86 gives the dependence of the radiation yield $\frac{dN}{dx}$ for the wavelength band 3500-5500 Å and of the maximum angle θ of the radiation on the refractive index n. The curves were obtained for particles with charge z = 1 (electrons, protons and so on). For particles with charge $z > 1$, the values of the ordinates of the curve $\frac{dN}{dx}$ have to be multiplied by z^2. In order to calculate $\frac{dN}{dx}$ for other wavelength ranges, the value obtained from the graph of Figure 86 should be multiplied by $9620\left(\frac{\lambda_2 - \lambda_1}{\lambda_1 \lambda_2}\right)$, where λ_1 and λ_2 are expressed in angstroms.

The quantum-mechanical theory of the V-C effect, developed in /32, 33, 99/, leads to results which differ only slightly from those of the

classical theory (formulas (9.1) and (9.4)). The corrections to these formulas, taking into account the recoil due to the emission of radiation quanta, are of the order of $\frac{\Lambda}{\lambda} 10^{-5}$, where Λ is the compton wavelength $\left(\Lambda = \frac{h}{mc} = 0.024\ \text{Å}\right)$.

Detailed information on the theory of the V-C effect is contained in the papers /15, 33/, as well as in Dzhelli's book /40/.

Use of Cerenkov counters for measuring the energy of ultra-fast protons. A very important feature of the V-C radiation is its independence of the rest mass of the initiating particles, but its strong dependence on their charge and velocity. A second feature is the sharp directionality of V-C radiation.

Finally, a very important fact is that the radiation has practically no inertia.

These features enabled the wide use of devices based on the V-C effect for the solution of certain problems in nuclear and elementary particle physics. Examples of the application of Cerenkov counters are given in Dzhelli's book /40/.

Here we shall only consider the use of Cerenkov radiation for an accurate determination of the velocity of ultra-fast protons /384, 49/.

The equipment for measuring the angle θ is shown schematically in Figure 87.

Protons from an accelerator passing through an inclined plate of flint glass ($n = 1.88$) cause emission of light. The V-C radiation, reflected from the metallized back wall of the plate, falls onto a prism and subsequently on the film in the camera. The angle of inclination of the prism is chosen so that the dispersion of the prism compensates for the dispersion of the Cerenkov radiation in the first order. This improves the sharpness of the image and the accuracy of measurement of the angle θ.

From the measured values of n and θ it is easy to determine the kinetic energy of the proton by (9.1) and (2.15):

$$T = M_p c^2 \left[\frac{n\cos\theta}{\sqrt{n^2\cos^2\theta - 1}} - 1\right]. \qquad (9.5)$$

Mather /384/ measured 340 Mev protons to within ± 0.8 Mev (0.2%). Zrelov and Stoletov /49/, using a similar method, measured 658 Mev protons to within ± 2 Mev (0.3%).

§ 10. Some methods of identifying fast charged particles and their energy measurements

In many physical investigations (for example, in the study of nuclear reactions or cosmic rays) it is necessary to determine the nature and energy of the radiating particles. In order to identify the particles, it is first necessary to determine their charge and mass. For this, at least two dynamical quantities, characterizing the interaction of the particles with electromagnetic fields or with matter should be measured simultaneously*. Some of the methods of identification of charged particles will be considered below.

* An exception is the extreme relativistic case.

Identification of particles from track characteristics in a photoemulsion. The track characteristics of a particle in a photoemulsion, i. e., the density of the grains, or of the clusters of grains, as well as the thickness and density of the track depend on the specific energy loss $\frac{dE}{dx}$ and on the specific ionization J produced by the particle. If we neglect the factors connected with the regression of the latent image or with the inhomogeneity of the silver halide in the emulsion*, then

$$J \sim \frac{dE}{dx} = z^2 f_1(\beta) = z^2 f_2\left(\frac{E}{M}\right). \tag{10.1}$$

where M, z, E, β are the mass, charge, energy, and velocity of the incident particle.

On the other hand, the range of a particle is connected with its parameters by the relation (see § 6)

$$R = \frac{M}{z^2} f_3(\beta). \tag{10.2}$$

Thus, simultaneous measurements of the track characteristics connected with the ionization (density of grains, density of clusters or of breaks between clusters of grains, track thickness) and with the range (total or residual range), facilitate the identification of the particles. Thus, integrating expression (10.1) we obtain

$$E = M f_3\left(R\frac{z^2}{M}\right). \tag{10.3}$$

Assuming further that

$$f_4\left(R\frac{z^2}{M}\right) = k\left(R\frac{z^2}{M}\right)^n, \tag{10.4}$$

we find for the range-energy relation in the emulsion

$$E = k z^{2n} M^{1-n} R_n^n, \tag{10.5}$$

where k is a constant;

n is a quantity weakly dependent on the mass.

A particular case of this equation is (6.10), relating the range with the energy of fast singly-charged particles in an emulsion.

The relation between the range and energy of heavy particles can be found by using (7.13) and the curves of Figure 76.

As was shown by the experiments of Lattes et al. /370/, the number of grains N_g in the track and the range of singly-charged particles are related by

$$N_g = MF\left(\frac{R}{M}\right). \tag{10.6}$$

The corresponding experimental curves for protons, deuterons and tritons are given in Figure 88 /239/. They make it possible to set

$$F\left(\frac{R}{M}\right) = k\left(\frac{R}{M}\right)^m,$$

so that

$$N_g = k M^{1-m} R^m \tag{10.7}$$

(m being an empirical constant).

* These factors lead to systematic errors in measurement; they can be taken into account or reduced to a minimum by choosing an appropriate technology of preparation and development of the photoemulsions /18, 437/.

It follows from (10.6) that for particles with masses M_1 and M_2 the ratio of the residual ranges R_1 and R_2, measured from the points where the particle velocities are identical, is equal to the ratio of the numbers N_1 and N_2 of developed grains on the residual ranges. The method based on this fact was used, for example, for the determination of the mass ratios of protons and π- mesons (see Figure 89).

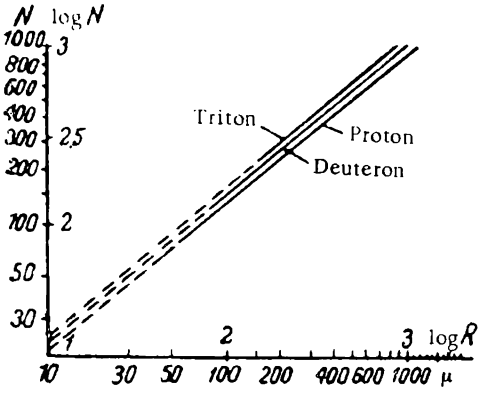

FIGURE 88. Number of grains in the track versus range of singly-charged particles of various masses /239/

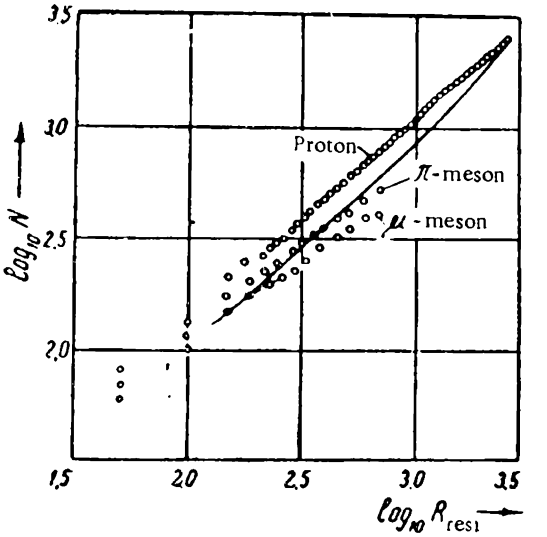

FIGURE 89. Number of grains in the tracks of protons, μ-mesons, and π-mesons in a photoemulsion as a function of the residual range (range in units of 9.85 microns) /370/. The straight line at an angle of 45° intersects the curves at points with equal grain density

The empirical relation (10.7) was used by Lattes /370/ in the investigation of π- and μ-mesons.

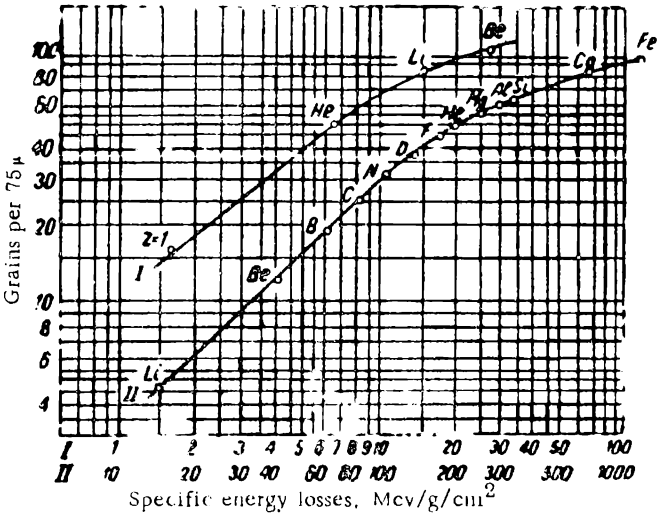

FIGURE 90. Grain density in the track as a function of the specific energy losses in the emulsion:

I—for the NTVS emulsion; II—for strongly underdeveloped NTA emulsion; the circles represent the hypothetical grain density in tracks formed by nuclei at relativistic velocities

The specific density of the grains $\frac{dN_g}{dR}$ (the number of grains per unit range length) is a function of the specific energy losses $\frac{dE}{dR}$. Generally, this function is not linear; in particular, the higher the specific energy losses (high specific ionization), the lower the relative sensitivity of the photoemulsion. The connection between $\frac{dN_g}{dR}$ and $\frac{dE}{dR}$ for an emulsion is considered in /233, 199/.

Figure 90 gives the experimentally determined dependence of the grain density along the track on the specific energy loss, and Figure 91 gives the curves of the dependence of the grain density on the residual ranges (measured from points with equal grain density) for particles with masses $0.25\,M_p$, $1\,M_p$ and $2M_p$ (M_p is the proton mass) /199/. Thus, the ratio of the residual ranges of singly-charged particles, corresponding to the same grain density, is equal to the mass ratios.

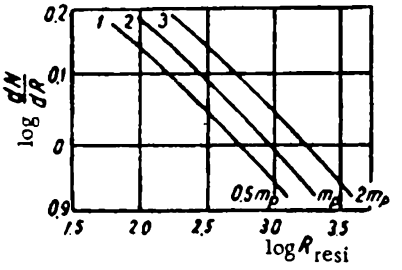

FIGURE 91. Grain density in the track versus residual range for protons (1), deuterons (2), and tritons (3) /199/

The method of measuring the grain density may only be used for the measurement of the π-meson mass, whereas the method of counting individual grains is only applicable if the number of grains does not exceed 50 over a path of about 100 microns of track section.

In these measurements the results are often normalized /228, 18/ to the specific ionization value and, consequently, to the density of the clusters on the ionization plateau, characteristic of high energy particles. The simultaneous effects of the relativistic increase in the ionization and of the density are taken into account (see § 5).

Curves giving the dependence of the grain density (N_g^*) and the grain cluster density (N_b^*) normalized to the plateau on the quantity $p\beta$ are given in Figure 92 /54/.

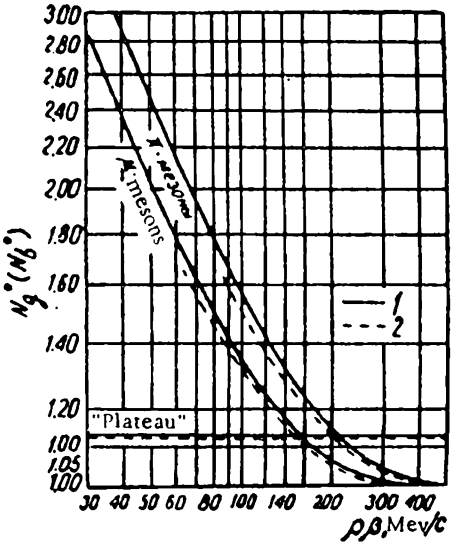

FIGURE 92. Grain density N_g^* (1) and grain cluster density N_b^* (2) normalized to the ionization plateau as a function of the quantity $p\beta$ for Ilford G-5 emulsion; $N_g^* = N_g/N_{g\min}$; $N_b^* = N_b/N_{b\min}$

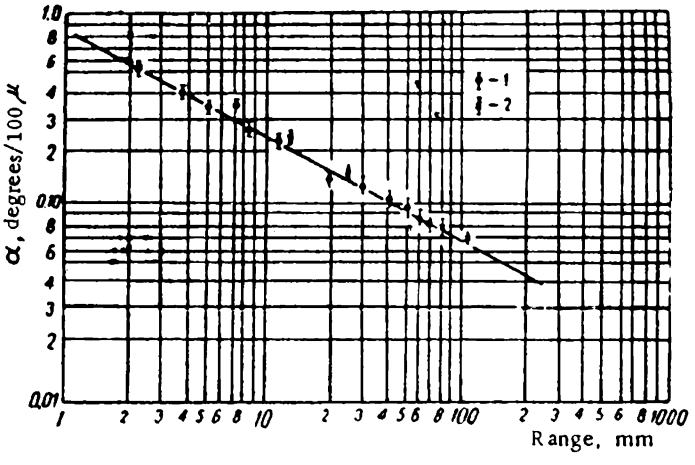

FIGURE 93. Dependence of the mean angle α of multiple scattering on the range of protons in an emulsion. The measurements were performed on π-mesons (1), and -mesons (2). Their proton equivalents were plotted on the graph

Identification of particles from the track curvatures in an emulsion. As a result of a large number of scattering events in multiple scattering, the track of a fast-charged particle in an emulsion is curved. It follows from the theory (§ 2) that the mean deflection angle $\bar{\alpha}_t$ per unit path length, i.e., the angle between two tangents to the projection of a section of the track on the plane of the plate, is equal to

$$\bar{\alpha}_t = \frac{kz\sqrt{t}}{p\beta}, \tag{10.8}$$

where t is the length of the measurement cell;

z, p, β are the charge, momentum and velocity of the particle, respectively.

The value of the scattering constant depends weakly on the velocity of the particle and on the length of the scattering cell.

If the angle $\bar{\alpha}_t$ is measured in degrees, t in microns, $p\beta$ in Mev/c, where c is the velocity of light, then for a nuclear emulsion $k \approx 26\mu$ Mev·degree per $(100\mu)^{1/2}$.

Combining the measurements of the scattering with those of the particle range R in the emulsion, or of the grain density in the track, it is possible to determine the mass and charge of the particle. This method is applicable in the investigation of fast particles in cosmic rays. The dependence of $\bar{\alpha}$ on the proton range is given in Figure 93.

Identification of highly-charged particles in a photoemulsion. Nuclei of heavy elements, possessing high energies, are detected in the primary cosmic radiation. However, the identification of these nuclei by the methods described above of grain counting with a simultaneous measurement of the residual range is impossible. In this case, either the photometric characteristics of the track (the thickness of the central part of the range, the length of the narrowing part of the track after maximum ionization) are measured, or the δ-electrons, knocked out from the atoms by the heavy particles, are counted.

Use is also made of the fact that the grain density at the end of the track of a multi-charged particle is much greater than the grain density in the track of a singly- or doubly-charged particle. The length of the narrowing part of the track, where intensive capture of electrons takes place, is then approximately proportional to the square of the nuclear charge forming the track (see § 7).

A more reliable method for determining the charge of heavy fast particles is the measurement of the number of δ-electrons per unit track length.

The cross section for the formation of δ-electrons with an energy from Q to $Q + dQ$ is quite well represented by (4.4). Multiplying this cross section by $n = NZ$, the number of electrons per 1 cm^3 of the medium, and integrating from Q_1 to Q_2, we obtain the number of δ-electrons per unit track length

$$N_\delta = \frac{2\pi n Z^2 z^2}{\beta^2}\left(\frac{e^2}{m_e c^2}\right)^2\left(\frac{m_e c^2}{Q_1} - \frac{m_e c^2}{Q_2}\right). \tag{10.9}$$

The upper limit Q_2 is determined by the sensitivity of the emulsion and by the possibility of counting the tracks of the δ-electrons, and the lower limit Q_1 is determined by the chosen criterion for counted δ-rays; if δ-rays containing no less than 3-4 grains are counted, then Q_1 is equal to 10-15 kev. At relativistic ($\beta \cong 1$) particle velocities, the density of the δ-rays is a single-valued function of the charge. In all other cases, in order to determine the nature of the particle (charge, mass), the measurement of the

density of the δ-rays is combined with that of the mean deflection angle $\bar{\alpha}_t$ per unit track length or with that of the range. The relation between these quantities for fast heavy nuclei with various z is illustrated by the curves of Figure 94 /226/.

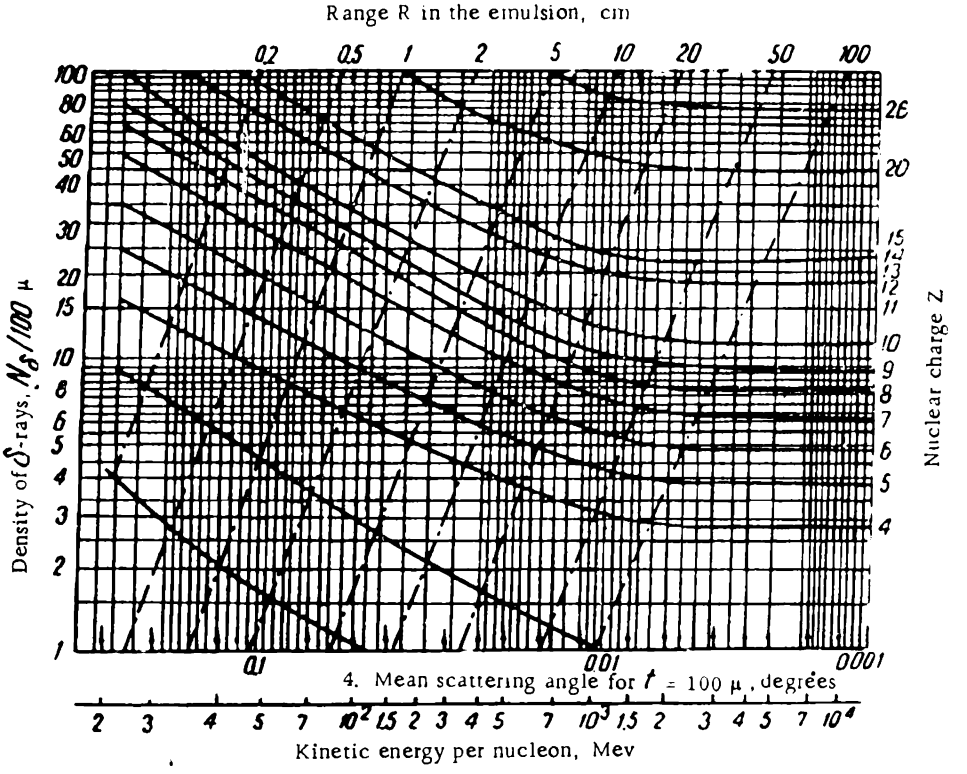

FIGURE 94. Relation between the density of δ-rays, the angle of multiple scattering and the range of multiply-charged ions in a photoemulsion. The dot-dashed curves are of equal range

Remarks on the identification of particles by means of a cloud chamber. The mass of a particle in a cloud chamber placed in a magnetic field can be determined by measuring:

1) the specific ionization $\frac{dJ}{dx}$ and the quantity $H\rho$;
2) the specific ionization $\frac{dJ}{dx}$ and the range R;
3) $H\rho$ and the range R;
4) $H\rho$ and the density of the δ-rays along the track.

The dependence of these quantities on $\frac{\beta}{\sqrt{1-\beta^2}}$ is shown in Figure 95.

Identification of non-relativistic charged particles by simultaneous measurements of the energy losses and of the total energy. For non-relativistic charged particles, the mean energy losses per unit path length and the ranges are expressed by means of relations (4.24) and (6.2), where $f(v)$ and $F(v)$ are functions of the velocity of the particle. If we neglect the influence of the logarithmic term in the expression for the mean energy losses, it is found that the product $E\frac{dE}{dx}$ is proportional to z^2M. A simultaneous measurement

of E and $\frac{dE}{dx}$ and of the product makes it possible to separate the particles according to their masses in a wide range of energy variations. Thus, for example, for particle energies of 5-25 Mev, the values of $E\frac{dE}{dx}$ in various media are in the ratios 1:1.8:2.6 for protons, deuterons and tritons, respectively /143/.

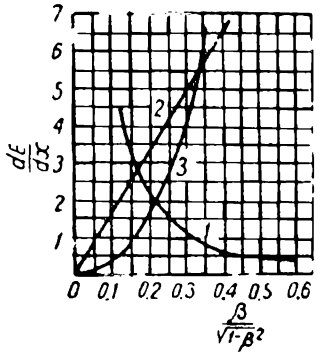

FIGURE 95. Dependence of dE/dx (curve 1; one division on the ordinate axis is equal to 10^4G·cm), $H\rho/(\mu/m)$ (curve 2; one division is equal to 10^2 oersted·cm) and $R(\mu/m)$ (curve 3; one division is equal to 10^{-3}cm) on $\beta/\sqrt{1-\beta^2}$

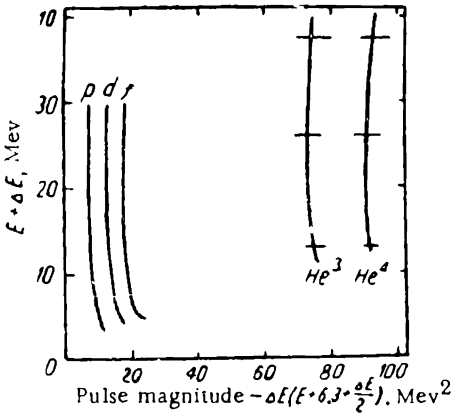

FIGURE 96. Theoretical dependence of the pulse magnitude in the „dE/dx—E" method with electronic corrections on the energy of incident particles of various masses and charges

This method has been successfully applied in a number of investigations of products of nuclear reactions /26, 142, 444, 507/. It is important here to choose the proper optimum "thickness" of the sensitive volume of the counter, since the resolution is determined by the ratio $\frac{\delta}{\Delta E}$, where is the half-width of the pulse spectrum obtained when a large number of monoenergetic particles pass through the counter; ΔE is the mean energy loss in the counter.

The curves in Figure 96 show the dependence of the pulse magnitude, proportional to $E\frac{dE}{dx}$, on the energy /444/.

Chapter II

PASSAGE OF ELECTRONS THROUGH MATTER

§ 11. Introduction

The passage of electrons through matter is associated, as are heavy charged particles, with elastic and inelastic collisions with the nuclei and electrons of the stopping medium. However, in contrast to heavy particles, the collision of an incident electron with an electron or nucleus of the stopping medium leads to a relatively large energy loss and to a considerable change in its direction of motion. Consequently, the intensity of a beam of electrons in heavy media decreases almost exponentially with increasing absorber thickness. For the same reason the path of an electron in matter is a wriggling broken line, and the ranges of electrons of equal energies have a considerable spread (§ 15).

Moreover, for electron energies $T > 0.5$ Mev, radiation losses become increasingly important with rising energy. These losses are due to the emission of electromagnetic radiation when electrons are stopped in the nuclear fields. In practice, these losses can be neglected for electron energies lower than 1 Mev. The principal mechanism of energy loss in this range is inelastic scattering on the bound electrons of the stopping medium, leading to the ionization and excitation of the atoms (§ 13). The ionization energy losses per unit path length of electrons and protons with the same velocity are almost the same. The scattering of electrons is mainly due to elastic collisions with the nuclei of the stopping medium (§ 12). The probability of elastic collisions with nuclei is considerably higher for electrons than for heavy incident particles. The difference between absorption and scattering in reducing the beam intensity is not as sharp as in the case of heavy charged particles (Chapter I).

The importance of scattering increases with decreasing electron energy and the angular distribution of the scattered electrons approaches a gaussian distribution; the mean scattering angle being proportional to the square root of the scatterer thickness (§ 12).

When the thickness of the scattering medium is large, the angular distribution of the scattered electrons becomes diffuse and does not depend on the thickness.

For electrons passing through metals, the interaction with the conduction electrons should be taken into account.

§ 12. Elastic scattering of electrons (positrons)

Classical (Rutherford) scattering of electrons on nuclei. When slow electrons are scattered on heavy nuclei, condition (2.36) is fulfilled. The scattering cross section is determined by Rutherford's formula (2.24)*. Considering the fact that the electron mass $m_1 = \frac{m}{\sqrt{1-\beta^2}}$ is much smaller than the mass of the nucleus, $M \equiv m_2$, and consequently, the scattering angle ϑ of the electrons in LS is the same as the scattering angle θ in CMS, we write formula (2.24) in the form:

$$\frac{d\sigma_R}{d\omega} = \sigma_R = \frac{Z^2}{4}\left(\frac{e^2}{mc^2}\right)^2 \left(\frac{1-\beta^2}{\beta^4}\right) \operatorname{cosec}^4 \frac{\vartheta}{2}, \qquad (12.1)$$

where $d\omega$ is the element of solid angle in LS;

Z is the charge of the scattering nuclei;

$$\beta = \frac{v}{c}.$$

$\frac{e^2}{mc^2} = 2.8 \cdot 10^{-13}$ cm is the classical radius of the electron.

The total cross section for back scattering $\left(\vartheta \geqslant \frac{\pi}{2}\right)$ of electrons is equal to

$$\sigma_R\left(\vartheta > \frac{\pi}{2}\right) = \pi Z^2 \left(\frac{e^2}{mc^2}\right)^2 \left(\frac{1-\beta^2}{\beta^4}\right) \simeq 0.25 Z^2 \left(\frac{1-\beta^2}{\beta^4}\right) \text{barn}. \qquad (12.2)$$

Thus, for 0.5 Mev electrons, the total cross section for back scattering on gold nuclei ($Z = 79$) is equal to 640 barn.

Quantum-mechanical calculations of the scattering cross sections of electrons on nuclei. Mott /71, 386/ determined the scattering cross section of fast electrons on nuclei, using Dirac's relativistic theory of the electron. In the calculations the nuclei were assumed to be material points (having no extension) and the screening of the nuclear coulomb fields by the electrons was not taken into account. The differential scattering cross section of unpolarized electrons is given in this approximation by

$$\frac{d\sigma_M}{d\omega} = \sigma_M = \frac{\lambda^2}{4\pi^2}\left\{q^2(1-\beta^2)|F|^2 \operatorname{cosec}^2\left(\frac{\vartheta}{2}\right) + |G|^2 \sec^2\left(\frac{\vartheta}{2}\right)\right\}, \qquad (12.3)$$

where $\frac{\lambda}{2\pi}$ is the reduced de Broglie wavelength;

$$q = \frac{\alpha}{\beta};$$

$$\alpha = \frac{Ze^2 \cdot 2\pi}{hc} = \frac{Z}{137};$$

$$\beta = \frac{v}{c}.$$

The quantities F and G are functions of α, q, ϑ and are expressed in terms of infinite series. Some investigators attempted to sum these series either by using approximate analytical expressions, or by numerical integration.

Among the first notable attempts of this kind the work of McKinley and Feshbach /387/ should be mentioned. Representing the functions F and G

* The scattering of electrons with energies $\sim 10^2$-10^3 ev has a more complicated character /97, 166/.

by the approximate analytical expressions

$$F = F_0 + A(\vartheta)\alpha^2 + B(\vartheta)\frac{\alpha^3}{\beta} + C(\vartheta)\frac{\alpha^4}{\beta^2} + D(\vartheta)\alpha^4,$$

$$G = G_0 + E(\vartheta)\alpha^2 + H(\vartheta)\frac{\alpha^3}{\beta} + I(\vartheta)\frac{\alpha^4}{\beta^2} + J(\vartheta)\alpha^4,$$

these authors calculated and tabulated the values of the coefficients A, B, C, D, E, H, I, J*. The final results of their calculations for three electron energies and various scattering angles are given in Figure 97. R_M (the Mott factor) is the ratio $\frac{\sigma_M}{\sigma_R}$, where σ_R is the Rutherford scattering cross section, given by formula (12.1).

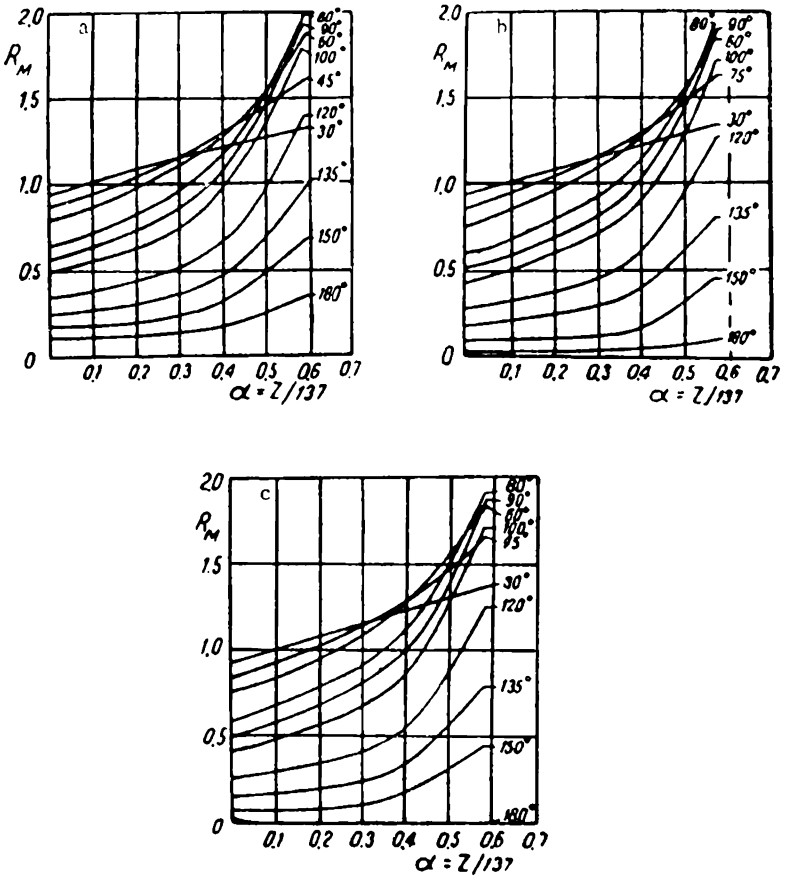

FIGURE 97. Ratio of the scattering cross section for electrons calculated by the Mott formula to that calculated by the Rutherford formula:

a — with an energy of 1 Mev /387/; b —with an energy of 2 Mev /387/; c — with an energy of 4 Mev /387/

McKinley and Feshbach noted that for $\frac{Z}{137} < 0.2$ and $\beta \approx 1$ one may use in the calculation of the scattering of fast electrons to a good approximation

* The values F_0 and G_0 were chosen so that the results of the calculations agreed with the earlier results of Bartlett and Watson /208/, and of Massey /386/, in which σ was calculated for Hg ($Z = 79$).

the following formula for the Mott factor

$$R_M = 1 - \beta^2 \sin^2 \frac{\vartheta}{2} + \pi\beta \left(\frac{Z}{137}\right) \left(1 - \sin \frac{\vartheta}{2}\right) \sin \frac{\vartheta}{2}. \qquad (12.4)$$

This expression corresponds to the initial sections of the curves of Figure 97. It follows from (12.4) that for slow electrons ($\beta \ll 1$), or for small scattering angles, $R \approx 1$, i.e., the magnitude of the cross section is the same as the Rutherford cross section. However, under these conditions, the classical impact parameter

$$\rho_{cl} = \frac{Ze^2}{mv^2\vartheta}$$

is smaller than the corresponding quantum-mechanical value.

The second term in (12.4) is independent of the charge of the scattering nuclei and leads to a reduction of the scattering cross section as compared with the Rutherford value. The third term in (12.4) leads to an increase in the scattering cross section of electrons, which is particularly noticeable for heavy elements. Thus, for large scattering angles and light elements, the theoretical quantum-mechanical scattering cross section of electrons is smaller than the Rutherford cross section. For intermediate scattering angles and heavy elements it is larger than the Rutherford cross section by a factor of 1.5-2 (see Figure 97).

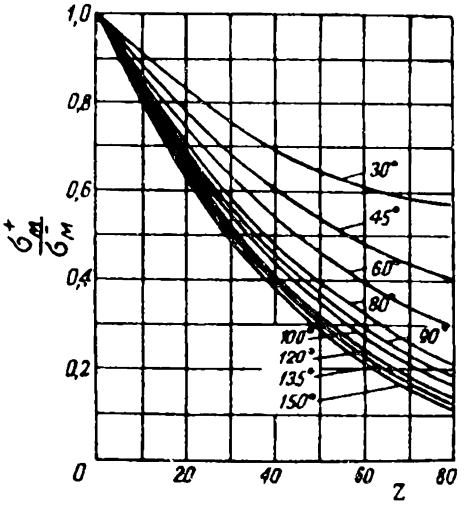

FIGURE 98. Theoretical dependence of the ratio of Mott scattering cross sections for positrons and electrons on the nuclear charge for $\beta \approx 1$.

The scattering cross section depends on the sign of the interaction potential and, therefore, in general, the value of the Mott factor is different for electrons and positrons. Particularly, when Z is replaced by $-Z$, expression (12.4) will give the scattering for positrons. The ratio $\frac{\sigma_M^+}{\sigma_M^-}$ is smaller than one, i.e., the scattering cross section of positrons is smaller than the scattering cross section of electrons for the same energy and scattering angle. The ratio decreases with increasing scattering angle and charge of the scattering nuclei as can be seen from Figure 98, where the ratio $\frac{\sigma_M^+}{\sigma_M^-}$, calculated in /249/ for the case $\beta \approx 1$, is given.

In the non-relativistic range ($\beta < 1$), the scattering cross sections of positrons and electrons are equal.

Results of more recent numerical calculations of $\frac{\sigma_M^-}{\sigma_R}$ and of $\frac{\sigma_M^+}{\sigma_R}$ for electron and positron energies from 0.05 Mev to 10 Mev and charges of the scattering Z nuclei from 6 to 92 are presented in Tables 65 and 66 /232/. The calculations were performed by electronic computers. Some of the results of /232/ were supplemented by Sherman /466/, who made computer calculations of the scattering cross sections σ_M for nuclei with Z, equal to 13, 48, 80, and electron velocities β, equal to 0.2, 0.4, 0.5, 0.6, 0.8, and 0.9. Sherman's results are presented in Table 67.

Allen et al. /144/ performed accurate calculations of the cross section for single scattering of electrons and positrons at small angles ($\theta < 30°$) by xenon.

TABLE 65

Calculated values of σ/σ_R for the scattering of electrons /232/

$\vartheta°$	E, Mev								
	10	4	2	1	0.7	0.4	0.2	0.1	0.05
				$Z = 6$					
0	1.000	1.000	1.000	1.000	1.000	1.000	1.000	1.000	1.000
15	0.999	0.999	1.000	1.000	1.001	1.002	1.003	1.004	1.004
30	0.961	0.962	0.963	0.967	0.970	0.977	0.987	0.996	1.001
45	0.888	0.890	0.894	0.903	0.911	0.929	0.954	0.976	0.990
60	0.788	0.790	0.797	0.814	0.828	0.860	0.906	0.946	0.974
75	0.666	0.669	0.680	0.705	0.728	0.776	0.846	0.909	0.953
90	0.532	0.537	0.551	0.586	0.617	0.683	0.781	0.868	0.930
105	0.397	0.403	0.421	0.466	0.505	0.590	0.714	0.826	0.905
120	0.269	0.277	0.298	0.352	0.440	0.501	0.651	0.786	0.882
135	0.1591	0.1680	0.1923	0.254	0.308	0.425	0.596	0.751	0.862
150	0.0742	0.0839	0.1106	0.1787	0.238	0.366	0.554	0.725	0.846
165	0.0206	0.0310	0.0591	0.1310	0.1938	0.328	0.527	0.708	0.836
180	0.0024	0.0129	0.0416	0.1148	0.1786	0.316	0.518	0.702	0.833
				$Z = 13$					
0	1.000	1.000	1.000	1.000	1.000	1.000	1.000	1.000	1.000
15	1.020	1.020	1.020	1.020	1.019	1.019	1.018	1.015	1.013
30	0.997	0.998	0.999	1.001	1.003	1.008	1.013	1.017	1.017
45	0.935	0.936	0.939	0.947	0.954	0.968	0.988	1.004	1.013
60	0.838	0.840	0.846	0.861	0.874	0.903	0.943	0.977	0.999
75	0.714	0.718	0.727	0.752	0.773	0.818	0.883	0.941	0.979
90	0.575	0.580	0.594	0.628	0.658	0.722	0.815	0.898	0.955
105	0.431	0.438	0.455	0.499	0.538	0.621	0.743	0.852	0.928
120	0.294	0.302	0.323	0.377	0.424	0.525	0.674	0.808	0.902
135	0.1742	0.1831	0.207	0.270	0.324	0.441	0.613	0.769	0.879
150	0.0813	0.0912	0.1179	0.1868	0.247	0.376	0.566	0.738	0.861
165	0.0226	0.0329	0.0614	0.1342	0.1980	0.334	0.536	0.719	0.850
180	0.0024	0.0131	0.0419	0.1163	0.1811	0.320	0.526	0.712	0.846
				$Z = 29$					
0	1.000	1.000	1.000	1.000	1.000	1.000	1.000	1.000	1.000
15	1.069	1.068	1.068	1.066	1.064	1.059	1.050	1.038	1.026
30	1.094	1.093	1.093	1.092	1.091	1.089	1.082	1.070	1.054
45	1.066	1.066	1.068	1.072	1.074	1.080	1.085	1.082	1.072
60	0.987	0.988	0.993	1.004	1.013	1.032	1.057	1.073	1.076
75	0.865	0.868	0.876	0.896	0.914	0.952	1.004	1.045	1.067
90	0.712	0.716	0.729	0.761	0.788	0.847	0.931	1.003	1.047
105	0.543	0.549	0.566	0.610	0.648	0.729	0.848	0.952	1.022
120	0.375	0.383	0.405	0.460	0.508	0.611	0.763	0.900	0.995
135	0.224	0.234	0.259	0.325	0.382	0.505	0.687	0.852	0.970
150	0.1052	0.1157	0.1446	0.218	0.282	0.420	0.626	0.813	0.950
165	0.0289	0.0402	0.0710	0.1497	0.218	0.366	0.587	0.789	0.937
180	0.0026	0.0141	0.0456	0.1261	0.1964	0.348	0.573	0.780	0.932
				$Z = 50$					
0	1.000	1.000	1.000	1.000	1.000	1.000	1.000	1.000	1.000
15	1.124	1.123	1.121	1.115	1.109	1.096	1.072	1.043	1.018
30	1.235	1.234	1.231	1.123	1.216	1.197	1.161	1.113	1.060
45	1.292	1.292	1.290	1.284	1.279	1.264	1.132	1.183	1.120
60	1.274	1.274	1.275	1.277	1.277	1.276	1.262	1.228	1.173
75	1.177	1.179	1.184	1.197	1.208	1.227	1.246	1.242	1.207
90	1.013	1.017	1.028	1.055	1.078	1.126	1.188	1.226	1.225
105	0.801	0.807	0.825	0.869	0.907	0.988	1.101	1.190	1.230
120	0.569	0.578	0.602	0.664	0.718	0.832	0.999	1.142	1.229
135	0.348	0.359	0.390	0.467	0.535	0.682	0.899	1.093	1.225
150	0.1651	0.1781	0.214	0.305	0.385	0.537	0.815	1.053	1.221
165	0.0452	0.0594	0.0983	0.1980	0.285	0.475	0.760	1.026	1.219
180	0.0033	0.0180	0.0581	0.1608	0.251	0.446	0.741	1.017	1.219

TABLE 65 (continued)

ϑ°	E, Mev								
	10	4	2	1	0.7	0.4	0.2	0.1	0.05
					$Z = 82$				
0	1.000	1.000	1.000	1.000	1.000	1.000	1.000	1.000	1.000
15	1.127	1.125	1.120	1.108	1.098	1.074	1.042	1.024	1.024
30	1.358	1.354	1.344	1.315	1.290	1.230	1.133	1.040	0.998
45	1.658	1.653	1.638	1.599	1.564	1.479	1.328	1.157	1.023
60	1.918	1.912	1.897	1.857	1.819	1.728	1.555	1.336	1.112
75	2.044	2.040	2.029	2.000	1.971	1.896	1.741	1.518	1.267
90	1.981	1.980	1.979	1.974	1.966	1.936	1.844	1.672	1.435
105	1.726	1.731	1.745	1.777	1.801	1.842	1.859	1.786	1.614
120	1.324	1.335	1.366	1.444	1.510	1.640	1.799	1.866	1.799
135	0.855	0.874	0.924	1.050	1.159	1.385	1.693	1.920	1.978
150	0.422	0.446	0.513	0.683	0.830	1.143	1.592	1.955	2.130
165	0.1158	0.1444	0.222	0.422	0.595	0.969	1.514	1.974	2.233
180	0.0068	0.0368	0.1187	0.328	0.511	0.908	1.486	1.978	2.267
					$Z = 92$				
0	1.000	1.000	1.000	1.000	1.000	1.000	1.000	1.000	1.000
15	1.103	1.102	1.097	1.086	1.076	1.058	1.038	1.034	1.029
30	1.321	1.316	1.304	1.270	1.240	1.174	1.075	1.005	1.007
45	1.702	1.694	1.674	1.619	1.569	1.456	1.267	1.080	0.978
60	2.119	2.110	2.085	2.019	1.958	1.815	1.561	1.272	1.038
75	2.418	2.410	2.388	2.326	2.268	2.127	1.859	1.521	1.193
90	2.482	2.477	2.465	2.429	2.393	2.295	2.083	1.770	1.413
105	2.264	2.266	2.272	2.284	2.290	2.280	2.198	1.991	1.679
120	1.797	1.809	1.840	1.918	1.981	2.096	2.206	2.177	1.979
135	1.191	1.213	1.273	1.423	1.551	1.809	2.141	2.226	2.287
150	0.598	0.629	0.715	0.932	1.120	1.510	2.048	2.436	2.561
165	0.1652	0.203	0.307	0.572	0.801	1.287	1.970	2.505	2.753
180	0.0091	0.0496	0.1600	0.441	0.685	1.206	1.940	2.523	2.826

TABLE 66

Calculated values of σ/σ_r for the scattering of positrons /232/

ϑ°	E, Mev								
	10	4	2	1	0.7	0.4	0.2	0.1	0.05
					$Z = -6$				
0	1.000	1.000	1.000	1.000	1.000	1.000	1.000	1.000	1.000
15	0.941	0.942	0.943	0.946	0.948	0.954	0.963	0.972	0.980
30	0.896	0.897	0.899	0.905	0.911	0.923	0.942	0.960	0.974
45	0.818	0.819	0.824	0.836	0.847	0.870	0.904	0.937	0.961
60	0.715	0.717	0.725	0.745	0.762	9.799	0.855	0.906	0.944
75	0.596	0.701	0.711	0.640	0.665	0.718	0.798	0.871	0.924
90	0.472	0.478	0.493	0.530	0.563	0.634	0.739	0.835	0.905
105	0.350	0.357	0.375	0.422	0.463	0.511	0.682	0.800	0.885
120	0.237	0.245	0.266	0.322	0.370	0.474	0.628	0.768	0.868
135	0.1388	0.1478	0.1724	0.235	0.290	0.408	0.582	0.740	0.853
150	0.0645	0.0743	0.1011	0.1696	0.229	0.357	0.547	0.719	0.841
165	0.0188	0.0291	0.0573	0.1292	0.1920	0.327	0.526	0.706	0.834
180	0.0024	0.0129	0.0415	0.1147	0.1786	0.315	0.518	0.701	0.832
					$Z = -13$				
0	1.000	1.000	1.000	1.000	1.000	1.000	1.000	1.000	1.000
15	0.940	0.941	0.942	0.943	0.948	0.953	0.963	0.973	0.982
30	0.877	0.878	0.881	0.886	0.895	0.909	0.930	0.952	0.968
45	0.790	0.792	0.797	0.807	0.822	0.848	0.887	0.924	0.953
60	0.685	0.688	0.696	0.714	0.736	0.776	0.836	0.893	0.953
75	0.568	0.573	0.584	0.612	0.640	0.697	0.781	0.860	0.918
90	0.448	0.454	0.469	0.506	0.542	0.616	0.725	0.826	0.900
105	0.331	0.338	0.356	0.402	0.446	0.537	0.671	0.794	0.883
120	0.223	0.231	0.253	0.308	0.359	0.465	0.622	0.765	0.868
135	0.1309	0.1398	0.1649	0.227	0.284	0.404	0.582	0.741	0.856
150	0.0609	0.0707	0.0979	0.1654	0.228	0.357	0.549	0.723	0.846
165	0.0174	0.0280	0.0561	0.1270	0.1924	0.328	0.530	0.711	0.840
180	0.0024	0.0130	0.0417	0.1139	0.1803	0.319	0.523	0.707	0.838

TABLE 66 (continued)

$\vartheta°$	E, Mev								
	10	4	2	1	0.7	0.4	0.2	0.1	0.05
				$Z = -29$					
0	1.000	1.000	1.000	1.000	1.000	1.000	1.000	1.000	1.000
15	0.919	0.920	0.921	0.926	0.931	0.938	0.952	0.967	0.979
30	0.835	0.837	0.840	0.850	0.858	0.878	0.908	0.938	0.963
45	0.738	0.740	0.746	0.763	0.777	0.810	0.859	0.908	0.946
60	0.631	0.635	0.644	0.669	0.690	0.737	0.809	0.877	0.929
75	0.519	0.524	0.537	0.570	0.599	0.663	0.758	0.848	0.914
90	0.406	0.412	0.429	0.471	0.508	0.589	0.709	0.820	0.900
105	0.298	0.305	0.325	0.376	0.422	0.518	0.663	0.794	0.887
120	0.200	0.208	0.213	0.291	0.344	0.456	0.622	0.772	0.877
135	0.1172	0.1268	0.1531	0.220	0.278	0.404	0.588	0.753	0.868
150	0.0547	0.0652	0.0936	0.1660	0.229	0.364	0.563	0.740	0.862
165	0.0156	0.0265	0.0562	0.1312	0.1981	0.339	0.547	0.732	0.859
180	0.0025	0.0136	0.0438	0.1208	0.1880	0.331	0.542	0.729	0.857
				$Z = -50$					
0	1.000	1.000	1.000	1.000	1.000	1.000	1.007	1.000	1.000
15	0.899	0.900	0.902	0.908	0.914	0.926	0.945	0.964	0.978
30	0.800	0.802	0.807	0.820	0.831	0.856	0.895	0.934	0.962
45	0.696	0.698	0.706	0.707	0.745	0.784	0.845	0.904	0.947
60	0.588	0.592	0.603	0.632	0.658	0.713	0.797	0.875	0.931
75	0.479	0.485	0.500	0.537	0.571	0.643	0.750	0.849	0.918
90	0.372	0.379	0.398	0.445	0.486	0.575	0.707	0.825	0.906
105	0.272	0.280	0.302	0.359	0.408	0.514	0.668	0.805	0.896
120	0.1817	0.191	0.217	0.282	0.339	0.459	0.635	0.787	0.888
135	0.1066	0.1171	0.1456	0.218	0.281	0.415	0.608	0.774	0.882
150	0.0500	0.0613	0.0921	0.1704	0.238	0.382	0.588	0.764	0.877
165	0.0146	0.0264	0.0586	0.1406	0.212	0.362	0.576	0.758	0.874
180	0.0027	0.0147	0.0475	0.1306	0.203	0.355	0.572	0.756	0.873
				$Z = -82$					
0	1.000	1.000	1.000	1.000	1.000	1.000	1.000	1.000	1.000
15	0.888	0.889	0.892	0.900	0.907	0.922	0.945	0.964	0.977
30	0.779	0.781	0.788	0.804	0.818	0.848	0.894	0.934	0.963
45	0.669	0.673	0.683	0.707	0.729	0.776	0.846	0.907	0.948
60	0.561	0.565	0.579	0.613	0.643	0.706	0.780	0.880	0.933
75	0.453	0.460	0.477	0.521	0.559	0.640	0.756	0.856	0.922
90	0.350	0.358	0.380	0.434	0.480	0.579	0.719	0.836	0.911
105	0.255	0.264	0.290	0.354	0.410	0.526	0.687	0.818	0.901
120	0.1702	0.1811	0.211	0.285	0.348	0.480	0.660	0.804	0.894
135	0.0997	0.1118	0.1446	0.227	0.297	0.442	0.638	0.793	0.888
150	0.0469	0.0599	0.0955	0.1844	0.260	0.415	0.623	0.785	0.885
165	0.0144	0.0282	0.0654	0.1586	0.237	0.399	0.614	0.780	0.882
180	0.0032	0.0171	0.0549	0.1496	0.229	0.394	0.612	0.778	0.882
				$Z = -92$					
0	1.000	1.000	1.000	1.000	1.000	1.000	1.000	1.000	1.000
15	0.888	0.889	0.892	0.900	0.907	0.923	0.945	0.963	0.976
30	0.778	0.780	0.786	0.803	0.818	0.849	0.894	0.935	0.963
45	0.667	0.671	0.681	0.707	0.729	0.777	0.848	0.908	0.948
60	0.558	0.563	0.577	0.612	0.643	0.708	0.802	0.881	0.934
75	0.450	0.457	0.475	0.520	0.559	0.642	0.759	0.858	0.922
90	0.348	0.356	0.378	0.434	0.482	0.583	0.723	0.838	0.911
105	0.253	0.263	0.289	0.356	0.413	0.531	0.691	0.820	0.902
120	0.1690	0.1803	0.211	0.288	0.353	0.487	0.666	0.806	0.895
135	0.0989	0.1116	0.1458	0.232	0.304	0.451	0.646	0.796	0.889
150	0.0465	0.0602	0.0973	0.1897	0.268	0.425	0.631	0.789	0.885
165	0.0146	0.0290	0.0680	0.1649	0.246	0.410	0.623	0.783	0.883
180	0.0033	0.0180	0.0576	0.1560	0.239	0.405	0.620	0.781	0.883

TABLE 67

Calculated values of σ_M (barn/steradian), S_M and R_M /466/

$\vartheta°$	Values of σ, R, S	$\beta = 0.2$	0.4	0.5	0.6	0.7	0.8	0.9
		T, Mev						
		0.01	0.046	0.079	0.128	0.204	0.340	0.664
		Mercury ($Z = 80$)						
15	σ_M	$2.64 \cdot 10^{9}$	$1.47 \cdot 10^{7}$	$5.35 \cdot 10^{6}$	$2.21 \cdot 10^{6}$	$9.07 \cdot 10^{5}$	$4.10 \cdot 10^{5}$	$1.39 \cdot 10^{4}$
	R_M	1.00	1.02	1.02	1.02	1.04	1.06	1.10
	S_M	$2.11 \cdot 10^{-3}$	$-4.25 \cdot 10^{-4}$	$1.60 \cdot 10^{-3}$	$3.45 \cdot 10^{-3}$	$4.04 \cdot 10^{-3}$	$3.77 \cdot 10^{-3}$	$2.79 \cdot 10^{-3}$
30	σ_M	$1.72 \cdot 10^{7}$	$9.30 \cdot 10^{5}$	$3.48 \cdot 10^{5}$	$1.51 \cdot 10^{5}$	$6.89 \cdot 10^{4}$	$3.03 \cdot 10^{4}$	$1.06 \cdot 10^{4}$
	R_M	1.01	1.00	1.02	1.08	1.14	1.22	1.29
	S_M	$-1.93 \cdot 10^{-3}$	$1.53 \cdot 10^{-2}$	$1.96 \cdot 10^{-2}$	$1.66 \cdot 10^{-2}$	$1.14 \cdot 10^{-2}$	$6.32 \cdot 10^{-3}$	$2.30 \cdot 10^{-3}$
45	σ_M	$3.63 \cdot 10^{6}$	$1.99 \cdot 10^{5}$	$7.93 \cdot 10^{4}$	$3.59 \cdot 10^{4}$	$1.68 \cdot 10^{4}$	$7.53 \cdot 10^{3}$	$2.66 \cdot 10^{3}$
	R_M	1.02	1.02	1.12	1.23	1.34	1.45	1.55
	S_M	$-9.65 \cdot 10^{-3}$	$3.93 \cdot 10^{-2}$	$2.01 \cdot 10^{-2}$	$2.02 \cdot 10^{-3}$	$-1.06 \cdot 10^{-2}$	$1.74 \cdot 10^{-2}$	$-1.76 \cdot 10^{-2}$
60	σ_M	$1.19 \cdot 10^{6}$	$7.45 \cdot 10^{4}$	$3.09 \cdot 10^{4}$	$1.42 \cdot 10^{4}$	$6.69 \cdot 10^{3}$	$2.99 \cdot 10^{3}$	$1.05 \cdot 10^{3}$
	R_M	0.976	1.12	1.27	1.41	1.55	1.67	1.78
	S_M	$5.6 \cdot 10^{-2}$	$2.18 \cdot 10^{-3}$	$-3.80 \cdot 10^{-2}$	$-6.16 \cdot 10^{-2}$	$-7.22 \cdot 10^{-2}$	$-7.10 \cdot 10^{-2}$	$-5.86 \cdot 10^{-2}$
75	σ_M	$5.21 \cdot 10^{5}$	$3.81 \cdot 10^{4}$	$1.59 \cdot 10^{4}$	$7.25 \cdot 10^{3}$	$3.37 \cdot 10^{3}$	$1.48 \cdot 10^{3}$	$5.11 \cdot 10^{2}$
	R_M	0.939	1.26	1.43	1.59	1.72	1.82	1.91
	S_M	$8.20 \cdot 10^{-2}$	-0.104	-0.143	-0.160	-0.162	-0.150	-0.117
90	σ_M	$2.94 \cdot 10^{5}$	$2.35 \cdot 10^{4}$	$9.64 \cdot 10^{3}$	$4.291 \cdot 10^{3}$	$1.94 \cdot 10^{3}$	$8.30 \cdot 10^{2}$	$2.78 \cdot 10^{2}$
	R_M	0.964	1.41	1.58	1.71	1.80	1.86	1.89
	S_M	$-3.59 \cdot 10^{-2}$	-0.234	-0.261	-0.271	0.265	-0.242	-0.190
105	σ_M	$2.10 \cdot 10^{5}$	$1.66 \cdot 10^{4}$	$6.56 \cdot 10^{3}$	$2.81 \cdot 10^{3}$	$1.22 \cdot 10^{3}$	$5.01 \cdot 10^{2}$	$1.60 \cdot 10^{2}$
	R_M	1.09	1.58	1.70	1.77	1.79	1.78	1.72
	S_M	-0.203	-0.333	-0.356	-0.367	-0.364	-0.340	-0.277

TABLE 67 (continued)

120	σ_M	$1.80 \cdot 10^5$	$1.29 \cdot 10^4$	$4.89 \cdot 10^3$	$2.00 \cdot 10^3$	$8.27 \cdot 10^2$	$3.19 \cdot 10^2$	94.4
	R_M	1.33	1.74	1.80	1.79	1.72	1.61	1.44
	S_M	−0.283	−0.372	−0.401	−0.424	−0.436	−0.429	−0.378
135	σ_M	$1.71 \cdot 10^5$	$1.10 \cdot 10^4$	$3.95 \cdot 10^3$	$1.54 \cdot 10^3$	$5.98 \cdot 10^2$	$2.13 \cdot 10^2$	56.3
	R_M	1.63	1.92	1.89	1.79	1.61	1.39	1.12
	S_M	−0.262	−0.342	−0.380	−0.418	−0.453	−0.479	−0.464
150	σ_M	$1.69 \cdot 10^5$	$9.86 \cdot 10^3$	$3.42 \cdot 10^3$	$1.27 \cdot 10^3$	$4.66 \cdot 10^2$	$1.52 \cdot 10^2$	34.2
	R_M	1.93	2.06	1.95	1.76	1.50	1.18	0.809
	S_M	−0.188	−0.257	−0.295	−0.337	−0.387	−0.446	−0.505
165	σ_M	$1.69 \cdot 10^5$	$9.31 \cdot 10^3$	$3.15 \cdot 10^3$	$1.13 \cdot 10^3$	$3.97 \cdot 10^2$	$1.20 \cdot 10^2$	22.6
	R_M	2.14	2.16	2.00	1.74	1.42	1.04	0.594
	S_M	$-9.56 \cdot 10^{-2}$	−0.137	−0.161	−0.189	−0.220	−0.281	−0.380
				Cadmium (Z = 48)				
15	σ_M	$9.51 \cdot 10^7$	$5.25 \cdot 10^6$	$1.95 \cdot 10^6$	$8.19 \cdot 10^5$	$3.58 \cdot 10^5$	$1.51 \cdot 10^5$	$5.03 \cdot 10^4$
	R_M	1.00	1.02	1.03	1.05	1.07	1.09	1.10
	S_M	$-1.14 \cdot 10^{-4}$	$1.81 \cdot 10^{-3}$	$1.64 \cdot 10^{-3}$	$1.22 \cdot 10^{-3}$	$7.56 \cdot 10^{-4}$	$3.58 \cdot 10^{-4}$	$7.35 \cdot 10^{-5}$
30	σ_M	$6.12 \cdot 10^6$	$3.54 \cdot 10^5$	$1.34 \cdot 10^5$	$5.68 \cdot 10^4$	$2.50 \cdot 10^4$	$1.06 \cdot 10^4$	$3.55 \cdot 10^3$
	R_M	1.00	1.06	1.10	1.13	1.15	1.18	1.20
	S_M	$4.37 \cdot 10^{-3}$	$2.30 \cdot 10^{-3}$	$-1.16 \cdot 10^{-3}$	$-3.67 \cdot 10^{-3}$	$-5.23 \cdot 10^{-3}$	$-5.8 \cdot 10^{-3}$	$5.13 \cdot 10^{-3}$
45	σ_M	$1.28 \cdot 10^4$	$7.76 \cdot 10^4$	$2.96 \cdot 10^4$	$1.26 \cdot 10^4$	$5.52 \cdot 10^3$	$2.33 \cdot 10^3$	776
	R_M	1.00	1.11	1.16	1.20	1.22	1.24	1.26
	S_M	0.0123	0.0119	−0.0188	−0.0227	−0.0242	−0.0232	−0.0188
60	σ_M	$4.50 \cdot 10^5$	$2.78 \cdot 10^4$	$1.05 \cdot 10^4$	$4.43 \cdot 10^3$	$1.93 \cdot 10^3$	803	264
	R_M	1.02	1.16	1.20	1.23	1.24	1.25	1.25
	S_M	$7.70 \cdot 10^{-4}$	−0.0427	−0.0510	−0.0550	−0.0554	−0.0515	−0.0410

TABLE 67 (continued)

$\vartheta°$	Value of σ, R, S	β=0.2	0.4	0.5	0.6	0.7	0.8	0.9
		T, Mev						
		0.01	0.046	0.079	0.128	0.204	0.340	0.664
75	σ_M	$2.12 \cdot 10^5$	$1.30 \cdot 10^4$	$4.86 \cdot 10^3$	$2.01 \cdot 10^3$	862	352	113
	R_M	1.06	1.19	1.22	1.22	1 22	1.20	1.17
	S_M	— 0.0372	−0.0832	−0.0919	−0.0959	−0.0953	−0.0886	−0.0710
90	σ_M	$1.21 \cdot 10^5$	$7.23 \cdot 10^3$	$2.65 \cdot 10^3$	$1.08 \cdot 10^3$	449	178	55.5
	R_M	1.02	1.20	1.21	1.20	1.16	1.11	1.05
	S_M	−0.080	−0.123	−0.133	−0.139	−0.139	−0.131	−0.108
105	σ_M	$7.99 \cdot 10^4$	$4.58 \cdot 10^3$	$1.64 \cdot 10^3$	646	261	99.6	29.5
	R_M	1.15	1.21	1.18	1.13	1.06	0.982	0.882
	S_M	−0.112	−0.153	−0.166	−0.175	−0.180	−0.176	−0.151
120	σ_M	$5.91 \cdot 10^4$	$3.22 \cdot 10^3$	$1.12 \cdot 10^3$	428	166	60.1	16.5
	R_M	1.21	1.21	1.16	1.07	0.961	0.841	0.701
	S_M	−0.122	− 0 163	−0.180	−0.195	−0.208	−0.213	−0.197
135	σ_M	$4.77 \cdot 10^4$	$2.48 \cdot 10^3$	840	310	115	39.0	9.60
	R_M	1.27	1.20	1.12	1.00	0.862	0.707	0.528
	S_M	−0.110	−0.151	−0.170	−0.190	−0.211	−0.231	−0.238
150	σ_M	$4.15 \cdot 10^4$	$2.07 \cdot 10^3$	684	245	87.2	27.4	5.87
	R_M	1.32	1.20	1.08	0.944	0.782	0.593	0.386
	S_M	−0.0822	−0.116	−0.134	−0.153	−0.177	−0.208	−0.247
165	σ_M	$3.83 \cdot 10^4$	$1.85 \cdot 10^3$	606	212	73.1	21.7	4.00
	R_M	1.35	1.20	1.07	0.907	0 .727	0.522	0.292
	S_M	−0.0435	−0.0630	−0.0736	−0.0863	−0.103	−0.128	−0.176
		Aluminum (Z=13)						
15	σ_M	$6.98 \cdot 10^5$	$3.84 \cdot 10^5$	$1.41 \cdot 10^5$	$5.80 \cdot 10^4$	$2.50 \cdot 10^4$	$1.04 \cdot 10^4$	$3.41 \cdot 10^3$
	R_M	1.00	1.01	1.02	1.02	1.02	1.02	1.02
	S_M	$2.97\ 10^{-5}$	$-1.92 \cdot 10^{-4}$	$-2.68 \cdot 10^{-4}$	$-3.24 \cdot 10^{-4}$	$-3.56 \cdot 10^{-4}$	$-3.55 \cdot 10^{-4}$	$-2.94 \cdot 10^{-4}$

TABLE 67 (continued)

30	σ_M	$4.54 \cdot 10^5$	$2.50 \cdot 10^4$	$9.13 \cdot 10^3$	$3.75 \cdot 10^3$	$1.61 \cdot 10^3$	$6.63 \cdot 10^2$	$2.17 10^2$
	R_M	1.01	1.02	1.02	1.02	1.01	1.01	1.00
	S_M	$-7.90 \cdot 10^{-4}$	$-1.80 \cdot 10^{-3}$	$-2.13 \cdot 10^{-3}$	$-2.36 \cdot 10^{-3}$	$-2.45 \cdot 10^{-3}$	$-5.35 \cdot 10^{-3}$	$-1.92 \cdot 10^{-3}$
45	σ_M	$9.52 \cdot 10^4$	$5.20 \cdot 10^3$	$1.89 \cdot 10^3$	$7.72 \cdot 10^2$	$3.28 \cdot 10^2$	$1.34 \cdot 10^2$	43.3
	R_M	1.01	1.01	1.01	1.00	0.987	0.975	0.956
	S_M	$-3.00 \cdot 10^{-3}$	$-5.14 \cdot 10^{-3}$	$-5.88 \cdot 10^{-3}$	$-6.40 \cdot 10^{-3}$	$-6.60 \cdot 10^{-3}$	$-6.33 \cdot 10^{-3}$	$-5.19 \cdot 10^{-3}$
60	σ_M	$3.27 \cdot 10^4$	$1.76 \cdot 10^3$	$6.35 \cdot 10^2$	$2.56 10^2$	$1.07 \cdot 10^2$	43.0	13.6
	R_M	1.02	0.999	0.986	0,966	0.939	0.912	0.875
	S_M	$-6.28 \cdot 10^{-3}$	$-9.73 \cdot 10^{-3}$	-0.0110	-0.0120	$-0\ 0125$	-0.0121	-0.0101
75	σ_M	$1.48 \cdot 10^4$	$7.87 \cdot 10^2$	$2.80 \cdot 10^2$	$1.11 \cdot 10^2$	45.7	17.9	5.50
	R_M	1.01	0.982	0.955	0.920	0.881	0.834	0.778
	S_M	$-9.90 \cdot 10^{-3}$	-0.0147	-0.0167	$-0,0184$	-0.0194	-0.0192	-0.0164
90	σ_M	$8.11 \cdot 10^3$	$4.22 \cdot 10^2$	$1.48 10^2$	57.7	23.1	8.76	2.58
	R_M	1.01	0.958	0.919	0.871	0.810	0.743	0.664
	S_M	-0.0130	-0.0191	-0.0220	-0.0244	-0.0203	-0.0269	-0.0240
105	σ_M	$5.09 \cdot 10^3$	$2.60 \cdot 10^2$	89.6	34.2	13.3	4.83	1.34
	R_M	1.00	0.936	0.882	0.818	0.740	0,649	0.546
	S_M	$-0,0150$	-0.0220	-0.0256	-0.0290	-0.0321	$-0,0341$	-0.0324
120	σ_M	3.56	1.78	6.04	2.25	8.47	2.93	0.748
	R_M	0,995	0,910	0.884	0,764	0.669	0,559	0.433
	S_M	$-0,0152$	$-0,0226$	-0.0266	$-0,0309$	-0.0353	-0.0394	-0.0406
135	σ_M	$2.74 \cdot 10^3$	$1.34 \cdot 10^2$	44.8	16.3	5.94	1.94	0.446
	R_M	0.992	0.887	0.811	0.717	0.607	0.479	0.334
	S_M	-0.0136	-0.0205	-0.0244	-0.0290	-0.0342	-0.0404	-0.0461
150	σ_M	$2.28 \cdot 10^3$	$1.10 \cdot 10^3$	36.4	1300	4058	1.42	0.288
	R_M	0.986	0.870	0,787	0,683	0.560	0.419	0.258
	S_M	-0.0102	-0.0155	-0.0187	-0.0226	-0.0276	-0.0343	-0.0444
165	σ_M	$2.05 \cdot 10^3$	98.0	32.1	11.3	3.90	1.16	0.211
	R_M	0.984	0,860	0.770	0,659	0,529	0.380	0.210
	S_M	$-5.48 \cdot 10^{-3}$	$-8.18 \cdot 10^{-3}$	$-0,0102$	-0.0125	$-0,0156$	$-0,0202$	-0.0290

The theoretical calculations are generally confirmed by experiments on the single scattering of electrons and positrons of 0.2-5 Mev (post-war experiments)*. Thus, Buechner et al. /181, 487/ have shown that the measured scattering cross sections of electrons of 1.27-2.27 Mev on nuclei of beryllium, aluminum, copper, silver, platinum and gold are equal in the range of angles 20-50° to the cross sections calculated by Mott's theory. In these experiments, the distance of closest approach of the electrons to the nuclei varied from $7 \cdot 10^{-13}$ cm (scattering on aluminum) to $100 \cdot 10^{-13}$ cm (scattering on gold), i.e., the scattering occurred in the unscreened part of the coulomb field (the radius of the K-shell of gold is equal to $\sim 700 \cdot 10^{-13}$ cm).

Some investigators /185, 348/ noted that the single-scattering cross sections of electrons with $T < 1$ Mev at large angles (100-150°) on light nuclei (aluminum), is in agreement with the theory, whereas the scattering cross sections on heavy nuclei (gold) at large angles exceed the calculated values. On the other hand, it was shown in /186, 418, 225/ that the scattering of electrons with energies of 0.2-4.3 Mev on heavy elements is in agreement with Mott's theory up to an angle of 150°.

When high-energy ($T > 5$ Mev) electrons are scattered, the screening and the finite dimensions of the nuclei should be taken into account (see below). The effect of the finite dimensions of the nucleus was studied experimentally for the first time in /372/ in the scattering of 15 Mev electrons. However, according to Paul and Reich /420/, the effect of the finite dimensions of the nucleus is already manifested in the scattering of electrons with energies of several megaelectronvolts on heavy nuclei. A similar conclusion follows from /473/, in which the experimental scattering cross sections of electrons with energies of 1.0-2.5 Mev are compared with the calculations of Doggett and Spencer (Tables 65, 66).

Earlier works investigating the scattering of positrons by nuclei in a cloud chamber did not reveal any qualitative difference between the scattering cross sections of positrons and electrons, although they did not contradict Mott's theory. Lipkin and White /371/ were the first who succeeded in obtaining reliable ratios of the scattering cross sections of ~ 1 Mev electrons and positrons on various nuclei. The measured ratios of electrons and positrons, scattered on copper and platinum ($T = 1.08$ Mev), were 0.52 and 0.31, and were found to be in good agreement with the theoretical values of 0.67 and 0.33. Allen et al. /144/ obtained the ratio of the experimental scattering cross sections of electrons and positrons with an energy of 9.8 Mev on xenon as equal to 1.3 (in agreement with the theory).

Effects of the screening and finite dimensions of the nucleus on electron scattering. The screening of the nucleus by the external electrons results in a decrease in the scattering cross sections as compared with the scattering cross sections in an unscreened coulomb field. This is particularly noticeable in small angle scattering. For a given scattering angle, the effect of the screening decreases with increasing electron energy and with decreasing charge of the scattering nuclei.

Depending on the value of the parameter $\alpha = \frac{Z}{137\beta}$, two limiting cases of electron scattering are distinguished, as in the case of heavy charged particle scattering (§ 2).

When the condition $\alpha \gg 1$ is fulfilled (slow electrons and heavy scattering media), the classical approximation is applicable, i.e., the cross section

* The results of earlier investigations are unreliable due to imperfect techniques which did not allow the separation of the elastic and the inelastic scattering of the electrons.

obeys Rutherford's formula (11.1) up to a certain limiting angle ϑ_a^*, as determined by expression (2.38).

In all other cases, the cross section for single scattering has has to be calculated by the quantum-mechanical formulas (Mott's theory, see above). In the limiting case ($\alpha \ll 1$), the calculated values of the scattering cross sections are correct up to a limiting angle ϑ_a^{**}, determined by formula (2.39a), in which $a = a_0 Z^{-1/3}$ is the effective screening radius. For $\vartheta < \vartheta_a^{**}$ the electron scattering will be smaller than that expected from theory due to the screening effects.

Bethe /150/ showed that in the Born approximation the ratio σ^{exp}/σ_R for non-relativistic electrons is determined by the factor $\left[1 - \frac{F(\xi)}{Z}\right]^2$, where $F(\xi)$ is the atomic form-factor, used in the theory of X-ray scattering:

$$\xi = \frac{\sin(\vartheta/2)}{\lambda} Z^{-\frac{1}{3}}.$$

Values of $f(\xi) = \frac{F(\xi)}{Z}$ are given in Table 68.

TABLE 68

Screening correction to the Rutherford formula (12.1) in the Born approximation /150/

ξ	$f(\xi)$	ξ	$f(\xi)$	ξ	$f(\xi)$
0	1	0.10	0.610	0.30	0.277
0.02	0.947	0.12	0.550	0.40	0.207
0.04	0.853	0.15	0.485	0.50	0.156
0.06	0.758	0.20	0.395	—	—
0.08	0.677	0.25	0.322	—	—

A more general method of consideration of the screening effects of the nuclear coulomb field by the atomic electrons, based on the Wentzel method, was worked out by Moliere /388, 389/. The main results of this theory are described in § 2.

The effect of the finite dimensions of the nucleus is noticeable in the scattering of high-energy electrons at large angles. This scattering is connected with small impact parameters, so that if we use the classical analogue, then in head-on collisions, the electron may pass through the periphery of the nucleus and will be subjected to the influence of only a fraction of its charge. Its deflection in this case will be smaller than in the coulomb field of a point charge. The study of such deflections provides valuable information on the charge distribution in the nucleus and on the nuclear form-factor /2/.

Polarization of electrons in single scattering on nuclei. When electrons are scattered their spin acquires a definite orientation, so that the scattered beam is either partially or completely polarized. The polarization of a beam of scattered electrons can be observed from the azimuthal asymmetry in secondary scattering. This fact was used in the well-known experiments on the verification of the parity non-conservation in weak interactions (see, for example, /2, 98/). If ϑ_1 is the scattering angle of the primary electron beam, then ϑ_2, the angle in secondary scattering, will also depend on φ_2, which is the azimuthal angle with respect to ϑ_1. The differential cross section for double scattering is given by the expression

$$\frac{d\sigma}{d\omega}(\vartheta_1, \vartheta_2, \varphi_2) = \frac{d\sigma_M}{d\omega}(\vartheta_1) \frac{d\sigma_M}{d\omega}(\vartheta_2) \left\{1 + S(\vartheta_1, \vartheta_2) \cos \varphi_2\right\}, \qquad (12.5)$$

where $\frac{d\sigma_M}{d\omega}$ is found by (12.3), and the polarization asymmetry factor $S(\vartheta_1,\vartheta_2)$ can be represented as a product $S(\vartheta_1)\,S(\vartheta_2)$, where each of the factors is a function of ϑ_1, or ϑ_2, only:

$$S_M(\vartheta) = \frac{2\lambda^2 q\,(1-\beta^2)^{1/2}}{(2\pi)^2 \sin\vartheta\left(\frac{d\sigma_M}{d\omega}\right)}\left\{F(\vartheta)\,G^*(\vartheta) + F^*(\vartheta)\,G(\vartheta)\right\}. \qquad (12.6)$$

Here we use the same notation as in formula (12.3). Values of $S_M(\vartheta) = \delta^{1/2}$ for various Z and β were calculated by Sherman /466/ and are given in Table 67. Figure 99 gives the dependence (the points) of the polarization asymmetry factor on β in double scattering by 90° ($\vartheta_1 = \vartheta_2 = 90°$) according to Sherman's calculations. This figure also gives the calculated curves of Mott /386/ and of Bartlett and Watson /208/.

The degree of polarization of scattered electrons depends on the energy of the incident electrons and on the charge of the scattering nuclei. Maximum polarization is observed for intermediate (~150 kev) electron energies and large scattering angles.

Scattering of electrons on electrons. In addition to elastic collisions with nuclei electrons are also scattered by inelastic collisions with the atomic electrons. In this case, when the energy of the incident electron exceeds the electron binding energy, an electron-electron collision can be regarded as a collision of two free particles.

The classical scattering cross section of non-relativistic electrons on electrons is given by (2.27). Since the scattering of a primary electron at an angle ϑ is accompanied by the escape of a recoil electron at an angle of $\left(\frac{\pi}{2} - \vartheta\right)$, and these electrons cannot be experimentally distinguished, the Rutherford scattering cross section of electrons on an electron is written in the form

$$\frac{d\sigma}{d\omega} = \sigma_R(\vartheta) = \left(\frac{e^2}{mv^2}\right)^2 \left(\frac{1}{\sin^4\vartheta} + \frac{1}{\cos^4\vartheta}\right) 4\cos\vartheta, \qquad (12.7)$$

where ϑ is the scattering angle in LS, and the factor 4 cos ϑ gives the ratio of the solid angle elements in LS and in CMS (see formulas (2.30) and (2.31)).

The total cross section for Rutherford scattering of electrons at angles larger than ϑ is obtained by integrating (12.7):

$$\sigma_R(\geqslant\vartheta) = 4\pi\left(\frac{e^2}{mv^2}\right)^2 (\mathrm{ctg}^2\vartheta + \mathrm{tg}^2\vartheta)\,\mathrm{cm}^2/\mathrm{electron}. \qquad (12.8)$$

The quantum-mechanical scattering cross section of non-relativistic electrons was calculated by Mott. $\sigma_M(\vartheta)$ is given by (2.28) for $Z = 1$.

For relativistic electrons the scattering cross section should be calculated by Möller's formula /390/

$$d\sigma_{\text{Möller}} = 4\pi\left(\frac{e^2}{mv^2}\right)^2 \left(\frac{\gamma+1}{\gamma^2}\right)\left[\frac{4}{(1-x^2)^2} - \right.$$
$$\left. - \frac{3}{(1-x^2)} + \frac{(\gamma-1)^2}{4\gamma^2}\left(1 + \frac{4}{1-x^2}\right)\right], \qquad (12.9)$$

where $\gamma = (1-\beta^2)^{-1/2}$ is the relativistic transformation factor;

$$x = \frac{2-(\gamma+3)\sin^2\vartheta}{2+(\gamma-1)\sin^2\vartheta}.$$

The cross section for electron-electron scattering is much smaller than the cross section for scattering on nuclei. For atoms with large Z, the scattering cross section of electrons on the nucleus should be Z times as large as the scattering cross section on the atomic electrons.

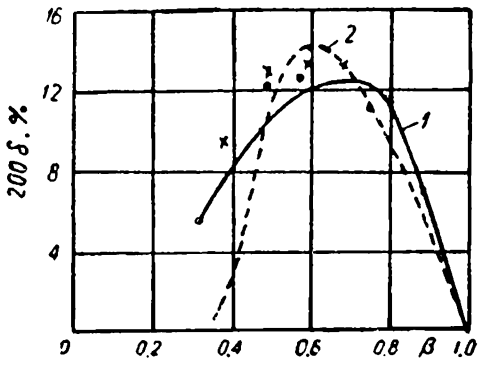

FIGURE 99. Polarization asymmetry factor versus energy in double scattering of electrons according to Sherman ($(\vartheta_1=\vartheta_2=90)^\circ$). According to the calculations of Bartlett and Watson /208/ — curve 1, Z = 80; according to the calculations of Mott /386/ — curve 2, Z = 79; according to Sherman /466/ — the points, Z = 80

The results of experimental investigations of the single scattering of electrons with energies of up to 200 Mev on electrons /203, 204, 331, 423, 467/ are in satisfactory agreement with Möller's formula. The results of some investigations on the scattering of positrons on electrons /138, 308/ are in qualitative agreement with Bhabha's calculations /183/. According to /308/, the ratio of the electron-electron to the positron-electron scattering cross sections for an incident particle energy of 1.3 Mev is equal to 1.82 ± 0.11, whereas according to Möller it is equal to 1.83.

Multiple scattering of electrons. All the formulas given here are only valid for the calculation of the angular distributions of singly scattered electrons. In single scattering, an electron passing a layer of thickness t suffers on the average up to one collision with a nucleus or with an electron of the stopping medium. The layer should in this case be sufficiently thin, so as to satisfy the following condition

$$t \ll \frac{1}{\sigma n}, \tag{12.10}$$

where σ is the effective scattering cross section;

n is the number of atoms per 1 cm^3 of the scattering medium.

The number of scattering events is determined by formula (1.2), σ being determined by one of the following expressions, (12.1), (12.3), (12.7) and (12.9).

If the thickness of the scatterer is

$$t \sim \frac{1}{\sigma n}, \tag{12.11}$$

then the deflection of a particle by a given angle ϑ may be due to several successive scattering events of the electron on nuclei or electrons. We then have plural scattering (§ 2).

If the number of collisions in passing a given thickness of scatterer exceeds twenty, and if at the same time the energy losses are small compared with the initial energy, one speaks of multiple scattering. The theory of plural and multiple scattering is given in §2, which may also be used in electron scattering. Finally, if the scattering foil is so thick that

$$t \gg \frac{1}{\sigma n} \tag{12.12}$$

and the energy losses are large, the passage of electrons can be considered as a diffusion process (see below).

Experimental investigations of multiple scattering of electrons were carried out by Kul'chitskii and Latyshev /58/, Hanson et al. /298/. The results of their investigations are in agreement with the theory given in § 2. Thus, Figure 100 gives the results of measurement /298/ of the angular distribution in multiple scattering of 15.7 Mev electrons in gold foils, and the appropriate theoretical cures (§ 2).

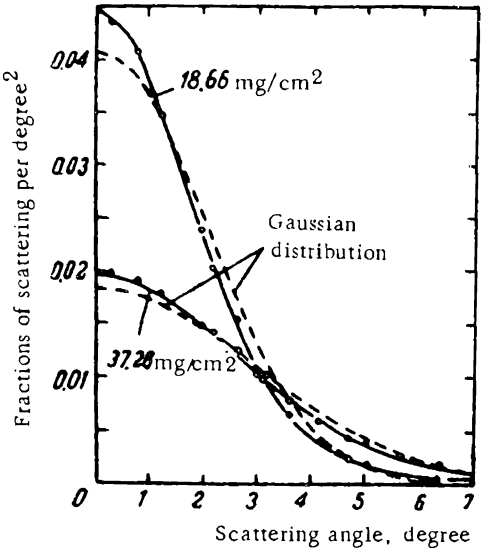

FIGURE 100. Angular distribution of 15.7 Mev multiply scattered electrons on gold foils of 18.66 and 17.28 mg/cm^2

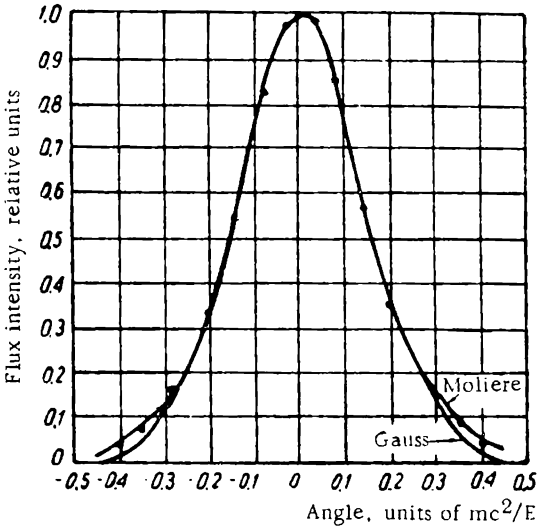

FIGURE 101. Angular distribution of 600 Mev electrons after multiple scattering in a thin (2.55 mg/cm^2) aluminum foil /398/

Further investigations, both at high /398/ and at low energies /333, 352/, showed that multiple scattering is satisfactorily described by Moliere's theory. Figure 101 gives curves for the comparison of the theoretical and experimental angular distributions of 600 Mev electrons passing through an aluminum foil of 2.44 mg/cm^2.

We note that multiple scattering has become very important for the determination of the energy of fast particles (cosmic rays, accelerated protons and mesons), see § 10.

Electron diffusion. For thick media (thickness exceeding approximately half the total range of the electrons, see § 13) the angular distribution of the scattered electrons takes the form

$$W(\theta) \sim \cos^2 \theta \tag{12.13}$$

and the mean scattering angle attains a maximum value of 33°, remaining constant upon a further increase in thickness (normal case or total diffusion).

The thickness at which the normal case is reached is called the normal thickness t_n. At some thickness t_r the number of back-scattered electrons (electrons leaving the scatterer on the side of the incident beam) reaches saturation. t_r is the thickness of back-scattering saturation or the thickness of back diffusion.

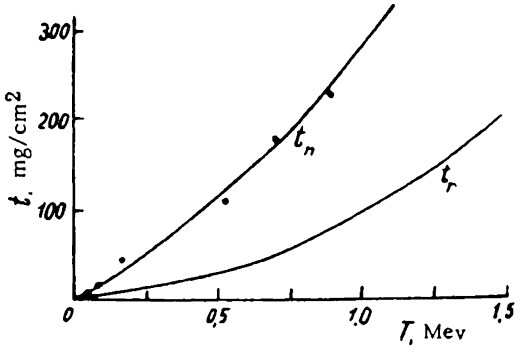

FIGURE 102. Normal thickness t_n and back-diffusion thickness t_r for electrons incident normally to the scatterer. Experimental points for aluminum

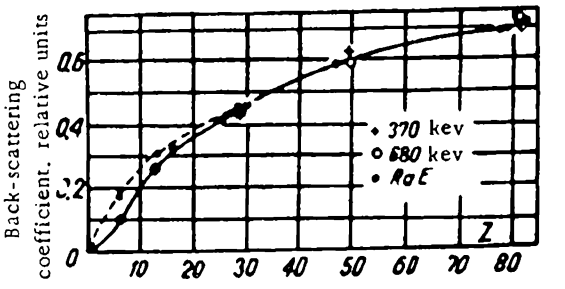

FIGURE 103. Coefficient of back scattering of electrons incident normally on the surface versus the atomic number of the scatterer. The points represent the results at various electron energies.

Figure 102 gives the dependence of the normal diffusion thickness t_n and of the back-diffusion thickness t_r on the energy of the incident electron beam (case of normal incidence of an electron beam on aluminum).

Finally, the curves in Figure 103 give the dependence of the back of scattering coefficient α_N, equal to the ratio of the number of back-scattered electrons in saturation to the number of primary electrons, on the atomic number of the scattering material. The back-scattering coefficient is very weakly dependent on the energy of the electrons, but is determined by the charge of the scatterer. According to Frank /241/, the coefficient of back scattering of electrons on an infinitely thick layer of lead is equal to 36 %, on copper 18 %, and on aluminum 5 % (T = 1-3.2 Mev). For positrons, the back-scattering coefficient is 30-40 % smaller than the corresponding coefficient for electrons (Z = 4 - 90). The energy distribution of the back-scattered electrons was studied by Bothe /185/. The ratio of the mean energy of the scattered electrons to the energy of the incident electrons increases with Z of the scattering medium (Figure 104). For normal incidence, the reflected electrons have a lower energy than for oblique incidence.

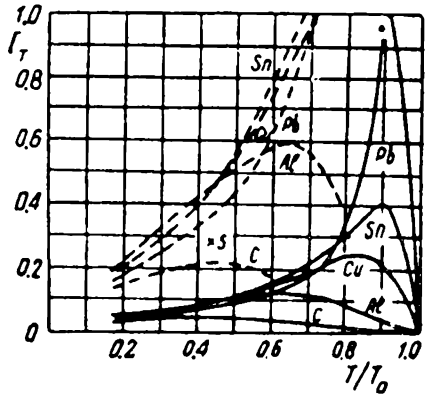

FIGURE 104. Energy distribution of electrons (T_0 = 680 kev), back-scattered by various materials. The broken lines are sections of the curves whose ordinates where increased by a factor of five.

Maximum energy transfer in inelastic collisions of electrons and positrons with atomic electrons. In a collision of identical particles, for example, collision of an electron with an electron, it is impossible to distinguish the scattered electron from the recoil electron. It is therefore usually assumed that the faster electron is the scattered one. Thus, if an electron with an energy T collides with a free stationary electron, the maximum energy transferred is

$$Q_{max} = \frac{T}{2} \equiv \frac{1}{2}(E - mc^2). \tag{13.1}$$

If a fast positron possessing energy Q collides with a free stationary electron, the maximum energy transferred is

$$Q_{max} = T.$$

It occurs in a head-on collision of a positron with an electron.

Cross sections for energy transfer in inelastic collisions. The classical cross section for the transfer of energy Q in the collision of an electron with energy T with a free electron is

$$d\sigma_{cl}(Q) = \sigma_{cl}(Q)\,dQ + \sigma_{cl}(T-Q)\,dQ,$$

where $\sigma_{cl}(Q)$ is determined by formula (2.41) so that

$$d\sigma_{cl} = \frac{2\pi e^4}{mv^2}\frac{dQ}{Q^2}\left[1 + \left(\frac{Q}{T-Q}\right)^2\right] \text{cm}^2/\text{electron}; \tag{13.2}$$

$d\sigma_{cl}$ is numerically equal to the probability of an electron collision as a result of which one electron will possess energy Q, and the other energy $(T-Q)$.

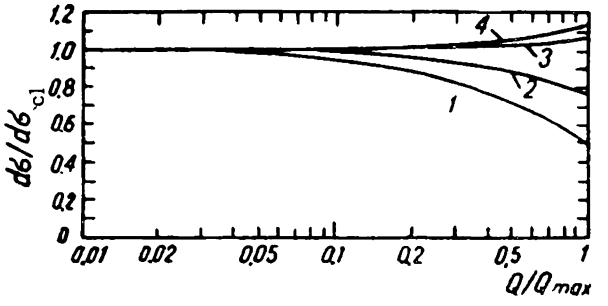

FIGURE 105. Ratio $d\sigma/d\sigma_{cl}$ for electron-electron collisions:

1 — non-relativistic case; 2 — T = 1 Mev; 3 — T = 10 Mev; 4 — highly-relativistic case

The quantum-mechanical expression for the cross section for energy transfer by an electron was obtained by Möller /390/ on the basis of Dirac's theory; it has the form

$$d\sigma = \frac{2\pi e^4}{mv^2}\frac{dQ}{Q^2}\left[1 + \left(\frac{Q}{T-Q}\right)^2 + \left(\frac{\gamma-1}{\gamma}\right)^2 - \frac{2\gamma-1}{\gamma^2}\left(\frac{Q}{T-Q}\right)\right], \tag{13.3}$$

where $\gamma = (1-\beta^2)^{-1/2}$ is the relativistic transformation factor.

In the non-relativistic case, when $T < mc^2$ or $(\gamma - 1) \ll 1$

$$d\sigma = \frac{2\pi e^4}{mv^2}\frac{dQ}{Q^2}\left[1 + \left(\frac{Q}{T-Q}\right)^2 - \left(\frac{Q}{T-Q}\right)\right]. \tag{13.3a}$$

Formula (13.3a) is sometimes referred to as the Mott-Williams formula.

For highly-relativistic electrons ($T \gg mc^2$; $\beta \approx 1$)

$$d\sigma = \frac{2\pi e^4}{mv^2}\frac{dQ}{Q^2}\left(\frac{T}{T-Q}\right)^2\left[1-\frac{Q}{T}+\left(\frac{Q}{T}\right)^2\right]^2. \qquad (13.3b)$$

Figure 105 gives the ratio $\frac{d\sigma}{d\sigma_{cl}}$ for electrons of various energies as a function of $\frac{Q}{Q_{max}}$.

Experimental verification of expressions (13.2) — (13.3b) was carried out in a number of experiments in which a wide electron energy range (0.1-250 Mev) was involved. Unfortunately, due to poor techniques, early studies did not provide a definite answer as to the difference between the classical and quantum-mechanical cross sections.

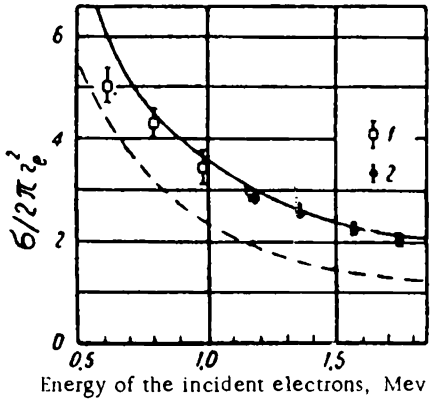

FIGURE 106. Cross section for transfer to the electron of half the initial energy by the quantum-mechanical and classical theories. The solid curve is calculated by Möller's theory, and the broken curve — the same, but neglecting the spin terms

In recent years, thanks to improvements in experimental techniques, the accuracy of measurement was considerably higher. In recent investigations the incident and scattered electrons were analyzed magnetically and a coincidence technique for the elimination of multiple scattering was used; the results were in agreement with (13.3) and they showed that the neglect of the spin terms leads to appreciably smaller cross sections than those obtained experimentally. This is illustrated, for example, by the graph of Figure 106, in which the points represent the experimental cross sections /138/ for transfer to the electron of half the initial energy (in units of $2\pi r_e^2$, where $r_e = \frac{e^2}{mc^2}$ is the classical radius of the electron). The solid curve in this figure was calculated by formula (13.3), the broken curve was calculated without allowance for the spin terms.

The cross section for energy transfer in LS in the collision of a positron with an electron, as a Dirac antiparticle and particle, was found by Bhabha /183/:

$$d\sigma = \frac{2\pi e^4}{mv^2}\frac{dQ}{Q^2}\left\{\left[1-\frac{\gamma^2-1}{\gamma^2}\frac{Q}{T}+\frac{1}{2}\left(\frac{\gamma-1}{\gamma}\right)^2\left(\frac{Q}{T}\right)^2\right]-\right.$$

$$-\left(\frac{\gamma-1}{\gamma+1}\right)\left(\frac{Q}{T}\right)\left[\frac{\gamma+2}{\gamma}-2\frac{\gamma^2-1}{\gamma^2}\left(\frac{Q}{T}\right)+\left(\frac{\gamma-1}{\gamma}\right)^2\left(\frac{Q}{T}\right)^2\right]+$$

$$\left.+\left(\frac{\gamma-1}{\gamma+1}\right)^2\left(\frac{Q}{T}\right)^2\left[\frac{1}{2}+\frac{1}{\gamma}+\frac{3}{2\gamma^2}-\left(\frac{\gamma-1}{\gamma}\right)^2\frac{Q}{T}\left(1-\frac{Q}{T}\right)\right]\right\} =$$

$$= d\sigma_{cl}\left[D+1+A\right]. \qquad (13.4)$$

The term D, the first term in the braces, gives the normal scattering without allowance for exchange effects; the third term in the braces, A, is due to the virtual effect of positron annihilation and formation of new positron-

electron pairs; finally, I gives the interference in phenomena represented by D and A.

In the non-relativistic case ($T \ll mc^2$) the expression in the braces is approximately equal to 1, and the cross section for energy transfer is the same as the classical expression (13.2). In the highly-relativistic case

$$d\sigma = \frac{2\pi e^4}{mv^2}\frac{dQ}{Q^2}\left[1 - \frac{Q}{T} + \left(\frac{Q}{T}\right)^2\right]^2. \qquad (13.4a)$$

Figure 107 gives the ratio $\frac{d\sigma}{d\sigma_{cl}}$ for positrons of various energies as a function of Q/Q_{max}. The role of the quantum-mechanical effects is shown in Figure 108 /424/, which gives the total cross section for energy transfer by 200 Mev positrons according to (13.4) as well as the cross section without allowance for the terms I and A in (13.4). The importance of I and A in the energy transfer cross sections was also noticed in experimental works /138, 308/.

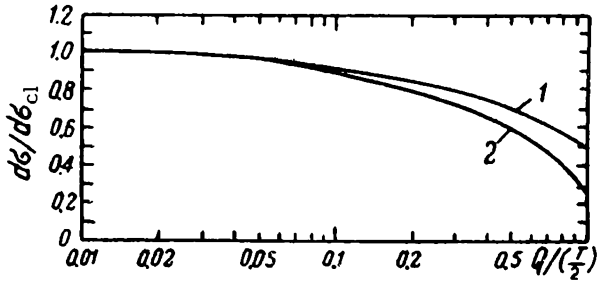

FIGURE 107. The ratio $d\sigma/d\sigma_{cl}$ for positrons according to Bhabha's theory:

1 — non-relativistic case; 2 — highly-relativistic case

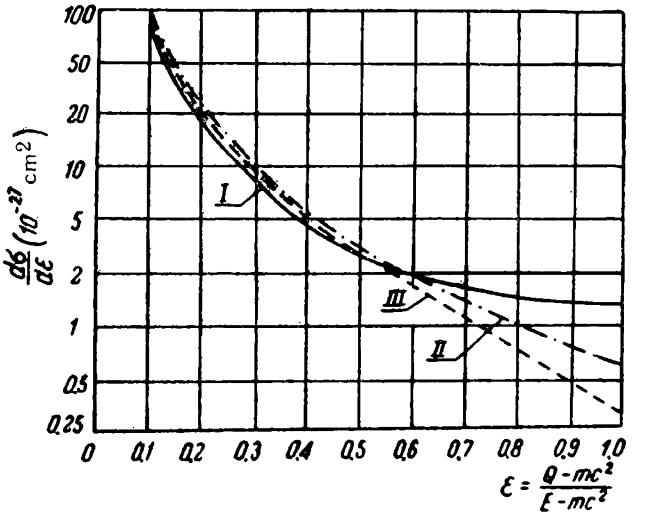

FIGURE 108. Differential cross sections for energy transfer by positrons with E = 200 Mev:

I — positron-electron scattering cross section according to the theory of Bhabha /152/ and Klein-Gordon; II — according to the Klein-Gordon formula without allowance for the annihilation terms.

Ionization energy losses. The ionization energy losses by electrons and positrons are calculated in the same way as the energy losses of heavy particles (§ 4) by (2.44); the calculation is done separately for close ($Q > H$) and for distant ($Q < H$) collisions.

Using formula (13.3) the energy losses by electrons in close collisions are

$$-\left(\frac{dE}{dx}\right)_{Q>H}=\frac{2\pi ne^4}{mv^2}\left[\ln\frac{T}{4H}+1-\frac{2\gamma-1}{\gamma^2}+\frac{1}{8}\left(\frac{\gamma-1}{\gamma}\right)^2\right]. \quad (13.5)$$

For positrons the corresponding expression is

$$-\left(\frac{dE}{dx}\right)_{Q>H}=\frac{2\pi ne^4}{mv^2}\left\{\ln\frac{T}{H}-\frac{\beta^2}{12}\left[11+\frac{14}{\gamma+1}+\frac{10}{(\gamma+1)^2}+\frac{4}{(\gamma+1)^3}\right]\right\}. \quad (13.6)$$

The energy losses in distant collisions for all charged particles, including electrons and positrons, are given in (4.14).

From (13.5) and (4.14), as well as from (13.6) and (4.14), we obtain expressions for the mean ionization energy losses per unit path length of electrons and positrons. For electrons

$$-\left(\frac{dE}{dx}\right)_{\text{ion}}=\frac{2\pi e^4n}{mv^2}\left[\ln\frac{T^2(\gamma+1)}{2I^2}+(1-\beta^2)-\frac{2\gamma-1}{\gamma^2}\ln 2+\frac{1}{8}\left(\frac{\gamma-1}{\gamma}\right)^2\right]; \quad (13.7)$$

for positrons

$$-\left(\frac{dE}{dx}\right)_{\text{ion}}=\frac{2\pi e^4n}{mv^2}\left[\ln\frac{2T^2(\gamma+1)}{I^2}-\frac{\beta^2}{12}\left(23+\frac{14}{\gamma+1}+\frac{10}{(\gamma+1)^2}+\frac{4}{(\gamma+1)^3}\right)\right]. \quad (13.8)$$

If the losses are measured in megaelectronvolts per centimeter, then the factor in front of the square brackets in formulas (13.7) and (13.8) is $0.153\,\rho\left(\frac{Z}{A}\right)\beta^{-2}$, where ρ is the density of the stopping medium (g/cm^3); Z and A are the charge and mass number of the stopping atoms;

$$\beta=\frac{v}{c}.$$

The value of I in (13.7) and (13.8) is the same as in the formulas for the energy losses of heavy charged particles.

In the non-relativistic case, $\beta<0.5$; $(\gamma-1)\ll 1$,

$$-\left(\frac{dE}{dx}\right)_{\text{ion}}=\frac{4\pi e^2n}{mv^2}\ln\frac{1.16mv^2}{2I}, \quad (13.9)$$

or, if $\frac{dE}{dx}$ is expressed in megaelectronvolts per centimeter

$$-\left(\frac{dE}{dx}\right)_{\text{ion}}=0.306\rho\left(\frac{Z}{A}\right)\beta^{-2}\ln\left(\frac{1.16T}{I}\right).$$

Comparing expression (13.9) with the corresponding formula for heavy charged particles (4.20) shows that they differ only by the value of the logarithmic term. This is due to the difference in the reduced masses in the electron-electron and heavy particle-electron systems; as was pointed out above, the maximum energy transferred to the electron is equal to $\frac{1}{4}mv^2$ and not $\frac{1}{2}mv^2$.

The ionization losses of electrons in intermediate and heavy media coincide with the ionization losses of protons of the same velocity to within 10%. Calculated values of the stopping powers of various media relative to air for fast electrons are given in Table 69.

An idea on the magnitudes of the mean ionization energy losses and their dependence on the energy of the incident electrons is given by the curves of Figures 109 and 110, calculated by the above formulas. In these calculations /405/ somewhat underestimated values, $I_{(Al)}$ = 148 ev,

$I_{(Cu)}$ = 310 ev (cf. Table 19), were taken, and no allowance was made for the density effect of the medium (see below). Table 70 gives data on the relative mass stopping powers of various materials for electrons, important for dosimetry /31, 405/.

TABLE 69

Stopping power (per electron) relative to air for fast electrons /446/

T, Mev	Beryllium Be	Polyethylene $(CH_2)_n$	Carbon C	Polystyrene	Lucite	Magnesium Mg	Aluminum Al
0.5	1.036	1.051	1.007	1.038	1.031	0.950	0.946
0.75	1.023	1.038	1.000	1.030	1.022	0.952	0.950
1.0	1.012	1.028	0.992	1.020	1.014	0.951	0.949
1.5	0.997	1.009	0.977	1.003	0.997	0.947	0.944
2.0	0.985	0.995	0.963	0.988	0.982	0.942	0.936
3	0.968	0.976	0.944	0.969	0.963	0.932	0.926
5	0.937	0.948	0.919	0.942	0.937	0.911	0.903
10	0.897	0.911	0.884	0.907	0.901	0.879	0.866
20	0.856	0.879	0.848	0.870	0.865	0.850	0.835
50	0.816	0.830	0.804	0.826	0.821	0.811	0.799
100	0.802	0.815	0.791	0.813	0.808	0.799	0.789

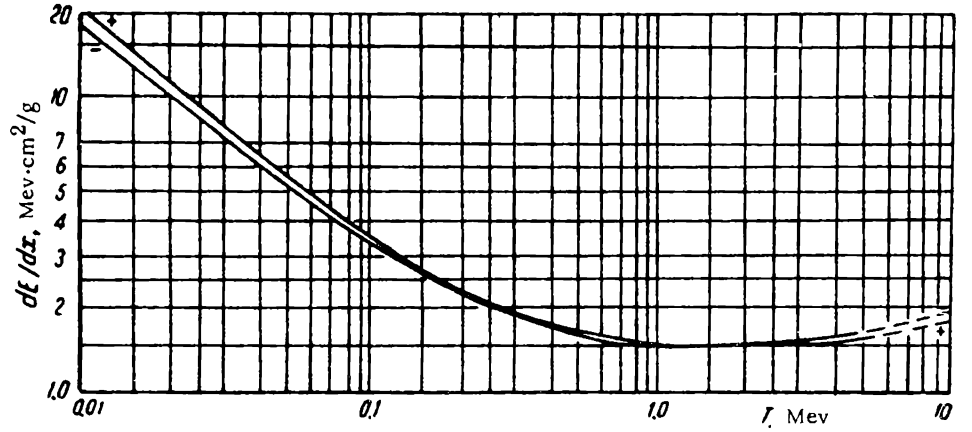

FIGURE 109. Specific energy losses by electrons (—) and by positrons (+) in aluminum according to Nelms' calculations /405/

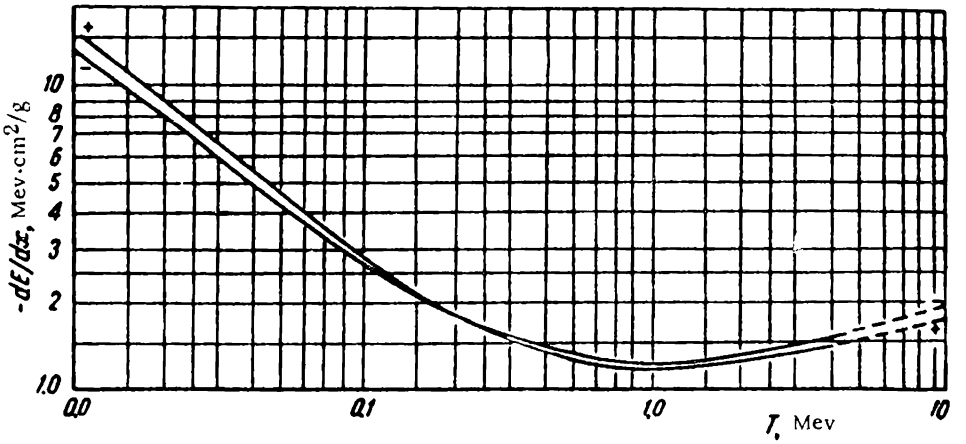

FIGURE 110. Specific energy losses of electrons (—) and positrons (+) in copper according to Nelms /405/

does not exceed

$$\Delta_0 = S_0\left[\ln\frac{2mv^2s_0}{(1-\beta^2)I^2} - \beta^2\right]. \qquad (13.11)$$

In subsequent works, corrections were introduced which take into account multiple scattering /518/, resonance widening of the distribution due to energy losses on strongly bound electrons /191, 192/ and radiation energy losses. The importance of the corrections for the density effect was also shown /277/. The density or polarization effects lead to a displacement of the whole distribution toward smaller energy losses. However, as the polarization effect is connected only with distant collisions in which the energy transfer is small (see § 4), it does not affect the form of the distribution curves in practice; see, for example, Figure 113. In the highly-relativistic case ($v \cong c$), the increase in the energy losses is compensated for by the density effect. In this case

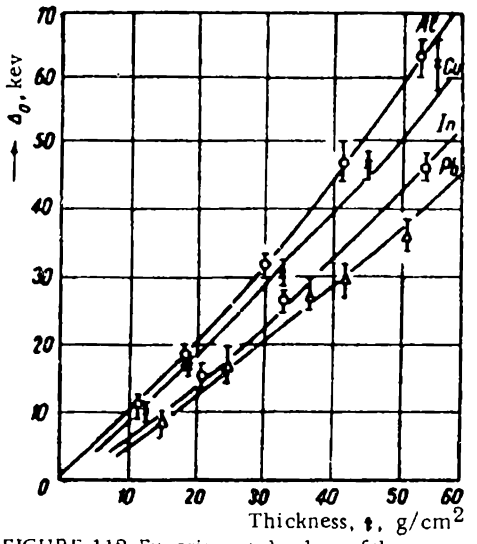

FIGURE 112. Experimental values of the most probable energy losses by 1.414 Mev electrons /352/ as a function of the absorber thickness; the curves are according to Landau's theory (§4)

$$\Delta_{\text{prob}(v=c)} = S_0\left[19.43 + \ln\left(\frac{t}{\rho}\right)\right]_{\text{Mev}}, \qquad (13.12)$$

where t is the absorber thickness (g/cm^2);
ρ is the density (g/cm^3).

The energy loss distribution of positrons was theoretically investigated by Rohrlich and Carlson /430/. It was shown that it is not significantly different from the distribution of the energy losses for electrons /25, 63, 191, 192/.

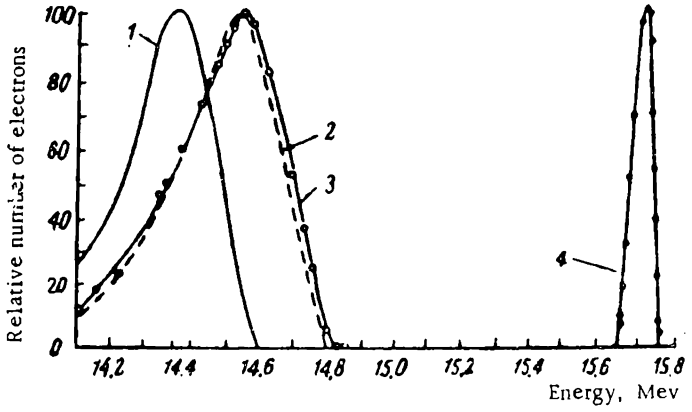

FIGURE 113. Experimental and theoretical distribution curves of the energy losses of electrons passing 0.86 mg/cm^2 of aluminum /278/:

1 — distribution curve according to Landau without allowance for density effect corrections; 2 — the same with correction; 3 — experimental curve; 4 — distribution of electrons in the primary beam.

The energy loss distribution of electrons was measured in many works. The technique of measurement usually consists in a magnetic analysis of

a beam of electrons passing through a foil of the material being investigated (cf. also § 5). The most probable losses are determined from the difference in the values of $B\rho$, for which the maximum detector current at the output of the analyzer is observed, in the absence and in the presence of the foil. The mean energy losses are determined from the displacement of the centers of gravity of the distribution curves of the electrons with and without the foil.

TABLE 70

Mass stopping power of various media relative to air*

T, Mev	S_m (without allowance for the density effect)							S_m (including the density effect)		
	Hydrogen H	Carbon C	Nitrogen N	Oxygen O	Phosphorus P	Calcium Ca	Water H_2O	Carbon C	Water H_2O	Cotton
0.001	3.564	1.079	1.018	0.965	0.692	0.598	1.254	1.079	1.254	1.231
0.002	3.223	1.062	1.014	0.973	0.752	0.685	1.223	1.062	1.223	1.202
0.003	3.084	1.055	1.013	0.976	0.776	0.720	1.211	1.055	1.211	1.190
0.004	3.004	1.051	1.012	0.978	0.791	0.741	1.203	1.051	1.203	1.184
0.005	2.949	1.049	1.011	0.979	0.800	0.755	1.198	1.049	1.198	1.179
0.006	2.904	1.045	1.010	0.979	0.806	0.764	1.193	1.045	1.193	1.174
0.007	2.877	1.045	1.011	0.981	0.813	0.773	1.192	1.045	1.192	1.173
0.008	2.851	1.044	1.010	0.982	0.818	0.780	1.189	1.044	1.189	1.171
0.009	2.830	1.043	1.010	0.982	0.821	0.785	1.118	1.043	1.188	1.169
0.01	2.811	1.042	1.010	0.983	0.825	0.790	1.186	1.042	1.186	1.167
0.02	2.709	1.037	1.009	0.985	0.843	0.816	1.177	1.037	1.177	1.158
0.03	2.661	1.034	1.088	0.986	0.851	0.828	1.172	1.034	1.172	1.154
0.04	2.630	1.033	1.008	0.987	0.857	0.836	1.169	1.033	1.169	1.152
0.05	2.609	1.032	1.008	0.987	0.860	0.841	1.168	1.032	1.168	1.150
0.06	2.592	1.031	1.008	0.988	0.863	0.846	1.166	1.031	1.166	1.148
0.07	2.579	1.030	1.008	0.988	0.866	0.849	1.165	1.030	1.165	1.147
0.08	2.568	1.030	1.007	0.988	0.868	0.852	1.164	1.030	1.164	1.146
0.09	2.559	1.029	1.007	0.988	0.869	0.854	1.163	1.029	1.163	1.146
0.1	2.550	1.029	1.007	0.989	0.871	0.856	1.162	1.029	1.162	1.144
0.2	2.502	1.027	1.007	0.990	0.879	0.869	1.158	1.023	1.158	1.140
0.3	2.476	1.025	1.006	0.990	0.884	0.875	1.155	1.019	1.155	1.138
0.4	2.458	1.024	1.006	0.991	0.887	0.880	1.154	1.014	1.154	1.136
0.5	2.444	1.024	1.006	0.991	0.889	0.883	1.153	1.010	1.152	1.134
0.6	2.433	1.023	1.006	0.991	0.891	0.886	1.152	1.007	1.148	1.130
0.7	2.424	1.023	1.006	0.992	0.893	0.888	1.151	1.003	1.144	1.126
0.8	2.417	1.022	1.006	0.992	0.894	0.890	1.150	1.000	1.140	1.122
0.9	2.410	1.022	1.006	0.992	0.896	0.892	1.150	0.997	1.134	1.116
1.0	2.404	1.022	1.006	0.992	0.897	0.894	1.149	0.994	1.133	1.115
2	2.366	1.020	1.005	0.993	0.903	0.903	1.146	0.971	1.105	1.088
3	2.347	1.019	1.005	0.993	0.907	0.908	1.144	0.954	1.086	1.069
4	2.333	1.018	1.005	0.994	0.909	0.912	1.143	0.942	1.071	1.054
5	2.324	1.018	1.005	0.994	0.911	0.914	1.142	0.932	1.059	1.042
6	2.316	1.017	1.005	0.994	0.912	0.916	1.141	0.923	1.049	1.032
8	2.305	1.017	1.005	0.994	0.914	0.919	1.140	0.909	1.032	1.016
10	2.297	1.016	1.004	0.995	0.916	0.921	1.139	0.898	1.019	1.003

* The mean excitation potentials I were assumed equal to $13Z$.

The experimental data on the spread in the energy losses by electrons, obtained until 1950, are considered, for example, in /166, 209/. We shall only discuss the more recent experimental investigations.

Studies on the spread in the energy losses for electrons with energies below 2 Mev /351, 353, 130, 310/ have shown that the measured values of the most probable energy losses by electrons in thin foils of materials from beryllium to lead are in agreement with those calculated by Landau's theory (see, for example, the experimental curve of Figure 112 from /351/). However, it was noted /351, 130/ that for heavy media the experimental distribution of the energy losses is considerably wider than the theoretical distribution.

Reich et al. /419, 420/ measured the energy loss distributions for electrons with energies of 2.8 and 4.7 Mev in foils of beryllium, carbon, iron and lead.

Results of investigations taking into account the corrections introduced by Blunck and Leisegang /191, 192/ were in good agreement with Landau's theory.

The necessity to take into account corrections for the density effect was confirmed by the measurements of Goldwasser et al. /277/. They studied the distribution of electrons with an initial energy of 15.7 Mev passing through gaseous absorbers as well as through their solid (polymerized) phases. In one case the distributions of electrons passing through the gas F_2C and its polymer Teflon (polytetrafluoroethylene) were compared. The measured probable energy losses of electrons in gases were in agreement with Landau's theory (without corrections for the density), and in polymers they were smaller by an amount equal to the correction for the density effect (see above). Goldwasser et al. /277/ have also shown that the most probable energy losses by electrons (T = 9.6 and 15.7 Mev) in light media (beryllium, aluminum, copper, polyethylene) are in agreement with those calculated by Landau's theory, if the correction for the density effect and the bremsstrahlung are taken into account. As an example, Figure 113 gives the experimental curves of the electron energy distribution before and after passing through an aluminum foil of 0.86 mg/cm^2 thickness, obtained in this work. This figure also gives the theoretical curves of Landau without corrections (solid curve) and with corrections (broken curve) for the density.

Similar results were obtained by Grishaev et al. /36/ who studied the energy losses by 18 Mev electrons.

Ziegler /519/ and Hudson /304/ investigated the energy distribution of high—energy electrons, passing through foils of light media. The measured and the theoretical results are given in Tables 71 and 72. These tables show the mean and most probable energy losses by fast electrons and the influence of the density effect and the radiation energy losses (§ 14) on the spread of the energy losses. The most probable energy losses in lithium, beryllium, carbon and aluminum are in agreement with the calculated losses. The width of the experimental distributions was 7-15% larger than that of the theoretical distributions.

Hall, Hanson and Jamnik /306/ measured, for the purpose of assessing the adequacy of the Landau theory for heavy stopping media, the most probable energy losses in a wide energy range (T = 3.4-19.4 Mev) and for a large number of stopping media (from aluminum to uranium). The technique of measurement was the usual one (magnetic analysis), and a Cerenkov counter (§ 9) served as a detector at the output of the spectrometer, which substantially reduced the background. The investigations have shown that the experimental curves are in satisfactory agreement with the theoretical curves (according to Landau) when allowance is made for density corrections, multiple scattering, radiation and the resonance broadening effect /191, 192/.

TABLE 71

Experimental and calculated values of the mean and most probable energy losses for 32 Mev electrons /519/

Loss characteristics, Mev·cm²/g	Beryllium, Be	Carbon, C	Aluminum, Al
$\varepsilon_m^{\text{total}} = \frac{dE}{\rho dx}$, experimental	2.0 ± 0.06	2.4 ± 0.11	—
$\varepsilon_m^{\text{rad}}$, theoretical	0.35	0.54	—
$\varepsilon_m^{\text{ion}}$, theoretical	1.66	1.87	—
$\Delta_0 = \frac{1}{\rho}\left(\frac{dE}{dx}\right)_{\text{prob}}$ experimental	1.25 ± 0.04	1.4 ± 0.042	1.6 ± 0.08
Δ_0, theoretical	1.25	1.5	1.35
Γ, experimental	0.32 ± 0.0016	0.34 ± 0.0017	0.47 ± 0.05
Γ, theoretical	0.27	0.30	0.30

TABLE 72

Experimental and calculated values of the most probable energy losses for 150 Mev electrons /304/

Target characteristics	Lithium, Li	Beryllium, Be	Carbon, C	Aluminum, Al
Target thickness, g/cm²	2.715	2.380	1.820	2.575
Experimental value of Δ_0, Mev	3.78 ± 0.12	3.16 ± 0.10	2.78 ± 0.09	3.83 ± 0.12
Theoretical value of Δ_0, Mev, including corrections for the density effect and for the radiation *	3.82	3.22	2.77	3.77
Experimental value of Γ (% of Δ_0), total width of the distribution at half height. .	23.8 ± 1.2	25.9 ± 1.3	29.0 ± 1.5	30.0 ± 1.0
Theoretical value of Γ including the correction for the density effect and for radiation *	21.4	22.9	25.1	28.2

* Corrections for the density effect were made according to Sternheimer /446/ and the mean ionization potentials were taken according to Coldwell /216/, see Table 19.

§ 14. Radiation energy losses. Total energy lost by an electron

Bremsstrahlung radiation. As a result of collisions with the nuclei of the stopping medium, an electron deviates from its initial direction of motion and may lose a part of its energy as radiation.

A charged particle, when accelerated, radiates electromagnetic energy. The acceleration of a particle with charge ze in the field of a nucleus with charge Ze and mass M is proportional to $\frac{zZe^2}{M}$. The radiation

intensity is proportional to the square of the acceleration, i.e., it is proportional to $\frac{Z^2 z^2}{M^2}$.

Thus, under otherwise identical conditions, the electromagnetic radiation losses are $3 \cdot 10^6$ times as much for an electron as for a proton. The radiation losses of heavy charged particles ($M \gg m$) are negligibly small compared with the ionization losses. However, for electrons, particularly of high energies ($T > 1$ Mev), moving in heavy media, the radiation losses amount to a considerable fraction of the total energy losses.

TABLE 73

Radiation length X_0 and critical energy E_{cr} for various media [20, 30, 14]

Medium	Z	x	X_0, g cm^{-2}	E_{cr}, Mev
Hydrogen, H	1	1.39	58	340
Helium, He	2	1.37	85	220
Carbon, C	6	1.32	42.5 (40)	103
Nitrogen, N	7	1.31	38 (35.4)	87
Oxygen, O	8	1.30	34.2 (32.1)	77
Aluminum, Al	13	1.28	23.9 (22.7)	47
Argon, A	18	1.26	19.4 (18)	34.5
Iron, Fe	26	1.24	13.8 (12.5)	24
Copper, Cu	29	1.23	12.8 (11.5)	21.5
Lead, Pb	82	1.16	5.8 (5.24)	6.9
Air	—	—	36.5 (34.2)	83
Water, H_2O	—	—	35.9 (33.9)	93

Remark. The values of X_0, indicated in parentheses, were obtained [14] with allowance for screening from the experimental data on the atomic form-factor (scattering of X-rays).

As will be seen in the following, in contrast to ionization losses which depend linearly on Z (the atomic number of the stopping medium), the radiation losses vary as Z^2. The dependence of the radiation losses on the energy is different from that of the ionization losses. Whereas the latter (see Figures 109-110) decrease with increasing energy for $T \leqslant 3\ mc^2$ and increas as $\ln T$ or more slowly for $T > 3\ mc^2$ (taking into account the polarization effect), the radiation losses for $T \leqslant mc^2$ are practically independent of the energy, and for $T \gg mc^2$ increase rapidly and almost linearly with the energy.

At high electron energies radiation losses are dominant. The electron energy at which the ionization and radiation energy losses are equal is called the critical energy E_{cr}. E_{cr} is some characteristic constant of the stopping medium (see Table 73).

The bremsstrahlung spectrum is continuous, the maximum energy of the bremsstrahlung quantum being equal to the initial kinetic energy of the electron

$$h\nu_{max} = T = E - mc^2, \tag{14.1}$$

where E is the total energy of the electron.

In the general case it is necessary to take into account the deceleration of the electrons in the field of the atomic electrons. This effect, as we shall see, is Z times weaker than the deceleration in the nuclear field.

Effective cross section for bremsstrahlung of electrons in the nuclear field. In the Born approximation, i.e., when condition (2.42) is fulfilled, the differential cross section for the emission by an electron with energy E of a bremsstrahlung quantum with an energy between $Q = h\nu$ and $Q + dQ$, according to /30, 92, 152/, is equal to

$$\sigma_{rad}(E, Q)\,dQ = 4\bar{\sigma}\frac{dQ}{Q}F(E, \eta), \tag{14.2}$$

where

$$\bar{\sigma} = Z^2\left(\frac{2\pi e^2}{hc}\right)\left(\frac{e^2}{mc^2}\right)^2 = 0.580\,Z^2\,\text{mbarn/nucleus}; \tag{14.3}$$

$F(E, \eta)$ being a slowly varying function of the initial total energy of the electron E and of the quantity $\eta = \frac{Q}{E}$.

Formula (14.2) is valid if the condition $E \gg mc^2$ is satisfied, the form of the function $F(E, \eta)$ depending on the parameter

$$\gamma = 100\frac{mc^2}{E}\frac{Q}{(E-Q)}Z^{-1/3} = 100\frac{mc^2}{E}\frac{\eta}{1-\eta}Z^{-1/3}, \tag{14.4}$$

representing the screening of the nucleus by the atomic electrons (§ 2). This parameter is proportional to the ratio of the radius a of the atom to the effective distance r from the nucleus at which the radiation event takes place. In fact, it follows from the uncertainty principle that

$$r \sim \frac{h}{2\pi q},$$

where q is the minimum momentum transferred to the nucleus in collisions.

In accordance with the conservation laws

$$q \cong \frac{1}{2}\left(\frac{mc^2}{E}\right)\left(\frac{Q}{E-Q}\right)mc$$

and, consequently,

$$r \sim \frac{h}{mc2\pi}\frac{E(E-Q)}{mc^2Q}.$$

On the other hand, the radius of the atom in the Thomas-Fermi model is determined thus:

$$a = a_0 Z^{-1/3},$$

where

$$a_0 = 137\left(\frac{h}{2\pi mc}\right).$$

Thus, γ is equal to

$$\gamma = \frac{a}{r} = 137\left(\frac{mc^2}{E}\right)\left(\frac{Q}{E-Q}\right)Z^{-1/3},$$

i.e., practically the same as (14.4).

For $\gamma = \frac{a}{r} \gg 1$, i.e., for effective radiation distances much smaller than the radius of the atom, the screening may be neglected.

For $\gamma \ll 1$, the variation of the momentum of the electron occurs far from the nucleus and the screening is large. The case $\gamma = 0$ corresponds to the so-called total screening.

The values of the function $F(E, \eta)$ for various values of the parameter γ were determined by Bethe and Heitler /156/.

In the absence of screening $(\gamma \gg 1)$

$$F(E, \eta) = \left[1 + (1-\eta)^2 - \frac{2}{3}(1-\eta)\right]\left[\ln \frac{2E}{mc^2}\frac{1-\eta}{\eta} - \frac{1}{2}\right]; \quad (14.5)$$

with full screening $(\gamma = 0)$

$$F(E, \eta) = \left[1 + (1-\eta)^2 - \frac{2}{3}(1-\eta)\right] \ln 183 Z^{-1/3} + \frac{1}{9}(1-\eta); \quad (14.6)$$

in the intermediate case $(\gamma < 2)$

$$F(E, \eta) = \left[1 + (1-\eta)^2\right]\left[\frac{f_1(\gamma)}{4} - \frac{1}{3}\ln Z\right] - \\ - \frac{2}{3}(1-\eta)\left[\frac{f_2(\gamma)}{4} - \frac{1}{3}\ln Z\right]; \quad (14.7)$$

in the intermediate case $(2 < \gamma < 15)$

$$F(E, \eta) = \left[1 + (1-\eta)^2 - \frac{2}{3}(1-\eta)\right]\left[\ln\left(\frac{2E}{mc^2}\frac{1-\eta}{\eta} - \right.\right. \\ \left.\left. - \frac{1}{2} - c(\gamma)^{-1/2}\right)\right]. \quad (14.8)$$

The numerical values of the functions $f_1(\gamma)$, $f_2(\gamma)$ and $c(\gamma)$ can be determined from the curves of Figure 114 and from Table 74.

As follows from the above formulas, the effect of the screening is displayed in the decrease of the emission probability of low-energy quanta as compared with the probability of the emission of high-energy quanta. In the case of full screening $(\gamma = 0)$, the cross section for the emission of a bremsstrahlung quantum is a function of $\frac{E-Q}{Q}$ only, i.e., the probability of the loss of a given part of the initial energy is independent of this energy.

As an example of the use of expressions (14.6), (14.7), (14.8), Figure 115 shows calculated curves of the dependence of the bremsstrahlung intensity, emitted in various media by electrons with an initial energy of 16.93 Mev, on Q /373/. Curve 1 corresponds to stopping in the absence of screening; in this case the quantity $\frac{Q\sigma(E, Q)}{4\sigma}$ is independent of Z. Curves 2 and 3 represent the distribution of the bremsstrahlung quanta in the passage of electrons in beryllium and gold with allowance for the screening. As the initial energy of the electrons increases, the plateau on the curves becomes more clearly pronounced.

For the weak relativistic case $(T \sim mc^2)$, the cross section for bremsstrahlung cannot be represented analytically.

In the non-relativistic case $(T < mc^2)$, the cross section for the emission of a photon in the Born approximation is

$$\sigma_{rad} = \frac{8}{3}\bar{\sigma}\left(\frac{\mu}{k}\right)\ln\frac{(\sqrt{T} + \sqrt{T-k})^2}{k}, \quad (14.9)$$

where $k = \frac{Q}{\mu}$; $T = E - \mu$; $\mu = mc^2$.

However, in the stopping of slow electrons, the condition of the Born approximation is not fulfilled. This is equally applicable to heavy stopping media.

TABLE 74

Numerical values of the function $c(\gamma)$, involved in formula (14.8), according to Bethe and Heitler /187/

γ	2	2.5	3	4	5	6	8	10	15
$c(\gamma)$	0.21	0.16	0.13	0.09	0.065	0.05	0.03	0.02	0.01

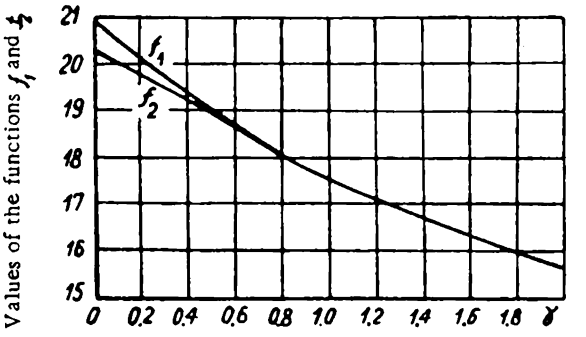

FIGURE 114. Graphs of the functions $f_1(\gamma)$ and $f_2(\gamma)$ involved in formula (14.7) /187/

The works /104, 392/ are devoted to a theoretical study of the bremsstrahlung of high-energy electrons. The results of calculations by Migdal /392/ for low energies agree with the results of Bethe and Heitler.

In Curtiss' work /215/ it is shown that for stopping of 63 Mev electrons in lead, the form of the spectrum of the bremsstrahlung is given by the formulas of Bethe and Heitler, but the absolute values of the cross sections are 7-8% smaller than the theoretical ones. Motz /397/ investigated the cross sections of electrons with energies of 0.5-1 Mev in beryllium, aluminum and gold and showed that in this case the Bethe-Heitler theory gives underestimated values.

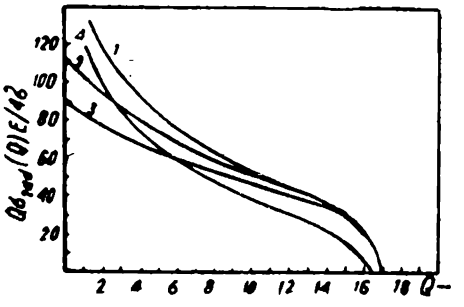

FIGURE 115. Bremsstrahlung intensity as a function of the energy of the photons created by 16.93 Mev electrons /373/:

1—for unscreened nuclei; 2—for beryllium, taking into account the screening; 3—for gold, taking into account the screening; 4—electron-electron collisions.

Radiation in the field of atomic electrons. Expressions (14.5) — (14.8) do not take into account the radiation appearing upon stopping in the field of the atomic electrons /67/. At high incident electron energies, the effective cross section for bremsstrahlung in the field of an atomic electron is almost the same as in the field of a nucleus of $Z = 1$. If $\gamma \gg 1$, the contribution of the radiation in the field of the electrons is given by (14.5), replacing Z^2 by Z, and the total cross section for bremsstrahlung is proportional to

$Z^2 + Z = Z(Z+1)$. In this case, the intensity of the bremsstrahlung which originates in the field of the nuclei is Z times higher than the intensity of the radiation originating in the field of the atomic electrons /66, 67, 84/. If the energy of the electrons is high, but $\gamma \approx 0$ (complete screening), the relative intensity of the bremsstrahlung produced in the field of the electrons increases to $\frac{x}{Z}$ - the fraction of the radiation in the nuclear field, where $x = 1.4$, 1.29 and 1.14 for $Z = 1.10$ and 92, respectively /517/; see also Table 73.

For low incident electron energies ($E \sim mc^2$), the probability of bremsstrahlung in the field of the atomic electrons is very small ($x \ll 1$).

Mean energy losses in bremsstrahlung. The mean energy losses upon the passage of electrons through a layer of thickness dx is

$$-\left(\frac{dE}{dx}\right)_{rad} = N\int_0^T Q_\sigma(E, Q)\,dQ = NE\varphi_{rad}, \tag{14.10}$$

where N is the number of atoms per 1 cm^3;

$$\varphi_{rad} = \frac{1}{E}\int Q_\sigma(E, Q)\,dQ \tag{14.11}$$

is the effective cross section for radiational energy losses.

For the highly-relativistic case in the absence of screening, i.e., when the following conditions are fulfilled

$$mc^2 < E < 137\,mc^2 Z^{-1/3},$$

the cross section for radiation losses is equal to

$$\varphi_{rad} = 4\bar{\sigma}\left(\ln\frac{2E}{mc^2} - \frac{1}{3}\right). \tag{14.12}$$

In the other highly-relativistic case taking into account complete screening ($E > 137mc^2 Z^{-1/3}$)

$$\varphi_{rad} = 4\bar{\sigma}\left(\ln 183\, Z^{-1/3} + \frac{1}{18}\right). \tag{14.13}$$

To take into account the radiation losses in the field of the atomic electrons, one has to use the value of $\bar{\sigma}$, in expressions (14.12) and (14.13), calculated by formula (14.3), in which Z^2 was replaced by $Z(Z+x)$, where in the first case $x = 1$, and in the second case $x > 1$ (see above).

In the non-relativistic case and in a pure coulomb field

$$\varphi_{rad} = \frac{16}{3}\bar{\sigma}. \tag{14.14}$$

It follows from these expressions that for low incident electron energies the effective cross sections for radiation losses are independent of the energy of the electrons and the mean losses are constant. For very high energies, the effective cross section for radiation losses increases as

ln E, and $\left(\frac{dE}{dx}\right)_{rad} \sim E \ln E$, if we disregard the screening, and it is independent of the energy, if we take the screening into account.

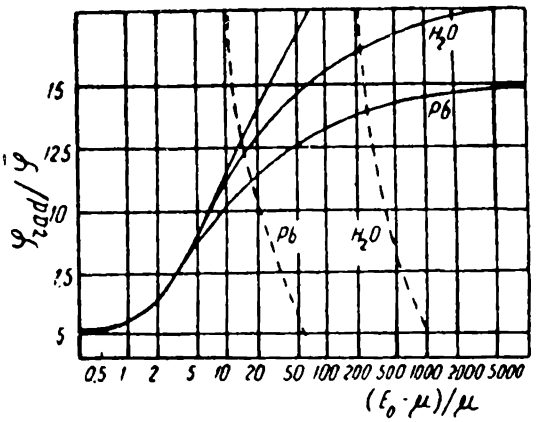

FIGURE 116. Effective cross section φ_{rad} for radiation energy losses by an electron in the Born approximation /30/. The straight section of the solid line at high energies was obtained without taking the screening into account and is valid for all media. The broken curves give the energy losses in inelastic collisions in the same units

This is demonstrated by the curves of Figure 116 /30/. In this figure the broken curves represent the theoretical dependence of the ionization energy losses on the energy (see above).

Radiation length and critical energy. In investigations of bremsstrahlung the so-called radiation or avalanche length unit X_0 is used. It is defined as the distance along which a fast electron loses $1/e$ of its energy. In accordance with formula (14.13), the radiation length unit is determined as*:

$$\frac{1}{X_0} = 4N\bar{\sigma} \ln (183 Z^{-1/3}). \tag{14.15}$$

Thus, for high-energy electrons, the mean relative radiation energy losses for total screening are given by

$$-\frac{1}{E}\left(\frac{dE}{dx}\right)_{rad} = \frac{1}{X_0}(1+b), \tag{14.16}$$

where $b = (18 \ln 183Z)^{-1}$ is a quantity whose mean value varies from 0.012 for air (Z = 7.3) to 0.015 for lead (Z = 82).

Values of x and X_0 for various media are given in Table 73. The values of E_{cr}, given in this table, correspond to those electron energies for which the losses per unit path length from ionizing collisions are equal to the radiation losses.

According to /150/

$$E_{cr} \cong \frac{1600\, mc^2}{Z} \tag{14.17}$$

* In calculating $\bar{\sigma}$, it is necessary to take $Z(Z+x)$ instead of Z^2, where x is a coefficient representing the contribution of the radiation in the electron field (see above).

and

$$\frac{\left(\frac{dE}{dx}\right)_{\text{rad}}}{\left(\frac{dE}{dx}\right)_{\text{ion}}} = \frac{EZ}{1600\,mc^2}, \tag{14.18}$$

where E is the total energy of the electrons;

Z is the atomic number of the stopping medium.

The total energy losses per unit path length are

$$-\left(\frac{dE}{dx}\right) = \left(-\frac{dE}{dx}\right)_{\text{ion}} + \left(-\frac{dE}{dx}\right)_{\text{rad}}. \tag{14.19}$$

TABLE 75

Calculated values of the total energy losses per unit path length for fast electrons in units of mc^2 /30/

$\frac{T}{mc^2}$	0.01	0.1	1	10	10^2	10^3	10^4
Air (normal conditions) .	0.0845	0.0145	0.0046	0.0049	0.0087	0.039	0.33
Water, H_2O	78	13.1	4.08	4.00	6.56	29.6	262
Aluminum, Al	147	26.9	8.65	8.98	19.1	116	1.095
Lead, Pb	255	64.5	24.5	40.5	204	1.910	19.30

The theoretical values of the total energy losses by electrons per unit path length in various stopping media are given in Table 75. In the calculations /30/, the contribution to the stopping of the atomic electrons was roughly taken into account by adding $0.8\,\sigma_{\text{rad}}/Z$ to the stopping by the nuclei.

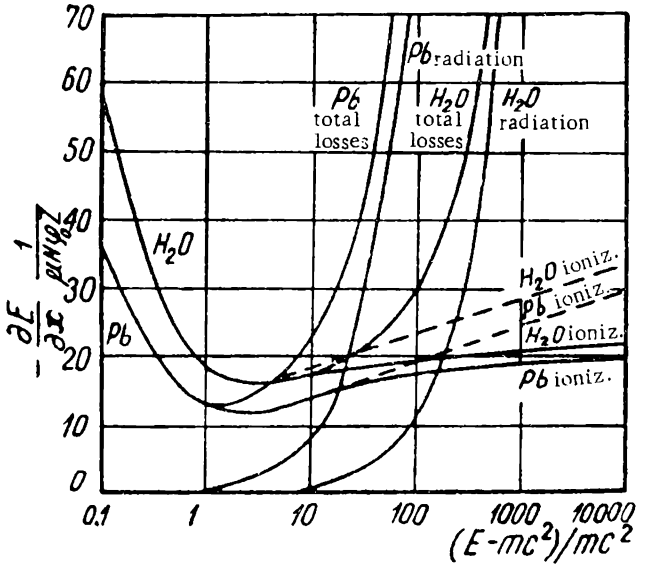

FIGURE 117. Mean energy losses by electrons in water and lead in units of $N\rho_0 Z\mu$ as a function of the kinetic energy of the electrons /30/. The broken curves — neglecting the density effect, the solid curves — taking the density effect into account

Figure 117 gives the theoretical dependence of the total ionization and radiation energy losses per unit path length on the energy of the electrons in water and lead. As can be seen from Figure 117 and Table 75, the energy losses in air and water for $E \gg 100$ Mev and in lead for $E \gg 10$ Mev are mainly due to bremsstrahlung. For $E \approx 10$ Mev the radiation and ionization energy losses in lead are equal; the total energy loss per 1 mm of electron path in lead is then ≈ 3.2 Mev.

Bremsstrahlung in thick targets. The spectral and angular distributions of the bremsstrahlung in thin targets were calculated by Bethe et al. /210/; see also /20/. Calculations of practical interest of the spectral distribution for thick targets, taking into account multiple scattering, were performed by Schiff /468/. Figure 118 shows curves, obtained according to Schiff's calculations, of the spectral distribution of photons formed upon the braking of 16 Mev electrons in a thick tungsten target.

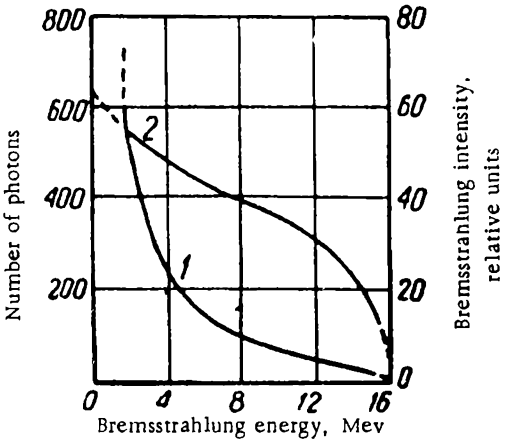

FIGURE 118. Spectral distribution of bremsstrahlung formed in a thick tungsten target bombarded by electrons:

1 — number of photons; 2 — bremsstrahlung intensity

Estimates /235/ of the mean energy fraction of the incident electrons used in forming the bremsstrahlung in thick targets are given in the following. This fraction for monoenergetic electrons with E up to 2.5 Mev is equal to $\approx 0.0007\ ZE$, i.e., amounts to $\approx 1\%$ for 500 kev electrons stopped in copper. For electrons of a continuous spectrum (beta-electrons) this fraction is equal to $\approx \frac{Z}{3000} E_0$, where E_0 is the maximum energy of the spectrum.

§ 15. Relationship between range and energy of electrons

With the appropriate reservations, the concept of electron range is meaningful if the ionization collisons are an important factor in the stopping process. In this case, according to formula (13.9),

$$\frac{dE}{dx} \approx \left(\frac{dE}{dx}\right)_{\text{ion}} \sim T^{-2} \text{ and } R \sim T^2,$$

where T is the kinetic energy of the electron.

At very high electron energies, when the main energy losses are radiational ($E>100\ mc^2$), we have according to § 14,

$$\frac{dE}{dx}\cong\left(\frac{dE}{dx}\right)_{\text{rad}}\sim E \text{ and } R(E)\sim \ln E;$$

in this case the range increases with energy faster in light media.

In this section we shall mainly consider those cases in which ionization losses are important.

In the study of the passage of an electron through matter, one should distinguish between its true path length L and its range R, i. e., the projection of the total true path on the direction of the initial motion (Figure 119). Due to the large statistical fluctuations of the energy losses in single collisions and to the importance of multiple scattering (§ 12), the true path lengths and the ranges of individual electrons with the same energy may differ greatly. In analogy with the description of the passage of heavy particles through matter (§ 2), here also one may use the concepts of the mean true path L of the electrons and their mean range S, as well as the corresponding values of the path straggling and spread. However, because of the complex character of the interaction of electrons with matter, the theoretical determination of these quantities and the relation between them are complicated.

It is important to realize that the mean true path length of electrons in a medium is 1.5-4 times their mean range. This ratio is higher the heavier the medium and the lower the energy of the electrons. In light media the scattering is weaker, but here, too, it is of importance for electron energies < 100 kev. In this case the electron range differs considerably from the path traversed by them.

The true path lengths of electrons can be measured directly in a cloud chamber, with a scintillation counter or in a photoemulsion. From the distribution of the true path lengths determined from these measurements it is possible to determine the mean path length L and to compare it with the theoretical value calculated by formula (4.45), in which $\frac{dT}{dx}$ is the total specific energy loss.

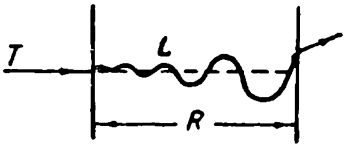

FIGURE 119. Schematic description of the true path length and the range of electrons in a medium

As a rule, the range of electrons is determined from the experimental transmission curves of electrons in the medium. The transmission curve gives the number of electrons which pass various absorber thicknesses as a function of the thickness. The transmission curve for monoenergetic electrons is shown schematically in Figure 120. It is characterized by the presence of a linear part on the fall-off section. The final sloping section of the curve intersects the distance axis at the point R_m which is called the maximum electron range. However, the accuracy of the determination of this quantity is poor, and its value for an electron beam of a given energy depends on the experimental conditions, i. e., the collimation of the beam, the sensitivity of the detecting device, the background level, the relative positions of the source and absorber, etc. Therefore, each individual experiment provides only an approximate value of R_m. Thus, R_m is determined as the maximum measured range, but is limited by the experimental

conditions. A more accurate value, dependent on the experimental conditions, is the extrapolated range R_0, which is determined by the intersection of the linear section of the transmission curve with the abscissa. R_0 is sometimes called the practical range. The extrapolated range in a sufficiently thick sample is almost independent of the mutual position of the source, detector and absorber. The reason for this is that after a sufficiently large number of scattering events the angular distribution is determined by diffusion, so that the mean scattering angle is independent of the angle (see §12). However, the other experimental conditions have a significant effect on the measured value of R_0. This should be borne in mind when comparing values obtained by various authors.

Finally, the concept of the mean range R_d is sometimes used; it is defined as the absorber thickness which absorbs half the incident electron beam.

The absorption curve of electrons having a continuous spectrum (e.g., beta-particles) differs considerably (Figure 121) from that of monoenergetic electrons. The curve of Figure 121 is bent toward the abscissa and does not have a clear linear section. The determination of the extrapolated range from this curve is difficult. Usually special analytical methods are used for curves of this kind /251, 188/.

Range—energy relation of monoenergetic electrons in aluminum. Aluminum is used as a standard stopping medium in experiments on the range of electrons. Figure 122 gives the absorption curves of monoenergetic electrons with energies of 427-1696 kev in aluminum /391/. The absorption curves for electrons of different energies (Figure 122) are similar and have well-pronounced linear sections, whose extrapolation makes it possible to determine R_0.

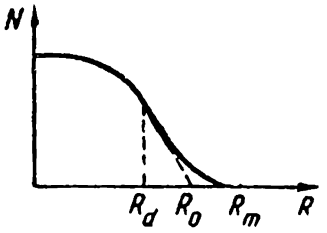

FIGURE 120. Schematic absorption curve of monoenergetic electrons in lead

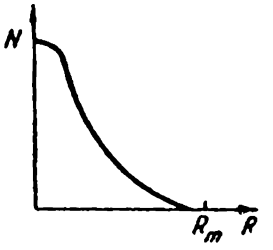

FIGURE 121. Schematic absorption curve of a continuous electron spectrum in matter

Figure 123 shows experimental absorption curves of electrons with energies from 3.70 to 11.85 Mev in aluminum /299/. The curves are normalized to the extrapolated range, and the intensity is given in arbitrary units.

The values of R_0 for aluminum satisfy the following empirical relationship for $T > 0.6$ Mev:

$$R_0(\text{g/cm}^2) = 0.526\ T(\text{Mev}) - 0.094. \qquad (15.1)$$

Numerous results of extrapolated ranges of low-energy electrons in aluminum were analyzed by Katz and Penfold /350/. The result of this analysis is shown by the solid curve of Figure 124. The points in this

figure represent the data of various measurements. The solid curve can be represented analytically by the formula

$$R = 0.412\ T^{(1.265-0.0954 \log T)}, \qquad (15.2)$$

which relates the extrapolated range in aluminum to the electron energy in the range 0.01-2.5 Mev.

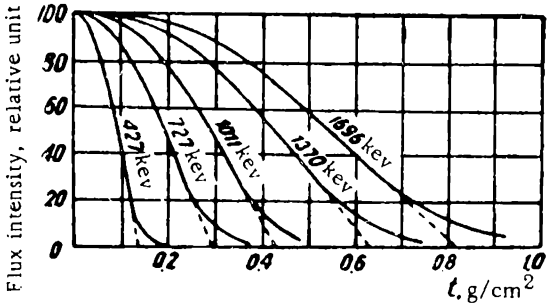

FIGURE 122. Absorption curves of monoenergetic electrons with energies of 0.4-1.7 Mev in aluminum /391/

The broken curve in Figure 124, corresponding to

$$R_0(\text{mg/cm}^2) = 0.5307\,(\text{Mev}) - 0.106, \qquad (15.3)$$

satisfies the experimental data for $T > 2.5$ Mev. The difference between the extrapolated ranges according to (15.1) and (15.3) is within the limits of experimental error. According to measurements /193/, for electrons with energies from 10 to 23 Mev the range in aluminum can be expressed by

$$R_m(\text{cm}) = 0.246\ E\ (\text{Mev}). \qquad (15.4)$$

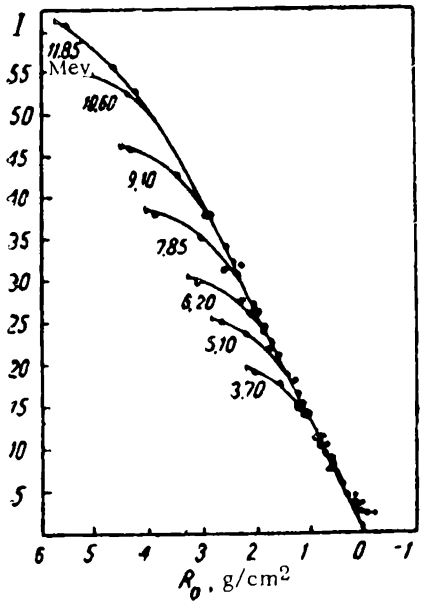

FIGURE 123. Absorption curves of monoenergetic electrons with energies of 3.7-11.9 Mev in aluminum /299, 300/

Whereas the experimental data on the ranges of electrons with energies higher than 100 kev agree with one another, they are quite contradictory for electron energies $T \leqslant 100$ kev. This is mainly due to the differences in the methods, and consequently, to the difference in the physical meaning of the ranges determined; the experimental difficulties in these investigations are also significant.

Feldman /250/ gives the results of systematic measurements of the practical maximum range of electrons with energies of up to 10 kev in various media. The measured ranges satisfy the formula

$$R_{mp}(\text{Å}) = 250\,\frac{A}{\rho}\left(\frac{T(\text{kev})}{Z^{1/2}}\right)^n, \qquad (15.5)$$

where

$$n = \frac{1.2}{1 - 0.29 \log_{10} Z};$$

A, Z are the mass number and nuclear charge of the stopping atoms;
ρ is the density.

For aluminum, in particular, the range—energy relation for T = 10 kev is given by

$$R_{m\rho}(\text{Å}) = 260\ T^{1.7}_{(\text{kev})} \tag{15.6}$$

It was pointed out in this work that the experimental values of $\frac{dE}{dx}$ for low-energy electrons ($T < 10$ kev) are lower than the theoretical values, calculated by (13.9).

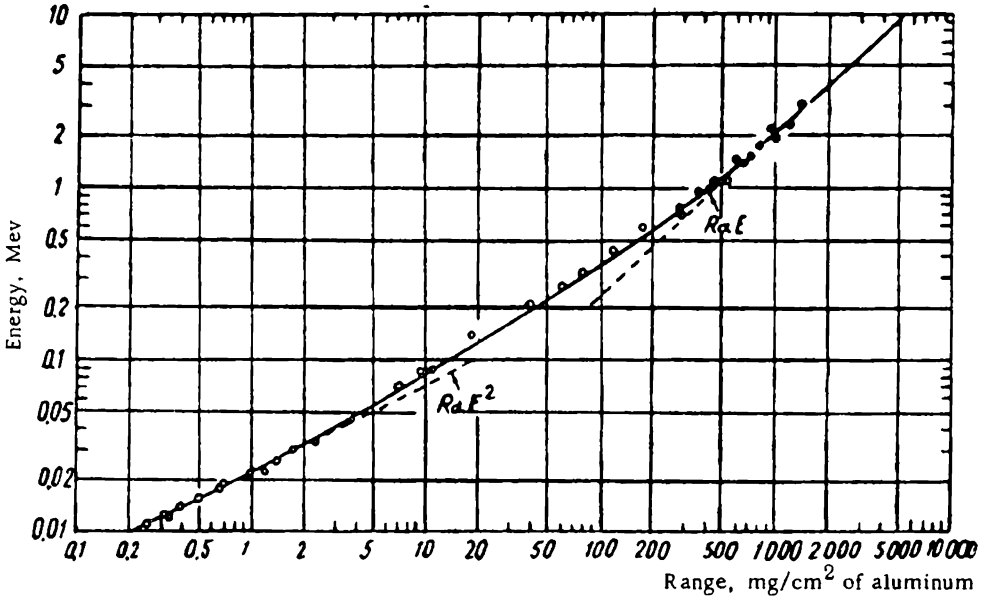

FIGURE 124. Semi-empirical range-energy relation of electrons in aluminum /350/. The points represent experimental data on the range of monoenergetic electrons. For the latter the curve gives the extrapolated range R_0, and for the beta-particles — R_{max}.

However, in /283/ it was shown that (13.9) gives mean electron ranges ($T \sim 10$ kev) in aluminum and gold which agree with the experimental values

On the basis of the experimental investigations of the range of monoenergetic electrons and positrons in aluminum, the authors of /276/ proposed the following formulas:

$$R^{-}_{m\rho}\left(\text{mg/cm}^2\right) = 773\ T^{1.70}_{(\text{Mev})} \tag{15.6a}$$

$$R^{+}_{m\rho}\left(\text{mg/cm}^2\right) = 759\ T^{1.72}_{(\text{Mev})}, \tag{15.6b}$$

$$10\ \text{kev} < T < 160\ \text{kev}.$$

The range of electrons (g/cm^2) in a medium is weakly dependent on Z, if the losses on bremsstrahlung are negligibly small. Results of the range-energy relation for electrons in aluminum may also be used for other media.

Ranges of electrons with a continuous energy spectrum. The absorption curve of electrons of a continuous spectrum, e. g., beta-electrons, differs considerably from that of monoenergetic electrons. In the initial section (see Figure 121) it has the form of the exponent $\exp(-\mu x)$, so that one may introduce the concept of absorption coefficient of beta-particles. As has been shown by experiments, the mass absorption coefficient $\frac{\mu}{\rho}$ is almost independent of the atomic weight of the absorber and increases slightly with Z.

The absorption coefficient of beta-particles in aluminum can be roughly determined from

$$\frac{\mu}{\rho}(\mathrm{cm}^2/\mathrm{g}) = \frac{22}{E_{0(\mathrm{Mev})}^{1.33}} \qquad (15.7)$$

Libby et al. /367/ have shown that for cylindrical geometry (absorbing medium in the form of a cylinder around a cylindrical counter) the following relation exists between the layer thickness for half absorption of beta-particles in aluminum and the maximum energy of the beta spectrum:

$$d_{1/2}(\mathrm{mg/cm}^2) = 38E_{0(\mathrm{Mev})}^{3/2}. \qquad (15.8)$$

The experimental data are given in Table 76.

A relation between the thickness of half absorption of beta-particles in aluminum and in other materials is given by

$$d_{1/2}(x) = d_{1/2(\mathrm{Al})}\frac{1.27}{\left(1+\frac{M_x}{100}\right)},$$

where M_x is the mean atomic weight of the absorbing material.

The above expressions are only suitable for simple beta spectra, i.e., for beta radiation sources in which the beta transition is only observed between the ground states of the nuclei.

TABLE 76

Experimental data on the relation between the limiting energy of the beta spectrum and the half absorption thickness /367/

β-particle source	Maximum β-particle energy, E_0, Mev	Absorbing medium	Half absorption layer $d_{1/2}$, mg/cm^2
T	0.0189	Helium, He	0.050
Zr^{93}	0.060	Aluminum, Al	0.35
Sm^{151}	0.0755	Aluminum, Al	0.63
C^{14}	0.155	Aluminum, Al	1.9
		Mylar	2.2
S^{35}	0.167	Aluminum, Al	2.3
		Mylar	2.7
Rb^{87}	0.270	Aluminum, Al	4.85
Ga^{45}	0.255	Aluminum, Al	4.9
Tc^{99}	0.296	Aluminum, Al	6.09
Tl^{204}	0.762	Aluminum, Al	22
Cl^{36}	0.716	Aluminum, Al	32
		Copper, Cu	26
		Tin, Sn	18-21
K^{40}	1.36	Aluminum, Al	67.0
P^{32}	1.708	Aluminum, Al	84.0
		Copper, Cu	60
		Tin, Sn	50
Y^{90}	2.275	Aluminum, Al	130

The maximum range of beta-particles determined from the absorption curve is a function of the maximum energy of the beta spectrum. The relation between the maximum range of beta-particles in aluminum and their maximum energy was studied by several authors. Feather /251/ compared such measurements with the values of E_0 determined by a

magnetic spectrograph, and proposed the following relation for aluminum

$$R_{\beta m}\,(\mathrm{g/cm^2}) = 0.543\ E_{0(\mathrm{Mev})} - 0.160, \tag{15.9}$$

which is true for $E_0 > 0.8$ Mev.

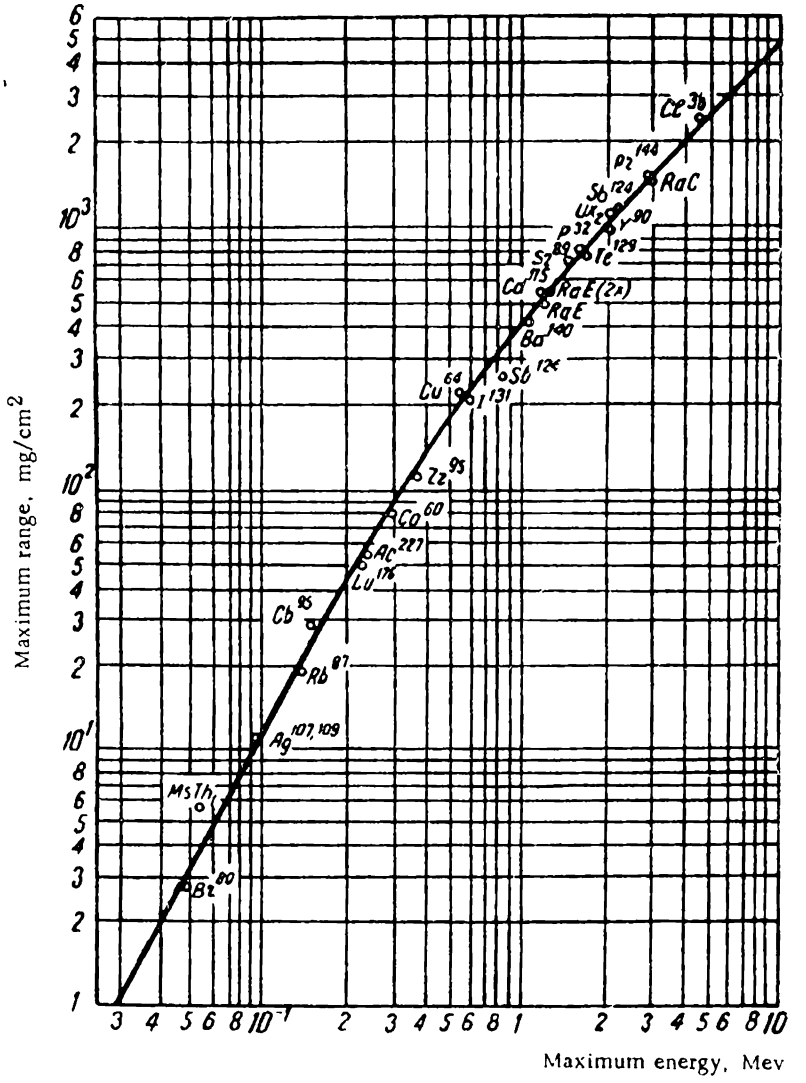

FIGURE 125. Experimental dependence of the maximum range of alpha-particles on their maximum energy in aluminum /91/

In recent years other semi-empirical relations have been proposed. For example, according to Glendenin /274/, the following expressions are valid for aluminum

$$R_{\beta m} = 0.542\ E_0 - 0.133 \qquad (0.8 < E_0 < 3\ \mathrm{Mev}), \tag{15.10}$$

$$R_{\beta m} = 0.407\ E^{1.38} \qquad (0.15 < E_0 < 0.8\ \mathrm{Mev}). \tag{15.10a}$$

According to Flammersfeld /252/

$$R_{\beta m} = 0.11\left(\sqrt{1 + 22.4E_0^2} - 1\right) \qquad (0 < E_0 < 3\ \mathrm{Mev}). \tag{15.11}$$

Finally, Bleuer and Zunti /188/ proposed the following empirical relation:

$$R_{\beta m} = 0.571\ E_0 - 0.161 \qquad (E_0 > 1 \text{ Mev}). \tag{15.12}$$

In (15.9) to (15.12) the range is expressed in grams per square centimeter, and the energy is expressed in megaelectronvolts.

In Figure 125 the solid curve gives the dependence of $R_{\beta m}$ on E_0 according to Flammersfeld's formula (15.11). The points in this figure represent values of $R_{\beta m}$ calculated by other expressions.

The curve of Figure 125 may be used for determining the end point energy of the beta-spectrum from the experimentally determined maximum range of the beta-particles. However, the determination of $R_{\beta m}$ is difficult, particularly in those cases when the beta disintegration is accompanied by the emission of gamma quanta. There are relatively few beta emitters free of gamma quanta, among them are RaE, P^{32}. They are used as standard sources in comparative methods /188, 251/.

Range of electrons in photoemulsions. The range—energy relation of electrons in special emulsions (sensitive to electrons) was studied in a number of experimental and theoretical works /199, 200/.

Table 77 gives experimental and calculated values of the mean range of electrons with energies of 30-350 kev in Kodak NT4 (NT2) photoemulsion, containing $10.8 \cdot 10^{23}$ electrons per cubic centimeter. In calculations by (13.9) I was taken as 125 ev for the emulsion.

Comparative investigation of absorption of monoenergetic electrons and positrons with energies of 0.25— 2.5 Mev in matter /21, 334/ have shown that in light media, for example in aluminum, the absorption is the same for both kinds of particles. In heavy media (gold), the absorption of positrons is weaker than that of electrons of the same energy. The difference increases with increasing charge of the absorber nuclei and with increasing absorber thickness. The reason for the stronger absorption of electrons is the difference in the cross sections for single and multiple scattering on nuclei (§ 12).

Mean electron ranges in various media, calculated by Bethe's formula, are given in Table 78.

§ 16. Connection between energy losses and ionization

Specific ionization. The total number of ion pairs, produced by an electron and by the secondary charged particles formed by it, is equal to

$$N_{\text{total}} = \frac{E}{w_e}, \tag{16.1}$$

where E is the initial energy of the electron;

w_e is the energy spent on the formation of one ion pair.

It was shown that the value of w_e is almost independent of the electron energy in a wide energy range.

The quantity

$$J_{\text{total}} = \frac{1}{w_e}\left(\frac{dE}{dx}\right)_{\text{ion}} \tag{16.2}$$

is called the probable specific ionization. It is the total number of ion pairs formed per unit range length of the electron.

The total ionization is the sum of the primary and secondary ionizations. On the average for each electron formed in primary ionization there are 1-2 secondary electrons (pairs).

TABLE 77

Experimental and theoretical electron ranges in Kodak NT4 emulsion /520/

T, kev	Mean range, R	Calculated range, R	Mean number of grains in the track
	microns		
30	7.0±0.3	6.0	11.0±0.4
40	10.8±0.4	9.9	13.8±0.5
50	15.8±0.5	14.6	20.4±0.8
60	21.4±0.6	20.0	22.4±0.6
80	32.7±0.6	32.8	35.5±1.4
100	46.7±1.5	47.8	43.3±1.0
147	95.4±1.2	92.0	74.2±1.8
200	141±6	149	95±3
250	201±8	211	133±5

TABLE 78

Calculated mean electron ranges /463/

T, Mev	Range, g/cm^2						
	Beryllium, Be	Polystyrene	Air	Aluminum, Al	Copper, Cu	Cadmium, Cd	Gold, Au
0.01	0.0003	0.00025	0.00029	0.00034	—	—	—
0.03	0.0021	0.0018	0.0020	0.0023	0.0029	—	—
0.05	0.0052	0.0043	0.0049	0.0056	0.0069	—	—
0.07	0.0094	0.0078	0.0088	0.0100	0.0122	0.0143	—
0.10	0.0173	0.0151	0.0162	0.0183	0.0222	0.0259	0.0308
0.20	0.0546	0.0459	0.0507	0.0508	0.0679	0.0784	0.0921
0.30	0.1026	0.0856	0.0952	0.1062	0.1260	0.1448	0.1690
0.40	0.1571	0.1306	0.1456	0.1619	0.1913	0.2191	0.2546
0.50	0.2156	0.1789	0.1996	0.2215	0.2609	0.2982	0.3455
0.60	0.2768	0.2294	0.2560	0.2836	0.3332	0.3802	0.4395
0.70	0.3397	0.2813	0.3139	0.3473	0.4073	0.4640	0.5358
0.80	0.4037	0.3342	0.3729	0.4120	0.4823	0.5489	0.6322
0.90	0.4684	0.3876	0.4324	0.4774	0.5580	0.6344	0.7297
1.00	0.5336	0.4415	0.4924	0.5431	0.6340	0.7201	0.8273
1.20	0.6646	0.5497	0.6129	0.6750	0.7862	0.8916	1.022
1.40	0.7959	0.6581	0.7335	0.8068	0.9381	1.062	1.216
1.60	0.9269	0.7662	0.8537	0.9380	1.089	1.232	1.408
1.80	1.057	0.8738	0.9733	1.068	1.239	1.406	1.599
2.00	1.187	0.9809	1.092	1.198	1.387	1.567	1.787
2.20	1.316	1.087	1.210	1.327	1.535	1.732	1.974
2.40	1.444	1.193	1.328	1.454	1.681	1.896	2.158
2.60	1.571	1.298	1.444	1.581	1.826	2.058	2.341
2.80	1.698	1.403	1.560	1.707	1.970	2.219	2.523
3.00	1.824	1.506	1.675	1.832	2.113	2.379	2.703
4.00	2.442	2.017	2.241	2.446	2.812	3.160	—
5.00	3.045	2.515	2.792	3.043	3.491	3.917	—
6.00	3.635	3.002	3.332	3.626	4.153	4.654	—
8.00	4.786	3.952	4.382	4.760	5.437	—	—
10.00	5.906	4.876	5.403	5.862	6.683	—	—
	(I=60ev)	(I_H=15.6 ev, I_C=76.4 ev)	(I_N=80.5 ev I_0=92 ev)	(I=150 ev)	(I=310 ev)	(I=480 ev)	(I=790 ev)

Thus, for example, a 4.9 Mev electron forms per 1 cm of path in air 25.4 primary pairs /226/ for a total number of 62.5 pairs per cm.

The measurement of the primary specific ionization is performed by a cloud chamber /512, 513/ or by investigating the dependence of the efficiency of the Geiger-Müller counters on the pressure /299, 393/; see § 8. The total ionization can be measured either in a cloud chamber or by ionization chambers or proportional counters.

TABLE 79

Primary specific ionization produced by electrons in various gases

Electron energy, Mev	Number of primary ion pairs per 1 cm path in the gas					References
	Hydrogen, H_2	Helium, He	Neon, Ne	Argon, A	Air	
0.205	8.45±0.095	7.56±0.16	18.45±0.36	41.7±0.77	—	/393/
0.500	6.04±0.065	5.58±0.066	13.4 ±0.17	30.5±0.34	—	/393/
0.885	5.44±0.054	5.08±0.043	12.5 ±0.14	27.7±0.31	—	/393/
1.17	5.30±0.053	—	—	—	—	/393/
1.55	5.32±0.059	5.02±0.06	12.4±0.13	27.8±0.39	—	/393/
4.9	—	—	—	—	25.4	/226/

Table 79 gives values of the number of primary ions formed by low-energy electrons ($T \leqslant 3\ mc^2$) per 1 cm of path in various gases, as well as the total specific ionization in air. Figure 126 gives experimental data on the specific primary ionization in hydrogen versus the momentum of electrons.

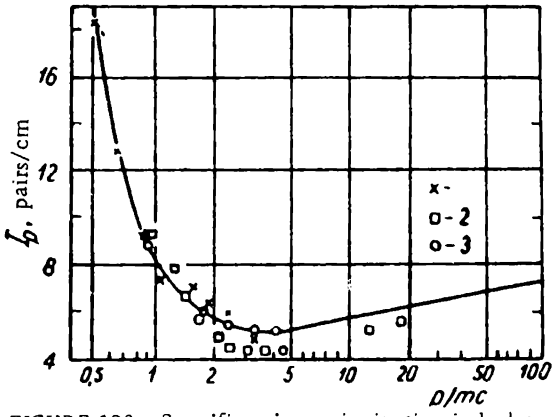

FIGURE 126. Specific primary ionization in hydrogen versus momentum of electrons. The curve was obtained by selecting the parameters in formula (16.3) which gave the best fit to the experimental points:

1—/512/; 2—/299, 300/; 3—/393/

The value of w_i is almost independent of the energy, and therefore the investigation of the primary and total specific ionizations, produced by high-energy electrons ($T > 3\ mc^2$), makes it possible to detect and measure the relativistic increase in the specific energy losses, as well as to assess the density effect. The relativistic increase in the ionization produced by electrons was first observed in the experiments of Corson and Brode /222/, who used a cloud chamber. This effect was studied more carefully and in greater detail in many subsequent works.

The points in Figure 126 represent experimental data on the specific primary ionization produced by electrons in various energies in hydrogen. These data were obtained by Kozins (1937), Hareford /299/ and McClure /393/ in studies of the dependence of the counting efficiency of electrons in gaseous counters on the pressure. The results of various measurements of Williams and Terroux are also included /512/. They studied the ionization produced by electrons with $v \approx 0.5$ c in hydrogen by a cloud chamber. The curve in Figure 126 corresponds to Bethe's theoretical formula /150/, giving the mean number of ionizing collisions per 1 cm of path in a gas under normal conditions

$$I_{\text{prim}} = 2\pi r_e^2 mc^2 nz^2 \frac{Za}{\beta^2}\left[\ln\left(\frac{2mc^2\beta}{(1-\beta^2)I} + b - \beta^2\right)\right], \qquad (16.3)$$

where r_e is the classical radius of the electron;
n is the number of atoms in 1 cm^3 of the stopping medium;
a and b are dimensionless constants, characterizing the electronic structure of the stopping atoms.

Bethe calculated the values of a and b only for hydrogen; for other media they are determined experimentally /393/. Usually there is a completely satisfactory agreement between the experiment and the theory.

A large number of investigators studied the specific total ionization and specific probable ionization. In contrast to the specific total ionization, the latter is connected with energy losses in collisions in which the electron is given an energy not less than some minimum T_0. The value of T_0 is determined by the lower sensitivity threshold of the detecting device. Whereas the specific total ionization is connected with the specific energy loss, determined by (13.7) or (13.9), the probable energy loss for relativistic electrons is given by

$$-\left(\frac{dE}{dx}\right)_{\text{prob}}^{\text{ion}} = \frac{2\pi ne^4}{wv^2}\left[\ln\frac{2mv^2T_0}{I^2(1-\beta^2)} - \beta^2 - \delta\right]; \qquad (16.4)$$

where the notation is the usual one.

Frost and Nielsen /253/ have shown that the specific probable ionization in air, hydrogen, helium and argon is in satisfactory agreement with (16.4) for electron energies of 0.25-0.8 Mev. It was shown in /409/ that the specific total ionization in air, argon and hydrogen increases by 5% when the electron energy is increased from 9 to 17.5 Mev.

Barber /194/ measured the specific probable ionization in hydrogen, helium and nitrogen for electron energies from 1 to 34 Mev with an ionization chamber. In nitrogen, the relativistic increase in the ionization from the minimum to T = 34 Mev is in agreement with the specific energy losses predicted by the theory (formula (16.4)). In helium, and in particular in hydrogen, the observed increase in the ionization was considerably lower than the theoretical prediction, and the density effect cannot explain this discrepancy. The author assumes that this is connected with the Cerenkov radiation (§ 9) and it leads to a situation where the value of w_e in hydrogen for T = 34 Mev is 3.3% higher than w_e in the minimum of the specific ionization curve.

Figures 127 and 128 give the experimental curves of the specific probable ionization in helium and nitrogen as obtained by Barber. The measured values of the minimum specific ionization in hydrogen, helium and nitrogen were (7.56 ± 0.09); (6.15 ± 0.08) and (53.2 ± 0.7) ion pairs/cm, respectively. Using these values, Barber determined, by expressions (16.2) and

(16.4), the values of w_e for hydrogen, helium and nitrogen (see Table 82). Dividing the difference in the specific energy losses, calculated by (13.9) and (16.4), by w_e and adding the result to the measured values of $\left(\frac{dE}{dx}\right)_{prob}$, the author determined the minimum specific total ionization for $T = 34$ Mev. The results of these calculations as well as other results are given in Table 80.

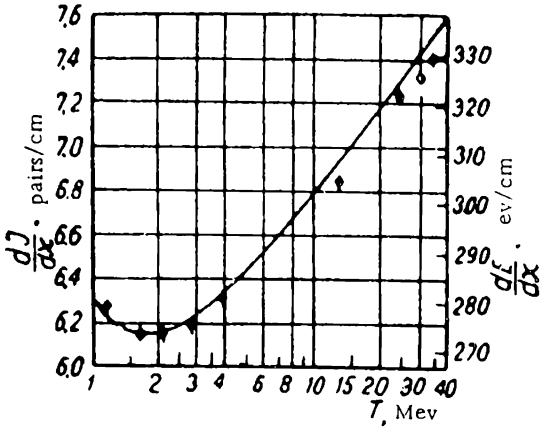

FIGURE 127. Specific ionization and probable energy losses by electrons in helium ($T_0 = 10.4$ kev)

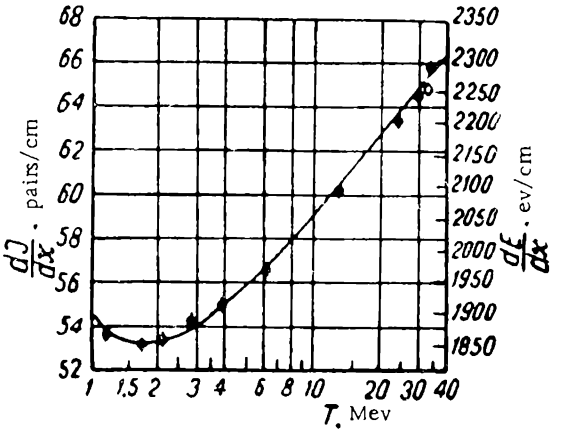

FIGURE 128. Specific ionization and probable energy losses by electrons in nitrogen ($T_0 = 70$ kev)

TABLE 80

Specific ionization in gases under $p = 760$ mm of mercury and $T = 0°$

Ionization characteristics	Hydrogen, H	Helium, He	Nitrogen, N	Air	Argon, A	References
Number of ion pairs per cm for minimum probable energy loss	6.48-0.34	8.13-0.51	—	46.1-2.2	53.1-2.8	/253/
Specific total ionization (pairs/cm) for T = = 17.5 Mev	8.4	—	—	64	101	/409/
Number of ion pairs per cm for minimum probable energy loss	7.56-0.09	6.15 ±0.08	53.2± 0.7	—	—	/194/
Minimum specific total ionization, pairs/cm	9.19-0 18	7.55-0.16	$61.6^{+1.7}_{-2.0}$	—	—	/194/
Specific total ionization (pairs/cm) for T=34 Mev	11.50± 0.22	9.67± 0.20	$82.0^{+1.7}_{-2.0}$	—	—	/194/

It was shown in /513/ that primary and probable ionization in hydrogen are not the same for electrons and positrons of the same energy ($T \simeq 230$-267 kev).

A relativistic increase in the specific ionization, limited by the density effect, was obtained in a dense condensed medium. An example is the work of Pickup and Voyvodic /421/, in which it was shown for the first time that the ionization minimum (observed at an electron energy of $\frac{E}{mc^2} \sim 3$) is followed by a small increase; for $\frac{E}{mc^2} \approx 20$, this increase is

$\sim$ 10% of the minimum and remains constant up to very high energies (ionization plateau, cf. also Figure 85). Subsequent work confirmed this result.

The light yield in crystal-scintillators has a similar dependence upon the electron energy /207/.

Energy spent on the formation of one ion pair. An important experimental fact, established in the investigation of ionization produced by electrons, X- and gamma-rays, is the weak dependence of w_e, the mean energy spent on the formation of an ion pair, on the energy of the electrons. Moreover, for a given medium the value of w_e differs only slightly from the values of w_α and w_p (the energies spent on the formation of an ion pair by alpha-particles and protons). For example, the absolute value of w_α(A), measured at $T_\alpha = 5.3$ Mev, is only 0.5% higher than the absolute value of w_e(A), measured for energies of 50-1000 kev.

TABLE 81

Experimental values of w_e for air

Electron energy, kev	w_e (air), ev/pair	Dependence of w_e on the electron energy	Technique of measurement	References
3-240	35.0 ± 0.5	Weak or no dependence	Proportional counter	/485/
70	35	The same	Extrapolation ionization chambers + calorimeter; source of S^{35}	/116/
1000	33.9	The same	Ionization chamber + dosimeter	/508/
5-20	34.1	The same	Ionization chamber + 4π — counter of beta-particles	/324/
1100	33	The same	Calorimeter + thermistors, beta sources	—
10-40	33.4-32.4	Weak	Electron beam	/275/
Up to 50	31.2	—	Cloud chamber with a magnetic field	/253/
17500	33	—	Betatron; microcalorimeter	/366/
49	33.7 ± 0.3	—	Extrapolation ionization chamber, beta-particles of S^{35}	/201, 202/
49	33.9	—	The same	/324/
49	33.6 ± 0.3	—	The same	/282, 329/
500-1700	33.9 ± 0.5N	No dependence	Extrapolation ionization chamber	/195/

Experimental data on the mean energy spent by electrons of various energies on the formation of one ion pair in air are given in Table 81. In early works of Bukhman and Eizl' it was shown that for electrons with energies of 4-60 kev the value of $w_{e(air)}$ is independent of the energy and is equal to 31-32 ev. Gerbes /275/ based on the analysis of these works and on his own measurements concluded that $w_{e(air)}$ is in the range 4-60 kev and decreases slowly with increasing energy. Pigge et al. established that w_e increases appreciably with increasing electron energy down to 0.3-1 kev.

In subsequent works carried out by means of an improved technique and at higher electron energies, values of $w_{e(air)}$, lying in the range of 31-35 kev, were obtained.

In 1956 the International Commission on Radiological Units recommended /31/ a value of $w_{e(air)}$ equal to 34.0 ev/pairs.

Argon or air are usually taken as a standard medium for measuring the relative values of $w_{e(air)}$ /324, 506/. The corresponding experimental data are given in Table 82.

TABLE 82

Experimental relative values of w_e for various gases

Gas	w_e (gas), ev	w_e (gas) / w_e (A)	w_e (gas), ev	w_e (gas) / w_e (A)	w_e (gas), ev	w_e (gas) / w_e (A)	w_e (gas), ev	w_e (gas) / w_e (A)	w_e (gas), ev	w_e (gas), ev
	/484/		/275/		/324/		/506/		/329/	/253/
Helium, He	32.5	1.20	—	—	42.3	1.60	40.3	1.57	—	26.0
Neon, Ne	—	—	29.1	1.07	36.6	1.39	35.3	1.48	—	—
Argon, A	27.0	1.00	27.3	1.00	26.4	1.00	25.8	1.00	—	27.9
Krypton, Kr	—	—	—	—	24.2	0.915	24.7	0.96	—	—
Xenon, Xe	—	—	—	—	22.0	0.83	22.0	0.82	—	—
Hydrogen, H_2	38.0	1.41	—	—	36.3	1.37	36.3	1.40	—	37.2
Air	35.0	1.29	33.4	1.22	34.0	1.29	33.9	1.37	33.9	31.2
Nitrogen, N_2	35.8	1.32	34.6	1.27	35.0	1.31	34 6	1.34	35.0	—
Oxygen, O_2	32.2	1.19	30.5	1.12	30.9	1.17	31.2	1.21	—	—
Carbon dioxide, CO_2	—	—	32.2	1.18	32.9	1.25	32.6	1.26	—	—
Ethylene, C_2H_4	—	—	—	—	26.2	0.99	26.4	1.02	—	—
Ethane, C_2H_6	—	—	—	—	24.8	0.94	—	—	24.6	—
Methane, CH_4	29.5	1.05	—	—	27.3	1.03	—	—	—	—
Radical CH_3	—	—	23.6	0.86	25.9	0.98	—	—	—	—

Jesse and Sadauskis used an ionization chamber with a collecting electrode in the form of a wire grid for measuring the absolute and relative values of w_e. The electrons were completely absorbed in the chamber so that the measurements gave the total ionization. The number of absorbed electrons were determined from the absolute rate of decay of beta sources determined with a 4π-counter.

The measured results of Jesse et al. are in good agreement with the results of measurement of w_e(A) /484/ made by proportional counters, filled with argon, with tracks of radioactive gases (H^3, C^{14}).

Among the important works on the determination of w_e are those of Weiss and Bernstein /506/, who used an extrapolation ionization chamber with plane electrodes, satisfying the Bragg-Gray principle*. The energy absorbed in the walls of the chamber was determined by a chemical ferrosulfate dosimeter. In calculating w_e from the measured results, the authors used the calculated values of the stopping powers of the media being investigated.

The values of w_e, measured by Weiss and Bernstein, are in good agreement with the values measured with a different technique by Jesse et al.

It should be mentioned that small impurity admixtures ($\approx$0.01-0.1 %) to certain noble gases lead to an increase in w_e (this refers also to the values of w_a and w_p, see § 8). The quantity $w_{e\,(He)}$ is particularly sensitive to impurities.

* In this case (see for example /3, 23/) the following relation exists between the energy E, absorbed in 1 g of material in the wall of the chamber, and the ionization produced in the gas filling the chamber

$$E = JwS_m,$$

where J is the ionization referred to 1 g of the gas, S_m are the relative mass stopping powers of the substance and of the gas.

The absolute values of $w_{e\ (A)}$ and $w_{\alpha\ (A)}$ are almost identical. The weighed mean of four independent measurements /189, 319, 464, 506/ of the absolute values of w_α gives 26.39 ev for $T_\alpha \cong 5.3$ Mev. At the same time, the weighed mean of four independent measurements /201, 512, 319, 282/ of the absolute value of $w_{e\ (A)}$ gives 26.25 ev (T = 49-1000 kev). Thus $w_{\alpha\ (A)}$ is $\sim 0.5\%$ higher than $w_{e\ (A)}$. Bay et al. /201/ obtained the following absolute values of the energy spent on the formation of one ion pair in air:

$$w_{e\ (air)} = 33.7 \pm 0.3 \text{ ev}, \quad w_{\alpha\ (air)} = 34.97 \pm 0.07 \text{ ev}.$$

The authors of /201, 202/ explain this as a consequence of the difference in the ionization conditions for alpha-particles and electrons; Jesse /320/ assumes that the inequality of w_α and w_e is due to the weak dependence of w_α on the energy of the alpha-particles. According to Jesse, the values of w_α and w_e should be exactly equal at very high alpha-particle energies.

BIBLIOGRAPHY

Publications in Russian

1. Artsimovich, L. A. Upravlyaemye termoyadernye reaktsii (Controlled Thermonuclear Reactions). — GIFML, Moskva. 1961.
2. Alikhanov, A. I. Slabye vzaimodeistviya (Weak Interactions). — GIFML, Moskva. 1960.
3. Aglintsev, K. K. Dozimetriya ioniziruyushchikh izluchenii (Dosimetry of Ionizing Radiations). — GITTL, Moskva. 1957.
4. Arifov, U. A. Vzaimodeistvie atomnykh chastits s poverkhnost'yu metalla (Interaction of Atomic Particles with the Surface of a Metal). — AN UzSSR, Tashkent. 1961.
5. Afrosimov, V. V. and N. V. Fedorenko. — ZhTF, 27:2557. 1957.
6. Afrosimov, V. V. and N. V. Fedorenko. — ZhTF, 27:2573. 1957.
7. Afrosimov, V. V., R. N. Il'in, and N. V. Fedorenko. — ZhETF, 34:1938. 1958; ZhTF, 28:2266. 1958.
8. Artsimovich, L. A. — ZhETF, 9:927. 1939.
9. Akhiezer, A. and I. Pomeranchuk. — J. Phys. USSR, 9:471. 1945.
10. Arutyunyan, F. R. — ZhETF, 34:800. 1958.
11. Avak'yants, G. M. and V. M. Lenchenko. — Izvestiya AN UzSSR, No. 2:29. 1957.
12. Bohr, N. Prokhozhdenie atomnykh chastits cherez veshchestvo (Passage of Atomic Particles through Matter). — IL., Moskva. 1950. [Translated from English.]
13. Baldin, A. M., V. I. Gol'danskii, and I. A. Rozental'. Kinematika yadernykh reaktsii (Kinematics of Nuclear Reactions). — GIFML, Moskva. 1959.
14. Belen'kii, S. Z. Lavinnye protsessy v kosmicheskikh luchakh (Avalanche Processes in Cosmic Rays). — GITTL, Moskva-Leningrad. 1948.
15. Bolotovskii, B. M. — UFN, 62:201. 1957.
16. Bethe, H. A., and E. E. Salpeter. Quantum Mechanics of One- and Two-Electron Atoms. — Springer-Verlag, Berlin. 1957.
17. Blokhintsev, D. I. Osnovy kvantovoi mekhaniki (Bases of Quantum Mechanics). — Vysshaya Shkola, Moskva. 1961.
18. Bonetti, A., S. Silvorz, S. R. Pelk, and L. Skarsi. Yadernye emul'sii (Nuclear Emulsions). — GIFML, Moskva. 1961. [Translated from English.]
19. Birks, J. B. Scintillation Counters. — Pergamon, London. 1953. [Russian translation. 1955]
20. Bethe, H. A. and Yu. V. Ashkin. — In: Experimental Nuclear Physics, Vol. 1, edited by E. Segré. Wiley, New York. 1953. [Russian translation. 1955]

21. Baskakova, K. A. and B. S. Dzhelepov. — DAN SSSR, 77:1001. 1951.
22. Baskakova, K. A. and V. M. Gorbachev. — ZhETF, 26:270. 1954.
23. Veksler, V., L. Groshev, and B. Isaev. Ionizatsionnye metody issledovaniya izluchenii (Ionization Methods of Investigation of Radiation). — GITTL, Moskva. 1949.
24. Vlasov, N. A. Neitrony (Neutrons). — GITTL, Moskva. 1955.
25. Vavilov, P. V. — ZhETF, 32:920. 1957.
26. Velyukhov, G. E., A. N. Prokof'ev, and S. V. Starodubtsev. — Izvestiya AN UzSSR, seriya fiziko-matematicheskikh nauk, 3. 1960.
27. Val'ter, A. K. et al. — Izvestiya AN SSSR, seriya fizicheskaya, 22:87. 1958; 24:884. 1960.
28. Gen et al. — Atomnaya Energiya, 7:473. 1959.
29. Grinberg, A. P. and I. Kh. Lemberg. — Izvestiya AN SSSR, seriya fizicheskaya, 23:887. 1959.
30. Heitler, G. The Quantum Theory of Radiation. — Clarendon Press, Oxford. 1936. [Russian translation. 1956]
31. Gusev, N. G. (editor). Edinitsy aktivnosti i dozy ioniziruyushchikh izluchenii (Activity Units and Doses of Ionizing Radiations). — IL., Moskva. 1959.
32. Ginzburg, V. L. — ZhETF, 10:589. 1940.
33. Ginzburg, V. L. — UFN, 69:537. 1959.
34. Gusev, N. G. Spravochnik po radioaktivnym izlucheniyam i zashchite (Manual on Radioactive Radiations and Shielding). — Medgiz, Moskva. 1956.
35. Gambosh, P. Statisticheskaya teoriya atoma i ee primenenie (Statistical Theory of the Atom and its Application). — IL, Moskva. 1951. [Translated from German.]
36. Grishaev, I. A., A. N. Fisun, A. S. Litvinenko, V. M. Grishko, B. I. Shramenko, and I. A. Onishchenko. — ZhETF, 37:1455. 1959.
37. Gerasimenko, V. I. — ZhETF, 41:1104. 1961.
38. Gerasimenko, V. I. and L. I. Rozentsveig. — ZhETF, 31:684. 1956.
39. Dobrotin, N. A. Kosmicheskie luchi(Cosmic Rays). — GITTL, Moskva. 1959.
40. Jelly, J. V. Cerenkov Radiation and Its Application. — Pergamon Press, London. 1958. [Russian translation. 1960]
41. Dukel'skii, V. M. and N. V. Fedorenko. — ZhTF, 25:2193. 1955.
42. Dmitriev, I. S., V. S. Nikolaev, L. N. Fateeva, and Ya. A. Teplova. — Izvestiya AN SSSR, seriya fizicheskaya, 24:1169. 1960.
43. Dukel'skii, V. M., V. V. Afrosimov, and N. V. Fedorenko. — ZhETF, 30:792. 1956.
44. Dmitriev, I. S. — ZhETF, 32:570. 1957.
45. Dmitriev, I. S., V. S. Nikolaev, L. N. Fateeva, and A. Ya. Teplova. — ZhETF, 42:16. 1962.
46. Drukarev, G. F. — ZhETF, 37:847. 1959.
47. Diven, B. C. — Proceedings of the International Conference on the Peaceful Uses of Atomic Energy, Vol. 4. p. 251. Geneva, 1955. [Russian translation. 1956]

48. Dolgirev, E. I., P. I. Maleev, and V. V. Sidorenko. Detektory yadernykh izluchenii (Detectors of Nuclear Radiations). — Sudpromgiz. Leningrad. 1961.
49. Zrelov, V. P. and G. D. Stoletov. — ZhETF, 36:658. 1959.
50. Il'in, R. N., V. V. Afrosimov, and N. V. Fedorenko. — ZhETF, 36:141. 1959.
51. Kuznetsov, M. I., P. I. Lukirskii, and N. A. Perfilov. — DAN SSSR, 100:665. 1955.
52. Kompaneets, A. S. — ZhETF, 15:235. 1945.
53. Kocharov, G. E. — Izvestiya AN SSSR, seriya fizicheskaya, 25:862. 1961.
54. Kunin, P. E. — In: Sbornik "Mezon", edited by Tamm, I. E., GITTL, Moskva. 1947.
55. Kaminker, D. M. and N. V. Fedorenko. — ZhTF, 25:1843. 1955.
56. Kaminker, D. M. and N. V. Fedorenko. — ZhTF, 25:2239. 1955.
57. Korsunskii, M. I., L. I. Pivovar, A. M. Markus, and Kh. L. Leviant. — DAN SSSR, 103:339. 1955.
58. Kul'chitskii, L. A. and G. D. Latyshev. — Phys. Rev., 61:254. 1942.
59. Komar, A. P., A. A. Vorob'ev, and V. A. Korolev. — DAN SSSR, 136:795, 137:541. 1961.
60. Konstantinova, M. P., E. V. Myakinin, A. M. Romanov, and T. V. Tsareva. — ZhETF, 41:49. 1961.
61. Klyucharev, A. P. — Izvestiya AN SSSR, seriya fizicheskaya, 24:887. 1960.
62. Landau, L. D. and E. M. Lifshitz. Mekhanika (Mechanics). — GIFML, Moskva. 1958.
63. Landau, L. D. — J. Phys. USSR, 8:201. 1944.
64. Landau, L. D. and E. M. Lifshitz. Kvantovaya mekhanika (Quantum Mechanics). — GITTL, Moskva. 1948.
65. Landau, L. D. and E. M. Lifshitz. Teoriya polya (Field Theory). — GITTL, Moskva. 1948.
66. Lifshitz, E. M. — ZhETF, 18:562. 1948.
67. Landau, L. D. and G. Rumer. — Proc. Roy. Soc., A166:213. 1938.
68. Leviant, Kh. L., M. I. Korsunskii, L. I. Pivovar, and I. M. Podgornyi. — DAN SSSR, 103:403. 1955.
69. Landau, L. D. and G. Rumer. — Proc. Roy. Soc., A166:213. 1938.
70. Levashov, A. E. Elementarnye chastitsy, Ch. I (Elementary Particles, Part I). — Kievskii universitet. 1960.
71. Mott, N. F. and H. S. W. Massey. The Theory of Atomic Collisions. — Clarendon Press, Oxford. 1949. [Russian translation. 1951]
72. Massey, H. S. W. and E. H. S. Burhop. Electronic and Ionic Impact Phenomena. — Clarendon Press, Oxford. 1952. [Russian translation. 1951]
73. Maikov, V. N. — Pribory i Tekhnika Eksperimenta, I, 50. 1959.
74. Malysheva, T. V. — Zavodskaya Laboratoriya, 23(3):319. 1957.
75. Migdal, A. B. — ZhETF, 10:1964. 1934.
76. Maksimov, M. Z. — ZhETF, 37:127. 1959.
77. Nelipa, N. F. Vvedenie v teoriyu mnogokratnogo rasseyaniya chastits (Introduction to the Theory of Multiple Scattering of Particles). — Atomizdat. Moskva. 1960.

78. Nikolaev, V.S., L.N. Fateeva, I.S. Dmitriev, and Ya. A. Teplova. — ZhETF, 32:965. 1957; 33, 306, 1325. 1957.
79. Nikolaev, V.S. — ZhETF, 33:534. 1957.
80. Nikolaev, V.S , I.S. Dmitriev, L.N. Fateeva, and Ya. A. Teplova. — ZhETF, 40:989. 1961.
81. Nikolaev, V.S., I.S. Dmitriev, L.N. Fateeva, and Ya. A. Teplova. — ZhETF, 39:905. 1960; Izvestiya AN SSSR, seriya fizicheskaya, 24:1169. 1960.
82. Orlov, Yu. F. — ZhETF, 30:613. 1956.
83. Nikolaev, V.S., L.N. Fateeva, I.S. Dmitriev, and Ya. A. Teplova. — ZhETF, 41:89. 1961.
84. Nemirovskii, P. —ZhETF. 18:899. 1948.
85. Osetinskii, G.M. — In: Sbornik "Yadernye reaktsii na legkikh yadrakh", Atomizdat, Moskva. 1957.
86. Oganesyan, Yu. I. — ZhETF, 36:936. 1959.
87. Pivovar, L.I., V.M. Tubaev, and M.T. Novikov. — ZhETF, 41:26. 1961.
88. Pomeranchuk, I. — ZhETF, 18:759. 1948.
89. Perfilov, N.A. — DAN SSSR, 28:424. 1940.
90. Parfanovich, D.M., A.M. Semchinova, and G.N. Flerov. — ZhETF. 33:343. 1957.
91. Paul, W. and H. Steinwedel. Interaction of Electrons with Matter. — In: "Beta- and Gamma-Spectroscopy" (editor: Kai Siegbahn), North-Holland Publishing Company, Amsterdam. 1955. [Russian translation. 1959]
92. Rossi, B. High-Energy Particles. — Prentice Hall, Incorporated, New York. 1952. [Russian translation. 1955]
93. Rybakov, B.V. — ZhETF, 28:65. 1955.
94. Rossi, B. and K. Greisen. Vzaimodeistvie kosmicheskikh luchei s veshchestvom (Interaction of Cosmic Rays with Matter). — IL., Moskva. 1948. [Translated from English.]
95. Rodicheva, M.F. — Zhurnal Nauchnoi i Prikladnoi Fotografii. 5:221. 1960; Uspekhi Nauchnoi Fotografii, 7:178. 1960.
96. Spivak, P E., L.A. Mikaelyan, I.E. Krutikov, and V.F. Apalin. — ZhETF, 39:1479. 1960.
97. Sena, L.A. Stolknoveniya elektronov i ionov s atomami gaza (Collisions of Electrons and Ions with Gas Atoms). — GITTL, Moskva. 1948.
98. Starodubtsev, S.V. and A.M. Romanov. Radioaktivnye prevrashcheniya yader i atomnaya obolochka (Radioactive Nuclear Transformations and the Atomic Shell). — AN UzSSR, Tashkent. 1958.
99. Sokolov, A.A. — DAN SSSR, 28:415. 1940.
100. Teplova, Ya. A., I.S. Dmitriev, V.S. Nikolaev, and L.N. Fateeva. — ZhETF, 34:559. 1958.
101. Teplova, Y.A., I.S. Dmitriev, V.S. Nikolaev, and L.N. Fateeva. — ZhETF, 32:974. 1957.
102. Tamm, I.E. —J. Phys. USSR. 1, 439. 1939.

103. Ter-Mikaelyan, M. L. — ZhETF, 36:253. 1959.
104. Ter-Mikaelyan, M. L. — ZhETF, 25:289, 296. 1953.
105. Fermi, E. Nuclear Physics. — The University of Chicago Press, Chicago. 1950. [Russian translation. 1951]
106. Frank, I. M. and I. E. Tamm. — DAN SSSR, 14:109. 1937.
107. Fedorenko, N. V. — UFN, 68:481. 1959.
108. Fedorenko, N. V. — ZhTF, 24:769, 784, 2113. 1954.
109. Fedorenko, N. V., V. V. Afrosimov, and D. M. Kaminker. — ZhTF, 26:1929. 1956.
110. Fedorenko, N. V. and V. V. Afrosimov. — ZhTF, 26:1941. 1956.
111. Fedorenko, N. V., V. V. Afrosimov, R. N. Il'in, and D. M. Kaminker. — ZhETF, 36:385. 1959.
112. Firsov, O. B. Doctorate thesis. — IAE, Leningrad. 1959.
113. Firsov, O. B. — ZhETF, 34:447. 1958.
114. Firsov, O. B. — ZhETF, 33:696. 1957.
115. Firsov, O. B — ZhETF, 36:1517. 1959.
116. Failla, G. — Proceedings of the International Conference on the Peaceful Uses of Atomic Energy, Vol. 14, p. 239. Geneva. 1955. [Russian translation. 1958]
117. Fogel', Ya. M. and R. V. Mitin. — ZhETF, 30:450. 1956.
118. Fogel', Ya. M., L. I. Krupnik, and B. G. Safronov. — ZhETF, 28:589, 711. 1955.
119. Fogel', Ya. M., N. F. Kozlov, L. A. Kalmykov, and B. Ya. Muratov. — ZhETF, 36:1312. 1959.
120. Fogel', Ya. M. — UFN, 71:243. 1960.
121. Filipenko, L. G. and I. P. Flaks. — ZhTF, 30:491. 1959.
122. Flaks, I. P., and E. S. Solov'ev. — ZhTF, 28:599, 612. 1958.
123. Tsvetaeva, N. M. — Atomnaya Energiya, 9 (6):507. 1960.
124. Cherenkov (Cerenkov), P. A. — DAN SSSR, 2:451. 1934; 14:105. 1937.
125. Cherenkov (Cerenkov), P. A. — DAN SSSR, 13:413. 1936; 20:653. 1938; 21:323. 1938.
126. Chudars, Ya. A. — Trudy Instituta Fiziki AN LatvSSR, 9:45. 1956.
127. Kharitonov, V. — DAN SSSR, 86:285. 1952.
128. Kharitonov, V. and A. Barskii. — DAN SSSR, 93:645. 1953.
129. Chavchanidze, V. V. — ZhETF, 26:179, 185. 1954.
130. Shpinel', V. S. — ZhETF, 22:421. 1952.
131. Shakhbazyan, V. A. — Izvestiya AN ArmSSR, seriya fiziko-matematicheskikh nauk, 9 (5):91. 1956.

Publications in other languages

132. Allison, S. K. and S. D. Warshaw. — Rev. Mod. Phys., 25:779. 1953.
133. Allison, S. K. — Rev. Mod. Phys., 30:1137. 1958.
134. Allison, S. K., J. Guevas, and M. Carcia-Munoz. — Phys. Rev., 120:1266. 1960.

135. Allison, S. K. and C. S. Littlejohn. — Phys. Rev., 104:959. 1956.
136. Allison, S. K. — Phys. Rev., 109:176. 1958.
137. Aron, W. A., B. G. Hoffmann, and F. C. Williams. — UCRL. 121. 1949.
138. Ashkin, A., L. A. Page and W. M. Woodward. — Phys. Rev., 94:357. 1954.
139. Alder, F., P. Huber, and F. Metzger. — Helv. Phys. Acta, 20:234, 236. 1947.
140. Alexander, G. and R. H. Johnston. — Nuovo cim., 5:363. 1957.
141. Ashmore, A. and A.V. Crewe. — Proc. Phys. Soc., A66:1172. 1953.
142. Alexander, J. M. and M. F. Gazdik. — Phys. Rev., 120:874. 1960.
143. Ashebrenner, F. A. — Phys. Rev., 98:657. 1954.
144. Allen, K. R. et al. — Proc. Phys. Soc., A69:355. 1956; A70:536. 1957.
145. Barkas, W. H. et al. — Phys. Rev., 102:583. 1956.
146. Bohr, N. — Phys. Rev., 58:654. 1940; 59:270. 1941.
147. Briggs, G. H. — Proc. Roy. Soc., A114:241. 1927.
148. Bethe, H. A. ,— Phys. Rev., 89:1256. 1953.
149. Bohr, N. — Phil. Mag., 25:10. 1913; 30:581. 1915.
150. Bethe, H. — Ann. Phys., 5:325. 1930; Z. phys., 76:293. 1932.
151. Bloch, F. — Z. phys., 81:363. 1933; Ann. phys., 16:285. 1933.
152. Bhabha, H. — J. Proc. Roy. Soc., A164:257. 1937.
153. Bethe, H. A. — Rev. Mod. Phys., 22:213. 1950.
154. Barkas, W. H. et al. — Nuovo cim., 8:185, 201. 1958.
155. Burkig, V. C. and K. R. McKenzie. — Phys. Rev., 106:848. 1957.
156. Bichsel, H., R. Mozley, and W. A. Aron. — Phys. Rev., 105:1788. 1957.
157. Bader, M., R. E. Pixley, F. S. Mozer, and W. Whaling. — Phys. Rev., 103:32. 1956.
158. Bakker, C. J. and E. Segré. — Phys. Rev., 82:489. 1951.
159. Brolley, J. E. and F. L. Ribe. — Phys. Rev., 98:1112. 1955.
160. Bogaardt, M. and B. Kondijs. — Physica, 18:249. 1952.
161. Bloembergen, N. and P. J. Van Heerden. — Phys. Rev., 83:561. 1951.
162. Bates, D. R., H. S. W. Massey, and A. L. Steward. — Proc. Roy. Soc., A216:437. 1953
163. Bates, D. R. and A. Dalgarno. — Proc. Phys. Soc., A65:919. 1952; A66:972 1953.
164. Barkas, W. H. — Phys. Rev., 89:1019. 1953.
165. Brunnings, J. H. M., E. Knippe, and E. Teller. — Phys. Rev., 60:657. 1941.
166. Birkhoff, R. D. — Handbuch d. Physik, Bd. 34. Berlin. 1957.
167. Bertolini, G., M. Bettoni, and A. Bisi. — Phys. Rev., 92:1586. 1953; Nuovo cim., 10, Suppl. 3, 299. 1953.
168. Bertolini, G., M. Bettoni, and A. Bisi. — Nuovo cim., 11:458. 1954.
169. Brinkman, H. G. and H. A. Kramers. — Proc. Acad. Sci. Amst., 33:973. 1930.
170. Bell, G. I. — Phys. Rev., 90:548. 1953.
171. Bichsel, H. and E. A. Uehling. — Phys. Rev, 119:1671. 1960.
172. Bichsel, H. — Phys. Rev., 120:1012. 1960.

173. Bichsel, H. — Phys. Rev., 112:1089. 1958.
174. Brandt, W. — Phys. Rev., 104:691. 1956.
175. Barkan, S. — Nuovo cim., 20:443. 1961.
176. Burcham, W. E. — Phil. Mag., 44:211. 1953.
177. Barkas, W. H., and S. von Friesen. — Nuovo cim. 19, Suppl. 1:41. 1961.
178. Bogaardt, M. L. and L. Vigneron. — Journ. phys. et rad., 1 :652. 1950.
179. Bichsel, H. — Helv. phys. acta, 25:119. 1952.
180. Blackett, P. M. S. and L. Lees. — Proc. Roy. Soc., A134:658. 1932.
181. Buechner, W. W., R. J. Van de Graaf, A. Sperduto, E. A. Burrill, and H. Feshbach. — Phys. Rev., 72:678. 1947.
182. Bohr, N. and J. Lindhard. — Dan. mat. fys. Medd., 28:7. 1954.
183. Bhabha, H. — J. Proc. Roy. Soc., A154:195. 1936.
184. Barnett, C. F. and P. M. Stier. —Phys. Rev., 109:355. 1958.
185. Bothe, W. — Z. Naturforsch., 4a, 88. 1949; 5a, 8. 1950.
186. Bayard, R. T. and J. Yntema. — Phys. Rev., 97:372. 1955.
187. Bethe, H. A. and W. Heitler. —Proc. Roys. Soc., A146:83. 1934.
188. Bleuler, E. and W. Zunti. — Helv. phys. acta, 19:137. 1946.
189. Bortner, T. E. and G. S. Hurst. — Phys. Rev., 90:160. 1953; 93:1326. 1954.
190. Biber, C., P. Huber, and A. Müller. — Helv. phys. acta, 28:503. 1955.
191. Blunck, O. and K. Westphalk. — Z. Phys., 130:641. 1951.
192. Blunck, O. and S. Leisegang. — Z. Phys., 128:500. 1950.
193. Breuer, H., D. Harder, and W. Pohlit. — Z. Naturf., 13a:567. 1956.
194. Barber, W. — Phys. Rev., 97:1071. 1955.
195. Brunner, C. — Naturwiss., 46:9. 1958.
196. Bradner, H., F. M. Smith, W. H. Barkas, and A. S. Bishop. — Phys. Rev., 77:462. 1950.
197. Bradt, H. L. and B. Peters. — Phys. Rev., 74:1828. 1948; 80:943. 1951.
198. Ballario, C., A. de Marco, R. D. Fortune, and C. Verwerk. — Nuovo cim., 19:1142. 1961.
199. Blau, M. — Phys. Rev., 75:279. 1949.
200. Blum, M. B. — J. phys. et rad., 12:861. 1951.
201. Bay, Z. and H. H. Seliger. — Phys. Rev., 120:141. 1960.
202. Ray, Z., W. B. Mann, H. H. Seliger, and H. O. Wycoff. — Rad. Res., 7:558. 1957.
203. Barkas, W. H., R. M. Deutsch, F. C. Gilbert, and C. E. Violet. — Phys. Rev., 86:59. 1952; 88:1135. 1952.
204. Barber, W. C., G. E. Becker, and E. L. Chu. — Phys. Rev., 89:950. 1953.
205. Bleuler, E. B. and D. Y. Tendam. — Phys. Rev., 99:1605. 1955
206. Blair, J. S. — Phys. Rev., 95:1218. 1955.
207. Bowen, T. — Nucleonics, 12:48. 1954.
208. Bartlett, J. H. and R. E. Watson. — Proc. Am. Acad. Arts. Sci., 74:53. 1940.
209. Bothe, W. Handbuch d. Physik, Bd 22/2. — Springer Verlag. 1933.
210. Bethe, H. A. and L. S. Maximon. — Phys. Rev., 93:768, 788. 1954.
211. Budini, L. and L. Taffara. — Nuovo cim., 4:23. 1956.
212. Chilton, A. B., J. N. Cooper, and J. C. Harris. — Phys. Rev., 93:413. 1954.

213. Cook, C. J., E. Jones, and T. Jorgensen. — Phys. Rev., 91:1417. 1953.
214. Crenshaw, C. M. — Phys. Rev., 62:54. 1942.
215. Curtiss, C. D. — Phys. Rev., 89:123. 1953.
216. Coldwell, D. O. — Phys. Rev., 100:291. 1955.
217. Cranshaw, T. E. and J. A. Harvey. — Can. J. Res., A26:243. 1948.
218. Chamidade, R. et al. — Compt. rend., 242:105. 1956.
219. de Carvalho, H. G. — Phys. Rev., 76:1729. 1949.
220. Carbonne, R. J., E. N. Fuls, and E. Everhardt. — Phys. Rev., 102:1524. 1956.
221. de Carvalho, H. G., and J. I. Friedman, — Rev. Sci. Inst., 26:261. 1955.
222. Corson, D. R. and R. B. Brode. — Phys. Rev., 53:773. 1938.
223. Chen, J. J. L. and S. D. Warshaw. — Phys. Rev., 84:355. 1951.
224. Cusack, W. and R. Stott. — Phil. Mag., 46:632. 1955.
225. Domoradan, K. K. and R. M. Curr. — Proc. Phys. Soc., A69:196. 1956.
226. Decher, R. and Kullenkampff. — Z. Phys., 137:638. 1954.
227. Dissanaike, G. A. — Phil. Mag., 44:1051. 1953.
228. Daniel, R. R., J. H. Davies, J. H. Mulvey, and D. H. Perking. — Phil. Mag., 43:753. 1952.
229. Dalitz. — Proc. Roy. Soc., A206:509. 1951.
230. Devons, S. and J. H. Towle. — Proc. Phys. Soc., A69:345. 1956.
231. Dalgarno, A. and H. N. Yadov. — Proc. Phys. Soc., A66:173. 1953.
232. Doggett, J. A. and L. V. Spencer. — Phys. Rev., 103:1597. 1956.
233. Demers, P. — Can. J. Res., 25:223. 1947.
234. Demichelis, F. — Nuovo cim., 13:562. 1959.
235. Evans, R. D. The Atomic Nucleus. — New York. 1955.
236. Everhardt, E., G. Stone, and R. G. Carbone. — Phys. Rev., 99:1287. 1955.
237. Evans, G. E., P. M. Stier, and C. E. Barnett. — Phys. Rev., 90:825. 1953.
238. Eillis, R. H., H. H. Rossi, and G. Failla. — Phys. Rev., 86:562. 1952.
239. Edmont, J. J. — Phys. et Rad., 10:22. 1949.
240. Erskine, G. A. — Proc. Roy. Soc., A224:362. 1954.
241. Frank, H. Z. — Naturforsch., 12a:750. 1957.
242. Fermi, E. — Phys. Rev., 57:485. 1940.
243. Fermi, E. and E. Teller. — Phys. Rev., 72:399. 1947.
244. Frost, R. H. and C. E. Nielsen. — Phys. Rev., 91:864. 1953.
245. Frolich, H. and R. L. Platzman. — Phys. Rev., 92:1152. 1953.
246. Friedlander, M. H., D. Keefl, and M. G. K. Menon, M. G. K. — Nuovo cim., 5:461. 1957.
247. Fuls, E. N., P. R. Jones, E. P. Ziemba, and E. Everhard. — Phys. Rev., 107:704. 1957.
248. Fano, U. — Phys. Rev., 63:222. 1946; 70:20. 1946; 72:20. 1947.
249. Feshbach, H. — Phys. Rev., 99:295. 1952.
250. Feldman, C. — Phys. Rev., 117:455. 1960.
251. Feather, N. — Proc. Cambr. Phil. Soc., 34:599. 1938.
252. Flammersfeld, A. — Naturwiss., 33:280. 1946.
253. Frost, R. H. and C. E. Nielsen, — Phys. Rev., 91:864. 1953.

254. Fano, U. — Phys. Rev., 93:117. 1954.
255. Faraggi, H. — Compt. Rend., 230:1398. 1950.
256. Fleischmann, H. — Z. Naturf., 15a:1090, 1096. 1960.
257. Farwell, G. W. and H. E. Wegner. — Phys. Rev., 95:1212. 1954.
258. Fulmer, C. B. and B. L. Cohen. — Phys. Rev., 108:1113. 1957.
259. Fulmer, C. B. and B. L. Cohen, — Phys. Rev., 109:94. 1958.
260. Gibson, W. M., D. I. Prowse, and Y. Rotblat. — Nature, 173:1180. 1954.
261. Gooding, T. J. and R. M. Eisberg. — Phys. Rev., 105:357. 1957.
262. Goudsmith, S. and J. Saunderson. — Phys. Rev., 57:24. 1940.
263. Green, D. W., J. N. Cooper, and J. S. Harris. — Phys. Rev., 98:466. 1955.
264. Gluckstern, R. L. — Phys. Rev., 98:1817. 1955.
265. Gryzinski, M. — Phys. Rev., 107:1471. 1957.
266. Gobeli, G. W. — Phys. Rev., 103:275. 1957.
267. Garstang, R. H. — Phys. Rev., 87:529. 1952.
268. Garin, A. and H. Faraggi. — J. Phys. Rad., 19:76. 1958.
269. Gray, L. H. — Proc. Cambr. Phil. Soc., 40:72. 1944.
270. Gilbody, H. B. and J. B. Hasted. — Proc. Roy. Soc., A240:382. 1957; Proc. Phys. Soc., A72:291. 1958.
271. Genin, R. J. — Phys. et Rad., 17:571. 1956.
272. Gerthsen, C. and Z. Grimm. — Phys., 120:476. 1943.
273. Gleason, G. I., I. D. Taylor, and D. L. Tabern, — Nucleonics, 8:5. 1951.
274. Glendenin, L. E. — Nucleonics, 2(1):12. 1948.
275. Gerbes,— Ann. Phys., 23:648. 1935; 30:169. 1937.
276. Gubernator, K. — Z. Phys., 152:183. 1958.
277. Goldwasser, E. L., F. E. Mills, and R. Hansch. Phys. Rev., 88:1137. 1952.
278. Goldwasser, E. L., F. E. Mills, and T. R. Robillard. — Phys. Rev., 98:1763. 1955.
279. Gerardin, C., R. Bilwes, and D. Magnac-Valette. — J. Phys. et Rad., 22:62. 1961.
280. Gove, H. E. — Phys. Rev., 99:1353. 1955.
281. Gooding, T. J. and H. G. Pigh. —Nucl. Inst. a. Meth., 7:189. 1960; 11:365. 1961.
282. Gross, W., G. Wingate, and G. Failla. - Radiology, 7:570. 1957.
283. Holliday, J. E. and E. J. Sternglass. — J. Appl. Phys., 30:1428. 1959.
284. Hubbard, E. L. and E. J. Lauer. — Phys. Rev., 98:1814. 1955.
285. Holloway, M. G. and M. S. Livingston. — Phys. Rev., 54:18. 1938.
286. Halpern, O. and H. Hall. — Phys. Rev., 73:477. 1948.
287. Heckmann, H. H., B. L. Perkirs, W. G. Simon, F. M. Smith, and W. H. Barkas.— Phys. Rev., 117:544. 1960.
288. Hirschfelder, J. O. and J. L. Magee. — Phys. Rev., 73:207. 1948.
289. Haworth, L. J. and L. D. P. King. — Phys. Rev., 54:48. 1938.
290. Huus, T. and C. B. Madsen. - Phys. Rev., 76:323. 1949.
291. Hubbard, E. L. and K. R. McKenzie, — Phys. Rev., 85:107. 1952
292. Halberli, W., P. Huber and E. Baldinger. — Helv. Phys. Acta, 25:467. 1952; 26:145. 1953.

293. Hasted, J. B. — Proc. Roy. Soc., A205:421. 1951; A212:235. 1952; A222:74. 1953; A227:466. 1955.
294. Hanna, G. C. — Phys. Rev., 80:530. 1950.
295. Henneberg, W. — Z. Phys., 86:592. 1933.
296. Hall, T. A. and S D. Warshaw. — Phys. Rev., 75:891. 1948; 77:954. 1950.
297. Heinz, O. — Phys. Rev., 95,610A. 1955; 94:1728. 1954.
298. Hanson, A. O., L. H. Lanzl, E. M. Lyman, and M. B. Scott. — Phys. Rev., 84:634. 1951.
299. Hareford, F. L. — Phys. Rev., 74:574. 1948.
300. Hareford, F. L. and Ch. P. Swann. — Phys. Rev., 78:727. 1950.
301. Huber, P. — Helv. Phys. Acta, 26:145. 1954.
302. Herwig, L. O. and G. H. Miller. — Phys. Rev., 94:1183. 1954.
303. Herwig, L. O. and G. H. Miller. — Phys. Rev., 95:413. 1954.
304. Hudson, A. M. — Phys. Rev., 105,1. 1957.
305. Henderson, G. H. — Proc. Roy. Soc., A102:496. 1922.
306. Hall, H. E., A. V Hanson, and D. Jamnik. — Phys. Rev., 115:633. 1959.
307. Henderson, C. and A. Scott. — Proc. Phys. Soc., A70:188. 1957.
308. Howe, H. A. and K. R. McKenzie. — Phys. Rev., 90:678. 1953.
309. Hanna, C. G., B. Pontecorvo, and D. Kirkwood. — Phys. Rev., 75:985. 1949; 74:497. 1948.
310. Hungerford, E. T. and R. D. Birkhoff. — Phys. Rev., 95:6. 1954.
311. Hooper, I.W., E.W. McDaniel, D. W. Martin, and D. S. Harmer. — Phys. Rev., 124:1123. 1961.
312. Igo, G. I., D. D. Clark, and R. M. Eisberg. — Phys. Rev., 89:879. 1953.
313. Gooding, T. J. and R. M. Eisberg. — Phys. Rev., 105:357. 1957.
314. Igo, G. and R. M. Thaler. — Phys. Rev., 106:126. 1957.
315. Igo, G., H. E. Wegner, and R. N. Eisberg. — Phys. Rev., 101:1508. 1956.
316. Jesse, W. P. and H. Forstat. — Phys. Rev., 73:926. 1948.
317. Jesse, W. P. and J. Sadauskis. — Phys. Rev., 78:1. 1950.
318. Jesse, W. P., H. Forstat, and J. Sadauskis. — Phys. Rev., 77:782. 1950.
319. Jesse, W. P. and J. Sadauskis. — Phys. Rev., 90:1120; 1953.
320. Jesse, W. P. — Phys. Rev., 122:1195. 1961.
321. Jackson, J. D. and H. Schiff. — Phys. Rev., 89:359. 1953.
322. Jshiwari, R., S. Yamashita, K. Yuasa, and K. Miyake. — Journ. Phys., Soc., Japan, 11:537. 1956.
323. Janssens, P. and M. Rene. — Nuovo cim., 760. 1955.
324. Jesse, W. P. and J. Sadauskis. — Phys. Rev., 107:766. 1957.
325. Jesse, W. R. and J. Sadauskis. — Phys. Rev., 102:389. 1956.
326. Jesse, W. P. and J. Sadauskis. — Phys. Rev., 88,417L 1952.
327. Jentschke, W. — Phys. Zs., 41:524. 1940.
328. Jesse, W. P. and J. Sadauskis. — Phys. Rev., 97:1668. 1955.
329. Jesse, W. P. — Phys. Rev., 109:2002. 1958.
330. Jesse, W. P. — Radiation Res., 13:1. 1960.
331. Kepes, I. I., B. Waldman, and W. C. Miller. — Ann. Phys. (USA), 6:90. 1959.

332. Kepler, R. G., C. A. d'Audlau, W. B. Fretter, and L. F. Hansen. — Nuovo cim., 7:71. 1958.
333. Knecht, O. and W. Bothe. — Z. Naturforsch., 8a:805. 1953.
334. Koester, L., H. Maier-Leibnitz, and K. Schmeiser. — Z. Ang. Phys., 5:9. 1953.
335. Kapitza, P. — Proc. Roy. Soc., 106:602. 1924.
336. Kanner, H. — Phys. Rev., 84:1211. 1951.
337. Kanter, H. — Ann. Phys., 20:144. 1957.
338. Knipp, J. and E. Teller. — Phys. Rev., 59:659. 1941.
339. Kelly, E. E. — Phys. Rev., 75:1006. 1949.
340. Kahn, D. — Phys. Rev., 90:503. 1953.
341. Kerne, J. P. — Phil. Mag., 40:369. 1949.
342. Kahn, W. — Phys. Rev., 90:383A. 1953.
343. Krasner, S. — Phys. Rev., 99:520. 1955.
344. Knipp, J. and R. C. Ling. — Phys. Rev., 80:106. 1950; 82:30. 1951.
345. Kaila, K. L. and N. K. Saha. — Proc. Phys. Soc., 69A:888. 1956.
346. Katcoff, S., J. A. Miskel, and C. W. Stanley. — Phys. Rev., 74:631. 1948.
347. Klein, O. and Y. Nishina. — Z. Phys., 52:853. 1929.
348. Kinzinger, E. and W. Bothe. — Z. Naturf., 7a:390. 1952.
349. Kinzinger, E. — Z. Naturf., 8a:312. 1953.
350. Katz, L. and A. S. Penfold. — Rev. Mod. Phys., 22:28. 1952.
351. Kagejama, S. and K. Nishimura. — J. Phys. Soc., Japan, 7:292. 1952; 8:682. 1953.
352. Kagejama, S. — J. Phys. Soc., Japan, 11:348. 1956.
353. Kalil, E. and R. D. Birkhoff. — Phys. Rev., 91:505. 1953.
354. Knecht, O., and W. Bothe. — Z. Naturf., 8a:805. 1953.
355. Koch, H. W. and J. W. Motz. — Rev.Mod. Phys., 31:920. 1959.
356. Keil, E., E. Zeitler, and W. Zinn. — Z. Naturf., 159:1031. 1960.
357. Kerlee, D. D., J. S. Blair, and G. A. Farwell. — Phys. Rev., 107:1343. 1957.
358. Lowry, R. A. and G. H. Miller. — Phys. Rev., 109:824. 1958.
359. Livingston, M. S. and H. A. Bethe. — Rev. Mod. Phys., 9:261. 1937.
360. Lindhard, J. and M. Scharff. — Dan. Mat. — Fys. Medd., 27:15. 1953.
361. Lonchamp, J. P. — J. Phys. Rad., 14:89. 1953; C.R., 239, 877. 1954.
362. Livesey, D. L. — Can. J. Phys., 34:203. 1955.
363. Lillie, A. B. — Phys. Rev., 87:716. 1952.
364. Lassen, N. O. — Dan. Mat. Fys. Medd., 25:11. 1948; 26:12. 1951; 30:8. 1955.
365. Lanon, R. E. and H. L. Kraybill. — Phys. Rev., 113:657. 1959.
366. Langhlin, et. al. — Radiology, 60:165. 1953.
367. Libby, W. F. — Phys. Rev., 103:1900. 1956; Anal. Chem., 19:2. 1947; 27:921. 1955.
368. Lorents, D. S. and E. J. Zimmermann. — Phys. Rev., 113:1199. 1959.
369. Lassen, N. O. — Phys. Rev., 75:1762. 1949.
370. Lattes, C. M. G., P. M. Fowler, and P. Güer. — Proc. Phys. Soc., 59:883. 1947.

371. Lipkin, H. G., and M. G. White. — Phys. Rev., 88:517. 1952.
372. Lyman, E. M., A. O. Hanson, and M. B. Scott. — Phys. Rev., 84:626. 1951.
373. Lanzl, L. and A. O. Hanson. — Phys. Rev., 83:959. 1951.
374. Lamb, W. E. — Phys. Rev., 58:696. 1940.
375. Larson, H. V. — Phys. Rev., 112:1927. 1958.
376. Leachman, R. B. and H. W. Schmitt. — Phys. Rev., 96:1366. 1954.
377. Metropolis, N., et al. — Phys. Rev., 110:185. 1958.
378. Millburn, Birnbaum, Grandall, and schechter. — Phys. Rev., 95:1268. 1954.
379. Miller. — Phys. Rev., 83:1261. 1951.
380. Madsen, C. B. — Dan. Mat. -Fys. Medd., 23:8. 1945.
381. Mano, G. — Ann. de phys., 1:407. 1934; J. Phys. et Rad., 5:628. 1934.
382. Madsen, C. B. — Dan. Mat. —Fys. Medd., 27:13. 1953.
383. Madsen, C. B. and P. Venkateswarln. — Phys. Rev., 74:648. 1948; 76:1782. 1948.
384. Mather, R. — Phys. Rev., 84:181. 1951.
385. Mather, P. and E. Segré. — Phys. Rev., 84:191. 1951.
386. Mott, N. F. — Proc. Roy. Soc., A124:425. 1929; A135:429. 1932.
387. McKinley, W. A. and H. Feshbach. — Phys. Rev., 74:1759. 1948.
388. Moliere, G. — Zs. Naturf., 2a:133. 1947.
389. Moliere, G. — Zs. Naturf., 3a:78. 1948.
390. Möller, C. — Ann. Phys., 14:532. 1932.
391. Marshall, J. and A. G. Ward. — Can. J. Res., A15:39. 1937.
392. Migdal, A. — Phys. Rev., 103:1811. 1956.
393. McClure, C. W. — Phys. Rev., 90: 796. 1953.
394. Maurer. - Ann. d. Phys., 5:340. 1930.
395. Milani. - Cited from Whaling /491/.
396. Miwa, M. and K. Kurijama. — J. Phys. Soc., Japan, 10:320. 1955.
397. Motz, J. W. — Phys. Rev., 100:1560. 1955.
398. Mozley, R. F., R. C. Smith and R. E. Taylor. — Phys. Rev., 111:647. 1958.
399. Nielsen, K. O. Electromagnetically Enriched Isotopes and Mass Spectroscopy (Ed. Smith, M. L.). - New York — London. 1956.
400. Newman, E. and F. E. Steigert. — Phys. Rev., 118:1575. 1960.
401. Neufeld. — J. Phys. Rev., 95:1128. 1954.
402. Neufeld, J. — Phys. Rev., 96:1470. 1954.
403. Northcliffe, C. L. — Phys. Rev., 120:1744. 1960.
404. Nigam, P. B., M. K. Sundaresan, and Ta-Yon Wu. — Phys. Rev., 115:491. 1959.
405. Nelms, A. T. — NBS Circular, 542. 1953; NBS Circular, 577. 1956.
406. Neufeld, J. and S. Snyder. — Phys. Rev., 107:96. 1957.
407. Nigam, B. P. and V. C. Mathur. — Phys. Rev., 121:1577. 1961.
408. Neufeld, J. — Health Phys., 1:315. 1958.
409. Ovadia et al. — Phys. Rev., 88:165A. 1952.
410. Nielsen, L. P. — Dan. Mat. Fys. Medd., 33:6. 1961.

411. Platzman, R. L. — Int. I. Appl. Rad. and Isot., 10:116. 1961.
412. Phillips, J. A. —Phys. Rev., 97:404. 1955.
413. Parkinson, D. B., R. G. Herb, J. C. Bellamy, and C. M. Hudson. — Phys. Rev., 52:75. 1957.
414. Phillips, J. A. — Phys. Rev., 90:532. 1953.
415. Phillipp, K. — Z. Physik, 17:23. 1923.
416. Porat, D. I. and K. Ramavataram. — Proc. Roy. Soc., A232:394. 1959.
417. Papineau, A. — J. Phys. et Rad., 17:566. 1956.
418. Pettus, W.G., H.G. Blosser, and F.L. Hareford. — Phys. Rev., 101:17. 1956.
419. Paul, W. and H. Reich. — Z. Physik, 127:429. 1950.
420. Paul, W. and H. Reich. — Z. Physik, 131:326. 1951.
421. Pickup, E. and L. Voyvodic. — Phys. Rev., 80:89. 1950.
422. Porat, D. I. and K. Ramavataram. — Proc. Phys. Soc., A77:97. 1961.
423. Page, L. A. — Phys. Rev., 81:1062. 1951.
424. Poirier. — Phys. Rev., 117:577. 1960.
425. Pradhan, T. — Phys. Rev., 105:1250 1957.
426. Ritter, V. O. et al. — Z. Naturf., 6a:243. 1951.
427. Rossi, B. — Nature, 130:699. 1932.
428. Rousset, A. et al. — Nuovo Cim., 14:365. 1959.
429. Del Rosario, L. — Phys. Rev., 74:304. 1948.
430. Rohrlich, F. and B. C. Carlson. — Phys. Rev., 93:386. 1954.
431. Roll, P. G. and F. E. Steigert. — Nucl. Phys., 16:534. 1960; 17:54. 1960.
432. Rich, M. and R. Madey. — Report UCRL, 2301. (1954)
433. Rosenblum, S. — Ann. de Phys., 10:408. 1928.
434. Reynolds, H.L., D.N.F. Dunbar, W. A. Wentzel, and W. Whaling. — Phys. Rev., 92:742. 1953.
435. Reynolds, H. L., D. W. Scott, and A. Zucker. — Phys. Rev., 95:671. 1954.
436. Roll, P. G. and F. E. Steigert. — Phys. Rev., 120:470. 1960.
437. Rotblatt, J. — Nature, 165:387. 1950; 167:550. 1951.
438. Ribe, F. — Phys. Rev., 85:1217. 1951.
439. Rosenzweig, W. — Phys. Rev., 115:1683. 1960.
440. Reynolds, H. K. and A. Zucker. — Phys. Rev., 96:393. 1954; 95:1353. 1954.
441. Pickup, E. and L. Voyvodic. — Phys. Rev., 80:89. 1950.
442. Russek, A. and M. Thomas. — Phys. Rev., 109:2015. 1958.
443. Reynolds, H. L., L. D. Wyly, and A. Zucker. — Phys. Rev., 98:474. 1954.
444. Stokes, R. H. et al. — Rev. Sci. Inst., 29:61. 1958; 31:768. 1960.
445. Schiff, H. — Can. J. Phys., 32:393. 1954.
446. Sternheimer, R. M. — Phys. Rev., 88:851. 1952; 91:256. 1953; 103:511. 1956.
447. Sternheimer, R. M. — Phys. Rev., 115:137. 1959.
448. Sternheimer, R. M. — Phys. Rev., 117:485. 1960.
449. Smith, J. H. — Phys. Rev., 71·32. 1947.
450. Sternheimer, R. M. — Phys. Rev., 93:351. 1954.

451. Sachs, D. C. and J. R. Richardson. — Phys. Rev., 93:351. 1954.
452. Sonett, C. P. and K. R. McKenzie. — Phys. Rev., 83:834. 1951; 89:1163. 1953.
453. Snitzer, E. — Phys. Rev., 89:1237. 1953.
454. Sharpe, J. — Proc. Phys. Soc., A65:859. 1952.
455. Sternheimer, R. M. — Phys. Rev., 118:1045. 1960.
456. Simmens, D. H. — Proc. Phys. Soc., A66:454. 1953.
457. Schmieder, K. — Ann. Phys., 35:445. 1939.
458. Stetter, G. — Z. Physik, 120:839. 1943.
459. Stone, W. G. and E. W. Cochran. — Phys. Rev., 107:702. 1957.
460. Snyder, H. S. and W. T. Scott. — Phys. Rev., 76:220. 1949.
461. Stetter, G. and W. Jentschke. — Phys. Zs., 36:44. 1955.
462. Spencer, L. V. and C. Blanchard. — Phys. Rev., 93:114. 1954.
463. Spencer, L. V. — Phys. Rev., 98:1597. 1955.
464. Sharpe, J. — Proc. Roy. Soc., A65:860. 1952.
465. Schambra, P. E., A. M. Rauth, and L. C. Northcliffe. — Phys. Rev., 120:1758. 1960.
466. Sherman, N. — Phys. Rev., 103:1601. 1956.
467. Scott, M. B., A. O. Hanson, and E. M. Lyman. — Phys. Rev., 84:638. 1951.
468. Schiff, L. J. — Phys. Rev., 70:87. 1946.
469. Sofftky, S. D. — Phys. Rev., 123:1885. 1961.
470. Stephens, K. G. and D. Walker. — Proc. Roy. Soc., A229:376. 1955; Phil. Mag., 45:543. 1954.
471. Stier, P. M. and C. F. Barnett. — Phys. Rev., 103:896. 1956.
472. Stelson, McCowan, cited from /501/.
473. Spiegel, V. et al. — Ann. Phys. (USA), 6, 70, 86. 1959.
474. Taylor, A. E. — Rep. Prog. Phys., 15:49. 1952.
475. Tunnicliffe, Ward. — Proc. Phys. Soc., A65:233. 1952.
476. Thomson. — Report UCRL, 1910. 1952.
477. Teasdale, cited from /452/.
478. Towler, et al. — Rev. Mod. Phys., 20:236. 1948.
479. Tamm, I. — Z. Physik, 62:545. 1930.
480. Uehling, E. A. — Ann. Rev. Nucl. Sci., 4:315. 1954.
481. Utterback, N. G. and G. H. Miller. — Phys. Rev., 116:976. 1959.
482. Vigneron, L. — J. Phys. Rad., 10:305. 1949.
483. Votruba, V. — Phys. Rev., 73:1468. 1948.
484. Valentine, J. M. and S. C. Curran. — Phil. Mag., 43:964. 1952; Proc. Roy. Soc. A211:75. 1955; Phil. Mag. 43:964. 1952.
485. Valentine, J. M. and S. C. Curran. — Rep. Prog. Phys., 21:1. 1958.
486. Varshni, V. P. — Ind. J. Phys., 32:373. 1958.
487. Van de Graaf, R. J., W. W. Buechner, and H. H. Feshbach. — Phys. Rev., 69:452. 1946.
488. Voyvodich. — Can. J. Res., A28:315. 1950.
489. Van Rossum, L. — J. Phys. Rad., 10:402. 1949.
490. Vigneron, L. — J. Phys. Rad., 14:145. 1953.
491. Whaling, W. Handbuch der Physik, Bd. 34, Berlin. 1957.

492. Whaling, W. Nuclear Spectroscopy, Part A, New York—London. 1964.
493. Walske, M. C. — Phys. Rev., 88:1283. 1952.
494. Walske, M. C. — Phys. Rev., 101:940. 1956.
495. Warshaw, S. D. — Phys. Rev., 76:1759. 1949.
496. Walker, D. — Prog. Nucl. Phys., 4:215. 1955.
497. Wick, G. C. — Nuovo cim., 1:302. 1945.
498. Weyl, P. K. — Phys. Rev., 91:289. 1953.
499. Wentzel, W. A. and W. Whaling. — Phys. Rev., 87:499. 1952.
500. Wilcox, H. A. — Phys. Rev., 74:1743. 1948.
501. Whitter, A. C. — Can. J. Phys., 32:275. 1954.
502. Wilson, R. R. — Phys. Rev., 60:749. 1941.
503. Wilson, R. R. and Brobeek. — Phys. Rev., 71:385. 1947.
504. Williams, E. J. — Rev. Mod. Phys., 17:217. 1945.
505. Williams, E. J. — Proc. Roy. Soc., A169:531. 1939; Phys. Rev., 58:292. 1940.
506. Weiss, J. and W. Bernstein. — Phys. Rev., 98:1829. 1955; 103:1253. 1956.
507. Wolfe, B., A. Silverman, and A. de Wire. — Rev. Sci. Inst., 26:564. 1955.
508. Wingate, C., W. Gross, and G. Failla. — Phys. Rev., 105:929. 1957.
509. Wentzel, G. — Ann. Phys., 69:335. 1922.
510. Wheeler, J. A. and W. E. Lamb. — Phys. Rev., 55:858. 1934.
511. Williams, E. M. — Proc. Roy. Soc., A125:420. 1929.
512. Williams, E. J. and F. B. Terroux. — Proc. Roy. Soc., A126:289. 1930.
513. Wiedecke, E. — Z. Phys., 154:150. 1959.
514. Webb, W. H., H. L. Reynolds, and A. Zucker. — Phys. Rev., 102:749. 1936.
515. Yadav, H. N. — Proc. Phys. Soc., A65:672. 1952.
516. Yang, C. N. — Phys. Rev., 84:599. 1951.
517. Young, I. R. — J. Appl. Phys., 28:524. 1957.
518. Ziemba, E. P., C. J. Lockwood, G. H. Morgan, and E. Everhardt. — Phys. Rev., 118:1552. 1960.
519. Ziegler, B. — Z. Physik, 151:556. 1958.
520. Zajac, B. and M. A. S. Rosse. — Nature, 162:923. 1948; 164:311. 1949.